University of Alberta

Dynamics of Enhanced Oil Recovery and Sequestration during CO_2 Injection in Fractured Reservoirs

by

Japan Trivedi

©

A thesis submitted to the Faculty of Graduate Studies and Research in partial fulfillment of the requirements for the degree of **Doctor of Philosophy**.

in

Petroleum Engineering

Department of Civil and Environmental Engineering

Edmonton, Alberta
Fall 2008

Library and Archives Canada

Published Heritage Branch

395 Wellington Street
Ottawa ON K1A 0N4
Canada

Bibliothèque et Archives Canada

Direction du Patrimoine de l'édition

395, rue Wellington
Ottawa ON K1A 0N4
Canada

Your file Votre référence
ISBN: 978-0-494-46439-7
Our file Notre référence
ISBN: 978-0-494-46439-7

NOTICE:
The author has granted a non-exclusive license allowing Library and Archives Canada to reproduce, publish, archive, preserve, conserve, communicate to the public by telecommunication or on the Internet, loan, distribute and sell theses worldwide, for commercial or non-commercial purposes, in microform, paper, electronic and/or any other formats.

The author retains copyright ownership and moral rights in this thesis. Neither the thesis nor substantial extracts from it may be printed or otherwise reproduced without the author's permission.

AVIS:
L'auteur a accordé une licence non exclusive permettant à la Bibliothèque et Archives Canada de reproduire, publier, archiver, sauvegarder, conserver, transmettre au public par télécommunication ou par l'Internet, prêter, distribuer et vendre des thèses partout dans le monde, à des fins commerciales ou autres, sur support microforme, papier, électronique et/ou autres formats.

L'auteur conserve la propriété du droit d'auteur et des droits moraux qui protège cette thèse. Ni la thèse ni des extraits substantiels de celle-ci ne doivent être imprimés ou autrement reproduits sans son autorisation.

In compliance with the Canadian Privacy Act some supporting forms may have been removed from this thesis.

While these forms may be included in the document page count, their removal does not represent any loss of content from the thesis.

Conformément à la loi canadienne sur la protection de la vie privée, quelques formulaires secondaires ont été enlevés de cette thèse.

Bien que ces formulaires aient inclus dans la pagination, il n'y aura aucun contenu manquant.

Canada

My work is dedicated to

"Lord Shree Swaminarayan" and H.D.H "Pramukh Swami Maharaj"

For their blessings and inspiration

My parents and brother

For their love and support

Friends - Without who it wouldn't be so easy

Abstract

With urgent need of greenhouse gas sequestration and booming oil prices, underground oil/gas reservoirs seem the only value added choice for CO_2 storage. A great portion of current CO_2 injection projects in the world is in naturally fractured reservoir. It is our aim to show that the matrix part of these reservoirs could be used as a permanent CO_2 storage unit while recovering oil from it.

This dissertation presents a different approach to the problem following a multi-stage research work. Initially, a series of laboratory experiments were performed at ambient conditions using artificially fractured (single) sandstone rocks to mimic fully miscible CO_2 injection. Different injection rates were tested and the efficiency of the process was analyzed in terms of maximized oil recovery. Next, CO_2 injection experiments at different miscible conditions were conducted to analyze the dominant transport mechanisms and to quantify enhanced oil recovery (EOR) / storage potential. CO_2 diffusion and other effective oil recovery mechanisms were studied during continuous injection at different rates into the fracture. After the continuous injection of CO_2, a soaking period was allowed following a blowdown period to produce the oil recovered by back-diffusion. The CO_2 storage and EOR capacity during the blowdown period were analyzed. Using dimensionless analysis and matrix-fracture diffusion groups, a critical number for optimal recovery/sequestration was obtained.

The pressure decay behavior during the shutdown was analyzed in conjunction with the gas chromatograph analysis of the produced oil sample collected during blowdown after the quasi-equilibrium reached during pressure decay. This gave insights into the governing

mechanism of extraction/condensation and miscibility for recovering lighter to heavier hydrocarbons during pressure depletion from fractured reservoirs.

The importance of miscible recovery from fractured reservoirs in current petroleum industry makes its comprehensive understanding, characterization, and quantitative prediction very critical. Therefore, as a final step, a universal procedure of inspectional analysis followed by a numerical sensitivity was performed for the scaling of fractured porous media. A new dimensionless group introduced by combining the effects of major governing groups will improve the understanding of pore scale mechanisms also it can be further used for the improvement of fractured reservoir models and upscaling laboratory results.

Acknowledgements

I am deeply indebted to my supervisor Dr. Tayfun Babadagli for his technical directions, motivation and moral support throughout this research. With the oil recovery enhancement, my technical, visional, goal directional and intrapersonal enhancement was also achieved through improvisation constantly pumped by Dr. Babadagli. I am thankful to Dr. Ergun Kuru, Dr. Minzhe Dong, Dr. Ahmed Bouferguene and Dr. Jozef Szymanski for serving as members on the examination committee. I am also thankful to Apache Canada Ltd. for providing field and well data, and permission to use them in this research. Assistance in obtaining the Midale field cores by Apache from the Saskatchewan Geological Survey is also appreciable. I, finally, would like to extend my gratitude to Mr. Rob Lavoie (CalPetra) for his invaluable assistance during data collection, trip to the Midale field and for sharing his experience on the operations done in the field over the last three decades.

This research was funded by NSERC (Strategic Grant No: G121990070) and Apache Canada Ltd. Partial funding was also obtained from an NSERC Grant (No: G121210595) and FSIDA (University of Alberta, Fund for Support of International Development Activities) Grant (#04-14O). The funds for the equipment used in the experiments were obtained from the Canadian Foundation for Innovation (CFI, Project #7566) and the University of Alberta. All these supports are greatly appreciated. I am also thankful for various scholarships from the FGSR (University of Alberta) and GSA (University of Alberta) to present my research at various conferences.

I would also like to thank Schlumberger (ECLIPSE), Computer Modeling Group (CMG) and COMSOL for their software supports.

This work could not have been completed without the help and support from a number of people; thanks to Nathan Buzik and Sean Watt for providing their technical expertise in preparing core-holder design and experimental set-ups; members of the EOGRRC group at the University of Alberta for stimulating discussions and knowledge exchange during group meetings.

Finally, I am greatly thankful to all invisible forces acting towards my dreams, desire and destiny.

TABLE OF CONTENTS

1 Introduction 1

1.1 Overview 1

1.2 Literature Review 6

1.2.1 Critical Injection Rate 6

1.2.2 First-Contact Miscible or Immiscible Matrix-Fracture Interaction Experiments 8

1.2.3 Effect of Flow on Diffusion/Dispersion in Fractured Porous Media 10

1.2.4 Scaling and Dimensionless Analysis 12

1.2.5 Multi-Contact Miscible CO_2 Injection into Fractures - Experimental Study 14

1.3 Problem Statement 15

1.4 Methodology 16

1.5 Outline 18

2 Efficiency of Diffusion Controlled Miscible Displacement in Fractured Porous Media 20

2.1 Introduction 20

2.2 Experimental Method 22

2.2.1 Porous Media 22

2.2.2 Fluids 23

2.2.3 Test Conditions 23

2.2.4 Core Preparation and Test Procedure 23

2.2.5 Measurement Technique 24

2.2.6 Effect of Water Saturation 25

2.2.7 Effect of Aging 25

2.2.8 Effect of Viscosity Ratio/Density 25

2.2.9 Effect of Gravity 26

2.3 Results and Analysis 26

2.4 Efficiency Analysis 28

2.5 Conclusions 29

3 Experimental and Numerical Modeling of the Mass Transfer between Rock Matrix and Fracture 40

3.1 Introduction 40

3.2 Experimental Study 43

3.2.1 Procedure 44

3.3 Experimental Observations 48

3.4 Modeling of Fracture-Matrix Transfer Process 53

3.4.1 Analogy between Monolith Catalysts (Reactor) and Matrix-Fracture Systems 54

3.4.2 Mathematical Model Formulation 56

3.4.3 Dispersion and Diffusion 60

3.5 Mass Transfer Rate Constant and Effective Diffusion into Porous Matrix 63

3.6 Conclusions 68

4 Efficiency Analysis of Greenhouse Gas Sequestration during Miscible CO_2 Injection in Fractured Oil Reservoirs 70

4.1 Introduction 70

4.2 Background 71

4.3 Dimensionless Parameters and the Effectiveness Factor for Matrix-Fracture Interaction by Diffusion during Injection of a Miscible Phase 72

4.4 Effective Parameters and Efficiency Correlations 76

4.5 Summary and Discussion 78

5 Scaling Miscible Displacement in Fractured Porous Media Using Dimensionless Groups 84

5.1 Background on Scaling Process 84

5.2 Dimensional Analysis (DA) 84

5.2.1 Inspectional Analysis (IA) 84

5.3 Derivation of the Dimensionless Groups for Flow in Fractured Porous Medium 86

5.4 New Dimensionless Number 90

5.4.1 Similarity and Comparison with the Immiscible Process 91

5.5 Validation of Proposed Group 92

5.5.1 Experiments 92
5.6 Physical Significant of the Proposed Group and Analysis 95
5.7 Concluding Remarks 97
6 Experimental Investigations on the Flow Dynamics and Abandonment Pressure for CO_2 Sequestration and Incremental Oil Recovery in Fractured Reservoirs: The Midale field Case 101
6.1 Introduction 101
6.2 Experimental Components 103
6.2.1 Diffusion Cell (Core Holder) 103
6.2.2 Injection Set-up 103
6.2.3 Production System 104
6.2.4 Data Acquisition System (DAQ) 104
6.2.5 Core Properties and Core Preparation 105
6.3 Experimental Procedure 105
6.3.1 Continuous CO_2 Diffusion for Oil Recovery 106
6.3.2 Blow Down 107
6.4 Effect of Rate – Existence of Critical Rate 107
6.5 Sequestration – Time and Economical Aspects 109
6.6 Effect of Miscibility – Sequestration and EOR 109
6.7 Rock Type – Sandstone and Limestone 110
6.8 Blow Down – Sequestration and EOR 110
6.9 Critical Observations 111
6.10 Cap Rock Sealing 112
6.11 Conclusions and Remarks 113
7 Experimental Analysis of CO_2 Sequestration Efficiency during Oil Recovery in Naturally Fractured Reservoirs 120
7.1 Overview 120
7.2 Introduction 120
7.2.1 Importance/Role of Diffusivity in Miscible and Immiscible Matrix-Fracture Transfer Process 121
7.3 Experimental Components 122
7.3.1 Core Properties and Core Preparation 122

7.3.2 Diffusion Cell (Core Holder) 122
7.3.3 Injection Set-up 123
7.3.4 Production System 123
7.3.5 Data Acquisition System (DAQ) 123
7.4 Experimental Procedure 124
7.4.1 Continuous CO_2 Diffusion for Oil Recovery 125
7.4.2 Blow Down 125
7.5 Experimental Results and Discussion 126
7.6 Matrix-Fracture Diffusion Simulation 129
7.7 Correlation for CO_2 Sequestration and Oil Production 131
7.8 Conclusions 133
8 Analysis of Observations on the Mechanics of Miscible Gravity Drainage in Fractured Systems 145
8.1 Problem Statement 145
8.2 Mechanisms: Miscible Gravity Drainage in NFRs 146
8.3 Soaking: Improving Extraction Mechanism 147
8.4 Effect of Diffusion/Dispersion and Injection Rate 148
9 Contributions and recommendations 150
9.1 Contributions and Conclusions 150
9.1.1 First Contact Miscible Experiments 150
9.1.2 Scaling of Matrix-Fracture Miscible Process and Critical Rate Definition 151
9.1.3 Simulation of Matrix-Fracture Process 152
9.1.4 Multi-Contact CO_2 Experiments 153
9.2 Recommendations for Future Research 155
10 Nomenclature 157
11 Appendix 164
12 Bibliography 172

LIST OF TABLES

Table 1.1 Miscible (major) CO_2 projects in the USA 3

Table 1.2 Miscible (major) CO_2 projects in Canada 4

Table 1.3 Imiscible (major) CO_2 projects world-wide 4

Table 2.1: Properties of displacing and displaced fluids. 31

Table 2.2: Detailed outline of experiments conducted. 32

Table 3.1: Properties of solute and solvent used in the study 46

Table 3.2: Details of experiments performed. 47

Table 4.1. Time-scales and dimensionless number associated with our physics similar to that of monolith (Bhattacharya et al. 2004). 79

Table 5.1: Dependent and independent variables, symbols and their dimensions. 88

Table 5.2: Dimensionless groups derived using the Inspectorial Analysis 90

Table 5.3: Experiments performed. 94

Table 5.4: Properties of solvent and solute used in experiments 94

Table 6.1: Core and fluid properties and experimental details 114

Table 7.1: Experiments details 134

Table 7.2: Hyperbolic behavior for oil recovery during production life 134

Table 7.3: Dimensionless numbers and TOP/TSI predicted values using $N_{M\text{-}FD}$ 135

Table 10.1: The unique dimensionless group from the above equations (marked as bold letters) 167

LIST OF FIGURES

Figure 2.1: Core-holder design. 30

Figure 2.2: Core samples cut for fracture creation and the core-holder used. 30

Figure 2.3: Experimental set-up. 31

Figure 2.4: Calibration chart for refractometer for mineral oil-heptane mixture. 33

Figure 2.5: Cumulative production with solvent injected (PV) for Berea sandstone horizontal orientation. 33

Figure 2.6: Cumulative production with solvent injected (PV) for Berea sandstone vertical orientation. 34

Figure 2.7: Cumulative production with solvent injected (PV) for aged Berea sandstone horizontal orientation. 34

Figure 2.8: Cumulative production with solvent injected (PV) for Indiana limestone horizontal orientation. 35

Figure 2.9: Cumulative production with solvent injected (PV) comparing aged and unaged Berea sandstone horizontal orientation. 35

Figure 2.10: Cumulative production with time for water imbibed cores. 36

Figure 2.11: Cumulative production with time for Berea sandstone horizontal orientation. 36

Figure 2.12: Cumulative production with time for aged Berea sandstone horizontal orientation. 37

Figure 2.13: Cumulative production with time for Berea sandstone vertical orientation. 37

Figure 2.14: Cumulative production at different flow rate and time axis for Berea sandstone horizontal orientation. 38

Figure 2.15: Cumulative production at different flow rate and time axis for Indiana limestone horizontal orientation..... 38

Figure 2.16: Cumulative production at different flow rate and time axis for aged Berea sandstone horizontal orientation..... 39

Figure 3.1(a): Core cutting and fracture preparation..... 45

Figure 3.1(b): Core holder design..... 45

Figure 3.2: Experimental set-up. 46

Figure 3.3: Solute recoveries during solvent diffusion for different oil types. 48

Figure 3.4: Solute recoveries during solvent diffusion for horizontal and vertical cases..... 50

Figure 3.5: Solute recoveries during solvent diffusion comparing Berea sandstone and Indiana limestone cores. 51

Figure 3.6: Comparison of the solute recoveries during solvent diffusion for the aged and non-aged samples. 52

Figure 3.7: Solute recoveries during solvent diffusion from high viscosity mineral oil aged and non-aged core samples. 52

Figure 3.8: Solute recoveries during solvent diffusion comparing 3" and 6" longer samples. 53

Figure 3.9: Diffusion and flux behavior in monoliths..... 55

Figure 3.10: Diffusion and flux in matrix-fracture system. 56

Figure 3.11(a): Geometrical representation of matrix-fracture system used in this study (not to scale)..... 57

Figure 3.11(b): Simulation match with the experimental results of solute (mineral oil) concentration (C_2) change for two different rates on aged Berea sandstone cores. 60

Figure 3.12: Mass transfer rate constant with velocity. 64

Figure 3.13: Comparison of the K_r (s^{-1}) values obtained through the numerical simulation and the ones obtained from Equation (3.17). 65

Figure 3.14: Comparison of D_e^M values used for the simulation matches with the ones obtained from Equation (3.18). 67

Figure 3.15: Concentration-time curves for matrix-fracture transfer at low and high rates... 67

Figure 4.1(a): Core cutting/fracture preparation and core holder assembly 79

Figure 4.1(b): Core holder design 80

Figure 4.2(a): Recovery of solute (oil) with injection of miscible solvent (heptane) 80

Figure 4.2(b): Simulation match (solid lines) with experimental results (symbols) 81

Figure 4.3: Power-law relationship between (TSP/TSI) and effectiveness factor (η_G). BHA: Berea sandstone-horizontal-mineral oil-aged, IH: Indiana limestone-horizontal- mineral oil, BHS: Berea sandstone-horizontal-mineral oil, BHK: Berea sandstone-horizontal-kerosene, HO: Heavy (mineral) oil, HOA: Heavy (mineral) oil-aged 82

Figure 4.4: Power-law relation of (TSS/TSI) with effectiveness factor (N_G) [Legend as given in Figure 4.3] 82

Figure 4.5: Comparison of (TSP/TSI) experimental value and the one obtained from Equation (4.7) [% error showing 10, 20 & 30 % error in predicted values] 83

Figure 4.6: Comparison of (TSS/TSI) experimental value and the one obtained from Equation (4.8) [% error showing 10, 20 & 30 % error in predicted values] 83

Figure 5.1 Geometrical representation of matrix-fracture system used in this study 97

Figure 5.2: Experimental set-up 98

Figure 5.3: Normalized oil production with respect to amount of solvent injected as a function of the gravity number (Ng). 98

Figure 5.4: Normalized oil production with respect to amount of solvent injected as a function of the Peclet number (*Pe*). 99

Figure 5.5: Normalized oil production with respect to amount of solvent injected as a function of (Peclet Number/Gravity Number). 99

Figure 5.6: Normalized oil production with respect to amount of solvent injected as a function of Matrix-Fracture Diffusion Group (N_{M-FD}). 100

Figure 5.7: Normalized oil production with respect to amount of solvent injected as a function of Fracture Diffusion Index (FDI). 100

Figure 6.1: Experimental set-up (A schematic is presented in chapter 7, Figure 7.2). 115

Figure 6.2: Core cutting, cleaning and fracture preparation. 115

Figure 6.3: Oil production for different rates and pressures. 116

Figure 6.4: CO_2 produced per amount of CO_2 injected for different rates and pressures. .. 117

Figure 6.5: CO_2 stored per amount of CO_2 injected for different rates and pressures. 117

Figure 6.6: CO_2 stored with time for different rates and pressures. 118

Figure 6.7: Core pressure change against time for four different cases. 118

Figure 6.8: Cap rock sealing capacity test. 119

Figure 7.1: Core Preparation. 136

Figure 7.2: Experimental Setup (Photo of the set-up is shown in Figure 6.1). 136

Figure 7.3: Oil recovery with the pressure blowdown for Berea sandstone. 137

Figure 7.4: Oil recovery with the pressure blowdown for Midale carbonate. 137

Figure 7.5: CO_2 production with the pressure blowdown for Berea sandstone. 138

Figure 7.6: CO_2 production with the pressure blowdown for Midale carbonate. 139

Figure 7.7: CO_2 storage with the pressure blowdown for Berea sandstone. 140

Figure 7.8: CO_2 storage with the pressure blowdown for Midale carbonate. 141

Figure 7.9: Normalized recovery factor with the CO_2 PV injected for Berea sandstone. 142

Figure 7.10: Normalized recovery factor with the CO_2 PV injected for Midale carbonate.. 142

Figure 7.11: Pressure decay and attainment of quasi-equilibrium behavior..... 143

Figure 7.12: Hydrocarbon recovery distribution for the Case-8 at different stages of the production life..... 143

Figure 7.13: (TOP/TSI) with matrix-fracture diffusion group ($N_{M\text{-}FD}$)..... 144

1 INTRODUCTION

1.1 Overview

Fossil fuels are likely to remain a major primary source of world's energy supply in today's industrialized world because of their inherent advantages such as availability, competitive cost, ease of transportation and storage, and well-advanced technology over other energy sources. Hence, the generation and emission of greenhouse gases, more specifically CO_2 and flue gas are likely to continue. The concentrations of CO_2 in the atmosphere have increased by 31% since 1750. Of the total CO_2 emissions in the United States in 2002, approximately 98% resulted from the combustion of fossil fuels (coal, petroleum, and natural gas). Industrial processes, including gas flaring and cement production, accounted for the other 2%. Fossil fuel combustion for electricity generation is the largest contributor to CO_2 emissions in the United States followed by fossil fuel combustion for transportation. In 2002, electricity generation accounted for 39% of CO_2 emissions in the United States while transportation accounted for about 32%. By weight, CO_2 is the most emitted greenhouse gas. In 2002, sources in the United States emitted 5,796 million metric tons of CO_2 compared to 27 million metric tons of methane and 1.1 million metric tons of nitrous oxides. The amount of anthropogenic CO_2 emitted to the atmosphere has risen from the preindustrial levels of 280 parts per million (ppm) to the present levels of over 365 ppm. It is estimated that ~6 gigatons of carbon enters the environment annually as a result of global energy-related CO_2 emission, North America being responsible for ~0%–25% of this total.

Because of the reasons outlined above, the sequestration of CO_2 turned out to be a critical issue in the last decade. There are several different ways to sequester CO_2. They can be classified as follows:

- CO_2 reactions with naturally or artificially formed alkine compounds, like silicate, oxide and hydroxide to store CO_2 in form of solid hydroxide to store CO_2 in form of solid carbonates.
- Storage of CO_2 in form of bicarbonate in solution by reaction of solid carbonate dissolution in the presence of water and CO_2.

- Deep-ocean injection, subterranean injection of captured CO_2 for biomass formation and accumulation.
- Stratigraphic and structural trapping in depleted oil and gas reservoirs.
- Adsorption trapping in uneconomic coal beds.
- Mineral immobilization
- Solubility trapping in reservoir oil and gas and formation water.

The mechanisms to sequester CO_2 geologically are: 1) stratigraphic and structural trapping in depleted oil and gas reservoirs, 2) solubility trapping in reservoir oil and formation water, 3) adsorption trapping in uneconomic coal beds, 4) cavern trapping in salt structures, and 5) mineral immobilization.

Recognition of the importance of CO_2 emissions has stimulated research toward mitigation of CO_2 effects as mandated under the Kyoto Protocol of the United Nations Framework Convention on Climate Change. The sequestration of CO_2 and/or flue gas is not cheap; however, the injection of those gases into oil or gas reservoirs to enhance production may offset some of the associated costs. Hydrocarbon miscible processes have received extensive field appraisal since 1950's, especially in the USA and Canada. CO_2 solvent flooding is one of the most successful EOR methods in the USA and worldwide.

A large proportion of the world's proven oil has been found in reservoir rocks that are naturally fractured. Due to poor sweep efficiency, waterflooding in such reservoirs may not be applicable if the matrix is not water-wet, very tight and heterogeneous, and oil viscosity is high. Use of vast and successful experience of miscible especially CO_2 flooding from homogeneous (un-fractured) reservoirs to fractured reservoir could benefit the tertiary recovery prospects and at the same time those reservoirs could be targeted for sequestration.

Table 1.1 Miscible (major) CO_2 projects in the USA

Pay zone (Basin)	Major fields	Formation	Porosity, %	Permeability md	Area, acres
San Andres (Tex/N.M)	Slaughter	Dolo/LS	9-15	1.3-123	20,328
	Vacuum				5,984
	Seminole Unit				16,679
	Wasson (Denver, Willard, ODC)				43,648
	Hanford				1,460
	Yates (Immiscible)				26,000
Silurian-Niagaran (Mich)	Dover	LS/Dolo	7-8	5-10	4,525
Canyon Reef (Tx)	SACROC	LS	4-5	19	49,900
	Cogdell				2,204
Devonian (Tx)	N.Cross-Devonian Unit S.Cross Devonian Unit Mid Cross Devonian Unit North Dollarhide Dollarhide Devonian	-	18-22	4-5	4,525
Lower Tuscaloosa (Miss.)	Little Creek	S	23-26	60-90	6,200
	West Mallalieu				8,240
	McComb				12,600
	Smithdale				4,100
	Brookhaven				10,800
Ismay Desert Creek (Utah)	Greater Aneth Area	LS	14	5	13,400
Canyon	Salt Creek	LS	20	12	12,000
Sims (Ok)	Sho-Vel-Tum	S	16	30	1,100
Delaware, Ramsey (Tx)	Twofreds East Ford El Mar	S	19-20	30-32	4,392 1,953 6,000
Abo (Tx)	T-Star (Slaughter Consolidated)	Dolo	7	2	1,000
Grayburg (Tx)	North Cowden Demo	Dolo	10	2-5	200
Clearfork (Tx)	Antosh Irish	Dolo	7-11	5	2,853
Springer (Ok)	Northeast Purdy Bradley Unit	S	13-14	44-50	4,100
Tensleep (Wyo)	Lost Soldier Wertz	S	9-10	20-30	1,345 1,400
Weber SS	Rangerly Weber sand	S	12	10	18,000
Morrow	Postle	S	16	30	11,000

Table 1.2 Miscible (major) CO_2 projects in Canada

Pay zone (Basin)	Major fields	Formation	Porosity, %	Permeability md	Area, acres
Midale	Weyburn Unit	LS/Dolo	15	10	9,900
Marly & Vuggy	Midale	Dolo/LS	16.3	75	30,483
Viking Cardium	Jofrre	S	13	500	6,625
	Pembina		16	20	80
Beaverhill Lake	Swan Hills	LS	8.5	50-60	-
Nisku	Enchant	Dolo	10-17	10-50	-

Table 1.3 Imiscible (major) CO_2 projects world-wide

Pay zone (Basin)	Major fields	Formation	Porosity, %	Permeability md	Area, acres	Start Date
Garzan (Turkey)	Bati Raman	LS	18	58	12,890	3/86
Forest Sands (Trinidad)	Area 2102	S	29-32	150-300	-	6/76
	Area 2121					1/74
	Area 2124					1/86
	EOR 34-Cyclic					84

LS – Limestone

S – Sandstone

Dolo - Dolomite

During the injection of fluids that are miscible with oil for enhanced oil recovery, oil recovery and transport of the injectant are controlled by fracture and matrix properties in naturally fractured reservoirs (NFR). For such systems, the transfer between matrix and fracture due to diffusion constitutes the major part of oil recovery. While injecting secondary or tertiary recovery materials that are miscible with matrix oil, i.e., hydrocarbon solvents, alcohols, CO_2, N_2 etc., because of the large permeability contrast between the matrix and the fracture; fracture network creates the path for the injected solvent to bypass and leave the oil in the matrix untouched. Significant amount of oil can be recovered from the unswept bypassed parts of the reservoir by maximizing the subsequent crossflow or

mass transfer between fracture and porous matrix. Likewise, when the greenhouse gases (CO_2, pure or in the form of flue gas) are injected into NFRs, the matrix part could be a proper storage environment and the transfer of the injected gas to the matrix needs to be well understood for the determination of process efficiency. The same process is encountered in the transportation of contaminants and waste material in NFRs. Understanding the effects of the different parameters on the dynamics of such processes is essential in modeling such processes. In fact, the description of matrix fracture interaction for dual-porosity dual-permeability models developed for NFRs is still a challenge.

Different solvent injection processes such as carbon dioxide, nitrogen, flue gas, natural gas, or other hydrocarbon gases (methane, ethane, propane, and butane) have one of the most important things in common; they all dissolve into the oil phase eventually causing mixing of oil and injected gas depending on the pressure applied. The efficiency of the mixing or dissolving here is always measured or characterized by mutual diffusion coefficient of solvent into the oil phase. Solute transport in fractures, however, is controlled not only by diffusion but also advective processes. The fracture dispersion coefficient and effective matrix diffusion coefficient are the most important parameters controlling the matrix diffusion. In the fractured porous media, the matrix diffusion is of primary importance in several problems such as geological disposal of nuclear waste, contaminant transport during ground water contamination, enhanced oil recovery and greenhouse gas sequestration. During CO_2 injection into naturally fractured oil reservoirs for enhanced oil recovery, a great portion of oil is recovered by matrix-fracture interaction. Diffusive mass transfer between matrix and fracture controls this process if CO_2 is miscible with matrix oil. The oil expelled from matrix is replaced by CO_2 and the matrix could be potentially a good storage medium for long term. Detailed analysis is needed for the co-optimization of the oil recovery and CO_2 storage, i.e., maximizing the oil recovery while maximizing the amount of CO_2 stored.

During CO_2 injection into fractured systems there still exist several unanswered questions. How the injection scheme is optimized? What is the optimal injection rate that delays the breakthrough time, and reduces the recycling cost keeping the process still efficient by producing oil at an economic rate? What range of reservoir pressure should be maintained for the best result (immiscible, miscible or near miscible process)? Which of the mechanisms of oil; swelling, gravity drainage or diffusion governs the production mechanism

during miscible recovery? What should be done when oil cut drops significantly during continuous CO_2 injection and most of the injected CO_2 needs to be recycled? How does the different hydrocarbon components' recovery get affected? Is sequestration goal a byproduct of oil production or hampers incremental recovery? These fundamental questions can only be answered by thorough experimental analyses.

1.2 Literature Review

1.2.1 Critical Injection Rate

Macroscopic/microscopic heterogeneities are the major reasons of unequal displacement rates between oil in place and solvent injected. Heterogeneities cause poor areal sweep efficiencies and early breakthroughs hampering oil recoveries. When a gas is injected to displace oil, the mobility ratio between the injected gas and displaced oil is typically highly unfavorable owing to low viscosity of gas that results in gravity segregation. In 1952, Hill defined a critical velocity above which viscous instability due to lower gravity compared to viscous forces can occur. Dumore (1964) modified the equation suggested by Hill (1952) with mixing of solvent and oil behind the front taken into consideration. Slobod and Howlett (1964) derived a critical rate for frontal stability in gravity drainage given by:

$$q_{oc} = \frac{k_o}{\Delta\mu_o}(\Delta\rho * g) \quad \text{.....(1.1)}$$

Gravity drainage rate for immiscible process in homogeneous porous media defined by Barkve and Firoozabadi (1992) is

$$q_{oc} = \frac{k_o}{\mu_o}(\Delta\rho * g - P_C^{(TH)} / L) \quad \text{.....(1.2)}$$

For miscible processes:

$$q_{oc} = \frac{k_o}{\mu_o}(\Delta\rho * g) \quad \text{.....(1.3)}$$

where

μ_o = Oil viscosity

k_o = Single phase oil permeability

$\Delta\rho$ = Density difference between injected/displaced fluids

$P_C^{(TH)}$ = Threshold capillary pressure

G = gravitational acceleration

L = Height

Tiffin and Kremesec (1986) noted recovery improvements for gravity-assisted vertical core displacement over horizontal displacement. They performed first contact as well as multi-contact miscible experiments. Their results indicated that the mass transfer strongly affects frontal stability and the efficiency increases at lower cross flow and mixing conditions.

Recovery mechanism of matrix-fracture systems has been studied at laboratory scale since 1970's. Thompson and Mungan (1969) compared displacement velocity to critical velocity (V_C) and showed its effect on recovery efficiency. Slobod and Howlett (1964) and Thompson and Mungan (1969) showed that the critical velocity defines the fingering behavior in displacement of more viscous and denser fluid in a miscible process.

Babadagli and Ershaghi (1993) proposed a fracture capillary number ($N_{f,Ca}$) as the ratio of viscous to capillary forces for immiscible displacement in fractured systems. The fracture capillary number is a ratio of viscous forces active in fracture to the capillary forces active in matrix. Stubos and Poulou (1999) introduced a modified diffusive capillary number as the ratio of diffusion to the capillary gradient driven rate. Their work mainly focused on drying of porous media with existence of two phases. Later, Babadagli (2002) showed a relationship between capillary imbibition recovery and matrix/fracture properties while there is a constant rate flow in the fracture using a scaling group where he included the length of the matrix. This group was derived based on the Handy's equation (Handy, 1960).

1.2.2 First-Contact Miscible or Immiscible Matrix-Fracture Interaction Experiments

Mahmoud (2006) and Wood et al. (2006) showed that the presence of vertical fracture improved the oil recovery through immiscible gas assisted gravity drainage (GAGD) compared to the unfractured counterpart. They observed that gas will try to stay on the top and expand laterally and if the gravity force loses its dominance to viscous forces, then the adverse effect of fractures can be observed.

Saidi (1987) studied the diffusion/stripping process in fractured media. He emphasized the compositional effects between gas in the fracture and oil in the matrix on recovery enhancement. Using the results of single matrix block analytical studies and multicomponent laboratory experiments Da Silva and Belery (1989) confirmed the importance of molecular diffusion in NFRs and concluded that it may override the other hydrocarbon displacement mechanisms. Morel et al. (1990) performed nitrogen diffusion experiments with horizontal chalk cores and studied the effect of initial gas saturation. They found that the recovery process is not purely dependent on diffusion mechanism. Hu et al. (1991) showed the importance of diffusion calculation as well as capillary pressure curve correction on the IFT change due to compositional change. Part (1993) studied the formation of drying patterns assuming only capillary forces and neglecting viscous effects. It was the first attempt to theoretically characterize drying patterns in porous media as well.

The effect of displacement rates and pressure on the recovery performance was investigated by Zakirov et al. (1991) in miscible displacement through fractured reservoirs. Firoozabadi and Markeset (1994) showed that the capillary pressure contrast between matrix and fracture could be the major driving force. Further, they studied the effect of matrix/fracture configuration and fracture aperture on first contact miscible efficiency. If the capillary contrast (capillary pressure) of the fractured and layered reservoirs are reduced or eliminated, gravity drainage performance can be improved (Dindoruk and Firoozabadi, 1997; Correa and Firoozabadi, 1996). Burger et al. (1996) and Burger and Mohanty (1997) found that capillary driven crossflow does not contribute significantly to mass transfer in near-miscible hydrocarbon floods.

The presence of water affects the pore-scale distribution of hydrocarbon phases (Pandey and Orr al., 1990, Mohanty and Salter, 1982). Connectivity and tortuosity of the pore structure influences the effective diffusivity and the relative permeability of each hydrocarbon phase. Hence, the mass transfer and bypassing are affected. LeRomancer et al. (1994) examined the effect of water saturation (<30%) on mass transfer in the matrix blocks of a fractured reservoir. As the water saturation increases, the liquid-hydrocarbon-phase area available for diffusion and the gas/liquid interfacial area decrease resulting in a reduction in mass transfer. At high water saturations, islands of oil will be isolated by water, effectively reducing mass transfer further. They also concluded that water saturation has no effect during nitrogen injection because of a strong capillary crossflow. Whylie and Mohanty (1997) further investigated the effects of water saturation on mass transfer from bypassed region and bypassing during miscible/near-miscible gas injection. They used 1-D model and calculated effective diffusion coefficient.

The orientation of the bypassed region with respect to gravity and enrichment of the solvents affect the mass-transfer rate. The mass-transfer was least for the vertically up orientation (against gravity), intermediate for the vertically down, and highest for the horizontal orientation for the experiments (Burger et al., 1996). Burger et al. (1996) also concluded in his analysis that in vertical orientation gravity does not induce the flow of oil to the outlet face; therefore, the recovery is primarily due to the diffusion. The oil-phase diffusivity is the controlling parameter in vertical mass transfer experiments.

Comings and Sherwood (1934) modeled the process considering moisture moment by capillary in drying granular materials. But determining mass transfer coefficients during flow in fracture is more complex process due to the involvement of injection rate effect and fracture properties. In most of the available commercial simulators, the mass transfer is assumed to proceed by diffusion within single phase. Recent studies from Jamshidnezhad et al. (2004) considered mass transfer between the same phases in the fracture and porous medium. They concluded that the displacement rates are of great importance for miscible process in NFRs.

Matrix fracture interaction in fractured rocks for different types of fluids was investigated computationally (Zakirov et al., 1991; Jensen et al., 1992) and experimentally (Li et al., 2000;

Le Romancer et al., 1994) in different studies. Analytical and numerical solutions for the diffusion process in the fracture and transport to the matrix are also available (Hu et al., 1991; Lenormand, 1998; LaBolle et al., 2000; Jamshidnezhad et al., 2004; Ghorayeb and Firoozabadi, 2000).

Experimental methods to measure diffusivity could be direct or indirect. The direct method is the one which requires the compositional analysis of the diffusing species while the indirect method changes one of the parameters affected by diffusion and the diffusivity is measured such as volume change, pressure variation or solute volatilization. As reported in the literature, direct methods are time consuming and expensive (Sigmund, 1976; Upreti and Mehrotra, 2002). Recently, studies (Upreti and Mehrotra, 2002; Riazi, 1996; Tharanivasan et al., 2004; Zhang et al., 2000; Sheikha et al., 2005) were reported on indirect method which measures change in pressure due to gas diffusion into liquid.

1.2.3 Effect of Flow on Diffusion/Dispersion in Fractured Porous Media

During the flow through porous media, the additional mixing caused by uneven flow or concentration gradient is called dispersion. It results from the different paths and speeds and the consequent range of transit times available to tracer particles convected across a permeable medium. Dispersive mixing is a resultant of molecular diffusion and mechanical dispersion. Perkins and Johnston (1963) provided an analysis of the dispersion phenomena and correlations for two types of dispersion; (1) longitudinal direction, and (2) transverse to the direction of gross fluid movement. Both, having different magnitude, have to be considered separately. Dispersive mixing plays important role in determining how much solvent will dissolve/mix with solute to promote miscibility. Molecular diffusion will cause mixing along the interface. The net result will be a mixed zone growing at a more rapid rate than would be obtained from diffusion alone. Diffusion is a special case of dispersion and a result of concentration gradient, with or without the presence of the velocity field (Bear, 1988; Sahimi et al., 1982).

Gillham and Cherry (1982) defined the hydrodynamic dispersion coefficient as the sum of coefficient of mechanical dispersion (D_{mech}) and the effective diffusion coefficient in porous

media (D_{eff}). The hydrodynamic dispersion coefficient is also referred as dispersion-diffusion coefficient (D_L).

$$D_L = D_{mech} + D_{eff} \quad \text{.....(1.4)}$$

The mechanical dispersion is proportional to the average linearized pore-water velocity (V) and the dispersivity (α) (Bear, 1979; Freeze and Cherry, 1979). The effective diffusion coefficient is related to diffusion coefficient in free solution and tortuosity.

Taylor (1953) showed that in case of substantial diffusion perpendicular to the average fluid velocity, the dispersion coefficient in the tube would be proportional to the square of the average fluid velocity. Later, Horne and Rodriguez (1983) concluded that in the diffusion dominated system, the dispersion coefficient in the single, straight, parallel plate fracture will be proportional to the square of the fluid velocity. Keller et al. (1999) showed that dispersion coefficient and velocity has linear relationship, where $D_L \ \alpha \ V$. Bear (1979) suggested that the relation between dispersion coefficient and the average fluid velocity would be $D_L = \alpha * V^n$. The range of the n value is limited to $1.0 \leq n \leq 2.0$.

From the findings of Ippolite et al. (1984) and Roux et al. (1998), it is known that the dispersion coefficient in the variable aperture fracture is the sum of molecular diffusion, Taylor dispersion and microscopic dispersion.

The Peclet number, Pe, for the flow in fracture is defined as;

$$Pe = \frac{V * b}{D_m} \quad \text{.....(1.5)}$$

where V is average fluid velocity in the fracture, b is the fracture aperture and D_m is the molecular diffusion coefficient.

Dronfield and Silliman (1993) conducted transport experiments in sand-roughened analog fracture and observed the following relationship: $D_L \ \alpha \ Pe^{1.4}$. He also suggested that the power term to be 2 for parallel plate fracture and 1.3 to 1.4 for rough fractures. Detwiler et al. (2000) studied the effect of Pe on D_L using experiments and numerical results. His observations were in accordance with those of earlier studies by Ippolite et al. (1984) and

Roux et al. (1998). Molecular diffusion dominates within the regime of $Pe<<1$. The Taylor dispersion and microscopic dispersion are related to *Pe*. The Taylor dispersion is proportional to Pe^2 while the microscopic dispersion is proportional to *Pe*. Detwiller et al. (2000) obtained the following quadratic relationship from the result of Roux et al. (1998) in the form of a first-order approximation of the total non-dimensional longitudinal dispersion coefficient:

$$\frac{D_L}{D_m} = \alpha_{Taylor}(Pe)^2 + \alpha_{macro}(Pe) + \tau \quad \text{.....(1.6)}$$

They further indicated that for typical *Pe* ranges, τ (tortuosity for fracture) can be neglected.

The Taylor dispersion coefficient defined for parallel plate fracture is: (Taylor 1953; Aris 1956; Fischer et al. 1979)

$$D_{L,Taylor} = \frac{1}{210}\frac{V^2 b^2}{D_m} \quad \text{.....(1.7)}$$

The mechanism of gas injection into a fractured porous media is governed by convection, dispersion and diffusion. Most mixing (dispersion) is mainly caused by adjacent rock block (rock matrix), the variations in velocity due to fracture roughness, mixing at fracture intersections, and the variations in velocity due to differing scales of fracturing variations in velocity caused by variable fracture density. The recovery in fractured reservoirs also requires the determination of transfer parameters between fracture and matrix, called transfer functions. Theoretical and empirical transfer functions for immiscible interaction are abundant in literature and an extensive of the review of those functions were provided previously (Babadagli and Zeidani, 2004; Civan and Rasmussen, 2005). More efforts are needed, however, to derive transfer functions capturing the physics of the miscible interaction.

1.2.4 Scaling and Dimensionless Analysis

The dimensionless analysis (DA) determines the minimum number and form of scaling groups based on the primary dimensions of any physical system (Fox and McDonald, 1998).

The dimensionless groups will not predict the physical behavior of the system only but these groups can also be joined together to be easily interpreted physically. The experimental validation for the final form of physically meaningful dimensionless group was also recommended (Fox and McDonald, 1998). The DA method does not require that the process being modeled be expressed by equations rather it is based on the knowledge of the pertinent variables affecting the process. Dimensionless numbers obtained through the inspectional analysis (IA) are generally considered to be more useful (Craig et al., 1957; Shook et al., 1992). Two succinct and apparently different methods for obtaining dimensionless numbers can be found in the general fluid flow literature. General fluid dynamics literature (Johnson, 1998; Fox and McDonald, 1998) suggests the use of DA, whereas petroleum related literature relies more on the IA (Shook et al., 1992). Dimensionless numbers obtained through the IA are generally considered to be more useful (Craig et al., 1957; Shook et al., 1992).

Scaling of miscible and immiscible processes using inspectorial analysis has led to better understanding of the process based on the dimensionless groups associated. In previous attempts, different studies derived dimensionless groups to represent the efficiency of the immiscible or miscible EOR processes. Mostly all of them were for homogeneous systems and only a few focused on heterogeneous reservoirs. Gharbi et al. (1998) and Gharbi (2002) used the IP to investigate the miscible displacement in homogeneous porous media. Grattoni et al. (2001) defined a new dimensionless group combining the effects of gravity; viscous and capillary forces which showed a linear relationship with the total recovery. For the application of the dimensionless groups, Kulkarni and Rao (2006a) presented the effect of major dimensionless groups on the final recovery based on various miscible and immiscible gas assisted gravity drainage field and laboratory experimental data. Wood et al. (2006) derived dimensionless groups for tertiary enhanced oil recovery (EOR) using CO_2 flooding in waterflooded reservoirs and presented a screening model for EOR and storage in Gulf Coast reservoirs.

1.2.5 Multi-Contact Miscible CO_2 Injection into Fractures - Experimental Study

A very limited number of experimental work have been reported in the context of oil recovery from naturally fractured reservoir using carbon dioxide as a solvent, and of these, sequestration related ones are even less. With the success of miscible flooding in different ongoing projects, researchers and industry have come together to focus on sequestration as well recently. Studies performed in these contexts are summarized below:

Karimaie et al. (2007) performed experiments for secondary and tertiary injection of CO_2 and N_2 in a fractured carbonate rock. In their work, 2 mm gap between core cylinder and core was used as a fracture while the core acted as a matrix. They used binary mixture of C1-C7 at 170 bar and 85 0C as solute. Gas was injected at 5 cc/min into the fracture to drain the oil (in secondary injection) or water (in tertiary injection) and then reduced to 1 cc/min. Within 10 hrs of secondary CO_2 injection, 75% of oil was recovered while it took 400 hrs (~17days) to recover 15% of oil using secondary N_2.

Darvish et al. (2006a; 2006b) used 96.6 mm long and 46 mm in diameter (4 mD, 44%) chalk cores. After saturating the core with live oil at 300 bar and 130 °C, CO_2 was injected at 5.6 cc/min to displace the oil from the fracture and then the rate was reduced to 1 cc/min.

Chakravarthy et al. (2006) used WAG and polymer gels to delay the breakthrough during CO_2 injection into fractured cores. They studied immiscible condition and used Berea cores (D = 2.5 cm (1 inch); L = 10 cm (3.9 inches)). They injected CO_2 continuously at 0.03 cc/min and 0.1 cc/min and compared core flooding experiments with continuous CO_2 injection, viscosified water injection followed by CO_2, and gel injection into fractured Berea sandstone.

Muralidharan et al. (2004) conducted experimental and simulation studies to investigate the effect of different stress conditions (overburden pressure) on fracture/matrix permeability and fracture width. They concluded that during constant injection average fracture permeability decreased about 91% and the average mean fracture aperture decreased about 71% while increasing overburden pressure from 500 psi to 1500 psi.

Torabi and Asghari (2007) studied CO_2 huff-and-puff performance on two Berea sandstone cores (k = 100 md and 1000 md; L = 30.48 cm; D = 5.08 cm). CO_2 was injected into 0.5 cm annular space between the core and core holder acting as a fracture. In their experiments, they injected CO_2 at six different pressure steps of constant pressure into saturated core. It followed by production at atmospheric pressure for 24 hours and removing CO_2/flash fluid from the top. Each step was continued until production ceases. No consideration was taken for sequestration. They observed drastic increase in the recovery factor from immiscible to near miscible/miscible conditions.

Asghari and Torabi (2007) performed gravity drainage experiments in sandstone core samples with fracture at the annular space and concluded that miscibility can increase the production substantially. One of their findings was that the recovery may decrease far above the miscibility. Injection and production was not at controlled rate, hence sudden increase or decrease in pressure may affect the results when comparing and also sequestration cannot be accomplished.

1.3 Problem Statement

It is obvious that underground oil/gas reservoirs are the only value added choice for CO_2 sequestration as the oil/gas recovered would offset the cost of the process. Most of the fractured reservoirs are suitable for CO_2 flooding, either miscible or immiscible. Continuous injection into a fractured medium may lead to early breakthrough and recovery of by-passed oil in the matrix is a major problem. Sequestering CO_2 into these by-passed matrix blocks is an added challenge. The physics of the matrix-fracture interaction process during CO_2 injection is still not known to great extent.

Injection rates play an important role in the recovery processes being more critical in the presence of fractures. Hence, a definition of critical rate for optimization with solvent and solute properties, matrix and fracture properties, pressure conditions as well as gravity effect consideration is a big challenge. Complexities are involved in understanding of the qualitative nature of the physics behind the matrix-fracture interaction process and quantitative representation of the controlling transfer parameters.

Moreover, comprehensive understanding of the pore scale mechanism is necessary so that these processes can be included in the development of models for miscible process in fractured medium and upscaling laboratory results. Studies on scaling the flow through fracture in oil saturated fractured reservoirs for a miscible displacement of oil by a solvent are limited. A model based on universal dimensionless groups that quickly predicts the efficiency of the recovery as well as sequestration is required.

Limited number of studies focused on the numerical modeling with enough experimental support. Very limited number of experimental work has been reported in the context of oil recovery from naturally fractured reservoir using carbon dioxide as a miscible solvent, and of these, sequestration related ones are even less. During continuous injection when the oil cut drops very low and still matrix possesses a large amount of bypassed oil, what could be done for incremental recovery has not been studied in depth. Lack of understanding of governing mechanisms may lead to excessive pressure depletion for oil recovery and this eventually causes severe damage to sequestration goals. Mechanistic knowledge of other methods of recovery such as huff-and-puff and soaking-and-depletion after continuous injection as well as the knowledge of optimal abandonment pressure for recovery and sequestration during depletion is completely unknown for fractured reservoirs.

Recently, pressure decay method has been used to quantify the diffusion between two fluid phases. However, the existence of this pressure decay in porous media (especially in fractured porous media) during CO_2 injection and its implication to recovery has not been studied to date. Also, the mechanisms of matrix diffusion, oil swelling, and extraction during miscible and immiscible processes need more focus to identify the operational criteria which help these mechanisms to affect positively towards recovery enhancement as well as CO_2 storage.

1.4 Methodology

Co-optimization of EOR and greenhouse gas sequestration is to manipulate the reservoir conditions and associated factors/parameters that will lead to the best outcome of the process. For this purpose, experimental analyses are needed initially.

The experimental study was performed in two phases:

a) First contact miscible experiments using heptane as solvent and mineral oil as solute,

b) Multi-contact miscible/immiscible experiments using CO_2 as solvent while n-decane and crude oil as solute.

With capillary drive and pressure drive not affecting the recovery due to first contact miscibility and gravity forces minimized as the orientation of the cores was horizontal, the influence of diffusion/displacement drive - only mechanism governing the process - was tested for recovery from naturally fractured reservoirs. The main focus was to study the dominance of the phase diffusion into matrix through fracture over viscous flow in the matrix-fracture system. The process efficiency in terms of the time required for the recovery as well as the amount of solvent injected was also investigated. This work mainly focuses on generalizing the effects of flow rate, matrix, fracture and fluid properties, to obtain a diffusion driven matrix-fracture transfer function and to propose a critical injection rate for an efficient miscible displacement.

The results of the continuous injection experiments were used to obtain process parameters governing the convection-diffusion equation by matching simulation results of matrix-fracture governing equations. For the co-optimization of the oil recovery and CO_2 storage efficiency analysis using a global effectiveness factor was defined based on experimental observations on artificially fractured core samples and finite element modeling results.

Using the Inspectional Analysis, a method based on the set of differential equations that governs the process of interest with the initial and boundary conditions into dimensionless forms, a set of dimensionless groups were derived. Based on the dimensionless groups derived, a new dimensionless group was proposed for better defining the effectiveness of the process. The new dimensionless group combined varying strength of all forces acting as different dimensionless groups during the process. Validation of the applicability and physical significance was done through the results of laboratory experiment of first contact as well as multi-contact experiments.

In the second phase, experiments were performed on fractured Berea sandstone and Midale carbonate cores obtained from a good quality matrix part of the field for continuous injection of CO_2. Effects of flow dynamics on sequestration and recovery were studied at different pressure ranges of miscible, immiscible and near miscible regions. At the end of the production life, system was shut down for enough time to allow the CO_2 and oil diffusion/back diffusion to occur. Then the pressure into the system was released to different pressure steps and kept shut (soaking period) for longer period of time at all the reduced steps of pressure. With the continuous data logging system pressure, CO_2 production rates and oil production weight as well as chromatography analysis of the liquid produced if required were collected for quantitative analysis. The storage capacity of the rock with change in pressure and the amount of oil recovered during blow down period were studied for critical understanding of abandonment pressure during the project life to achieve the goal of sequestration and recovery optimization.

The pressure decay behavior during the shutdown (soaking) was analyzed in conjunction with the gas chromatograph analysis of produced oil sample collected at initial stage (stock tank oil used for saturation of the core), during continuous injection, during the first blowdown followed by quasi-equilibrium during first shutdown (soaking) and during the last cycle of blowdown after the quasi-equilibrium reached during pressure decay. This practice gave an insight into the governing mechanism of extraction/condensation driven by diffusion and miscibility for recovering lighter to heavier hydrocarbons during pressure depletion from fractured reservoirs.

In summary, first contact and multi-contact diffusion experiments in oil saturated porous media were performed for better physical understanding of miscible/immiscible matrix-fracture diffusion interaction. For evaluating the performance of enhanced oil recovery and CO_2 sequestration, a dimensionless analysis yielding a new matrix-fracture diffusion transfer group was performed.

1.5 Outline

Chapter-2 of this dissertation is focused on first contact miscible experiments to understand the flow dynamics. Chapter-3 and Chapter-4 are based on numerical simulation to obtain

parameters that affects the miscible displacement process and defining the efficiency process using empirical correlations. In Chapter-5, dimensionless groups based on Inspectional Analysis of the matrix-fracture transfer equations are derived and a new group (matrix-fracture diffusion group) is proposed for critical rate definition and efficiency analysis.

In Chapter-6, CO_2 injection experiments on the artificially fractured Berea sandstone and carbonate cores from the Midale reservoir at miscible, near miscible and immiscible conditions are explained with detailed analysis. Chapter-7 focuses on in-depth understanding of the role of diffusion in CO_2 sequestration and EOR mechanisms during the project life. Also, in this chapter results from all miscible vertical gravity drainage (first contact or multi-contact) are used to obtain a critical value of matrix-fracture interaction group proposed earlier in Chapter-5. The mechanistic insight of the governing mechanism of miscible gravity drainage flow in fractured NFRs is described in Chapter-8. Each Chapter (from Chapter-2 to Chapter-7) is a paper published in journals or presented at conferences. They all have individual literature survey at the beginning and concluding remarks at the end of the chapter. As each chapter used different terminology and different symbols sometimes to define the same parameter, the terms and symbols are defined in Nomenclature separately for each chapter at the end of the thesis. Chapter-8 and Chapter-9 are general analyses and conclusions/contributions with recommendation for future research, respectively.

2 EFFICIENCY OF DIFFUSION CONTROLLED MISCIBLE DISPLACEMENT IN FRACTURED POROUS MEDIA

2.1 Introduction

A large proportion of the world's proven oil reserves have been found in naturally fractured reservoirs (NFRs). During the injection of fluids that are miscible with oil for enhanced oil recovery, the transport of the injectant and the oil recovery are controlled by fracture and matrix properties in this type of reservoirs. For such systems, the transfer between matrix and fracture due to diffusion is a significant oil recovery mechanism. Similar processes can be encountered during the sequestration of greenhouse gases, and the transport of contaminants in subsurface reservoirs. Understanding the effects of different parameters on the dynamics of the transfer due to diffusion is essential in modeling such processes. In fact, the description of matrix fracture interaction for dual-porosity dual-permeability models developed for NFRs is still a challenge.

Oil recovery mechanism of matrix-fracture systems has been studied at laboratory scale since 1970's. Thompson and Mungan (1969) compared displacement velocity to critical velocity (V_C) and showed its effect on recovery efficiency. Using the results of single matrix block analytical studies and multicomponent laboratory experiments Da Silva and Belery (1989) confirmed the importance of molecular diffusion in NFRs and concluded that it may override the other hydrocarbon displacement mechanisms. Firoozabadi and Markeset (1994) showed the effect of matrix/fracture configuration and fracture aperture on first contact miscible efficiency. Matrix fracture interaction in fractured rocks for different types of fluids was investigated computationally (Zakirov et al., 1991; Jensen et al., 1992) and experimentally (Li et al., 2000; Le Romancer et al., 1994) in different studies. Saidi (1987) studied the diffusion/stripping process in fractured media. Morel et al. (1990) performed diffusion experiments with chalk and studied the effect of initial gas saturation. Analytical and numerical solutions for the diffusion process in the fracture and transport to the matrix

A version of this chapter has been published
Trivedi J. and Babadagli T., 2008. Transport in Porous Media. 71(3): 379.

are also available (Hu et al., 1991; Lenormand, 1998; Labolle et al., 2000; Jamshidnezhad et al., 2004; Ghorayeb and Firoozabadi, 2000).

More recently, static experiments were reported on the diffusion process from fracture to matrix (Babadagli et al., 2005; Rangel-German and Kovscek, 2000; Hatiboglu and Babadagli, 2006). There are also experimental methods for calculating diffusion coefficients between two fluid systems (Yang and Gu, 2003; Civan and Rasmussen, 2002; Raizi, 1996; Stubos and Poulou, 1999). But within the porous media transfer by diffusion depends on the conditions at the boundaries and fracture geometry as well as flow conditions. The mechanism of gas injection into a fractured porous media is governed by convection, dispersion and diffusion. Most mixing (dispersion) is mainly caused by adjacent rock block (rock matrix), variations in velocity due to fracture roughness, mixing at fracture intersections, variations in velocity due to differing scales of fracturing variations in velocity due to variable fracture density. Recovery in fractured reservoirs requires the determination of transfer parameters between fracture and matrix, called transfer functions. The theoretical derivations of such transfer functions are available in literature (Babadagli and Zeidani, 2004; Civan and Rasmussen, 2005).

In general four factors contribute to crossflow/mass transfer between matrix-fracture:

- Pressure drive
- Gravity drive
- Dispersion/diffusion drive
- Capillary drive

When the bypassed fluid and displacement fluids are first contact miscible (FCM), there is no capillary crossflow. When the fluids are multicontact miscible (MCM) or immiscible, there can be some capillary-driven crossflow. Burger et al. (Burger et al., 1996; Burger and Mohanty, 1997) found that capillary driven crossflow does not contribute significantly to mass transfer in near-miscible hydrocarbon floods. The other three has to be focused for understanding of crossflow/mass transfer between fracture and surrounding matrix block during miscible displacements. The current work was done at room temperature and pressure conditions; hence the pressure drive was also out of focus.

A version of this chapter has been published
Trivedi J. and Babadagli T., 2008. Transport in Porous Media. 71(3): 379.

Our work mainly focuses on studying the effects of flow rate, matrix, fracture and fluid properties during the recovery of oil mainly under the influence of dispersion/diffusion drive.

2.2 Experimental Method

Series of experiments were conducted with solvent injection into fractured cores. The detailed experimental outline has been given in **Tables 2.1** and **2.2**. Parameters investigated in this study are as follows:

- Flow rate (injection rate) in the fracture,
- Gravity effect,
- Water saturation in the matrix,
- Rock type,
- Effect of aging (wettability),
- Effect of viscosity ratio.

2.2.1 Porous Media

Different samples representing two characteristic sedimentary rocks were used to study the effect of the rock type: (1) Berea sandstone (average permeability = 500 md and average porosity = 20% and (2) Indiana limestone (average permeability =15 md and average porosity = 11%). For porosity measurement, core samples were weighted and placed in a desiccator filled with oil. The desiccator was connected to a vacuum pump. The core was saturated under constant vacuum for 48-72 hours. The weight of the core after saturation was measured and the porosity of the matrix was calculated from the difference between the weight of the saturated and unsaturated core. The porosity of Berea sandstone cores ranges from 19 to 21 % and that of Indiana limestone cores is between 10 to 12 %. The permeability of the Berea sandstone and Indiana limestone cores were calculated using the data obtained from constant rate water injection experiments and the Darcy equation. Experiments were conducted on a few samples from the same block and the average values

A version of this chapter has been published
Trivedi J. and Babadagli T., 2008. Transport in Porous Media. 71(3): 379.

were obtained as 500 md and 15 md for Berea sandstone and Indiana limestone, respectively.

2.2.2 Fluids

Two different oil types, light mineral oil and kerosene were used as displaced fluids. Heptane was used as the -miscible- displacing fluid. The properties of fluids are given in **Table 2.1**.

2.2.3 Test Conditions

All tests were performed at room-temperature (60^0F) and atmospheric pressure. Solvent was injected at a constant rate while the oil was produced at atmospheric pressure.

2.2.4 Core Preparation and Test Procedure

The core samples and the set-up for the experiments are presented in **Figures 2.1** to **2.3**. The cores are cylindrical samples, 6 inches in length and 2 inches in diameter **(Figure 2.1)**. Cores were cut through the center in direction of longitudinal axis. They cores were weighted and fully saturated with oil under constant vacuum using vacuum pump for 48-72 hours to achieve maximum saturation. The weight of the cores after saturation was measured. Porosity was obtained from the weight difference before and after saturation. The two pieces were then held together tight with heat-shrinkable rubble sleeves. The fractured core packed with rubber sleeve was placed into a Plexiglas core-holder of 6 inches length and 2.5 inch diameter. The annular area between core and core-holder was filled with silicon. This was done to ensure no flow between the core and the core-holder. The silicon used was industry grade liquid silicon, which solidifies by adding curing agent with time.

After the set-up of the core was done, the injection and producer ports were placed at the centers of both ends of the core-holder. This way the injection was done through the fracture directly **(Figure 2.2)**. For horizontal experiments to minimize the effect of gravity on oil recovery from matrix the core was positioned in such a way that two matrix blocks placed at the same horizon are separated by a single vertical fracture. The configuration with matrix at top and bottom separated by a horizontal fracture is different and not studied in this research simply to avoid the different gravitational forces effective on both matrix

A version of this chapter has been published
Trivedi J. and Babadagli T., 2008. Transport in Porous Media. 71(3): 379.

blocks. Therefore, the position of the fracture is vertical but the whole core system was placed and the injection was in horizontal direction.

The same core preparation method was used in all experiments. Note that each core was used only once to avoid the property change due to cleaning procedure. The cores are assumed to have similar properties as they were plugged out from the same block. The list of the experiments conducted in this study is given in **Table 2.2**.

Heptane was continuously injected through the fracture at a constant rate. The flow rate and the cumulative volume injected were monitored using ISCO-500 D pumps. The effluent was collected over time to time and analyzed with a refractometer **(Figure 2.3)**.

The permeability contrast between matrix and fracture was kept as high as possible to ensure that the viscous flow dominates only in the fracture and the matrix oil is recovered only by diffusion. No overburden was applied on the cores and the average value of fracture permeability on the cores was measured as around 8-10 Darcies. This value yields enough contrast between matrix and fracture permeabilities for viscous flow to be effective only in the fractures.

2.2.5 Measurement Technique

Because of the small density difference between oil and solvent used here, the need of a different technique which does not depend on density for determining the composition of the produced liquid raised. Measurement of refractive index (RI) was used to determine the relative proportions of the mixture from the production end. The ratio of the speed of light in air to the speed of light in another media is called "refractive index" (RI). A bench-type Refractometer supplied by Fisher Scientific was used. The minimum reading of scale indicates down to 4 places of decimal of the RI values. The accuracy is +/- 0.0002 refractive units. Proper care was taken to conduct all the readings at same temperature to avoid any effect of temperature change on the final reading. The RI values for the pure compounds were measured and a calibration curve was generated with the known percentage of oil mixed with heptane. This curve is presented in **Figure 2.4**. Using this curve composition of the produced liquid was determined.

A version of this chapter has been published
Trivedi J. and Babadagli T., 2008. Transport in Porous Media. 71(3): 379.

2.2.6 Effect of Water Saturation

Most of the reservoirs at present state are water flooded. Sometimes the percentage of water present is higher than the oil. Considering this fact we decided to create similar situation. Two (100%) oil-saturated Berea sandstone cores, packed in heat-shrinkable Teflon sleeve, were prepared similar way as mentioned earlier in other experiments. These cores were exposed to water by spontaneous imbibition using imbibition tubes. The recovery was monitored against time. When oil production through imbibition reached plateau, the cores were taken out and placed into Plexiglas core-holder as discussed above, similar to the other experiments for solvent injection. Note that this is a secondary -miscible- recovery after a primary waterflooding. The solvent injection rates applied for these water imbibed cores were 3 ml/hr and 6 ml/hr.

2.2.7 Effect of Aging

Aging the rock with oil over a period of time may change the wettability of the rock type and may cause considerable effect on oil recovery process. Though there is no water in the cores, aging over longer period of time changes the affinity as well as the contact angle of oil to the rock. To study this effect, four Berea sandstone cores were aged in mineral oil over one month. The experimental results as well as the imbibition tests reported in other papers (Babadagli and Ershaghi, 1993; Babadagli, 2000) indicated that the longer contact time altered the wettability of the rock to mineral oil. Although the polar components are not as high as in crude oils, the mineral oil we used showed change in the affinity to oil after aging. Solvent was injected into these aged samples at the flow rates of 3, 4.5, 6 and 9 ml/hr.

2.2.8 Effect of Viscosity Ratio/Density

In order to analyze the effects of viscosity and density of the non-wetting phase, we conducted some experiments with kerosene as a non-wetting phase. Cores were saturated with kerosene under vacuum and prepared in a similar way as other experiments.

A version of this chapter has been published
Trivedi J. and Babadagli T., 2008. Transport in Porous Media. 71(3): 379.

2.2.9 Effect of Gravity

Gravity also contributes to recovery, mostly when the fracture orientation is vertical. In our work, we studied the recovery from three samples with vertical orientation of fracture. After preparing the cores following the same procedure, we mounted them vertically and injected solvent at three different rates of 1, 3 and 6 ml/hr from the top of the sample downward to the bottom. For these experiments, we used only mineral oil as the displaced phase.

2.3 Results and Analysis

The recovery curves for the above mentioned experiments are presented in **Figures 2.5** to **2.8** as pore volume injected vs. pore volume recovered. Here, recovery of mineral oil was used as y-axis. In a sense, this is the solvent concentration in the system. We used heptane as solvent to mimic miscible CO_2 displacement in fractured oil reservoirs. As our preliminary target was oil recovery, we preferred this type of representation in y-axis rather than solvent concentration.

With capillary drive and pressure drive not affecting the recovery and gravity forces minimized as the orientation of the cores was horizontal, the only mechanism governing the process could be diffusion/displacement drive. The diffusion dominant process yields slower recovery of oil with a delayed solvent breakthrough when the solvent injection rate was low, but it results in higher ultimate recovery for the horizontal mineral oil-Berea sandstone cases **(Figure 2.5)**. When comparing the recovery trends for a lower (BSH-3) and a higher (BSH-6) rate, BSH-6 shows faster initial recovery compared to BSH-3. But after certain period of time, the BSH-3 case overpasses the production as an evidence of diffusion controlling mechanism. It is also evident that during the initial phase of the recovery, the displacement was driven by diffusion between fracture and matrix for lower rates rather than viscous flow in fracture. Hence, 3ml/hr flow rate overrides the recovery of 6 ml/hr flow rate. Performance of kerosene was also included in this plot. The recovery rate and ultimate recovery for the kerosene case is remarkably lower than those of mineral oil cases for the same injection rate. The effect of viscosity and oil type on this process needs more detailed study and this part of research is on-going

A version of this chapter has been published
Trivedi J. and Babadagli T., 2008. Transport in Porous Media. 71(3): 379.

The recovery rate behavior for the cases of solvent injection with vertical orientation of Berea sandstone cores is very similar to that of the horizontal case. But the ultimate recoveries for all vertical orientated cores turned out to be the same despite different solvent injection rates **(Figure 2.6)**, unlike the horizontal orientation. The gravity drainage mechanism might have played a role in the oil recovery process. Similar to the horizontal Berea sandstone cases, the recovery curve at lower solvent injection rate overpasses the one at higher solvent injection rate after a certain period of time for the cores with vertical orientation, i.e., BSV-1, BSV-3 and BSV-6. Initial difference in the recoveries is not much compared to the difference between the two equivalent horizontal cases (BSH-3 and BSH-6). Still at a certain point, the recovery of BSV-1 curve overpasses the recovery curves of higher solvent injection rate cases (BSV-3 and BSV-6). The location of this crossover point occurs almost at the same time as noticed during horizontal experiments.

In the case of limestone, the recovery trends with 3 ml/hr and 6 ml/hr injection rates are almost similar to the Berea sandstone cases **(Figure 2.8)**. But the ultimate recoveries are very low almost half to that of the Berea sandstones.

With the aged samples of Berea sandstone cores, the recovery is lower than the same cores without aging **(Figure 2.9)**. For the cases of BSH-3A and BSH-6A, aging has a negative effect on miscible displacement efficiency compared to cases BSH-3 and BSH-6 **(Figure 2.7)**. It is notable that slowest solvent injection rate (3 ml/hr) yielded the highest ultimate recovery. Similar recovery trends and ultimate recoveries were obtained from all other four rates.

The recovery curves for the previously depleted matrix cases by water imbibition are shown in **Figure 2.10**. The BSH-3W case showed higher ultimate recovery than BSH-6W. The ultimate recovery after solvent injection into previously water flooded cores were only 55%, much lower than the one without water flooded (95%). Proving that solvent has diffuses easily into oil phase rather than water. It shows that starting the process by solvent injection (diffusion) results in higher ultimate recovery than injecting solvent into already waterflooded cases.

A version of this chapter has been published
Trivedi J. and Babadagli T., 2008. Transport in Porous Media. 71(3): 379.

It is clear that the injection rate is a critical parameter as well as the matrix and fluid properties on the process. Higher injection rates resulted in earlier breakthrough and less residing time in order for the matrix fracture interaction due to diffusion to take place. This was more significant for some cases and it even affected the ultimate recovery from the matrix. Therefore, it is essential to define a critical rate as a function of matrix and fluid properties. This can be done in two different ways depending on what type of efficiency is considered. For example, if the critical parameter in the efficiency of the process is the amount of oil produced per amount of solvent injected, one can define a critical rate (Babadagli and Ershaghi, 1993). If the critical parameter is the time to complete the process rather than the amount of injected fluid, then one can define an optimal injection rate as suggested by a previous study for water imbibition transfer between matrix and fracture (Babadagli, 2000).

2.4 Efficiency Analysis

In many enhanced oil recovery processes including miscible processes, the amount of solvent injected per oil recovery is the critical parameter. However, oil recovery rate, i.e., process time required to reach the ultimate recovery could also be important because the time value of money might offset the cost of extra injected solvent. Therefore, the time to reach the ultimate recovery could be equally important parameter with the amount of solvent injected in certain circumstances, especially when the oil prices are high. Hence, the efficiency of the process was analyzed with respect to the diffusion time as well. For this exercise, the amount of oil produced was plotted against time instead of total amount of solvent injected. The plots are given in **Figures 2.10** to **2.13**. Using those plots, the amount of total oil produced (PV) was plotted against the flow rate at different times. **Figures 2.14** to **2.16** show the optimal rate for maximum oil recovery at different diffusion time scale. The optimal rate was observed to be around 6 ml/hr for the sandstone and limestone horizontal experiments without aging **(Figures 2.14** and **2.15)**. At the end of the process after 40-50 hrs, the slower rate (3 ml/hr) overpasses the production obtained from the 6 ml/hr case. This indicates the dominance of the diffusional flow (matrix-fracture interaction) compared to the viscous flow (in fracture). One can conclude from these results that, for faster and higher ultimate recovery, the process should be operated at 6 ml/hr at

A version of this chapter has been published
Trivedi J. and Babadagli T., 2008. Transport in Porous Media. 71(3): 379.

the start and should be switched to 3 ml/hr. **Figure 2.16** suggests that there is no optimal rate for the aged sample as they all followed a similar recovery trend as given in **Figure 2.12** regardless the rate. Interestingly enough, the ultimate recoveries of aged samples vary significantly compared to that obtained from unaged samples.

2.5 Conclusions

Dominance of the phase diffusion into matrix through fracture over viscous flow in the fracture was shown in this study. Though the higher solvent injection rate yields high production rate of oil in the initial period of the project life, considering the long run, the low rate solvent injection strategy is the best with most of the production contribution from matrix through the diffusion process. Solvent injected at lower rate has more time to diffuse into matrix in transverse direction before it breaks through, hence results into higher ultimate recovery than that of higher rate solvent injection strategy.

With some water existing in the rock from previous waterflooding, one can still obtain oil recovery from matrix by the diffusion process. Note that the ultimate recovery obtained from the waterflooding followed by the solvent diffusion process would be much lower than the cases with solvent diffusion only.

The efficiency of the process was investigated using two different parameters. When the amount of oil produced per time is the critical efficiency parameter, a rate of 6 ml/hr was found to be the optimal rate for almost all the cases except less water-wet samples. This approach for efficiency analysis is useful for enhanced oil recovery applications.

In this study, we have not varied two critical parameters; the size of the matrix (length or width) and oil type (mainly for viscosity variation). Further attempts were made in subsequent studies where the process has been theoretically modeled using the experimental observations and considering those parameters (Trivedi and Babadagli, 2007a-b). Also, this study focused on first contact miscibility. The multi-contact miscible diffusion at reservoir temperature and pressure is more complex. This case requires more effort and could be critical especially in the CO_2 injection for EOR and sequestration.

A version of this chapter has been published
Trivedi J. and Babadagli T., 2008. Transport in Porous Media. 71(3): 379.

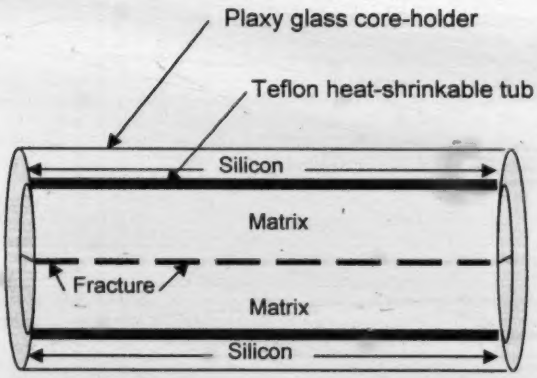

Figure 2.1: Core-holder design.

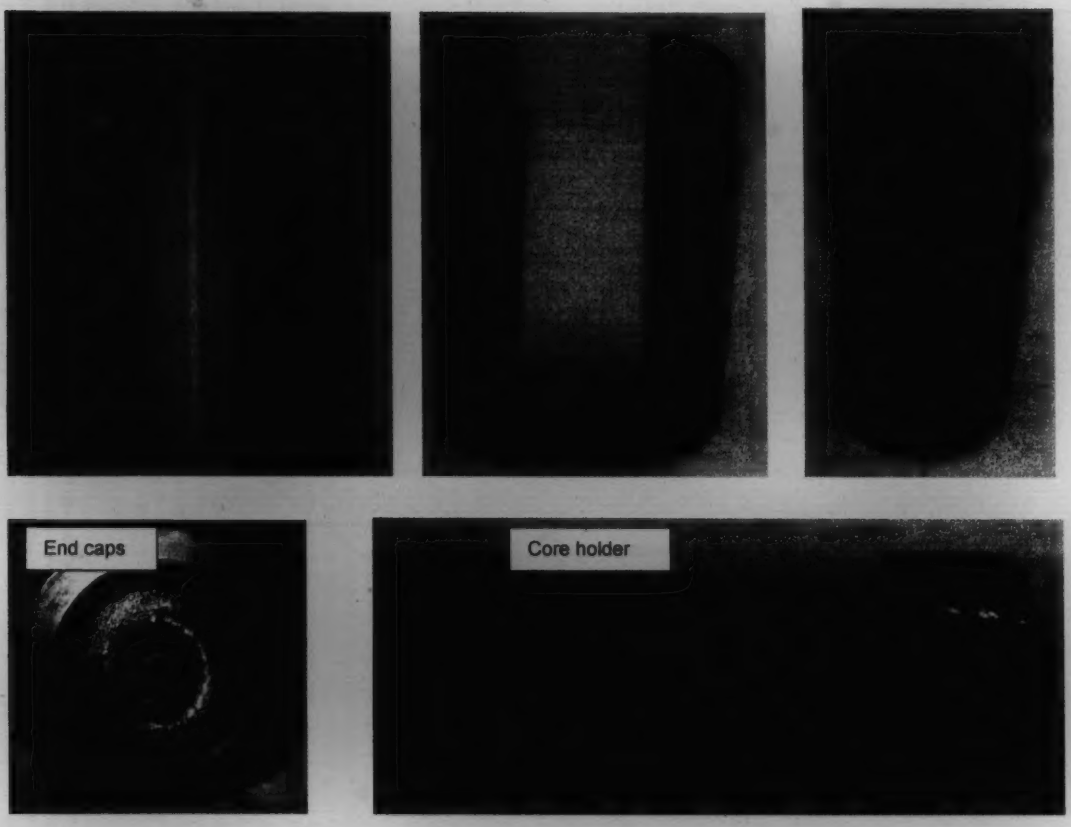

Figure 2.2: Core samples cut for fracture creation and the core-holder used.

A version of this chapter has been published
Trivedi J. and Babadagli T., 2008. Transport in Porous Media. 71(3): 379.

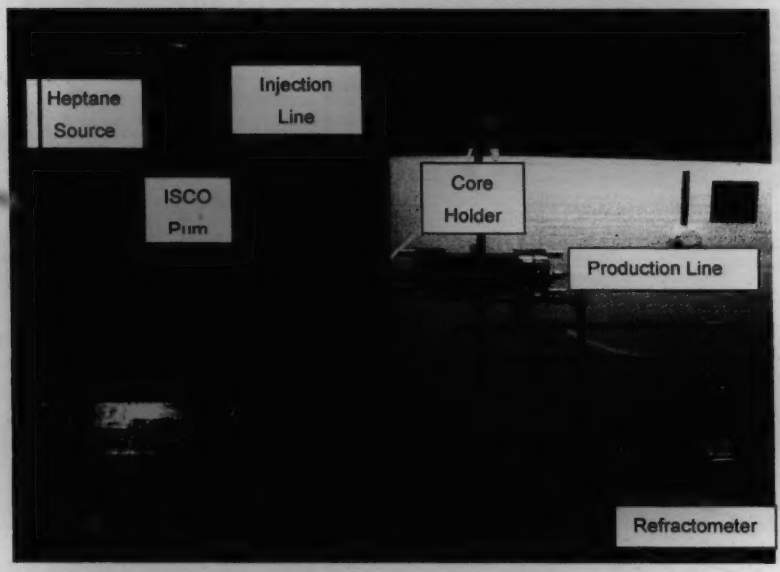

Figure 2.3: Experimental set-up.

Table 2.1: Properties of displacing and displaced fluids.

Properties	Displacing Fluid	Displaced Fluid	
	Heptane	Mineral Oil	Kerosene
Density (g/cc)	0.69	0.83	0.81
Viscosity (cp)	0.410	33.5	2.1
Refraction Index	1.3891	1.469	1.475

A version of this chapter has been published
Trivedi J. and Babadagli T., 2008. Transport in Porous Media. 71(3): 379.

Table 2.2: Detailed outline of experiments conducted.

Case	Core Type	Fracture Orientation	Oil Type	Aged	S_{wi} (%)	Flow rate (ml/hr)
BSH-3	Berea Sandstone	H	MO	No	0	3
BSH-6	Berea Sandstone	H	MO	No	0	6
BSH-9	Berea Sandstone	H	MO	No	0	9
BSH-3A	Berea Sandstone	H	MO	Yes	0	3
BSH-4.5A	Berea Sandstone	H	MO	Yes	0	4.5
BSH-6A	Berea Sandstone	H	MO	Yes	0	6
BSH-7.5A	Berea Sandstone	H	MO	Yes	0	7.5
BSH-3K	Berea Sandstone	H	Kerosene	No	0	3
BSH-6K	Berea Sandstone	H	Kerosene	No	0	6
BSV-1	Berea Sandstone	V	MO	No	0	1
BSV-3	Berea Sandstone	V	MO	No	0	3
BSV-6	Berea Sandstone	V	MO	No	0	6
BSH-3W	Berea sandstone	H	MO	No	>0	3
BSH-6W	Berea sandstone	H	MO	No	>0	6
ILH-3	Indiana Limestone	H	MO	No	0	3
ILH-6	Indiana Limestone	H	MO	No	0	6

B – Berea
S – Sandstone
I – Indiana
L – Limestone
H – Horizontal
V – Vertical
A – Aged over period of 1 month
W – Water imbibed for primary recovery
MO – Mineral Oil

A version of this chapter has been published
Trivedi J. and Babadagli T., 2008. Transport in Porous Media. 71(3): 379.

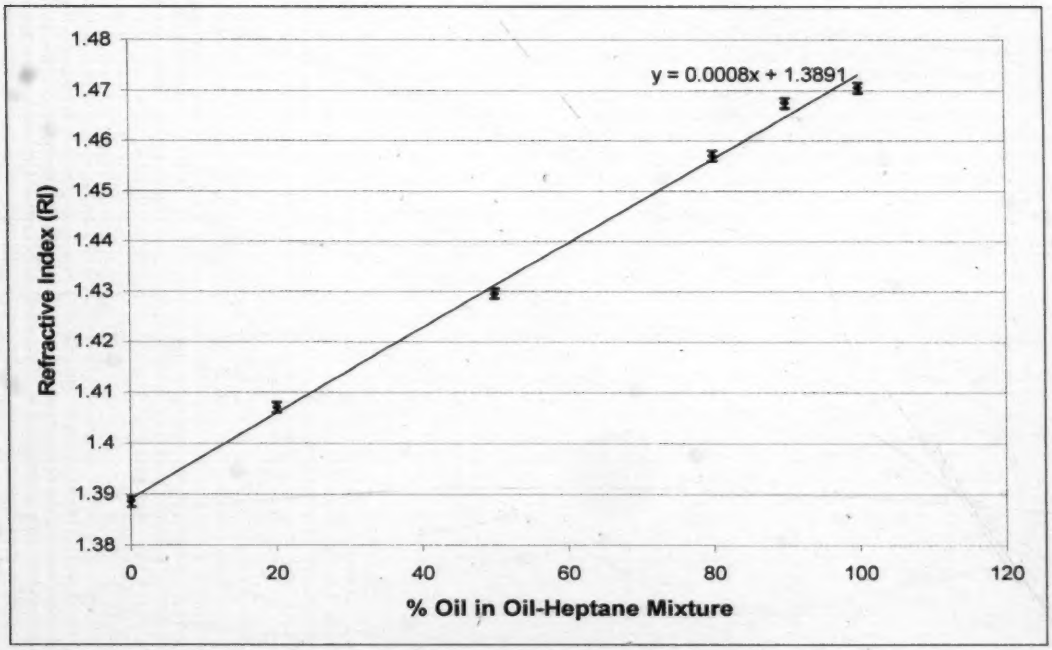

Figure 2.4: Calibration chart for refractometer for mineral oil-heptane mixture.

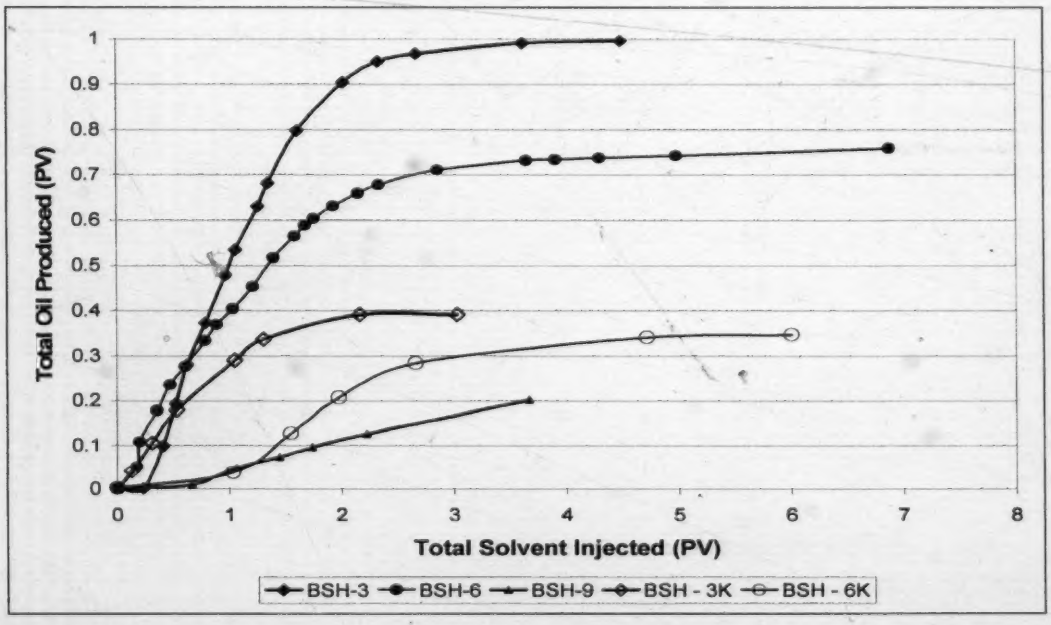

Figure 2.5: Cumulative production with solvent injected (PV) for Berea sandstone horizontal orientation.

A version of this chapter has been published
Trivedi J. and Babadagli T., 2008. Transport in Porous Media. 71(3): 379.

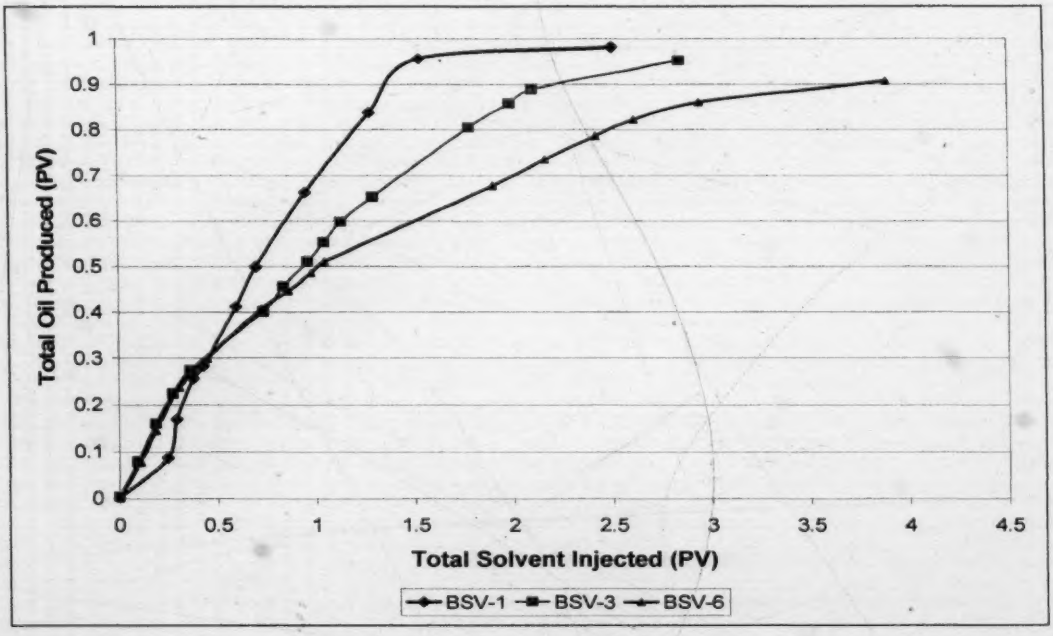

Figure 2.6: Cumulative production with solvent injected (PV) for Berea sandstone vertical orientation.

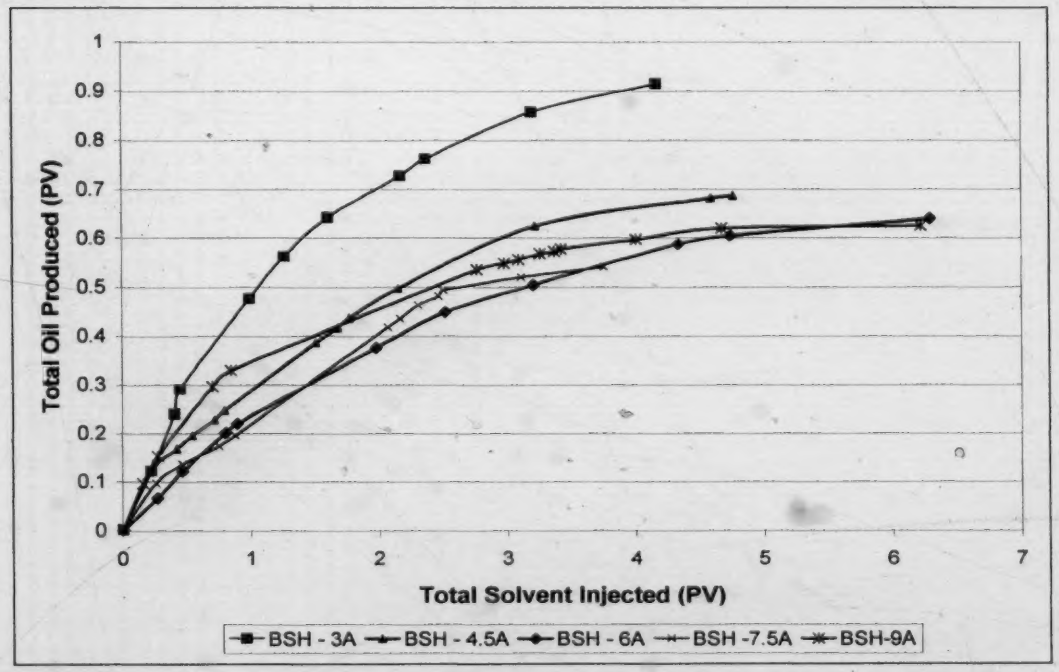

Figure 2.7: Cumulative production with solvent injected (PV) for aged Berea sandstone horizontal orientation.

A version of this chapter has been published
Trivedi J. and Babadagli T., 2008. Transport in Porous Media. 71(3): 379.

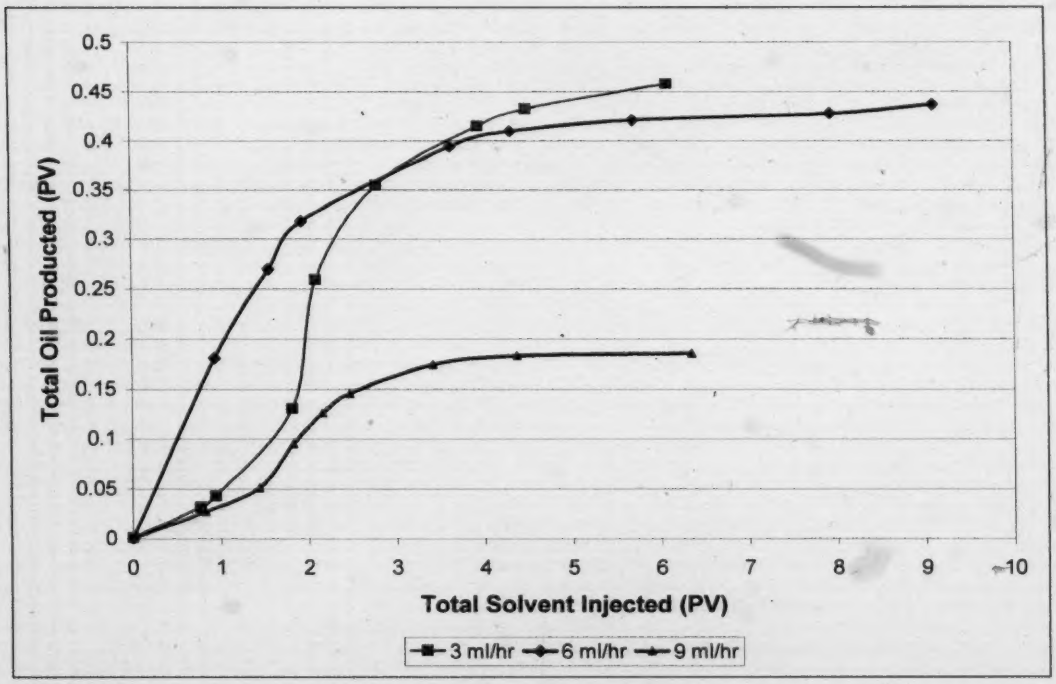

Figure 2.8: Cumulative production with solvent injected (PV) for Indiana limestone horizontal orientation.

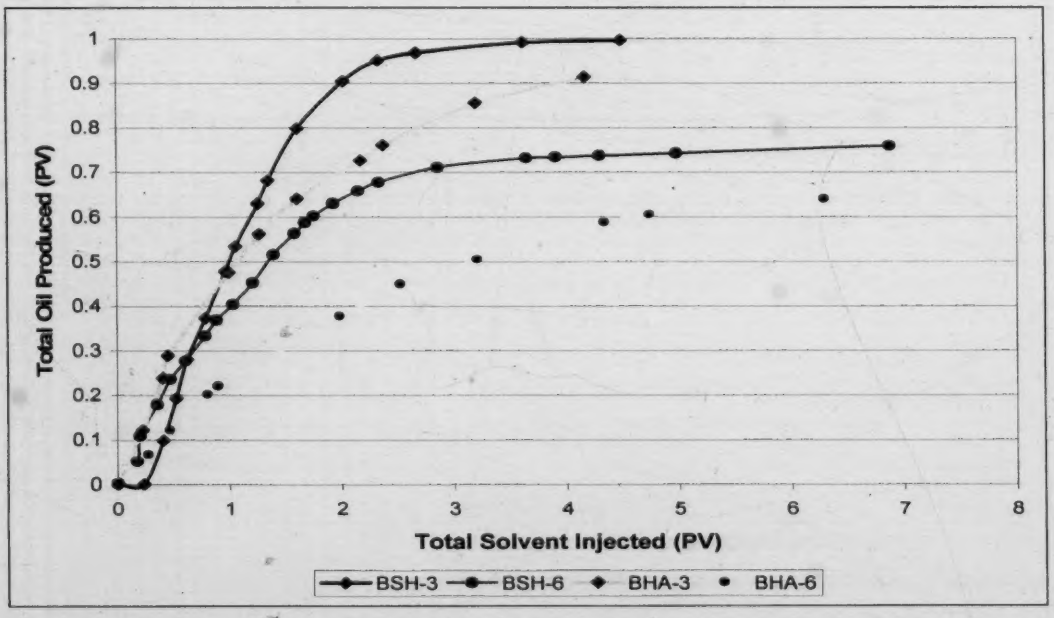

Figure 2.9: Cumulative production with solvent injected (PV) comparing aged and unaged Berea sandstone horizontal orientation.

A version of this chapter has been published
Trivedi J. and Babadagli T., 2008. Transport in Porous Media. 71(3): 379.

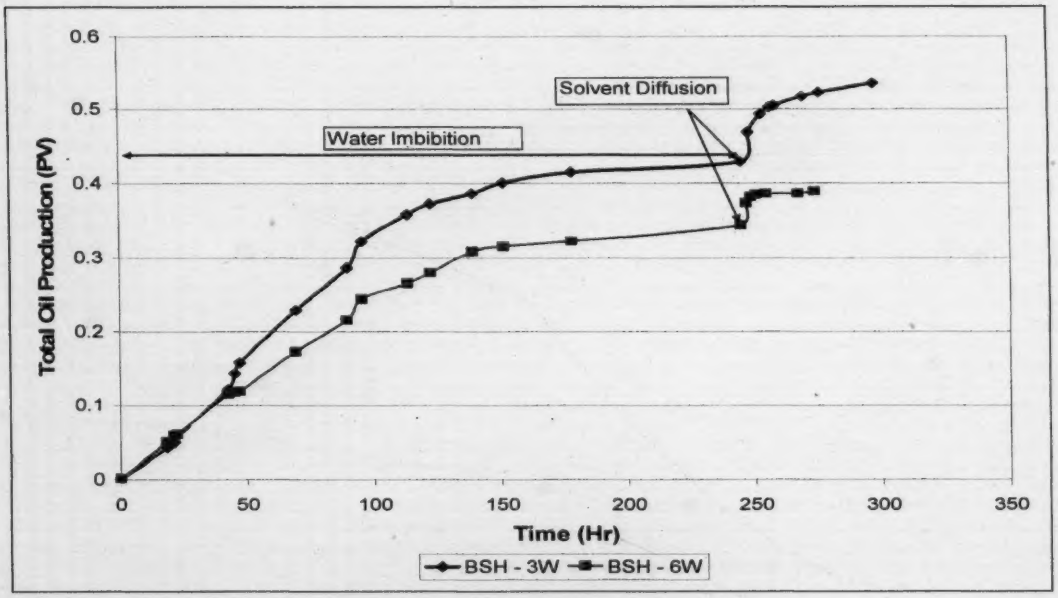

Figure 2.10: Cumulative production with time for water imbibed cores.

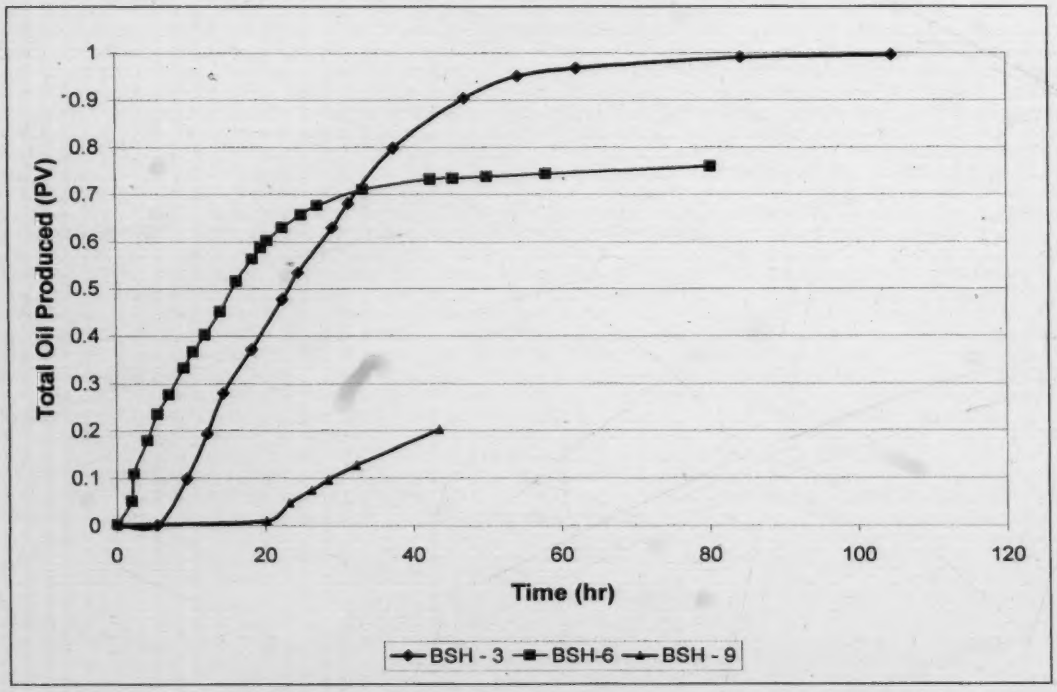

Figure 2.11: Cumulative production with time for Berea sandstone horizontal orientation.

A version of this chapter has been published
Trivedi J. and Babadagli T., 2008. Transport in Porous Media. 71(3): 379.

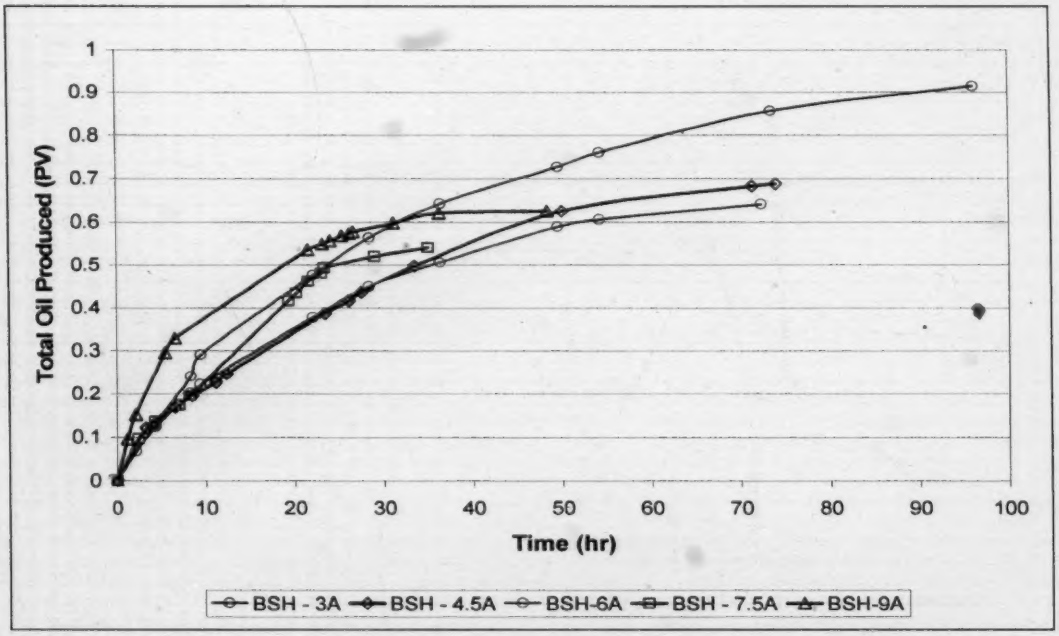

Figure 2.12: Cumulative production with time for aged Berea sandstone horizontal orientation.

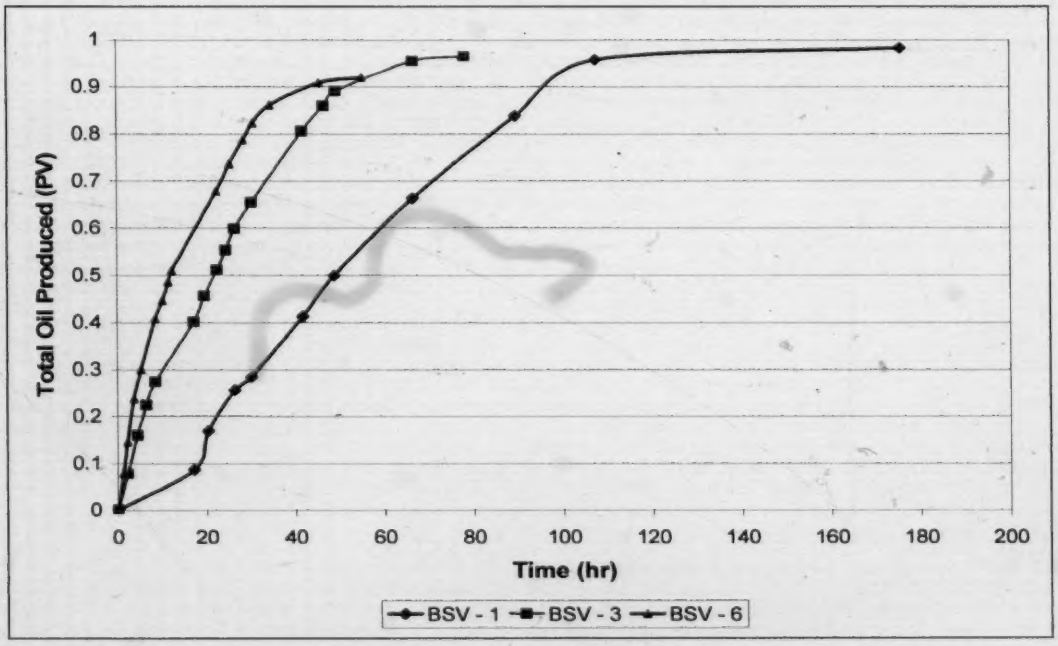

Figure 2.13: Cumulative production with time for Berea sandstone vertical orientation.

A version of this chapter has been published
Trivedi J. and Babadagli T., 2008. Transport in Porous Media. 71(3): 379.

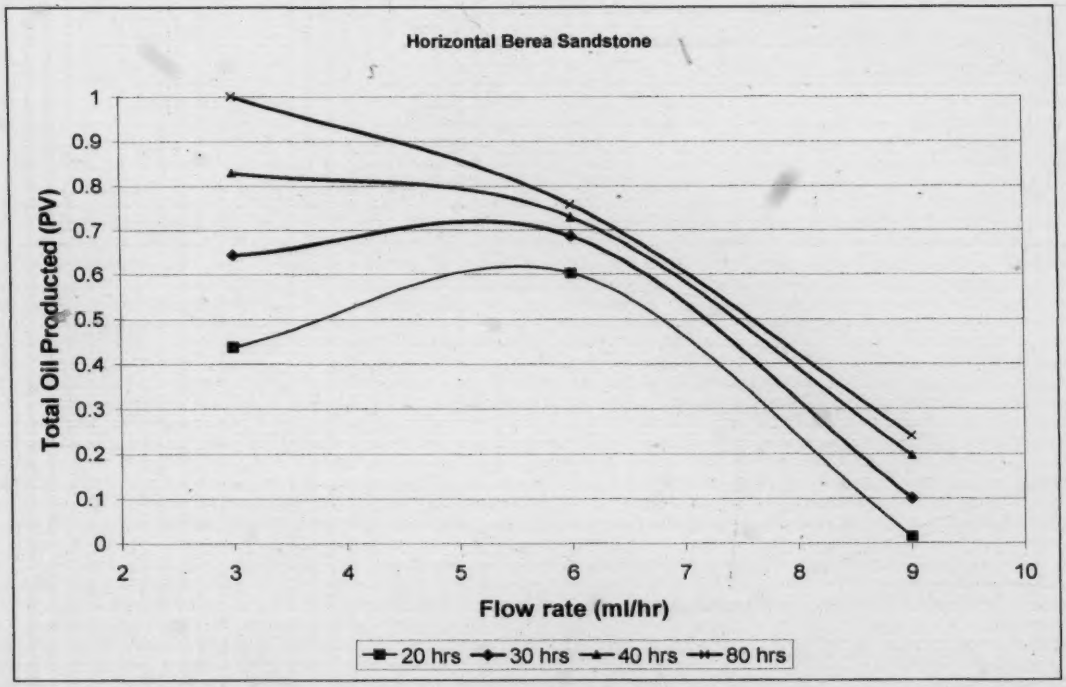

Figure 2.14: Cumulative production at different flow rate and time axis for Berea sandstone horizontal orientation.

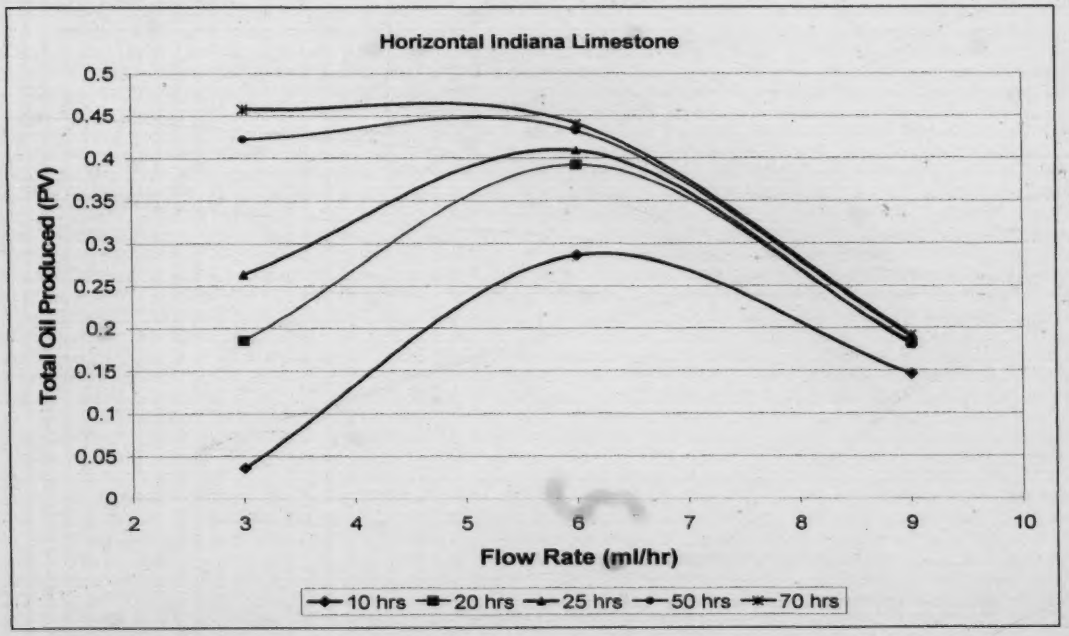

Figure 2.15: Cumulative production at different flow rate and time axis for Indiana limestone horizontal orientation.

A version of this chapter has been published
Trivedi J. and Babadagli T., 2008. Transport in Porous Media. 71(3): 379.

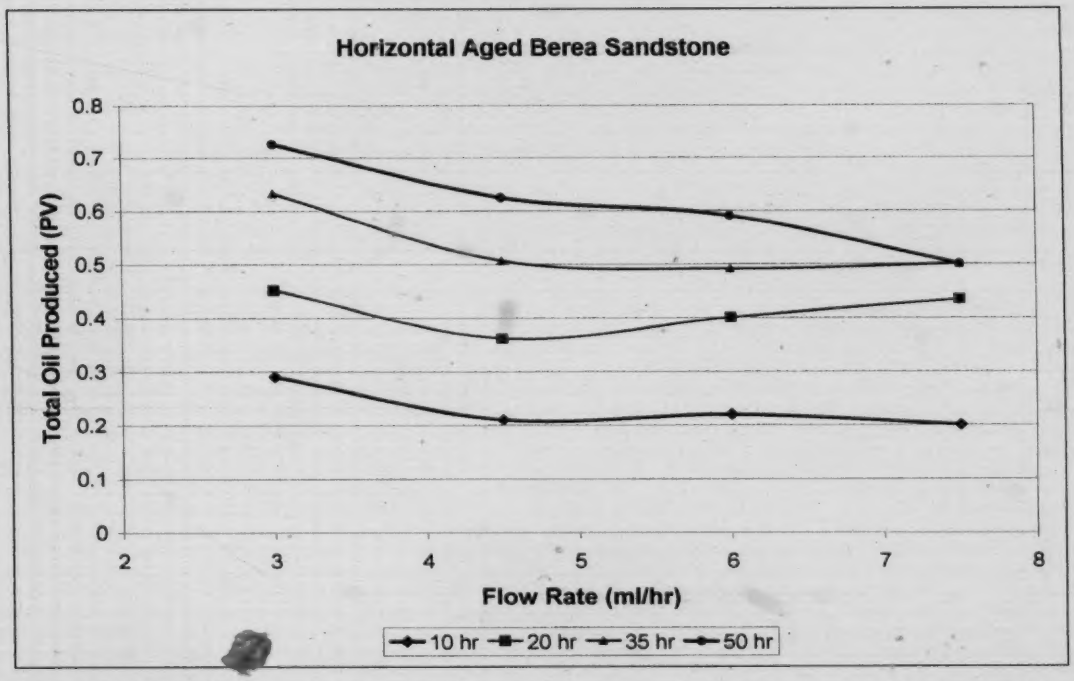

Figure 2.16: Cumulative production at different flow rate and time axis for aged Berea sandstone, horizontal orientation.

A version of this chapter has been published
Trivedi J. and Babadagli T., 2008. Transport in Porous Media. 71(3): 379.

3 EXPERIMENTAL AND NUMERICAL MODELING OF THE MASS TRANSFER BETWEEN ROCK MATRIX AND FRACTURE

3.1 Introduction

The target oil in naturally fractured reservoirs (NFR) exists in rock matrix. During the injection of tertiary recovery materials that are miscible with matrix oil, i.e., hydrocarbon solvents, alcohols, CO_2, N_2 etc., fracture network creates the path for the injected solvent to bypass and leave the unwept oil zones in the matrix. Significant amount of oil can be recovered from this upswept bypassed zone by maximizing the subsequent crossflow or mass transfer between fracture and media. Likewise, when greenhouse gases (CO_2, pure or in the form of flue gas) is injected into NFRs, the matrix part could be a proper storage environment and the transfer of the injected gas to matrix needs to be well understood for the determination of the process efficiency. The same process is encountered in the transportation of contaminants and waste material in NFRs.

In general four factors contribute to crossflow/mass transfer: (a) Pressure, (b) gravity, (3) dispersion/diffusion, and (d) capillary drive. When the bypassed fluid and displacement fluids are First Contact Miscible (FCM), there is no capillary crossflow. When the fluids are Multi Contact Miscible (MCM) or immiscible, there could be a certain degree of capillary-driven crossflow. Burger et al. (Burger et al., 1996; Burger and Mohanty, 1997) found that capillary driven crossflow does not contribute significantly to mass transfer in near-miscible hydrocarbon floods. The other three forces play a critical role in the mass transfer between matrix and fracture and need to be well understood in terms of the effective parameters and efficiency of the process.

Previously we had performed experiments to clarify the effective parameters on the mass transfer during solvent injection into fractured systems (Trivedi and Babadagli, 2006). In this study, the critical rate was defined as the maximum rate beyond which no change in the ratio of matrix recovery to injected solvent is obtained by increasing rate. As the injection rate is increased, the injected fluid flowing in the fracture would yield an early breakthrough

A version of this chapter has been published
Trivedi J. and Babadagli T., 2008. Chemical Eng. J. doi:10.1016/j.cej.2008.05.032.

without spending enough time to contact with the matrix. Hence, increasing rates may result in a faster recovery but higher amount of solvent is needed due to weaker mass transfer interaction to cause oil production from matrix. This results in an inefficient use of solvent. Therefore, slower rates are desirable for a better interaction and stronger mass transfer yielding higher matrix oil recovery to solvent injected ratio. This, however, reduces the recovery time. Thus, the definition of critical rate is an important issue and the rate depends on rock and fluid characteristics. The concept of critical velocity was first introduced by Thompson and Mungan (1969). They compared displacement velocity to critical velocity (V_C) and showed its effect on recovery efficiency. Firoozabadi and Markeset (1994) showed that the capillary pressure contrast between matrix and fracture could be the major driving force. Further, they studied the effect of matrix/fracture configuration and fracture aperture on first contact miscible efficiency.

Advanced visualization studies were also conducted to understand the physics of matrix-fracture interaction. Part (1993) studied the formation of drying patterns assuming only capillary forces and neglecting viscous effects. It was the first attempt to theoretically characterize drying patterns in porous media as well. Computational (Zakirov et al., 1991; Jensen et al., 1992) and experimental (Lenormand, 1998; Hunjun Li et al., 2000) studies on the interaction of matrix and fracture for different types of fluids were also reported.

The diffusion process and correlations of the capillary pressure with variation of interfacial tension were also investigated (Morel et al., 1993; Hu et al., 1991; Gabitto, 1998). Morel et al. (1993) performed diffusion experiments with chalk and studied the effect of initial gas saturation. The diffusion/stripping process in fractured media was well described by Saidi (1987). Recently, there has been success in determining diffusion coefficients between two miscible fluid systems (Yang and Gu, 2006; Civan and Rasmussen, 2002; Raizi, 1996; Stubos and Poulou, 1999) but the process is totally different within the fractured porous media, affected by many parameters such as, matrix properties, condition at the boundaries, fracture geometry and flow conditions.

The presence of water affects the pore-scale distribution of hydrocarbon phases Pandey and Orr al., 1990, Mohanty and Salter, 1982). Connectivity and tortuosity of the pore structure influences the effective diffusivity and the relative permeability of each hydrocarbon phase.

A version of this chapter has been published
Trivedi J. and Babadagli T., 2008. Chemical Eng. J. doi:10.1016/j.cej.2008.05.032.

Hence the mass transfer and bypassing are affected. LeRomancer et al. (1994) examined the effect of water saturation (<30%) on mass transfer in the matrix blocks of a fractured reservoir. As the water saturation increases, the liquid-hydrocarbon-phase area available for diffusion and the gas/liquid interfacial area decrease, and mass transfer decreases. At high water saturations, islands of oil will be isolated by water, effectively reducing mass transfer further. They concluded that water saturation has no effect during nitrogen injection because of a strong capillary crossflow. Whylie and Mohanty (1997) further investigated the effects of water saturation on mass transfer from bypassed region and bypassing during miscible/near-miscible gas injection. They used 1-D model and calculated effective diffusion coefficient.

The orientation of the bypassed region with respect to gravity and enrichment of the solvents affect the mass-transfer rate. The mass-transfer was least for the vertically up orientation (against gravity), intermediate for the vertically down, and highest for the horizontal orientation for the experiments (Burger et al., 1996). Burger et al. (1996) also concluded in his analysis that in vertical orientation gravity does not induce the flow of oil to the outlet face; therefore the recovery is primarily the result of diffusion. The oil-phase diffusivity is the controlling parameter in vertical mass transfer experiments.

Comings and Sherwood (1934) modeled the process considering moisture moment by capillary in drying granular materials. But determining mass transfer coefficients during flow in fracture is more complex process due to the involvement of injection rate effect and fracture properties. In most of the available commercial simulators, the mass transfer is assumed to proceed by diffusion within single phase. Recent studies from Jamshidnezhad et al. (2004) considered mass transfer between the same phases in the fracture and porous medium. In their work displacement was considered as one-dimensional and a few experiments were compared with the simulation results.

As seen, the miscible interaction process between matrix and fracture in naturally fractured subsurface reservoir has been studied for different purposes. The previous efforts were made usually to understand the physics of the interaction process through experimental studies. Limited number of studies focused on the numerical modeling usually without enough experimental support. Deriving correlations using dimensionless numbers to define

A version of this chapter has been published
Trivedi J. and Babadagli T., 2008. Chemical Eng. J. doi:10.1016/j.cej.2008.05.032.

matrix-fracture interaction terms is a critical task and that requires a combination of experimental and simulation work. Though much effort was devoted in defining the immiscible matrix-fracture interaction through dimensionless terms, less attention has been given to modeling miscible interaction, especially using controllable parameters such as injection rate and fluid characteristics. Also in simulation of the matrix-fracture fracture miscible interaction processes, 2- or 3-D models have to be considered due to transverse mass transfer to and from the fracture and longitudinal diffusion/dispersion within the matrix and fracture individually. The understanding of the qualitative nature of the physics behind the matrix-fracture interaction process and quantitative representation of the controlling transfer parameters are the objectives of this paper and this was achieved through a series of experimental and numerical simulation works.

3.2 Experimental Study

Experiments were performed to study and analyze the process of diffusion and dispersion during flow of solvent into the fracture adjacent to the oil saturated matrix qualitatively with change in length, solute type (hence the viscosity and density) and aging time with oil in the fractured porous media. These parameters affect the various forces, viscous and diffusion in particular, and alter the amount of oil produced and solvent diffused into the matrix with amount of solvent injected over the period of solvent injection process. Experimental observations will be useful in comparing and matching the results from the numerical simulations. Experimental analysis coupled with the numerical modeling will also be used to define and formulate critical parameters controlling the matrix-fracture interaction/transfer, which are not practically obtainable through direct experimental measurements or computations. To simplify the understanding of diffusion drive mechanism, we used first contact miscible (FCM) case and neglected capillary-driven crossflow. All the experiments were performed at room temperature and pressure to nullify the crossflow/mass transfer due to pressure drive.

A version of this chapter has been published
Trivedi J. and Babadagli T., 2008. Chemical Eng. J. doi:10.1016/j.cej.2008.05.032.

3.2.1 Procedure

Cylindrical plugs were cut from 20 inches long cylindrical rods of Berea sandstone (k= 500 md; ϕ = 0.21) and Indiana limestone (k= 15 md; ϕ = 0.11) to 6 inches in length and 2 inches in diameter. Then, the samples were fully saturated with different solute under constant vacuum for 48 hours using a vacuum pump. The saturated cores were cut into two pieces through the center in the direction of longitudinal axis for the purpose of creating a fracture. These pieces were held together using heat-shrinkable rubber sleeves.

The fractured core was then placed into Plexiglas holder and the annular space was filled with silicon to ensure no flow to the annulus between the core and core holder. The solvent was injected at constant rate from the center of the core and production line was placed at the center of other end. Injection and production were maintained only through the fracture while the flow into matrix was only through diffusion/mass transfer.

Flow through fractures was considered in several studies. There are three common ways of injection: (a) Injection through matrix and production through matrix, while the fracture was located in the middle of the two matrix blocks, (b) Injection through fracture and produce through fracture, while there is only one (or two) matrix block adjacent to fracture, and (c) Injection through circular annular acting as a fracture. In our experiments, we applied the injection scheme as defined in option (b) considering the fact that the flow will be controlled by high permeability fractures.

Some experiments were also performed with aged samples. In those cases cores were aged for a period of one month. Effect of solute viscosity and density were analyzed by using different solute types (mineral oil, heavy mineral oil, and kerosene).

The samples collected at the production end were analyzed using refractometer. Using the calibration curve from the known percentage of mixture, refractive index (RI) values were converted to obtain relative proportions in the production mixture. All the experiments were performed at room temperature.

A version of this chapter has been published
Trivedi J. and Babadagli T., 2008. Chemical Eng. J. doi:10.1016/j.cej.2008.05.032.

Core preparation and experimental set-up are shown in **Figures 3.1** and **3.2**, respectively. The properties of fluids used are given in **Table 3.1**. Detailed outline of experiments performed is listed in **Table 3.2**.

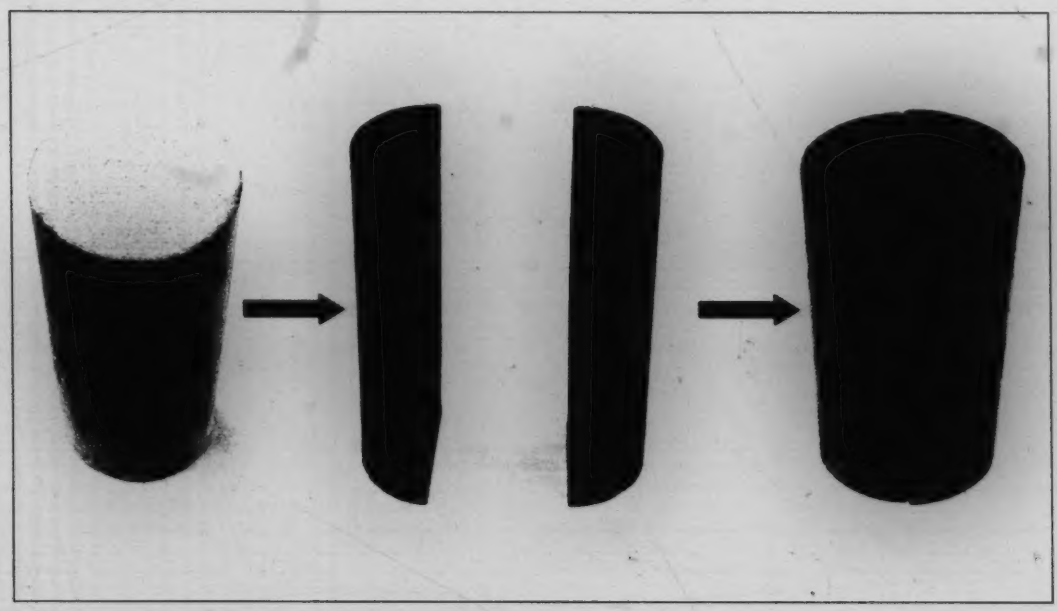

Figure 3.1(a): Core cutting and fracture preparation.

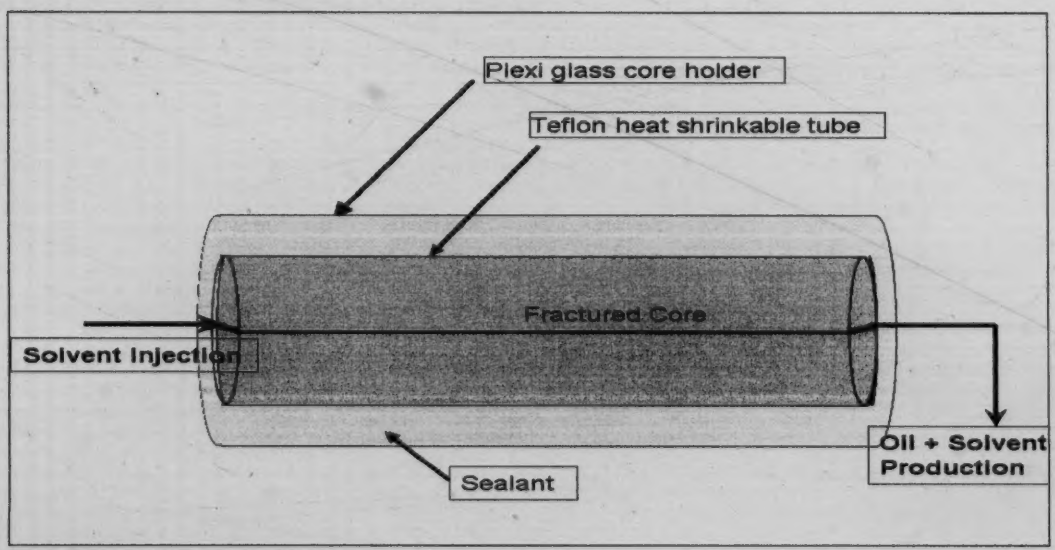

Figure 3.1(b): Core holder design.

A version of this chapter has been published
Trivedi J. and Babadagli T., 2008. Chemical Eng. J. doi:10.1016/j.cej.2008.05.032.

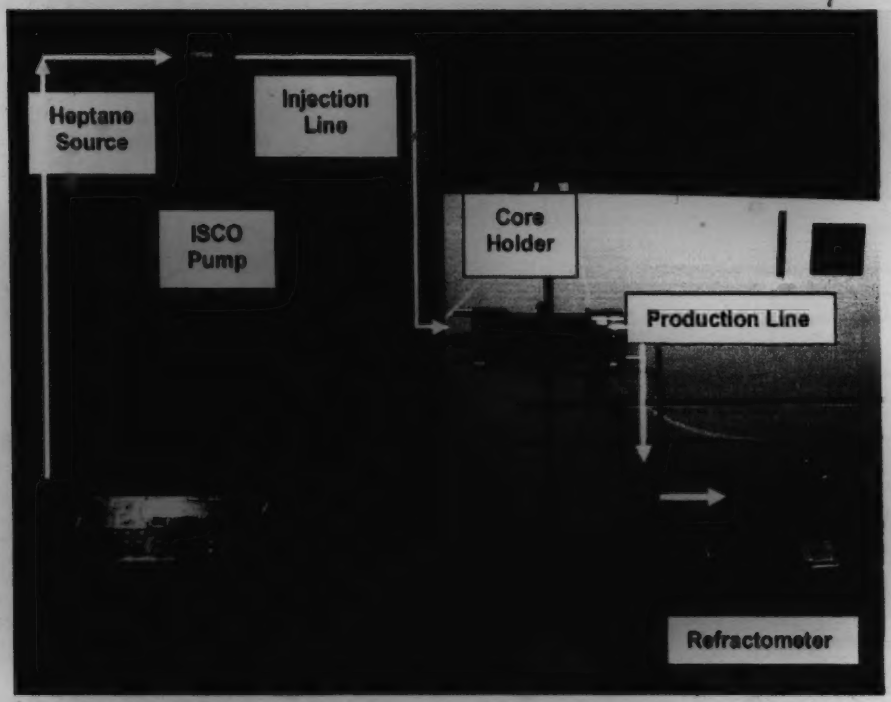

Figure 3.2: Experimental set-up.

Table 3.1: Properties of solute and solvent used in the study.

	Chemical Name	Density (g/cc)	Viscosity (cp)	Refraction Index (RI)
Solvent	Heptane	0.69	0.410	1.3891
Solute	Mineral Oil (MO)	0.83	33.5	1.469
	High Viscosity Mineral Oil (HO)	0.85	150	1.469
	Kerosene	0.81	2.1	1.475

A version of this chapter has been published
Trivedi J. and Babadagli T., 2008. Chemical Eng. J. doi:10.1016/j.cej.2008.05.032.

Table 3.2: Details of experiments performed.

Case	Core Type	Angle (Deg)	Solute Type	Flow rate (ml/hr)	Matrix length (inches)	Aged
BSH-3	Sandstone	0	MO	3	6	No
BSH-6	Sandstone	0	MO	6	6	No
BSH-9	Sandstone	0	MO	9	6	No
BHA-3	Sandstone	0	MO	3	6	Yes
BHA-4.5	Sandstone	0	MO	4.5	6	Yes
BHA-6	Sandstone	0	MO	6	6	Yes
BHA-9	Sandstone	0	MO	9	6	Yes
BSK-3K	Sandstone	0	Kerosene	3	6	No
BSK-6K	Sandstone	0	Kerosene	6	6	No
BSV-3	Sandstone	90	MO	3	6	No
BSV-6	Sandstone	90	MO	6	6	No
HO-3	Sandstone	0	HO	3	6	No
HO-6	Sandstone	0	HO	6	6	No
HO-3 (3")	Sandstone	0	HO	3	3	No
HO-6 (3")	Sandstone	0	HO	6	3	No
HOA-3	Sandstone	0	HO	3	6	Yes
HOA-6	Sandstone	0	HO	6	6	Yes
ILH-3	Limestone	0	MO	3	6	No
ILH-6	Limestone	0	MO	6	6	No

H – Horizontal

V – Vertical

A – Aged over period of 1 month

MO – Mineral Oil

HO – High Viscosity Oil

A version of this chapter has been published
Trivedi J. and Babadagli T., 2008. Chemical Eng. J. doi:10.1016/j.cej.2008.05.032.

3.3 Experimental Observations

We used the plot of total solvent injection (as pore volume) vs. total oil (solute) recovered (as pore volume) to represent the results. The recovery of solute (oil) in y-axis corresponds to solvent concentration in the system. Because our main target was oil recovery in this particular study, we preferred to use solute recovered in y-axis rather than solvent concentration.

The diffusion dominant displacement front progresses slower when injecting solvent at a lower rate for all three solutes (oils) **(Figure 3.3)**. Although the solute recovery rates are slower compared to that of higher rate solvent injection, the final recoveries are higher for the lower rates. It was observed that the initial phase of the recovery curves are dominated by displacement or viscous forces and the diffusion comes into picture at later stage. Such phenomena can be detected at the point when recovery curve of BHS-3 overpasses that of BHS-6 as marked by an arrow in **Figure 3.3**.

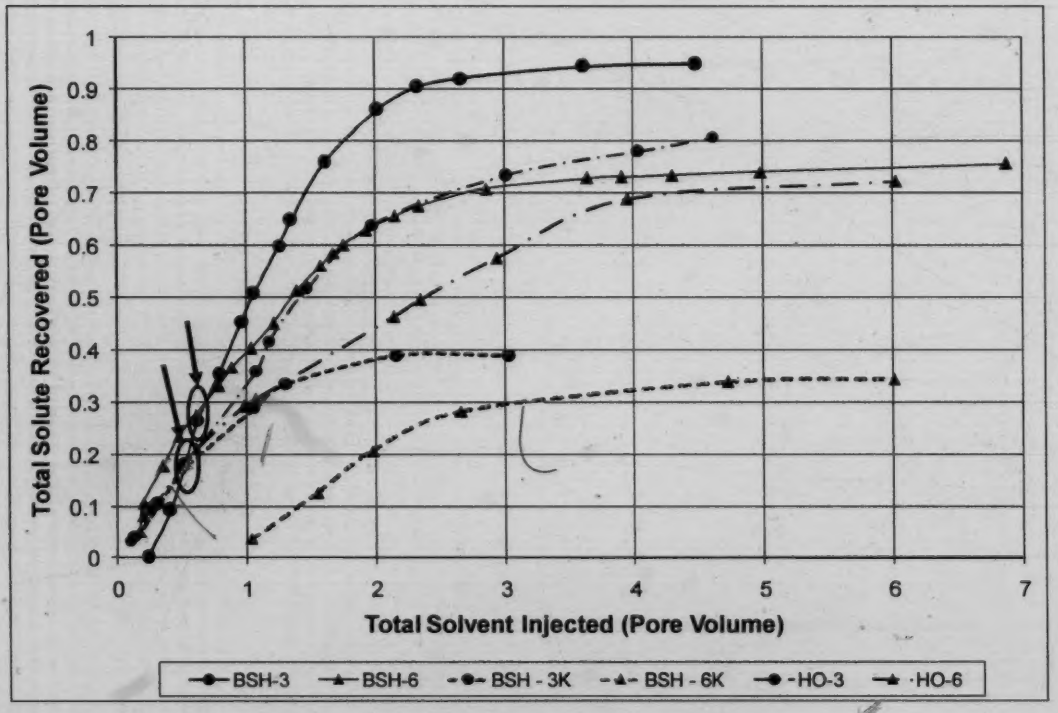

Figure 3.3: Solute recoveries during solvent diffusion for different oil types.

A version of this chapter has been published
Trivedi J. and Babadagli T., 2008. Chemical Eng. J. doi:10.1016/j.cej.2008.05.032.

Different solute types, i.e. different densities and viscosities, may take part in the diffusion process between matrix and fracture. Some experiments were conducted to elaborate the range of viscosity and density of solute used. We used high viscosity mineral oil and kerosene for this purpose. Though the ultimate recoveries are lower for heptane diffusing into high viscosity mineral oil saturated sandstone, the crossover of lower rate injection case (HO-3) to higher rate injection case (HO-6) was evident **(Figure 3.3)**. Interestingly, it occurred after certain amount of pore volume solvent injected (or time). In case of kerosene, we were not able to capture this point. It possibly occurred either at very early stage of the process or did not ever happen. The lower-rate-diffusive-transfer dominates the solute production throughout the process. Based on these observations, one can conclude that density difference controls the process rather than the viscosity difference.

In contrast to the horizontal case where the effect of different flow rates was significant on ultimate recovery, the ultimate recoveries were similar during solvent diffusion at different rates in the vertically oriented sandstone **(Figure 3.4)**. However, solute recovery trends were in agreement with those of horizontal cases. It is worth noting that the BV-3 case overpasses the BV-6 case at around 40% of solute production. This turning point is higher than the point where BHS-3 overpasses the BHS-6. The total amounts of solute produced were also higher with almost similar amount of solvent required to reach the plateau of ultimate recovery, which makes a strong point of gravity influence.

A version of this chapter has been published
Trivedi J. and Babadagli T., 2008. Chemical Eng. J. doi:10.1016/j.cej.2008.05.032.

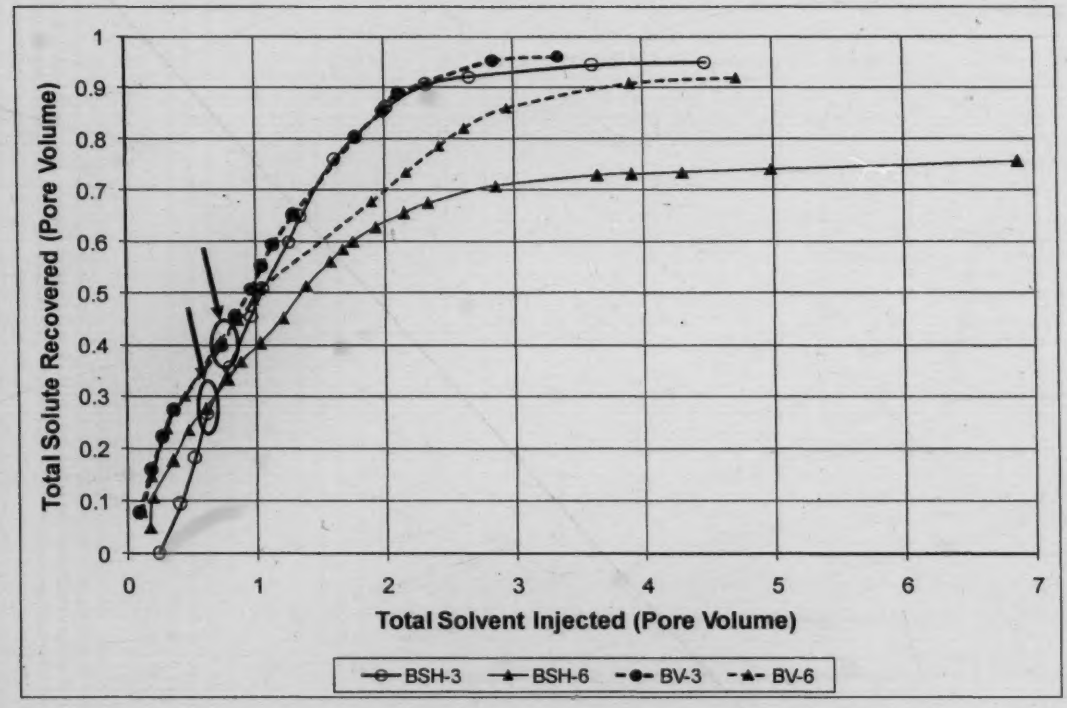

Figure 3.4: Solute recoveries during solvent diffusion for horizontal and vertical cases.

The role of porosity and permeability was proved to be significant when similar injection and experimental conditions were applied for mineral oil saturated Berea sandstone and Indiana limestone **(Figure 3.5)**. The ultimate recovery from the limestone sample is almost half of the recovery observed in the sandstone cores. The trend was very much alike of sandstones where slower rate process overpasses the higher rate process at the same point of recovery. Noticeably this transition took place at nearly 35% oil production, just a bit higher than that of horizontal and vertical sandstone cases (30%). This point comes much later stage of time compared to that in sandstone, meaning that the poor porosity and permeability of the medium yield less efficient process.

Core aging affects the recovery trends. The recovery rate of mineral oil is slower and the ultimate recovery is lower for the aged Berea sandstones compared to those of non-aged samples. **Figure 3.6** points out the influence of aging on miscible flood efficiency. The comparison of such effect on recovery curves is illustrated using the cases of 3 ml/hr and 6 ml/hr flow rates for non-aged mineral oil saturated Berea sandstones and aged one (for a

A version of this chapter has been published
Trivedi J. and Babadagli T., 2008. Chemical Eng. J. doi:10.1016/j.cej.2008.05.032.

period of one month). No significant difference in terms of ultimate recovery was observed between aged and non-aged samples for heavy-mineral oil **(Figure 3.7).** The amount of pore volume injected for obtaining ultimate recovery was also found unchanged with marginal difference compared to that of non-aged-viscous-oil-sandstone cases.

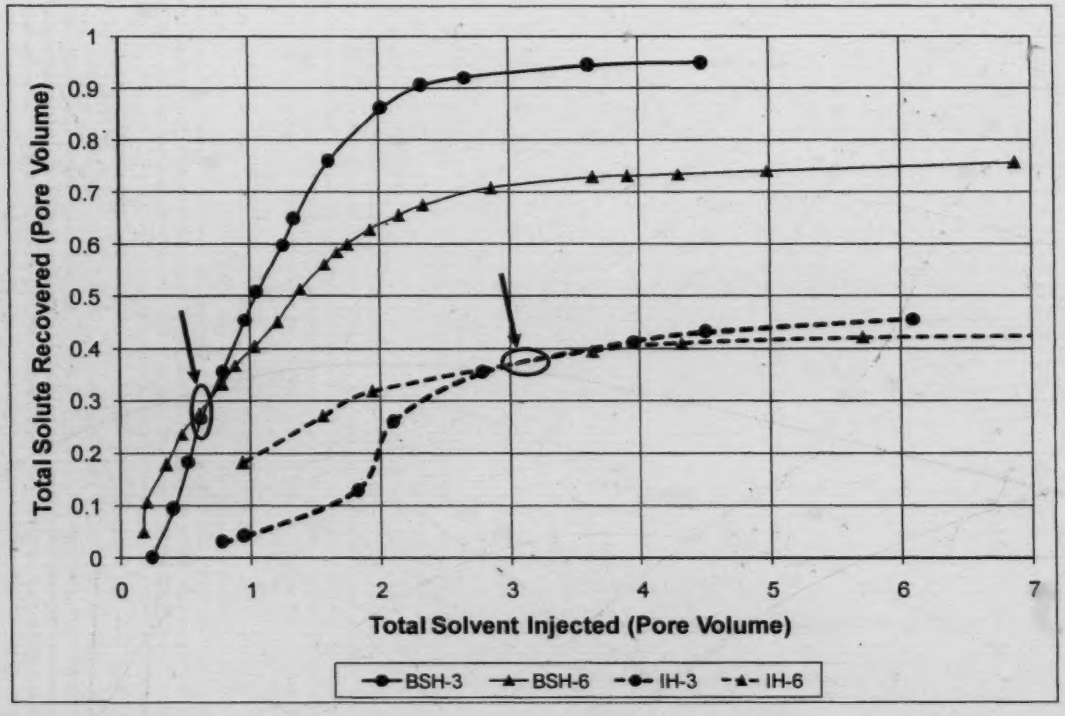

Figure 3.5: Solute recoveries during solvent diffusion comparing Berea sandstone and Indiana limestone cores.

A version of this chapter has been published
Trivedi J. and Babadagli T., 2008. Chemical Eng. J. doi:10.1016/j.cej.2008.05.032.

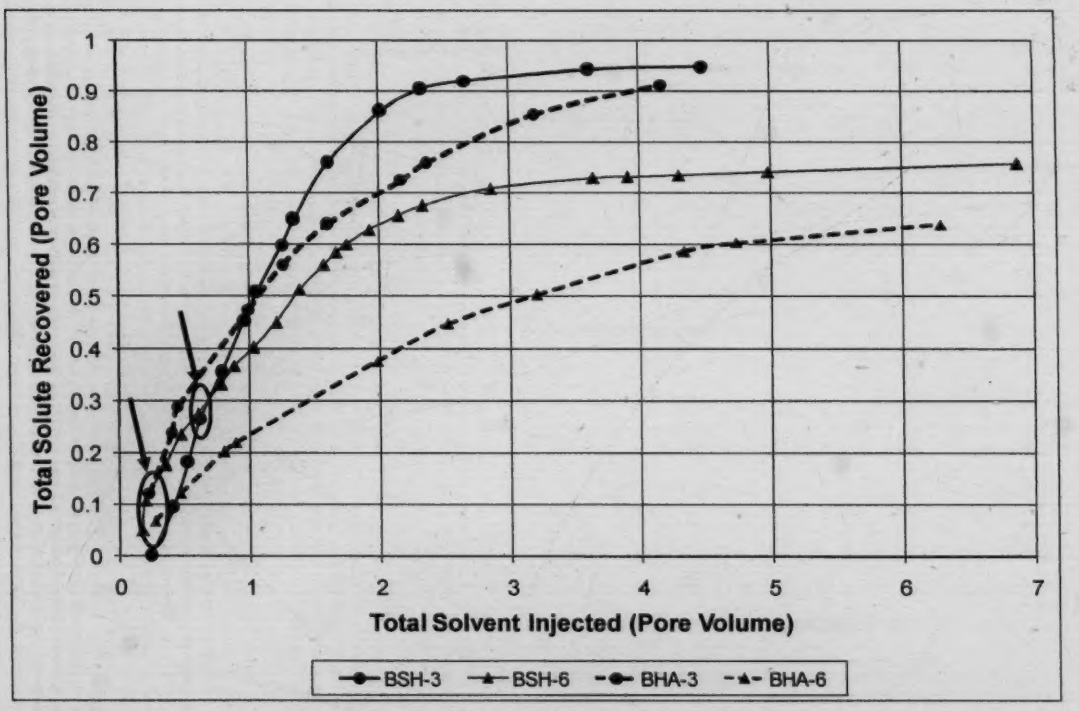

Figure 3.6: Comparison of the solute recoveries during solvent diffusion for the aged and non-aged samples.

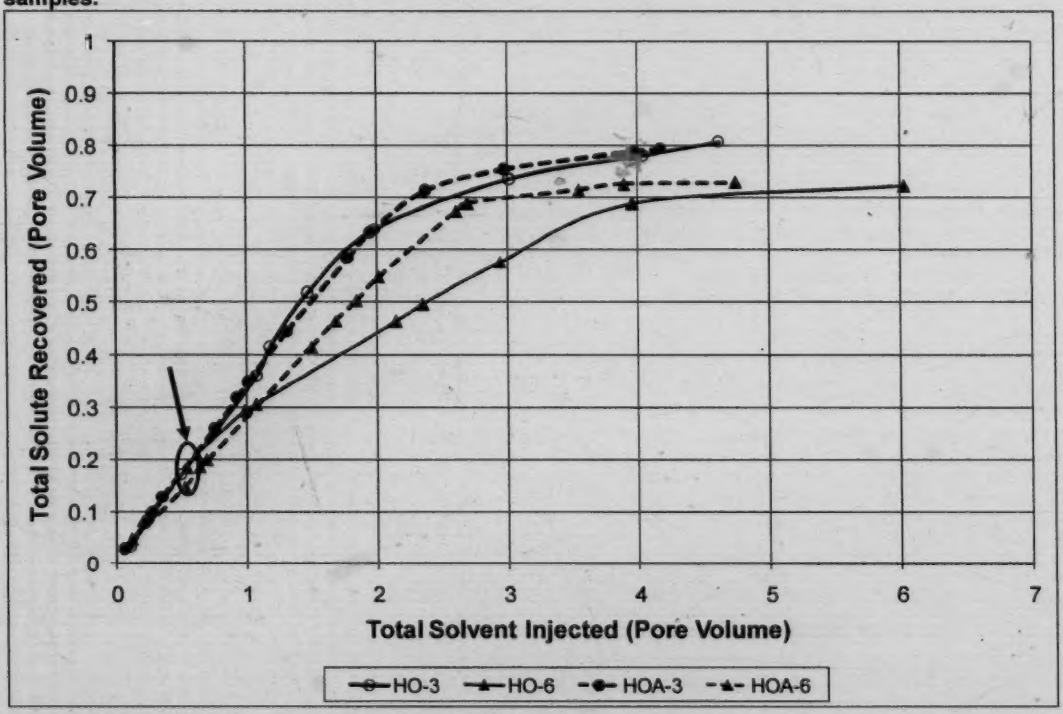

Figure 3.7: Solute recoveries during solvent diffusion from high viscosity mineral oil aged and non-aged core samples.

A version of this chapter has been published
Trivedi J. and Babadagli T., 2008. Chemical Eng. J. doi:10.1016/j.cej.2008.05.032.

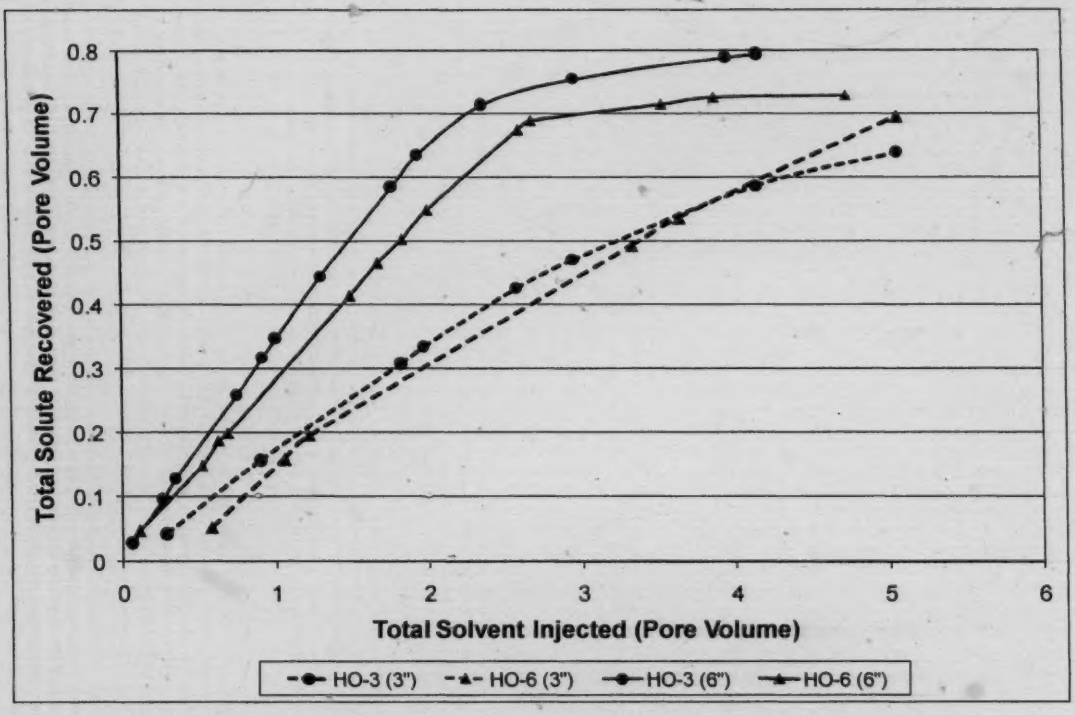

Figure 3.8: Solute recoveries during solvent diffusion comparing 3" and 6" longer samples.

When the size of the core was changed from 6 inch to 3 inch **(Figure 3.8)**, no significant effect was observed between the ultimate recoveries of the flow rate of 3 ml/hr and 6 ml/hr cases. But, more solvent needs to be injected to reach the same ultimate recovery in case of shorter samples, implying that the recovery rate is lower. Solvent does not have enough time to contact with the rock matrix to diffuse into the matrix to sweep out the solute before it breaks through for the shorter samples. Hence, the length of the matrix size in determining the efficient transfer conditions is also important.

3.4 Modeling of Fracture-Matrix Transfer Process

Fracture-matrix transfer process was modeled numerically and presented in the form of dimensionless groups to analyze the effects of different parameters quantitatively. The process experimentally analyzed in the previous section was simulated using finite element modeling with the governing advection-convection equations and the Darcy equation. Only

A version of this chapter has been published
Trivedi J. and Babadagli T., 2008. Chemical Eng. J. doi:10.1016/j.cej.2008.05.032.

parameters other than those unavailable from the laboratory scale experiments are diffusion/dispersion coefficients and mass transfer coefficients in the matrix as well as in the fracture. These parameters were obtained through matching the numerical modeling results to their experimental equivalents and then they were correlated to fluid-rock properties and flow velocity.

3.4.1 Analogy between Monolith Catalysts (Reactor) and Matrix-Fracture Systems

Monolithic catalysts have gained recent interest for reducing pollution (Cybulski and Moulin, 1998) due to simultaneous advantages of very low pressure drop, short diffusion resistance, excellent mass transfer and high surface to volume ratio. They are also widely used in selective catalytic reduction of NO_x, hydrogenations of liquid phase, power generation using gas turbines (Cybulski and Moulin, 1994; Forzatti, 2001).

Monolithic catalysts/reactors **(Figure 3.9)** consist of a matrix of uniformly aligned parallel channels. The diameter of the channel ranges from 0.5 to 10 mm and length can be up to 1 meter long. These channels are fabricated on either ceramic or metallic supports called substrates. On the walls of the channels a catalytic active layer (a porous layer), 10 to 200 μm thick, can be applied. It is commonly called as *washcoat*. The flow is laminar in monolithic reactor for most of the applications with the Reynolds number typically in the range 10-1000. The reactants in the fluid phase are transported to the surface of the catalyst by convection and from the surface of the catalyst to the active sites of the catalyst by diffusion. The reactants react on the active catalysts sites which results in release or absorption of heat. The presence of catalytic reactions at the wall of the channel acts as a source or sink, which imposes temperature or concentration gradients in the radial directions.

The magnitude of radial gradients depends on the relative rates of heat and mass transfer and chemical reaction. There are two important types of potential mass transfer limitation in these reactors. The first is diffusion limitation in the washcoat owing to fast reaction. The rate of reaction is controlled by the intrinsic kinetics only and the reactor is said to be in kinetically controlled regime. If the rate of diffusion is lower than the intrinsic rate of reaction, the bulk and surface conditions are different. In the extreme case, the catalyst

A version of this chapter has been published
Trivedi J. and Babadagli T., 2008. Chemical Eng. J. doi:10.1016/j.cej.2008.05.032.

concentration at the surface may go zero and the rate is controlled solely by the rate of mass transfer.

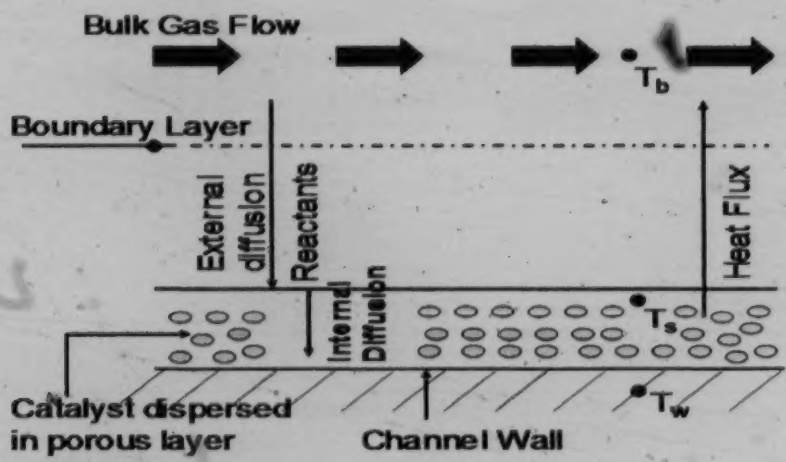

Figure 3.9: Diffusion and flux behavior in monoliths.

The monolith reactors system **(Figure 3.9)** is analogous to the matrix-fracture system in subsurface reservoirs as depicted in **Figure 3.10**. The network of fracture channels run through less permeable porous media than fractures. Porous media can be visualized as porous washcoat. Injected solvent passes through fractures transferring to matrix interface through diffusion and convection. Within the matrix pores, solvent is transported through diffusion. For simplification, the whole network of channels is represented by a single channel with assumption of equivalent passages with no interaction. The same assumption applies while simulating the matrix-fracture system. The only difference is the size of porous media. Unlike the monolith reactor the size of porous media is considerably large in the fractured reservoirs. This may cause higher concentration or temperature gradients in the transverse directions, which is normal to the flow direction and hence the Sherwood numbers becomes remarkably higher than that exists into typical monolith catalyst. The physics of the process, however, is very much similar in both cases.

The mass or heat transfer within a single matrix can be described by two inherently coupled processes: external transfer from the bulk to the matrix and internal transfer inside the

A version of this chapter has been published
Trivedi J. and Babadagli T., 2008. Chemical Eng. J. doi:10.1016/j.cej.2008.05.032.

porous matrix. Hence, the steady-state behavior of a single matrix can be mathematically described by convection – diffusion equation in the fluid phase coupled with the diffusion–reaction equation within the porous media involving more than one spatial dimension similar to the single monolith channel reactor.

The shape of the washcoat geometry has large influence on the final conversion of reactants and mass transfer rate because of their small size (μm scale). While the matrix assumed here is of significantly larger size (cm scale) and considered rectangular shape. The effect of matrix shape is not the scope of this research and has to be focused separately.

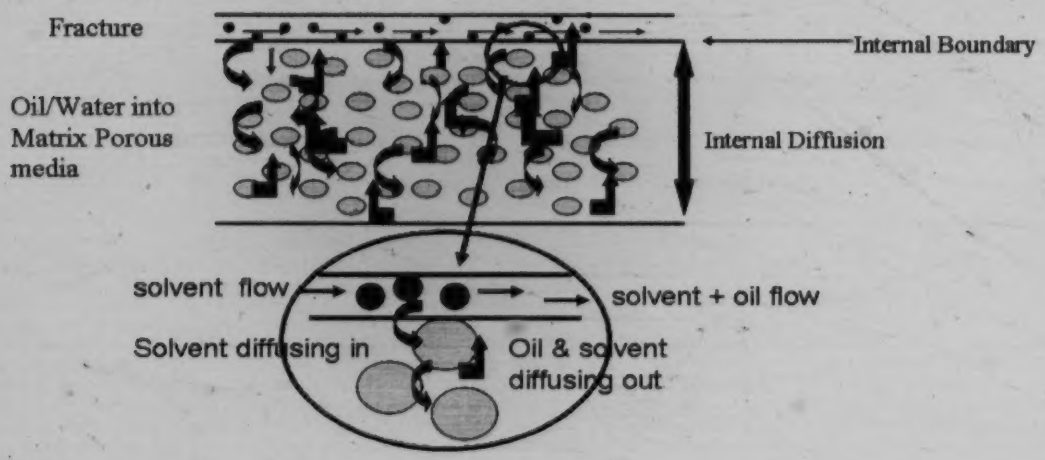

Figure 3.10: Diffusion and flux in matrix-fracture system.

3.4.2 Mathematical Model Formulation

The assumptions in the derivation of the equations are as follows:

- All fractures of the system are equivalent with uniform flow distribution and represent the network of fractures by a single straight channel.
- The oil is assumed to be dispersed uniformly within the porous matrix.

- In this analysis, we do not impose any restriction on the geometric shape of the fracture, except that the cross section of the fracture is invariant with the axial position.
- The flow is laminar and fully developed.
- The aspect ratio of the channel is assumed to be small; that is, the hydraulic diameter is much smaller than the length of the fracture (which is true for most of the practical applications). This assumption justifies the use of fully developed velocity profile within the channel and also leads to the simplification of negligible axial diffusion in both fluid phase and matrix compared to the convective transport rate.
- The flow in the fracture is assumed isothermal.
- Solvent flows only through fractures; there is no flow in the matrix surrounding fracture.
- The variations of physical properties (such as density, viscosity, diffusivities, and so on) and velocity with temperature and compositions are neglected.

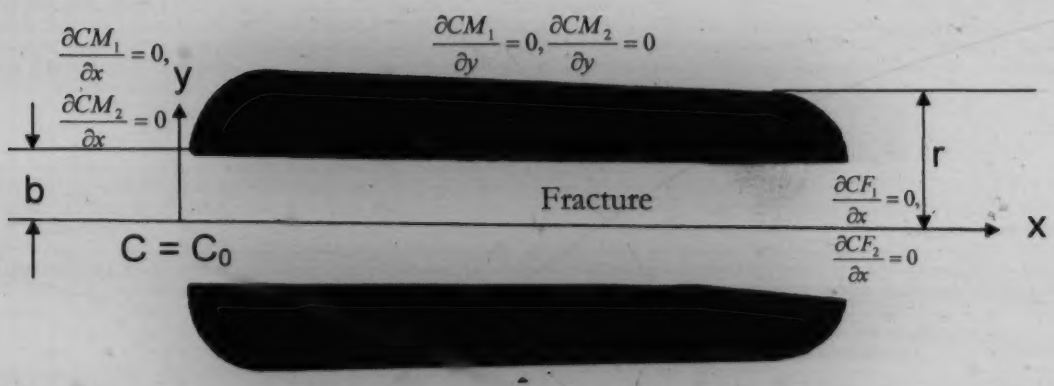

Figure 3.11(a): Geometrical representation of matrix-fracture system used in this study (not to scale).

Figure 3.11(a) represents the matrix-fracture system (length = l and radius = 2r) with inlet, outlet as well as the boundary conditions. The pore space of the matrix is initially filled with a displaced fluid ($C_M = 1$) and is flooded with a displacing fluid ($C_F = 1$) from one side x = 0 at the center, where fracture (half aperture = b) is located. The x-axis is the principle flow

direction, while the y-axis is the direction perpendicular to the flow. The displacing fluid (solvent) flows/injected at constant rate through fracture at the inlet x = 0; there is no flow in the matrix surrounding fracture.

The diffusion- convection equations for fracture and matrix are defined as:

Domain 1 – Fracture

$$\frac{\partial CF_1}{\partial t} - D_L \frac{\partial^2 CF_1}{\partial x^2} - D_L \frac{\partial^2 CF_1}{\partial y^2} = -K_V (CF_1 - CM_1) - u_F \frac{\partial CF_1}{\partial x} \quad \text{..... (3.1)}$$

$$\frac{\partial CF_2}{\partial t} - D_L \frac{\partial^2 CF_2}{\partial x^2} - D_L \frac{\partial^2 CF_2}{\partial y^2} = -K_V (CF_2 - CM_2) - u_F \frac{\partial CF2}{\partial x} \quad \text{..... (3.2)}$$

Domain 2 – Matrix

$$\frac{\partial CM_1}{\partial t} - D_e^M \frac{\partial^2 CM_1}{\partial x^2} - D_e^M \frac{\partial^2 CM_1}{\partial y^2} = K_V (CF_1 - CM_1) \quad \text{..... (3.3)}$$

$$\frac{\partial CM_2}{\partial t} - D_e^M \frac{\partial^2 CM_2}{\partial x^2} - D_e^M \frac{\partial^2 CM_2}{\partial y^2} = K_V (CF_2 - CM_2) \quad \text{..... (3.4)}$$

Initial conditions:

$CF_1(x, y, 0) = 0$; $CM_1(x, y, 0) = 0$; $CF_2(x, y, 0) = 1$; $CM_2(x, y, 0) = 1$; $CF_1(0, t) = CF_0$.... (3.5)

Boundary conditions:

$$\left.\frac{\partial CM_1}{\partial y}\right|_{(x,r,t)} = 0 \qquad \left.\frac{\partial CM_2}{\partial y}\right|_{(x,r,t)} = 0 \quad \text{..... (3.6)}$$

$$\left.\frac{\partial CF_1}{\partial x}\right|_{(\infty,t)} = 0 \qquad \left.\frac{\partial CF_2}{\partial x}\right|_{(\infty,t)} = 0 \quad \text{..... (3.7)}$$

$$D_L \frac{\partial CF_1}{\partial y} = -D_e^M \frac{\partial CM_1}{\partial y};\ D_L \frac{\partial CF_2}{\partial y} = -D_e^M \frac{\partial CM_2}{\partial y} \quad \text{at t = t} \forall x, b \quad \text{..... (3.8)}$$

A version of this chapter has been published
Trivedi J. and Babadagli T., 2008. Chemical Eng. J. doi:10.1016/j.cej.2008.05.032.

We used Finite Element Method (FEM) to solve the partial differential equation using COMSOL multiphysic (2006). The finite element method approximates a PDE problem with a problem that has a finite number of unknown parameters. The advantages of FEM are the ease of handling complex geometries, straightforward implementation of non-uniform meshes and the simple incorporation of flux boundary conditions. Galerkin method is used to solve the partial differential equations.

The system is described by Eqs. (3.1) through (3.4), with the initial and boundary conditions given in Eqs. (3.5) through (3.8). The grid size in the fracture is maintained constant while the grid size varies in the matrix. Transient analysis with time dependent solver (direct (Spooles) linear system solver) is used. The Spooles linear solver makes use of the symmetry in the diffusion equation and saves memory. A second order in space and time discretization is adopted with an implicit time stepping to achieve accurate results. The temporal simulations with increasing time steps starting with a small time step are made. The simulation results were compared with the results of experimental performed earlier. From the numeric simulations, values of $K\nu$ and D_e^M were obtained. In fact, they are the two critical parameters controlling the matrix-fracture interaction and functions of several different flow, fluids, fracture, and matrix properties. All other parameters were experimentally available, measurable, or computable. Comparison of simulated and experimental results is shown for two different cases in **Figure 3.11(b)**.

Note that the early time behavior (initial straight line portion before the curvature) was observed to be dominated by the K_ν and the later part by the D_e^M. The early time behavior is not controlled by the D_e^M. Therefore, the solution of the equation is assumed to be unique.

A version of this chapter has been published
Trivedi J. and Babadagli T., 2008. Chemical Eng. J. doi:10.1016/j.cej.2008.05.032.

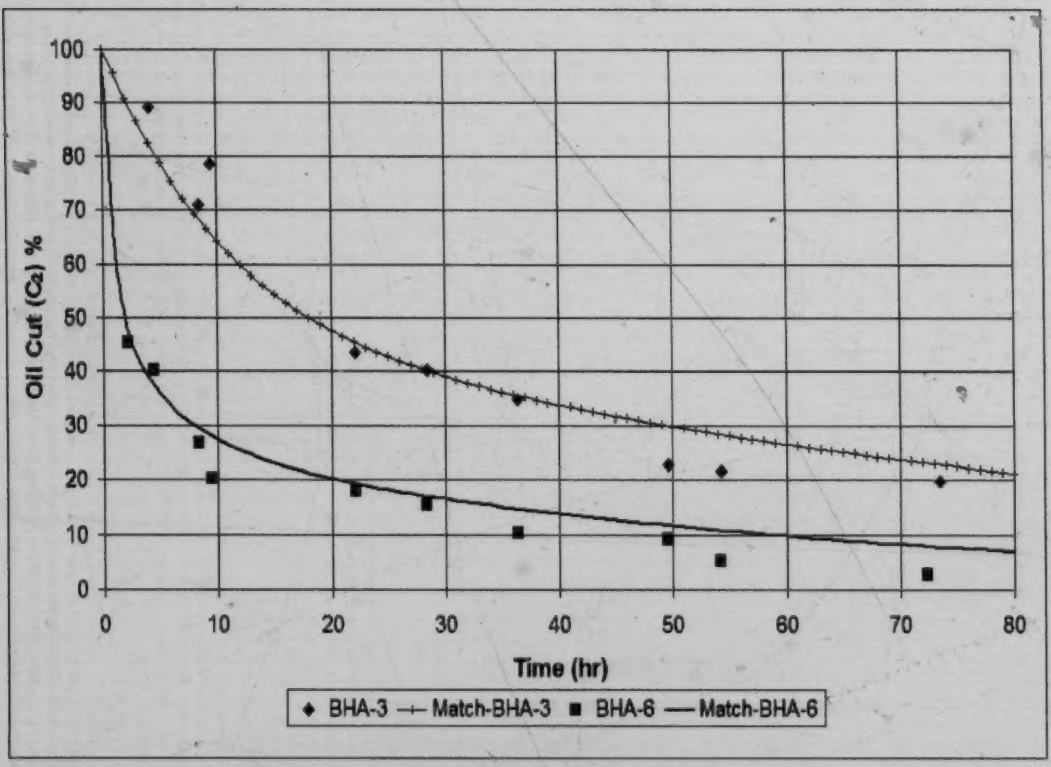

Figure 3.11(b): Simulation match with the experimental results of solute (mineral oil) concentration (C_2) change for two different rates on aged Berea sandstone cores.

3.4.3 Dispersion and Diffusion

Miscible recovery is the process in which solvent and solute are completely miscible with each other either first-contact or multi-contact. The concentration changes from that of solute to solvent inside the porous media till the equilibrium reaches. Due to miscible nature of the process (no interfacial tension), in such process there is no existence of capillary or inter-phase forces. Theoretically complete sweep is possible and 100% recovery of solute can be achieved at the equilibrium stage. The driving forces are molecular diffusion and convection.

During the flow through porous media, the additional mixing caused by uneven flow or concentration gradient is called dispersion. It results from the different paths and speeds and the consequent range of transit times available to tracer particles convected across a

A version of this chapter has been published
Trivedi J. and Babadagli T., 2008. Chemical Eng. J. doi:10.1016/j.cej.2008.05.032.

permeable medium. Dispersive mixing is a resultant of molecular diffusion and mechanical dispersion. Perkins and Johnston (1963) have provided an analysis of the dispersion phenomena and correlations for two types of dispersion; (1) longitudinal direction, and (2) transverse to the direction of gross fluid movement. Both, having different magnitude, have to be considered separately. Dispersive mixing plays important role in determining how much solvent will dissolve/mix with solute to promote miscibility. Molecular diffusion will cause mixing along the interface. The net result will be a mixed zone growing at a more rapid rate than would obtain from diffusion alone. Diffusion is a special case of dispersion and a result of concentration gradient, with or without the presence of the velocity field (Bear, 1988; Sahimi et al., 1982).

Gillham and Cherry (1982) defined the hydrodynamic dispersion coefficient as the sum of coefficient of mechanical dispersion (D_{mech}) and the effective diffusion coefficient in the porous media (D_{eff}). The hydrodynamic dispersion coefficient is also referred as dispersion-diffusion coefficient (D_L).

$$D_L = D_{mech} + D_{eff} \quad \text{.....(3.9)}$$

The mechanical dispersion is proportional to the average linearized pore-water velocity (V) and the dispersivity (α) (Bear, 1979; Freeze and Cherry, 1979). The effective diffusion coefficient is related to diffusion coefficient in free solution and tortuosity.

Taylor (1953) showed that in case of substantial diffusion perpendicular to the average fluid velocity, the dispersion coefficient in the tube would be proportional to the square of the average fluid velocity. Later, Horne and Rodriguez (1983) concluded that in the diffusion dominated system, the dispersion coefficient in the single, straight, parallel plate fracture will be proportional to the square of the fluid velocity. Keller et al. (1999) showed that dispersion coefficient and velocity has linear relationship, where $D_L \ \alpha \ V$. Bear (1979) suggested that the relation between dispersion coefficient and the average fluid velocity would be $D_L = \alpha * V^n$. The range of the n value is limited to $1.0 \leq n \leq 2.0$.

From the findings of Ippolite et al. (1984) and Roux et al. (1998), it is known that the dispersion coefficient in the variable aperture fracture is the sum of molecular diffusion, Taylor dispersion and microscopic dispersion.

A version of this chapter has been published
Trivedi J. and Babadagli T., 2008. Chemical Eng. J. doi:10.1016/j.cej.2008.05.032.

The Peclet number Pe for the flow in fracture is defined as;

$$Pe = \frac{V * b}{D_m} \quad \text{.....(3.10)}$$

where V is average fluid velocity in the fracture, b is the fracture aperture and D_m is the molecular diffusion coefficient.

Dronfield and Silliman (1993) conducted transport experiments in sand-roughened analog fracture and came up with a relation as $D_L \alpha\ Pe^{1.4}$. He also suggested that the power term to be 2 for parallel plate fracture and 1.3 to 1.4 for rough fractures. Detwiler et al. (2000) studied the effect of Pe on D_L using experiments and numerical results. His investigations were in accordance with that of earlier from Ippolite et al (1984) and Roux et al. (1998). Molecular diffusion dominates within the regime of $Pe<<1$. The Taylor dispersion and microscopic dispersion are related to Pe. The Taylor dispersion is proportional to Pe^2 while microscopic dispersion is proportional to Pe. Detwiller et al. (2000) showed quadratic relation from the result of Roux et al. (1998) in the form of a first-order approximation of the total non-dimensional longitudinal dispersion coefficient:

$$\frac{D_L}{D_m} = \alpha_{Taylor}(Pe)^2 + \alpha_{macro}(Pe) + \tau \quad \text{.....(3.11)}$$

They further mentioned that for typical Pe ranges, τ (tortuosity for fracture) can be neglected.

The Taylor dispersion coefficient defined for parallel plate fracture is: (Taylor, 1953; Aris, 1956; Fischer et al., 1979)

$$D_{L,Taylor} = \frac{1}{210}\frac{V^2 b^2}{D_m} \quad \text{.....(3.12)}$$

$$\frac{D_{L,Taylor}}{D_m} = \frac{1}{210}\frac{V^2 b^2}{D_m^2} \quad \text{.....(3.13)}$$

A version of this chapter has been published
Trivedi J. and Babadagli T., 2008. Chemical Eng. J. doi:10.1016/j.cej.2008.05.032.

$$D_{L,Taylor} = \frac{D_m}{210} * (Pe)^2 \quad \text{.....(3.14)}$$

In our case, we assumed $D_L \ \alpha \ (Pe)^{1.5}$, an average value of Taylor and microscopic dispersions, and used this calculated value for the dispersion coefficient in fracture. The value of D_m in our set of experiments will be the mutual diffusion coefficient of heptane and particular oil type. It is 3.2×10^{-9} m^2/s and 3×10^{-8} m^2/s for heptane-mineral oil and heptane-kerosene, respectively.

3.5 Mass Transfer Rate Constant and Effective Diffusion into Porous Matrix

In simple terms, mass transfer is moving of fluid material from one point to another. For porous media it is the getting the material into and out of pores. Also for reactive process, the speed at which a chemical reaction proceeds, in terms of amount of product formed or amount of reactant consumed is also important. When there is no reaction, transfer rate is mostly due to diffusion and mixing. This transfer rate between two fluid pairs, solvent and solute, is presented by mass transfer rate constant (K_v). The increase of K_v indicates better mixing of solvent and solute, which results in faster approach to equilibrium conditions.

Figure 3.12 clearly suggests that K_v is related to velocity, solvent-solute properties, and matrix properties as well as aging. Increase of velocity results into rapid circulation, enhanced mixing and better mass transfer. It is also evident that with the same type of cores and aging time, the increase in K_v is controlled mainly by the velocity **(Figure 3.12)**. As the velocity increases, the rate constant value increases and the values vary from each other with considerable margin.

A version of this chapter has been published
Trivedi J. and Babadagli T., 2008. Chemical Eng. J. doi:10.1016/j.cej.2008.05.032.

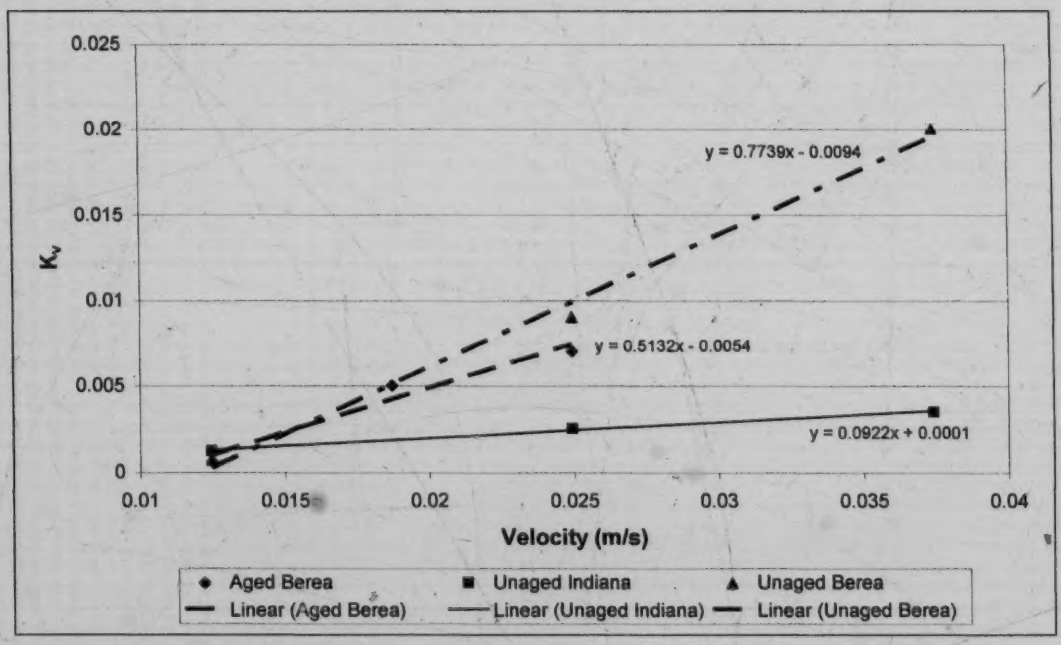

Figure 3.12: Mass transfer rate constant with velocity.

Different amount of solute recoveries were observed when cores were aged for different periods of time after complete saturation **(Figures 3.6** and **3.7)**. Though there is no water present in core samples, this can be interpreted as wettability change. To quantify the effect of aging time (or wettability change), we used spontaneous water imbibition data presented by Hatiboglu and Babadagli (2004) and Trivedi and Babadagli (2008a) and on the same core and oil types based on Handy's approach (1960).

$$Q_w^{\,2} = \left(\frac{2P_C \kappa_w \phi A^2 S_w}{\mu_w} \right) t \qquad \text{.....(3.15)}$$

The initial slop of the straight line from Q^2 against time were measured and normalized against the highest slope to obtain the P_c (known as effective capillary pressure). The changing slope reflects changing wettability caused by the aging as all other rock and fluid properties remained the same as observed by Trivedi and Babadagli (2008a).

The capillary pressures obtained from the experimental results of Hatiboglu and Babadagli (2004) and Trivedi and Babadagli (2008a) were normalized based on the capillary pressure of

A version of this chapter has been published
Trivedi J. and Babadagli T., 2008. Chemical Eng. J. doi:10.1016/j.cej.2008.05.032.

kerosene and multiplied with viscosity ratio of solvent to solute to get wettability factor Trivedi and Babadagli (2008a). To incorporate the effect of solute viscosity we defined the following dimensionless term (wettability factor, W_{factor}).

$$W_{factor} = \left(\frac{P_C}{P_{CK}}\right)\left(\frac{\mu_2}{\mu_1}\right) \quad \text{.....(3.16)}$$

P_c is obtained for each oil and rock type using Eq. 15 and P_{CK} is the P_c value for kerosene, which gives the highest slope due to its strong imbibition into matrix driven by its low viscosity.

To quantify the transfer rate constant for different wettability and porosity cores, it was represented as a function of velocity, wettability factor (W_{factor}), porosity of matrix, viscosity and density ratio of solute and solvent.

$$K_V = V * (W_{Factor})^{-0.15} * (\phi)^{0.9} * \left(\frac{\mu_2}{\mu_1}\right)^{0.06} * \left(\frac{\rho_2}{\rho_1}\right) \quad \text{.....(3.17)}$$

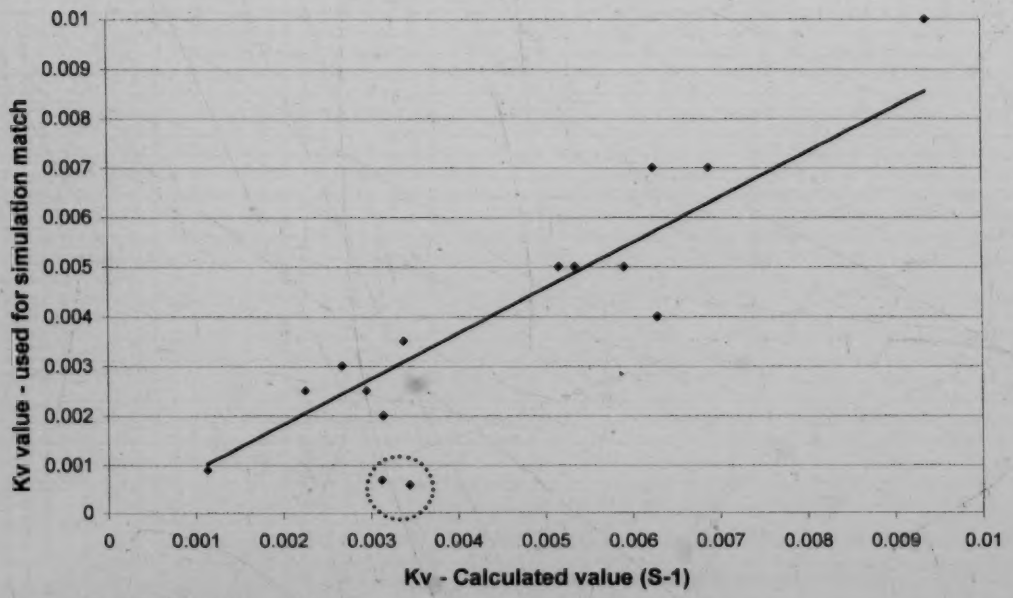

Figure 3.13: Comparison of the K_v (s^{-1}) values obtained through the numerical simulation and the ones obtained from Equation (3.17).

A version of this chapter has been published
Trivedi J. and Babadagli T., 2008. Chemical Eng. J. doi:10.1016/j.cej.2008.05.032.

Within porous media, the solute and solvent are transferred into and out of the pores by dispersion-diffusion mechanism. Since the solvent is injected into the fracture, there is no direct flow into the matrix porous media. Hence, we are not concerned with dispersion into the adjacent matrix. But there is an induced flow because of the flux transferred from the fracture at the interface and diffusion within the matrix. This complex process inside the porous media can be seen as an effect of dispersion into fracture and mass transfer between two fluids, solvent and solute. Therefore, the resultant effective diffusion coefficient into the porous media is not only because of tortuosity but also because of mass transfer rate constant and dispersion occurring into fracture.

This effective diffusion coefficient into the matrix is represented as a function of solvent and solute properties, rock properties, mass transfer rate constant and the Taylor dispersion coefficient as follows:

$$D_e^M = \sqrt{D_{L,Taylor} * \frac{\left(\frac{k}{K_V}\right) * \phi * \left(\frac{\mu_2}{\mu_1}\right)}{\left(\frac{\rho_2}{\rho_1}\right)}} \quad \text{.....(3.18)}$$

where k is the matrix permeability, K_V is the mass transfer rate constant, ϕ is the matrix porosity. The value of effective diffusion coefficient within the matrix (D_e^M) was one of the parameters tuned to obtain the match with experimental results of solvent concentration in the effluent. The effective matrix diffusion coefficient (D_e^M) calculated as shown above was in good agreement with that used during simulations **(Figure 3.14)**.

Note that the matrix size was not found critical in the correlations given in Eqs. 3.17 and 3.18. A good agreement was obtained for both shorter and longer samples as shown in **Figures 3.13** and **3.14**. The only two points off line in **Figure 3.13** are for the low rate (3 ml/hr) experiments. In those cases, the process is strongly controlled by the diffusion as the solvent has significantly more time to contact with matrix due to slow flow rate in the fracture. In other words, the effects of flow and diffusion in fracture are minimal.

A version of this chapter has been published
Trivedi J. and Babadagli T., 2008. Chemical Eng. J. doi:10.1016/j.cej.2008.05.032.

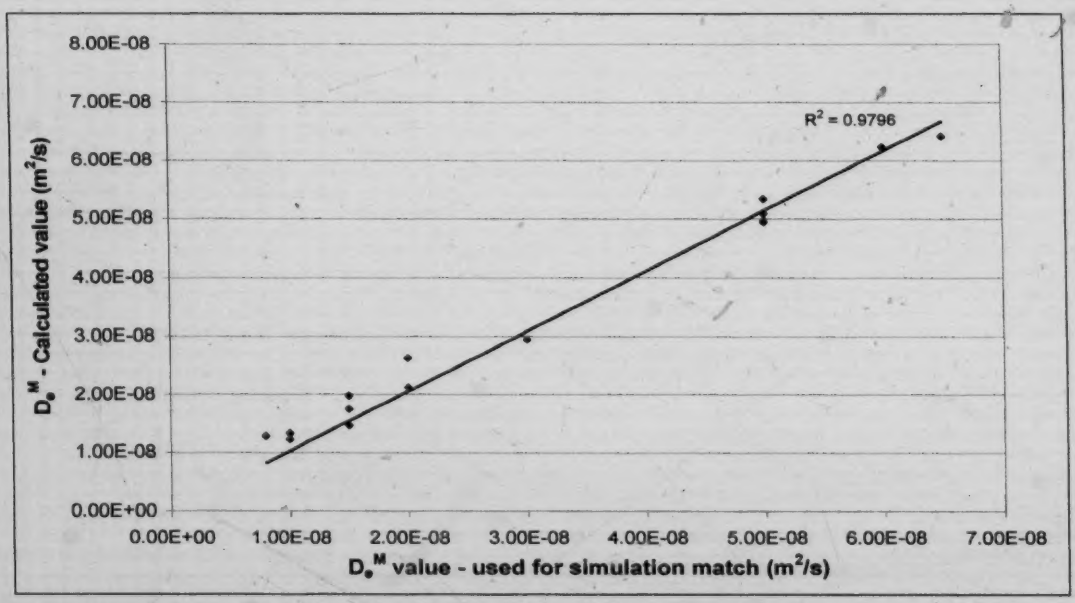

Figure 3.14: Comparison of D_e^M values used for the simulation matches with the ones obtained from Equation (3.18).

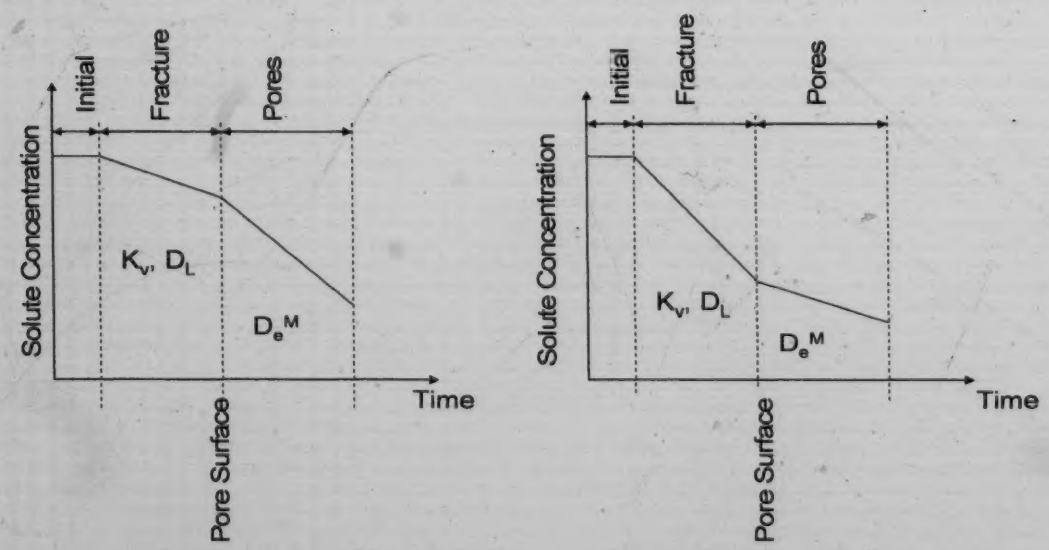

- Low velocity
- D_L is low, Less dominating (first period)
- K low

- High velocity
- D_L is High, More dominating (first period)
- K High

Figure 3.15: Concentration-time curves for matrix-fracture transfer at low and high rates.

A version of this chapter has been published
Trivedi J. and Babadagli T., 2008. Chemical Eng. J. doi:10.1016/j.cej.2008.05.032.

In our process, mass-transfer occurs in two different ways. One is in the fracture and it takes place between fluid mixtures until the oil in the fracture is exhausted. This process is controlled dominated by K_v and D_L. The second one is in the matrix pores and controls the remaining part of the process. This part is governed by K_v and D_e^M. This fact is well justified in the experimental results when the higher rate solute recovery curve dominates in the earlier period of time during which the essential solute fracture has been recovered. At later stages, dominated by D_e^M, the lower rate solute recovery curve overpasses the one with the higher rate suggesting the influence of pore diffusion. This process was schematically presented as the concentration-time curve in **Figure 3.15**.

3.6 Conclusions

1. The experimental results indicated that the recovery through the fracture is dominated by the Peclet number (dispersion effect) and mass transfer rate constant (K_V). Hence, at the earlier stage of the production life (when the fracture oil recovery is effective) higher rate solvent injection should be preferred.

2. Considering overall effect and assuming the solute inside the matrix pores is larger in amount compared to that in the fracture, the effective diffusion coefficient (D_e^M) is the major controlling parameter and slower rate solvent injection with more retention time for effective diffusive flux to transfer from matrix yields better recovery.

3. The porous media aged over a period of time behaved different than that of non-aged one depending on the solute properties. The wettability factor presented here and further used in the study proved handy tool for inclusion of aging effect.

4. Length of the matrix being one of the important parameter because of the solvent breakthrough was noticed during experiments. Shorter cores, having less time for solvent to diffuse in transverse direction into porous matrix, showed lower solute

A version of this chapter has been published
Trivedi J. and Babadagli T., 2008. Chemical Eng. J. doi:10.1016/j.cej.2008.05.032.

recovery in a given time and rate compared to the longer ones. This drives to the importance of fracture spacing and matrix size in field applications.

5. We, however, did not observe significant effect of matrix size on the mass transfer rate constant (K_V) and effective diffusion coefficient in matrix (D_e^M).

6. The mass transfer rate and effective matrix diffusion coefficient were found to be linearly dependent on the average fluid velocity in fracture and also affected by wettability as well as rock properties.

7. K_V and D_e^M, not available from any means of laboratory experiments, can be easily computed for miscible solvent processes in fractured porous media using the correlations provided here with fairly good amount of accuracy.

A version of this chapter has been published
Trivedi J. and Babadagli T., 2008. Chemical Eng. J. doi:10.1016/j.cej.2008.05.032.

4 EFFICIENCY ANALYSIS OF GREENHOUSE GAS SEQUESTRATION DURING MISCIBLE CO_2 INJECTION IN FRACTURED OIL RESERVOIRS

4.1 Introduction

One of the viable ways to sequester CO_2 is to inject it into partially depleted oil reservoirs as the cost of the sequestration process will be reduced by additional oil recovery. Co-optimization of the process, however, is needed and this requires the manipulation of reservoir conditions and associated factors/parameters that will lead to the best outcome of the process. The criteria for CO_2 use in enhanced oil recovery applications are well defined (Taber et al., 1997a & 1997b). CO_2 injection for enhanced oil recovery is applicable to a wide range of reservoir types including naturally fractured ones. It is critically important to test those types of reservoir for the suitability to storage as well. Several studies listed the reservoir screening criteria for CO_2 sequestration in geological environments (Bachu, 2002; Kovscek, 2002; Jessen et al., 2005). Some of them (Kovscek, 2002; Jessen et al., 2005) scrutinized the conditions for CO_2 storage during enhanced oil recovery (EOR) applications based on static reservoir conditions and oil/injectant properties. More investigation, especially parametric analysis, is needed for dynamic conditions. This approach will eventually lead to define the conditions for an efficient application of CO_2 injection for sake of oil recovery and storage.

We propose a parametric analysis using dimensionless groups to define the conditions for efficiency of the process in this study. Similar analyses were proposed before for enhanced oil recovery by miscible injection into non-fractured medium. Scaling of miscible and immiscible processes using inspectorial analysis also led to better understanding of the process based on the dimensionless groups associated (Gharbi et al., 1998; Gharbi, 2002; Kulkarni and Rao, 2006; Wood et al., 2006; Grattoni et al., 2001). Kulkarni and Rao (2006) presented the effect of major dimensionless groups on the final recovery based on various miscible and immiscible gas assisted gravity drainage field data and laboratory experimental data. Wood et al. (2006) derived dimensionless groups for tertiary EOR using CO_2 flooding

A version of this chapter has been published
Trivedi J. and Babadagli T., 2008c. Env. Sci. and Tech.

in water flooded reservoirs and presented a screening model for EOR and storage in the Gulf Coast reservoirs. Yet, less has been listed about fractured reservoirs especially with the flow conditions taken into consideration. In order to test the efficiency of such process, new dimensionless groups need to be defined. This requires substantial amount of laboratory experiments and analytical/numerical analysis of the process. The analysis using the dimensionless groups (obtained from parameters affecting the process) will lead to the better understanding of the efficiency of CO_2 injection process for enhanced oil recovery and storage in naturally fractured reservoirs.

4.2 Background

Previously we had performed experiments to clarify the effective parameters on the mass transfer during solvent injection into fractured systems (Trivedi and Babadagli 2006). The work was mainly focused on generalizing the effects of flow rate, matrix, fracture and fluid properties, and gravity to obtain a diffusion driven matrix-fracture transfer function and to propose a critical injection rate for an efficient miscible displacement. We had defined dimensionless fracture-matrix index (FDI) as a performance indicator. The FDI $(\frac{\sqrt{k_f} * v * f(\theta) * \rho_s}{k_m * D * \rho_o})$ is the ratio of viscous terms effective in the fracture (v is the volumetric injection rate of the diffusing phase, $f(\theta)$ is the function of wettability, and k_f is fracture permeability) and the diffusive matrix-fracture interaction term effective in the matrix (k_m is matrix permeability, D is the diffusion co-efficient between oil and solvent). ρ_o and ρ_s and are the oil and solvent densities, respectively. This term was correlated to the ratio of total oil produced to total solvent injected. Further, we extended the study with additional experiments to account for the effect of oil viscosity and matrix length (Trivedi and Babadagli, 2008a). To simplify the understanding of diffusion drive mechanism we used first contact miscible solvent-solute pairs and neglected capillary-driven crossflow. Heptane was used as a solvent to mimic the miscibility behavior of CO_2 with oil phase as a commonly encountered process during enhanced oil recovery applications.

The model consists of a core with a single artificial fracture. We used different flow rates of 3ml/hr, 6ml/hr and 9 ml/hr for the horizontal experiments, and 1 ml/hr, 3 ml/hr and 6

A version of this chapter has been published
Trivedi J. and Babadagli T., 2008c. Env. Sci. and Tech.

ml/hr for the vertical experiments. Rock types used were Berea sandstone (k= 500 md; = 0.21) and a few Indiana limestone (k= 15 md; = 0.11) samples. Three different types of oil, namely, kerosene (2.1 cp viscosity and 0.81 g/cc density) mineral oil (33.5 cp viscosity and 0.83 g/cc density), and heavy mineral oil (150 cp viscosity and 0.85 g/cc density), were used. Also a few experiments were performed with Berea sandstone aged over longer period of time after saturating with oil to see the effect of aging time that alters the wettability of the rock sample. All the experiments were performed at room temperature and pressure to nullify the crossflow/mass transfer due to pressure drive. For details about the experimental study and the results, readers are referred to the relevant publication (Trivedi and Babadagli, 2008a).

In the succeeding study, we modeled the experiments using finite element (Trivedi and Babadagli, 2008b) and obtained the process parameters governing the convection-diffusion equation. Result of few of the experiments in **Figure 4.2(a)** while the matches for the experimental and simulation results of oil (solute) produced against time are shown in **Figure 4.2(b)**. The values of diffusion coefficients and rate of mass transfer constants obtained from the simulation results are used in this paper. In this paper, we focused on the efficiency of oil recovery and storage processes and formulated it using dimensionless groups and the term called global effectiveness factor.

4.3 Dimensionless Parameters and the Effectiveness Factor for Matrix-Fracture Interaction by Diffusion during Injection of a Miscible Phase

In addition to diffusive resistance due to matrix, strong concentration gradients traverse to the direction of flow may occur in the fracture-matrix system. These gradients arise as a combination of the laminar channel flow in fracture and high rates of reaction at the wall of matrix. Under these conditions the concentration at the matrix-fracture interface may be significantly lower than the average concentration in the bulk fluid (the fluid-solid interface may be significantly lower than). These concentration values are used to calculate the well-known Sherwood number:

$$Sh = \frac{2R}{(< C_A > - C_{AW})} \left.\frac{\partial C}{\partial r}\right|_{r=R} \qquad \text{(4.1a)}$$

A version of this chapter has been published
Trivedi J. and Babadagli T., 2008c. Env. Sci. and Tech.

where,

$$< C_A >= \frac{\int_0^R v_z(r) C_A(r) r \partial r}{\int_0^R v_z(r) r dr} \quad \text{.....(4.1b)}$$

The Sherwood number (Sh) is a function of axial position z and varies along the length of the channel (fracture) as the concentration profile develops. Mass transfer coefficient or Sh has a higher value where the concentration boundary layer is developing. It decreases along the length of the channel approaching an asymptotic value Sh_∞ as z approaches the concentration entry length. The asymptotic value corresponds to the fully developed concentration profile. In our simulations, we calculated the value of Sh at the exit or production end at the end of the production life.

In addition to the equations listed above, we used some dimensionless terms and numbers as given in right column of **Table 4.1** in developing the global effectiveness factor. The Biot number (Bi_m) is a ratio of convective to diffusive mass transfer. For the same characteristic length and effective diffusion coefficient, the value of K_m, mass transfer coefficient, is indicative of convective to diffusive transfer. It is noted that, as the flow rate increases, the value of K_m and hence the value of the Biot number increases, which indicates the reduction of diffusive transfer. From the value of the Sherwood number, mass-transfer coefficients and the Biot numbers were calculated. For this purpose, the Sherwood number is obtained from Eqs. (4.1-a & 4.1-b). Then, the K_m, mass transfer coefficient, is obtained using the following form of the Sherwood number:

$$Sh = \frac{K_m d_h}{D_L} \quad \text{.....(4.2-a)}$$

Once the K_m term is found, the Biot number is obtained using the following equation as given also in **Table 4.1**:

$$Bi_m = \frac{K_m L_{TF}}{D_L} = \frac{t_{TM}}{t_M} \quad \text{.....(2-b)}$$

Another dimensionless term used in this analysis is the Thiele modulus, ϕ_L (see Table 4.1). It provides a convenient measure of the importance of diffusion on the apparent conversion rates. The Thiele modulus is a square root ratio of transverse diffusion time for matrix (t_{TM}) to the reaction time (t_R). When the diffusion is slow (i.e., $\phi_L >> 1$), transport limitations make the measured overall reaction rates slow compared to the intrinsic reaction rates.

The local Damkohler number (Da_L) is the same as surface Thiele modulus (ϕ_S^2) and it is presented as:

$$Da_L = \phi_S^2 = \frac{L_{TM} L_{TF} K_V}{D_L} \quad \text{.....(4.3)}$$

If the Thiele modulus is less than one, it indicates that diffusion does not play an important role in overall reaction rate. The reaction kinetics for all the experiments performed here fall well into the diffusion limited region (>1).

The Thiele modulus is useful in assessing the relative importance of diffusion but a more direct indication of the degree to which diffusion, matrix dimensions and shape influence the overall reaction rate is the effectiveness factor. For simple kinetics, the local effectiveness factor depends on the local Thiele modulus. The generic solution for the effectiveness factor can be approximated in one dimension using the analytical solution for an isothermal flat plate (Froment and Bischoff, 1990):

$$\eta_L = \frac{\tanh(\phi_L)}{\phi_L} \quad \text{.....(4.4)}$$

where η_L is defined as local effectiveness factor.

The effectiveness factor of unity indicates that diffusion is not important, whilst a value less than one indicates that diffusion limitation is occurring. The effectiveness factor can exceed unity in non-isothermal cases and complex kinetics.

For first order isothermal systems, the global (η_G) and local (η_L) effectiveness factors are related by,

$$\frac{1}{\eta_G} = \frac{1}{\eta_L} + \frac{\phi_L^2}{Bi_m} \quad \text{.....(4.5)}$$

As explained before, the Biot number is obtained using the Eqs. 4.1 through 4.2-a. The η_L is obtained from Eq. 4.4 using ϕ_L which is given in **Table 4.1**. Trivedi and Babadagli (2008b) obtained K_L by matching the experimental results to the solution of the diffusion-convection equations for fracture and matrix. They also derived an equation for the K_L as functions of phase densities and viscosities, porosity, wettability factor (given in Eq. 4.6 below), and velocity of the solvent injected in the fracture.

The effectiveness factor decreases as the thickness of the porous media increases. This is due to higher mass transfer resistance inside the porous media. The concentration gradients are much higher in fluid phase (from center of fracture to boundary between matrix and fracture) than inside of the matrix (from boundary of matrix and fracture to matrix outer wall). This indicates that the overall reaction rate is mostly limited by interphase diffusion.

Small values of η (< 0.01) indicate a fast intrinsic reaction rate and severe diffusive limitations to mass transfer. The slightly larger effectiveness factor (and thus smaller) can be attributed in part to faster diffusion of reactant species within the system.

When the global effectiveness factor is plotted against the ratio of Total Solute Produced (TSP) and Total Solvent Injected (TSI) **(Figure 4.3)**, it shows an increasing trend and very good match with power law fit for all experimental points. The slower rate causes more time for solvent to diffuse into matrix saturated with solute (oil). This results in lower gradient in the transverse direction and lower values of mass transfer coefficient as well as lower Sherwood number. This eventually leads to higher effectiveness factor. The higher rate processes work the other way and results into lower effectiveness factor. If the purpose of the injection is purely enhanced oil recovery, it is desired to maximize the recovery with minimized injected solvent. The maximum (TSP/TSI) occurred around the value 0.22 to 0.25 of global effectiveness factor in our study.

In case of the injection of (miscible) greenhouse gases such as CO_2 (or flue gas) or contaminant transportation, the injected material is desired to be stored in the matrix of

reservoir instead of being transported through fracture network. Therefore, the process needs also to be evaluated in terms of the amount stored in the rock matrix. It is noticeable that a similar trend was observed when effectiveness was plotted against the ratio of Total Solvent Stored (TSS) and TSI **(Figure 4.4)**. As similar to **Figure 4.3**, the power-law behavior was evident. The value of global effectiveness factor here was also in a range of 0.22 to 0.25 for maximization of (TSS/TSI).

4.4 Effective Parameters and Efficiency Correlations

We went one step further and correlated the effective parameters to two different efficiency indicators; (TSP/TSI) and (TSS/TSI) for generalization purposes. In this exercise we considered fluid density, fluid viscosity, porosity of the matrix, solvent injection rate, wettability of the rock material, matrix size, diffusion coefficient and mass transfer rate. The final equations were presented in terms of dimensionless groups and parameters.

In chapter 3, we had quantified the effect of aging time and defined the following dimensionless term (wettability factor, W factor).

$$W_{factor} = \left(\frac{P_C}{P_{CK}}\right)\left(\frac{\mu_2}{\mu_1}\right) \quad \text{.....(4.6)}$$

P_c is an "effective capillary pressure" representing the wettability of the sample. The P_{CK} is the P_c value for kerosene, which is the lightest oil we used in the experiments and represents the most water wet case due to its strong imbibition into matrix driven by its low viscosity. Therefore, the (P_c) term is normalized as to the kerosene having unity for this oil type and lower values for the other (heavier) oil samples. Details on the derivation and use of Eq. 4.6 can be found in chapter 3. It is important to note that though there is no water phase present in our experiments of first-contact miscible flooding, a difference in oil recovery was noticed for core samples saturated with mineral oil over different periods of time. It is believed that this was mainly due to the nature of oil (existence of polar groups) and its interaction with the rock surface causing changes in the pore structure or surface characteristics (desorption, acidic effect etc.). To quantify this effect the term W_{factor} is introduced.

A version of this chapter has been published
Trivedi J. and Babadagli T., 2008c. Env. Sci. and Tech.

We also included the Reynolds number (*Re*) and Peclet number (*Pe*), besides the global effectiveness factor and wettability factor and applied multivariable regression analysis to obtain a relationship between the efficiency indicators [(TSP) / (TSI) and (TSS) / (TSI)] and dimensionless groups described above.

The following equations show those relationships:

$$(TSP)/(TSI) = (\mathrm{Re})^{-0.15} * (Pe)^{0.009} * (\eta_G)^{0.75} * (W_{factor})^{-0.03} \quad \text{..... (4.7)}$$

$$(TSS)/(TSI) = (\mathrm{Re})^{0.04} * (Pe)^{0.09} * (\eta_G)^{0.6} * (W_{factor})^{-0.03} \quad \text{..... (4.8)}$$

Figures 4.5 and **4.6** display the comparison of the experimental values of the efficiency indicators and calculated values using Eqs. 4.7 and 4.8, respectively. **Figure 4.7** shows % error lines in the (TOP/TSI) predicated results with the one obtained from experiments. All the points are within the range of 20% error except two points at very low TOP/TSI values. Similarly in (TSS/TSI) values shows less than 20% prediction error, except one point shown by red circles. Considering 10% experimental error, the predicted values fall very much into the reliable range.

Total solute produced per total solvent injected is critical in enhanced oil recovery and this ratio defines the efficiency of the process. The effect of diffusion has been included in effectiveness number and the rate of mass transfer constant directly relates to velocity. Thus, the two major parameters driving the flow dynamics, diffusion coefficient and velocity, are incorporated in a single dimensionless number – the effectiveness number. The Peclet number has negligible influence while the Reynolds number has inverse relation but influence is still very less compared to effectiveness factor and these influences are only because of parameters other than diffusion coefficient and velocity. The Peclet number and Reynolds number effect have been included in effectiveness factor and therefore they have relatively very low impact on the TOP/TSI and TSS/TSI. The controls the efficiency of the process as can be inferred from the correlation given in Eq. 4.7 and is related to the Sherwood number and the mass transfer Biot number as described earlier.

A version of this chapter has been published
Trivedi J. and Babadagli T., 2008c. Env. Sci. and Tech.

Total solvent stored in the matrix per total solvent injected is critical in greenhouse gas sequestration and groundwater contamination (or waste disposal). In this case, Eq. 4.8 defines the efficiency of the process.

Noticeably, the global effective factor has the greatest influence among all. Though the power terms of W_{factor}, Re and Pe weigh low comparably, they are someway affecting the final result.

4.5 Summary and Discussion

The global effectiveness factor, defined as functions of the mass transfer Biot number and the Sherwood number, is the major governing parameter in obtaining the optimal value of the solute produced and solvent stored. Incorporation of different parameters evaluated into dimensionless numbers has led us to obtain an optimal value of effectiveness factor which maximizes the ratio of TSP/TSI as well as TSS/TSI. This effectiveness factor is in the range of 0.22 to 0.25.

The net effect of various dimensionless numbers associated with the process such as, the Reynolds, Peclet, and Sherwood numbers and wettability factor, has been represented in form of empirical equation for maximizing TSP/TSI as well as TSS/TSI. Given the fluid pairs, reservoir properties, flow condition and diffusion/mass transfer parameters (K_l and D_e^M) calculated from simulations or empirical equation (see Trivedi and Babadagli 2008b for the correlations for these two values); one can easily check the efficiency of the process using correlations in Eq. 4.7 and Eq. 4.8. Though the effectiveness factor and equations may vary for different case of particular solvent or tracer and solute or water/oil, they depict the ease of efficiency checking tool.

The correlations presented here could also be tested with different solvent and solute pairs. The experiments were conducted at the atmospheric conditions; results may differ with application of pressure drive. In this work, we have not varied the matrix size. The optimal height of the matrix for effective solvent transfer could be studied separately. Only a few experiments were done with limestone. A wider range of porosity/permeability could also be tested.

A version of this chapter has been published
Trivedi J. and Babadagli T., 2008c. Env. Sci. and Tech.

Table 4.1. Time-scales and dimensionless number associated with our physics similar to that of monolith (Bhattacharya et al. 2004).

Convection time	$t_C = \frac{L}{< u >}$	**Biot number**	$Bi_m = \frac{K_m L_{TF}}{D_L} = \frac{t_{TM}}{t_M}$
Transverse diffusion time into fracture	$t_{TF} = \frac{L_{TF}^2}{D_L}$	**Sherwood number**	$Sh = \frac{K_m d_h}{D_L}$
Transverse diffusion time into matrix	$t_{TM} = \frac{L_{TM}^2}{D_e^M}$	**Reynolds number**	$\mathrm{Re} = \frac{\rho V d_h}{\mu}$
Reaction (Mixing) time	$t_R = \frac{1}{K_V}$	**Peclet number**	$Pe = \frac{V\ b}{D_m}$
Mass transfer time into matrix	$t_M = \frac{L_{TM}^2}{K_m L_{TF}}$	**Local Thiele modulus** (first order)	$\phi_L = L_{TM}\sqrt{\frac{K_V}{D_e^M}} = \sqrt{\frac{t_{TM}}{t_R}}$

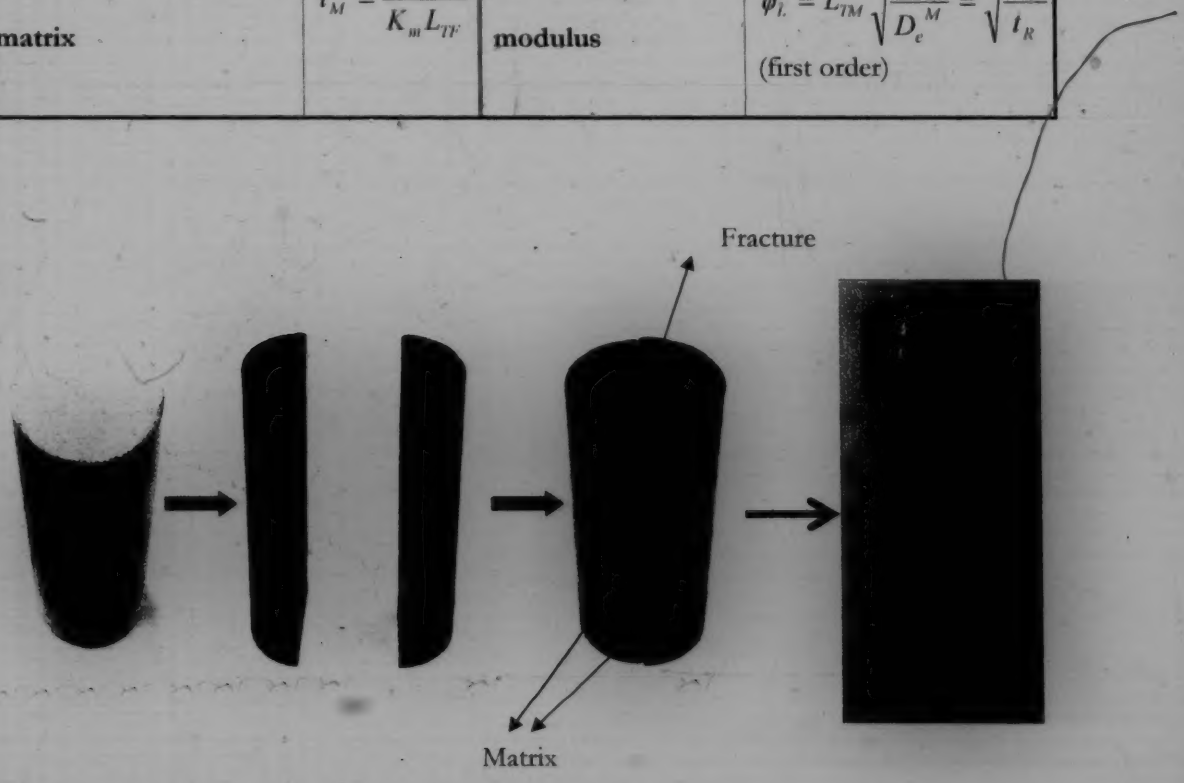

Figure 4.1(a): Core cutting/fracture preparation and core holder assembly

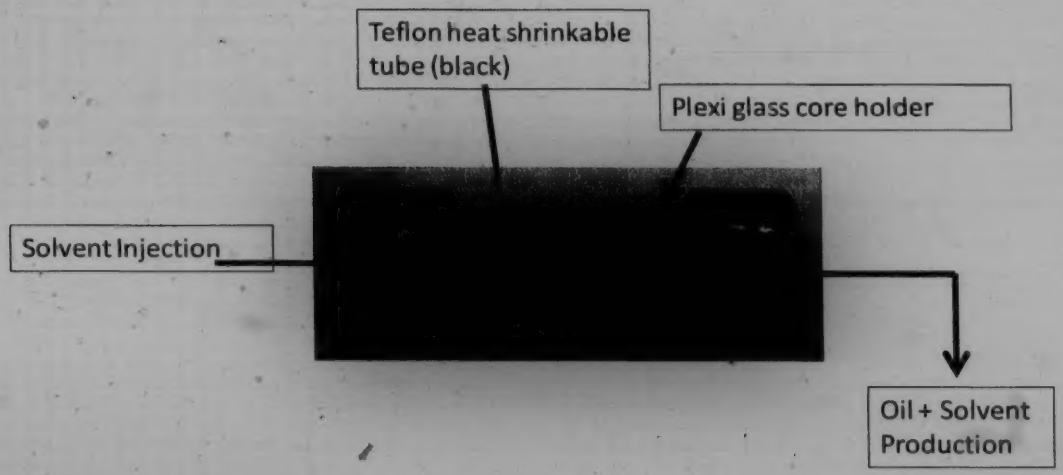

Figure 4.1(b): Core holder design

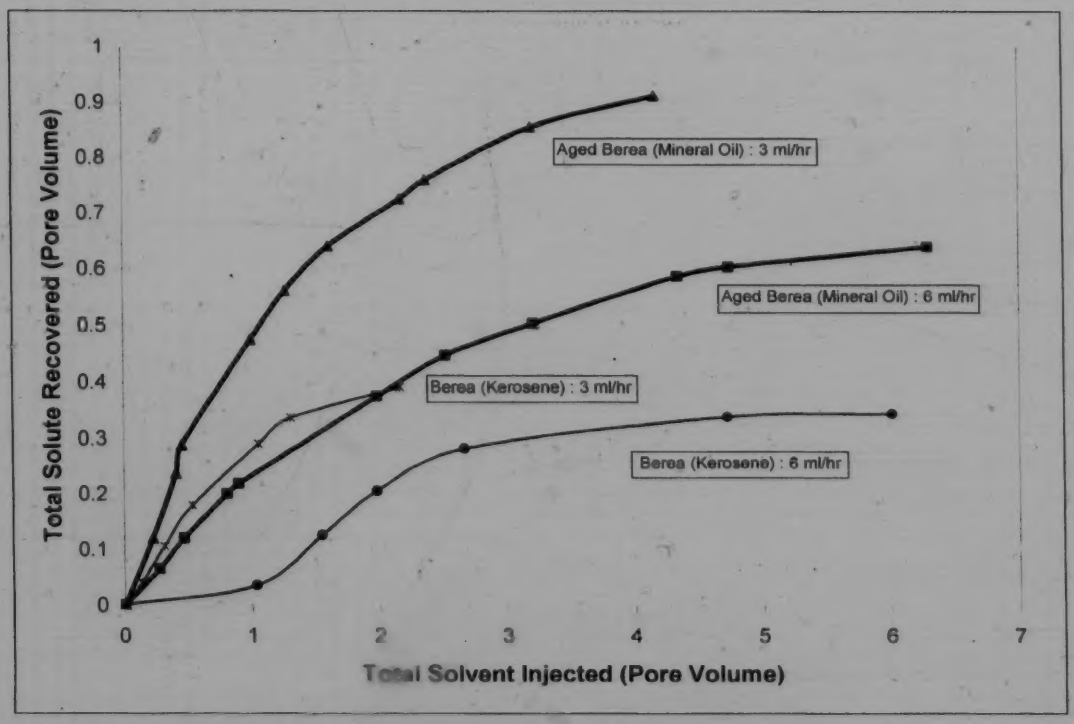

Figure 4.2(a): Recovery of solute (oil) with injection of miscible solvent (heptane)

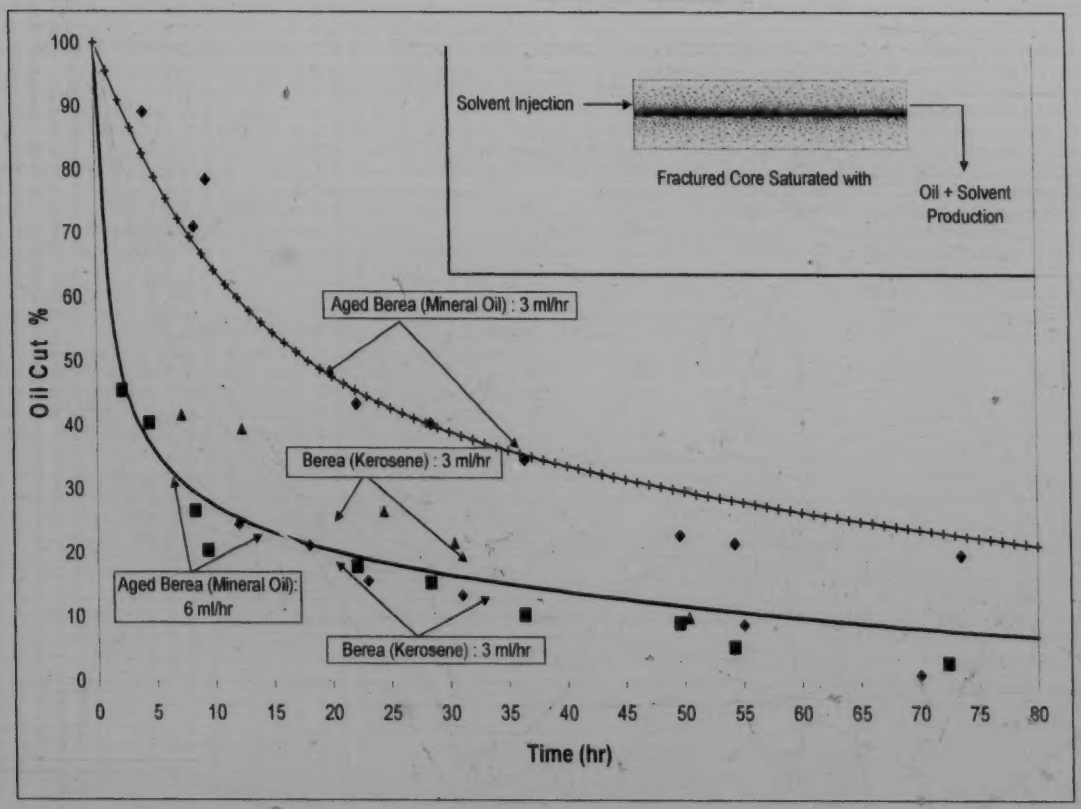

Figure 4.2(b): Simulation match (solid lines) with experimental results (symbols)

A version of this chapter has been published
Trivedi J. and Babadagli T., 2008c. Env. Sci. and Tech.

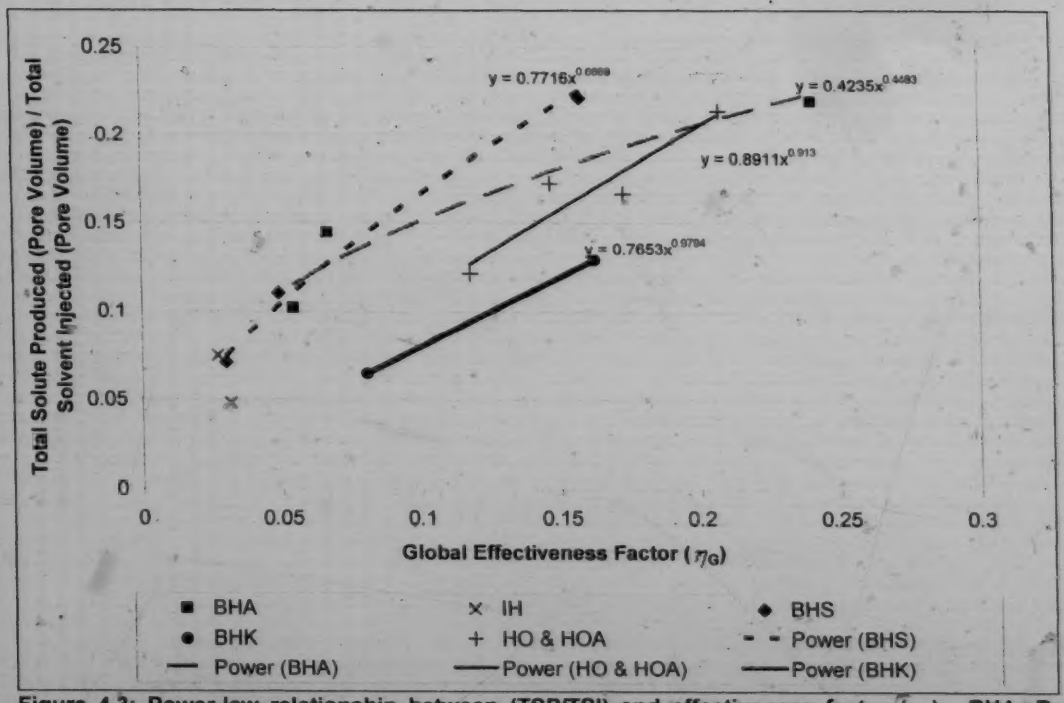

Figure 4.3: Power-law relationship between (TSP/TSI) and effectiveness factor (η_G). BHA: Berea sandstone-horizontal-mineral oil-aged, IH: Indiana limestone-horizontal- mineral oil, BHS: Berea sandstone-horizontal-mineral oil, BHK: Berea sandstone-horizontal-kerosene, HO: Heavy (mineral) oil, HOA: Heavy (mineral) oil-aged.

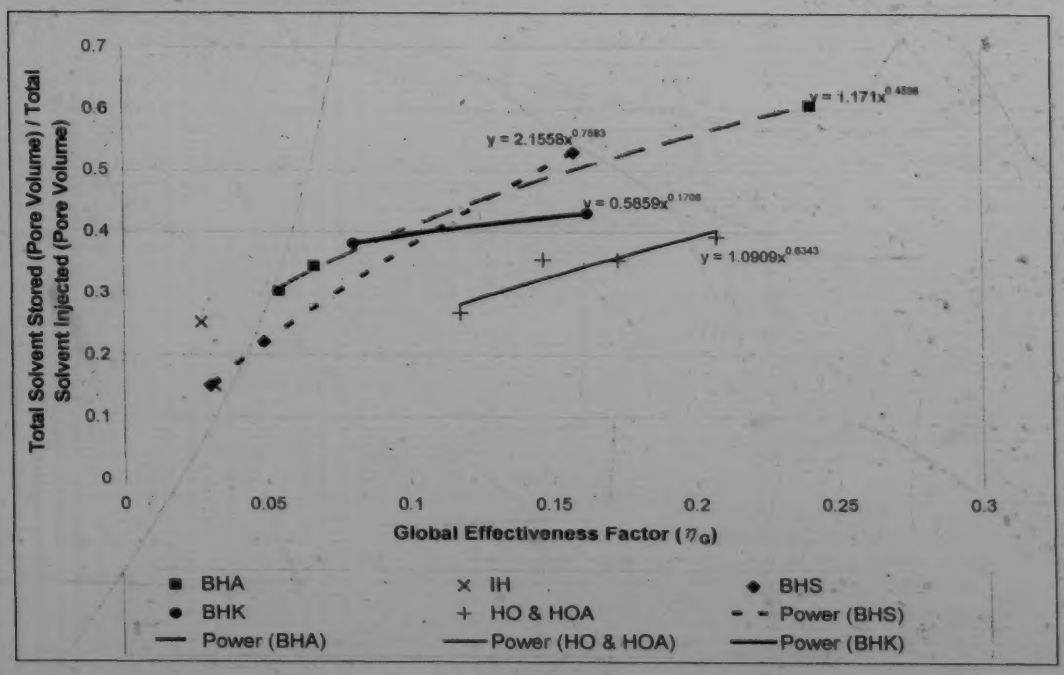

Figure 4.4: Power-law relation of (TSS/TSI) with effectiveness factor (N_G) [Legend as given in Figure 4.3].

A version of this chapter has been published
Trivedi J. and Babadagli T., 2008c. Env. Sci. and Tech.

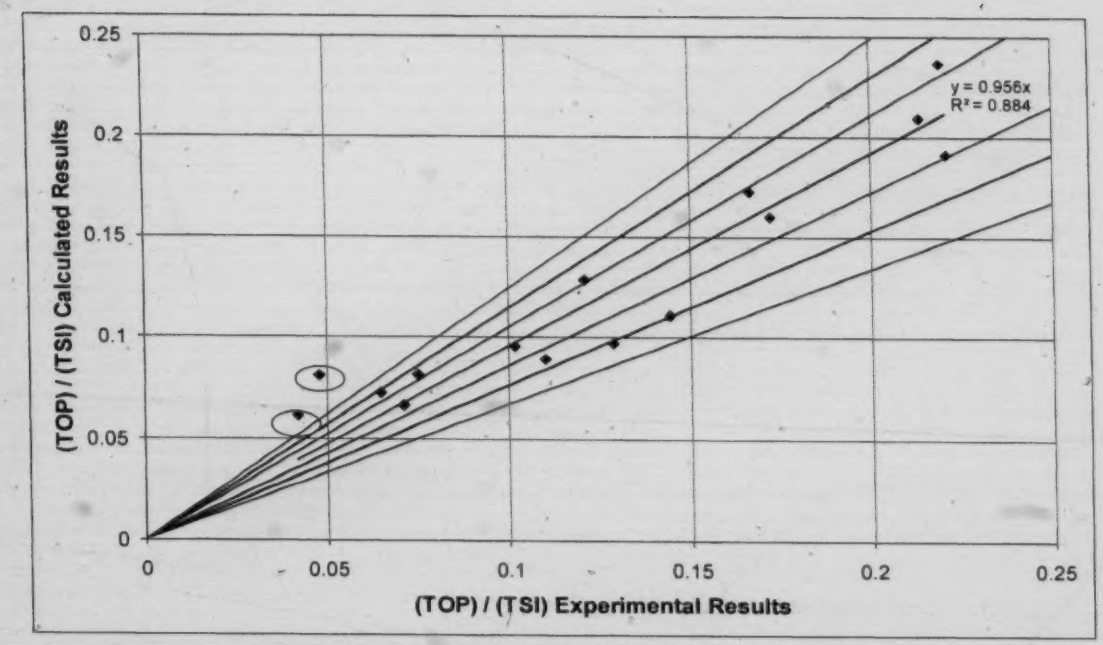

Figure 4.5: Comparison of (TSP/TSI) experimental value and the one obtained from Equation (4.7) [% error showing 10, 20 & 30 % error in predicted values]

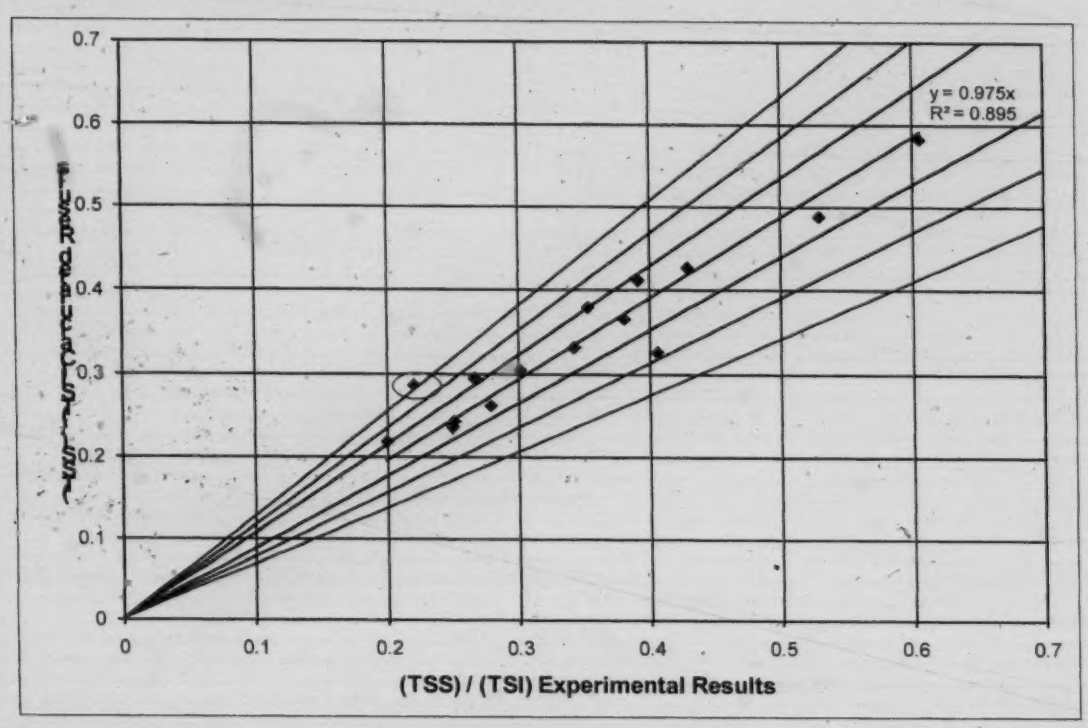

Figure 4.6: Comparison of (TSS/TSI) experimental value and the one obtained from Equation (4.8) [% error showing 10, 20 & 30 % error in predicted values]

A version of this chapter has been published
Trivedi J. and Babadagli T., 2008c. Env. Sci. and Tech.

5 SCALING MISCIBLE DISPLACEMENT IN FRACTURED POROUS MEDIA USING DIMENSIONLESS GROUPS

5.1 Background on Scaling Process

Scaling is a procedure of extrapolation of results obtained at one scale to another, usually from a small-scale laboratory observation to a large-scale process. Two different methods for obtaining dimensionless numbers can be found in the literature, Dimensional Analysis (DA) and Inspectional Analysis (IA).

5.2 Dimensional Analysis (DA)

The DA determines the minimum number and form of scaling groups based on the primary dimensions of any physical system (Fox and McDonald, 1998). The dimensionless groups will not predict the physical behavior of the system only but these groups can also be joined together to be easily interpreted physically. The experimental validation for the final form of physically meaningful dimensionless group has also been recommended (Fox and McDonald, 1998). The DA method does not require that the process being modeled be expressed by equations rather it is based on the knowledge of the pertinent variables affecting the process.

Historical developments in the field of fluid mechanics and dynamics point to dimensionless numbers as a mean of comparison. Two succinct and apparently different methods for obtaining dimensionless numbers can be found in the general fluid flow literature. General fluid dynamics literature (Johnson, 1998; Fox and McDonald, 1998) suggest DA, whereas petroleum related literature relies more on IA (Shook et al., 1992)

5.2.1 Inspectional Analysis (IA)

Dimensionless numbers obtained through the IA are generally considered to be more useful (Craig et al., 1957; Shook et al., 1992). The IA is the extension of the DA, where a final

A version of this chapter has been published
Trivedi J.J. and Babadagli T., 2008. J. Pet. Sci. Eng. doi:10.1016/j.petrol.2008.03.001.

dimensionless formulation is tested against the variables from which it has been developed. Unlike the DA approach, the IA is based on the set of differential equations that governs the process of interest with the initial and boundary conditions into dimensionless forms. The flow equations included in the analysis improve the description of the reservoir behavior. Because the flow equations neither alter the number of primary dimensions nor introduce new parameters to the system, the DA still holds. The primary goal of the IA on the expanded set of equations is to introduce the necessary boundary conditions. Boundary conditions can be introduced through the process of transformation from dimensional to dimensionless space or through later rearrangement of already developed dimensionless equations.

Both methods have certain advantages and disadvantages. The availability of the mathematical equations representing the process is essential in the IA. As the IA is based on the existing differential equation with acting boundary, it is a simpler and preferred method in petroleum engineering related literature.

Scaling of miscible and immiscible processes using inspectorial analysis also have led to better understanding of the process based on the dimensionless groups associated (Gharbi et al., 1998; Gharbi, 2002; Kulkarni and Rao, 2006a; Wood et al., 2006; Grattoni et al., 2001). Grattoni et al (1998) defined a new dimensionless group combining the effects of gravity and viscous forces to capillary forces. This group showed a linear relationship with the total recovery for all the scenarios tested. Kulkarni and Rao (2006a) presented the effect of major dimensionless groups on the final recovery based on various miscible and immiscible gas assisted gravity drainage field data and laboratory experimental data. Wood et al. (2006) derived dimensionless groups for tertiary enhanced oil recovery (EOR) using CO_2 flooding in waterflooded reservoirs and presented a screening model for EOR and storage in Gulf Coast reservoirs. Yet, less has been listed about fractured reservoirs especially with the flow conditions taken into consideration. Previously, we proposed a group, FDI (Fracture Diffusion Index), as a ratio of viscous forces in the fracture and diffusion forces in the matrix (Trivedi and Babadagli, 2006) using the analogy to capillary imbibition controlled immiscible displacement in fractured porous medium. In this study, we derived the groups affecting the miscible process and proposed a new dimensionless number with its physical significance towards the efficient recovery process.

A version of this chapter has been published
Trivedi J.J. and Babadagli T., 2008. J. Pet. Sci. Eng. doi:10.1016/j.petrol.2008.03.001.

5.3 Derivation of the Dimensionless Groups for Flow in Fractured Porous Medium

Figure 5.1 represents the matrix-fracture system (length = L and radius = 2r) with inlet, outlet as well as the boundary conditions. The pore space of the matrix is initially filled with a displaced fluid (C = 0) and is flooded with a displacing fluid (C = 1) from one side x = 0 at the center, where fracture (half aperture = b) is located. The displaced fluid is assumed to be dispersed uniformly into the porous matrix. It is assumed that both fluids, displacing and displaced, are incompressible and complete mixing across the fracture width takes place at all times. Both media has uniform properties. In this analysis, we do not impose any restriction on the geometric shape of the fracture, except that the cross section of the fracture is invariant with the axial position. The x-axis is the principle flow direction, while the y-axis is the direction perpendicular to the flow. The displacing fluid (solvent) flows/injected at constant rate through fracture at the inlet x = 0; there is no flow in the matrix surrounding fracture. The displacement is one-dimensional in two media. Under these conditions, Equations 5.1 to 5.5 can be written in scalar forms with the appropriate initial and boundary conditions. Equations 5.1 and 5.2 describe coupled one dimensional equation, one for fracture and the other for the adjoining porous matrix. For simplicity, we assumed no reaction between solvent and solute. Assuming the diffusive flux from fracture to matrix is acting perpendicular to the fracture, the coupling parameter between matrix and fracture are the continuity of fluxes and concentrations along the interface (Tang et al., 1981).

The equations associated with the process:

Fracture:

$$\frac{\partial C_F}{\partial t} + u_{Fx}\frac{\partial C_F}{\partial x} - D_L\frac{\partial^2 C_F}{\partial x^2} + \frac{\phi_m D_m}{b}\frac{\partial C_M}{\partial y} = 0 \quad \text{..... (5.1)}$$

For matrix:

$$\frac{\partial C_M}{\partial t} - D_m\frac{\partial^2 C_M}{\partial y^2} = 0 \quad \text{..... (5.2)}$$

A version of this chapter has been published
Trivedi J.J. and Babadagli T., 2008. J. Pet. Sci. Eng. doi:10.1016/j.petrol.2008.03.001.

$$u_{FX} = -\frac{k_F}{\mu_F}\left(\frac{\partial P_F}{\partial x} + \rho_F g\right) \quad \text{..... (5.3)}$$

$C_F = 0$ at t = 0 $\forall x, y$ ..... (5.4)

$u_{FY} = 0$ at y = 0 $\forall x, t$ ..... (5.5)

$u_{FY} = 0$ at y = b $\forall x, t$ ..... (5.6)

$$\frac{1}{b}\int_0^b u_{FX}\, dy = u_T \text{ At x=0} \quad \text{..... (5.7)}$$

$$P_F = P_{wf} + \rho_m g(b - y) \text{ at x=L} \quad \text{..... (5.8)}$$

Here C_F and C_M are the concentrations of solute in fracture and matrix, respectively, (M/L^3). $2b$ is the constant fracture aperture (L), r is the half fracture spacing (L), D_l represents the coefficient of hydrodynamic dispersion in the fracture (L^2/T), D_m is the effective molecular diffusion coefficient in the matrix (L^2/T), which includes the effect of tortuosity. The dependent and independent variables associated with the process are tabulated with their respective symbols and dimensions in **Table 5.1**.

A version of this chapter has been published
Trivedi J.J. and Babadagli T., 2008. J. Pet. Sci. Eng. doi:10.1016/j.petrol.2008.03.001.

Table 5.1: Dependent and independent variables, symbols and their dimensions.

Dependent and Independent Variables	Symbols	Dimensions	Dependent and Independent Variables	Symbols	Dimensions
Porosity (Fracture)	$\emptyset_F$	$M^0L^0T^0$	Porosity (Matrix)	$\emptyset_M$	$M^0L^0T^0$
Velocity	u_T	$M^0L^1T^{-1}$	Length of Fracture	L	$M^0L^1T^0$
Permeability (Fracture)	K_F	$M^0L^2T^0$	Permeability (Matrix)	K_M	$M^0L^2T^0$
Solvent viscosity	μ_s	$M^1L^{-1}T^{-1}$	Oil viscosity	μ_o	$M^1L^{-1}T^{-1}$
Solvent density	ϱ_s	$M^1L^{-3}T^0$	Oil density	ϱ_o	$M^1L^{-3}T^0$
Amount of solvent injected (Pore volume)	Q_I	$M^0L^0T^0$	Amount of solute produced (Pore volume)	Q_P	$M^0L^0T^0$
Fracture width	b	$M^0L^1T^0$	Matrix width	r	$M^0L^1T^0$
Diffusion Coefficient	D_{eff}	$M^0L^2T^{-1}$	Dispersion Coefficient	D_L	$M^0L^2T^{-1}$
Viscosity difference	$\Delta\mu$	$M^1L^{-1}T^{-1}$	Density difference	$\Delta\varrho$	$M^1L^{-3}T^0$
Gravity force	g	$M^0L^1T^{-2}$			

In this process, we will study the ratio of total oil produced and total solvent injected as the efficiency indication parameter. Hence, our goal is to find the dimensionless group which affects the objective function given below and maximize it.

$$(Q_P / Q_I) = f(\phi_F, \phi_M, K_F, K_M, v_T, \mu_S, \mu_O, \rho_S, \rho_O, \Delta\mu, \Delta\rho, L, b, r, D_{eff}, D_L, g) \quad \text{..... (5.9)}$$

With some simplifications,

The fluid densities and viscosities may be appropriately grouped together.

A version of this chapter has been published
Trivedi J.J. and Babadagli T., 2008. J. Pet. Sci. Eng. doi:10.1016/j.petrol.2008.03.001.

Since the solvent is injected into the fracture, the Darcy flow equation applies only to flow in fracture. Hence, the permeability of the matrix does not play a role into the set of equations representing the system.

$$(Q_P / Q_I) = f\left(\frac{\phi_F}{\phi_M}, K_F, v_T, \frac{\mu_O}{\mu_S}, \frac{\rho_O}{\rho_S}, \frac{\Delta\mu}{\mu_S}, \frac{\Delta\rho}{\rho_S}, \frac{L}{b}, \frac{L}{r}, \frac{D_L}{D_{eff}}, g\right) \quad \text{.....(5.10)}$$

This expression has no unique form. We have used the IA method to identify/derive the dimensionless groups associated with the process. The procedure of IA is presented in Appendix. Since the IA is a parameter rather than dimensions procedure, it can produce dependent dimensionless scaling groups. To remediate, Shook et al (1992) proposed writing the dimensional matrix for dimensionless groups in a form. They used linear (affine) transformations, which works well if the grouping and elimination of translation factors is physically meaningful. The eight dimensionless scaling groups obtained after applying this procedure are shown in the first column of **Table 5.2**. These scaling groups can be reduced further to obtain a set of independent dimensionless groups. The minimum numbers of independent scaling groups are equal to the rank of the non-square coefficient matrix. This method of minimizing the number of dimensionless scaling groups was suggested by Shook et al (1992). Logarithm of the eight groups originally obtained, shown in the first column of **Table 5.1**, are taken to make them linear. The rank of the resultant coefficient matrix is determined by the method of elementary row operations. Further reducing the groups and then exponentiation, the remaining dimensionless scaling groups are shown in second column of **Table 5.2**.

A version of this chapter has been published
Trivedi J.J. and Babadagli T., 2008. J. Pet. Sci. Eng. doi:10.1016/j.petrol.2008.03.001.

Table 5.2: Dimensionless groups derived using the Inspectorial Analysis.

Dimensionless groups after IA	Dimensionless groups minimized (suggested by Shook et al., (1992))
$\left(\frac{D_L}{Lu_T}\right)$	$\left(\frac{D_L}{D_m}\right)$ = (Dispersion diffusion ratio)
$\left(\frac{\phi_m D_m L}{bru_T}\right)$	$\left(\frac{\phi_m r}{L}\right)$ = (1/aspect ratio for matrix)
$\left(\frac{D_m L}{r^2 u_T}\right)$	$\left(\frac{D_m}{bu_T}\right)$ = (1/Pe)
$\left(\frac{\mu_S}{\mu_0}\right)$	$\left(\frac{\mu_S}{\mu_0}\right)$ = (1/M) = (1/Mobility factor)
$\left(\frac{k_F \Delta\rho g}{\mu_0 u_T}\right)$	$\left(\frac{\Delta\rho}{\rho_0}\right)$ = Density Number
$\left(\frac{k_F \rho_0 g}{\mu_0 u_T}\right)$	$\left(\frac{k_F \Delta\rho g}{\mu_0 u_T}\right)$ = Gravity Number
$\left(\frac{k_F \rho_0 g b}{\mu_0 u_T L}\right)$	$\left(\frac{b}{L}\right)$ = (1/Aspect ratio for fracture)
$\left(\frac{k_F \Delta\rho g b}{\mu_0 u_T L}\right)$	

$$(Q_P / Q_I) = f\left(\frac{D_L}{D_{eff}}, Pe, Ar_M, M, N_\rho, N_g, Ar_F\right) \quad \text{.....(5.11)}$$

5.4 New Dimensionless Number

None of the scaling groups individually can define the efficiency of the process of interest. Hence a new dimensionless group combining varying strength of all forces acting as different dimensionless groups during the process is necessary.

We propose here a new group, Matrix-Fracture Diffusion Number, ($N_{M\text{-}FD}$), by inverse multiplication of (G2), (G3) and (G6).

A version of this chapter has been published
Trivedi J.J. and Babadagli T., 2008. J. Pet. Sci. Eng. doi:10.1016/j.petrol.2008.03.001.

$$(1/N_{M\text{-}FD}) = \left(\frac{k_f \Delta\rho g}{\mu_0 u_T}\right)\left(\frac{D_m}{b u_T}\right)\left(\frac{\phi_m r}{L}\right) \quad \text{.....(5.12)}$$

Since,

$$\frac{D_{L,Taylor}}{D_m} = \frac{1}{210}\frac{u_T^2 b^2}{D_m{}^2} = \frac{1}{210}(Pe)^2 \quad \text{.....(5.13)}$$

The group (G1) is also indirectly incorporated in the expression 12.

$$(1/N_{M\text{-}FD}) = \left(\frac{k_f \Delta\rho g D_m}{\mu_0 u_T^2 b}\right)\left(\frac{\phi_m r}{L}\right) = \frac{Ng}{Pe}\frac{1}{Ar_M} \quad \text{.....(5.14)}$$

$$(N_{M\text{-}FD}) = \left(\frac{\mu_0 u_T^2 b}{k_f \Delta\rho g D_m}\right)\left(\frac{L}{\phi_m r}\right) = \frac{Pe * Ar_M}{Ng} \quad \text{.....(5.15)}$$

5.4.1 Similarity and Comparison with the Immiscible Process

Similar dimensionless groups were introduced using different techniques before for different purposes. Stubos and Poulou (1999) introduced a modified diffusive capillary number by taking the ratio of diffusion to capillary gradient driven rates. Their work mainly focused on drying of porous media with existence of two-phase.

$$\frac{D_{eff} * \mu_l * (C_e - C_o)}{\sigma * \rho_l * \sqrt{\phi k_m}} \equiv Ca_D \quad \text{.....(5.16)}$$

Babadagli and Ershaghi (1993) proposed a fracture capillary number ($N_{f,Ca}$) as the ratio of viscous to capillary forces for immiscible displacement in fractured systems. The fracture capillary number is a ratio of viscous forces active in fracture to the capillary forces active in matrix:

$$N_{f,Ca} = \frac{\sqrt{k_f} * V_T * \mu_w}{k_m * P_{c,\max}} \quad \text{.....(5.17)}$$

A version of this chapter has been published
Trivedi J.J. and Babadagli T., 2008. J. Pet. Sci. Eng. doi:10.1016/j.petrol.2008.03.001.

The derivation of Eq. 5.17 is based on the viscous forces effective in fractures and capillary forces in matrix. This ratio is given by

$$\frac{(V_T)(dy)(\mu_w)(dx)(b)}{(k_m * P_{c,\max})(dx)(dy)} \quad \text{.....(17-a)}$$

Where, *dx* and *dy* are fracture and matrix dimensions and *b* is the fracture width. Eq. 5.17 was obtained by replacing the term (b) by $\sqrt{k_f}$.

In a different study, Babadagli (2002) also showed a relationship between capillary imbibition recoveries while there is a constant rate flow in the fracture using a scaling group where he included the length of the matrix. This group was derived using Handy's equation (Handy, 1960) and the final form was

$$\left(\frac{V_T^{2} * \mu_w}{P_{c,eff} * k_m}\right)\left(\frac{L_y}{L_x}\right)^2 \quad \text{.....(5.18)}$$

The expression for the ($N_{M\text{-}FD}$) proposed here (Eq. 5.15) is similar to Eq. 5.18 and also to some extent to fracture capillary number, $N_{f,Ca}$ (Eq. 5.17), where the capillary forces are replaced by diffusive forces in the matrix with addition of gravity factor.

5.5 Validation of Proposed Group

5.5.1 Experiments

To validate the applicability of the new group proposed and its physical significance as well as its behavior, we preformed first contact miscible core scale experiments using heptane as solvent and mineral oil as solute. The process mimics miscible CO_2 injection in naturally fractured reservoirs. To analyze the effects of viscosity and density of the solute, we conducted some experiments with kerosene. Rock types used were Berea sandstone and Indiana limestone.

A version of this chapter has been published
Trivedi J.J. and Babadagli T., 2008. J. Pet. Sci. Eng. doi:10.1016/j.petrol.2008.03.001.

The procedure of the experimentation is as follows.

- The cores (6 inches in length and 2 inches in diameter) were cut into two pieces through the center in direction of longitudinal axis for the purpose of creating a fracture.
- The cut cores were weighed and fully saturated with oil under constant vacuum using vacuum pump for 48-72 hours to achieve maximum saturation. For aged experiments the saturation was time was over a period of a month.
- The weight of the cores after saturation was measured. Porosity was measured from the weight difference before and after saturation.
- The saturated two pieces were held together using heat-shrinkable rubber sleeves.
- The fractured core then placed into a plexiglas holder and the annular space was filled with silicon to ensure no flow to the annulus between the core and core holder.
- Solvent was injected at constant flow rates of 3ml/hr, 6ml/hr and 9 ml/hr for the horizontal experiments, and 1 ml/hr, 3 ml/hr and 6 ml/hr for the vertical experiments from the center of the core holder. The production lines were also placed at the center at the other end.
- The samples collected at the production end were analyzed using bench-type refractometer.

The experimental set-up is shown in **Figure 5.2**. The details of experiments performed are shown in **Table 5.3** with particular fluid type and rock properties used while the fluid properties are shown in **Table 5.4**.

A version of this chapter has been published
Trivedi J.J. and Babadagli T., 2008. J. Pet. Sci. Eng. doi:10.1016/j.petrol.2008.03.001.

Table 5.3: Experiments performed.

Case	Core Type	$Ø_M$	Solute (oil) Type	Flow rate (ml/hr)	L (inches)	Aged	Orientation
1	Sandstone	21%	MO	3	6	No	Horizontal
2	Sandstone	21%	MO	6	6	No	Horizontal
3	Sandstone	21%	MO	9	6	No	Horizontal
4	Sandstone	21%	MO	3	6	Yes	Horizontal
5	Sandstone	21%	MO	4.5	6	Yes	Horizontal
6	Sandstone	21%	MO	6	6	Yes	Horizontal
7	Sandstone	21%	MO	9	6	Yes	Horizontal
8	Sandstone	21%	Kerosene	3	6	No	Horizontal
9	Sandstone	21%	Kerosene	6	6	No	Horizontal
10	Sandstone	21%	MO	1	6	No	Vertical
11	Sandstone	21%	MO	3	6	No	Vertical
12	Limestone	11%	MO	3	6	No	Horizontal
13	Limestone	11%	MO	6	6	No	Horizontal

Table 5.4: Properties of solvent and solute used in experiments

	Chemical Name	Density (g/cc)	Viscosity (cp)	Refraction Index (RI)
Solvent	Heptane	0.68	0.410	1.3891
Solute	Mineral Oil (MO)	0.79	33.5	1.469
	Kerosene	0.81	2.1	1.475

A version of this chapter has been published
Trivedi J.J. and Babadagli T., 2008. J. Pet. Sci. Eng. doi:10.1016/j.petrol.2008.03.001.

In each case of the experiment performed, the amount of solvent injected and the amount of solvent and solute produced were monitored during the run time and later used for calculation.

5.6 Physical Significant of the Proposed Group and Analysis

The critical parameter defining the efficiency of the process could be the amount of solvent introduced per oil produced as in the case of enhanced oil recovery applications (the opposite is the case in greenhouse gas sequestration or groundwater contamination processes). The amount of solvent introduced into the system and the oil produced at the completion point of the process, i.e., when the recovery curve levels off and reaches its plateau, was found from the experimental results. This point was defined as TOP/TSI (Total Oil Produced (TOP) / Total Solvent Injected (TSI)).

The values of (TOP/TSI) were plotted against different dimensionless group. **Figure 5.3** shows normalized oil production (TOP/TSI) with respect to amount of solvent injected as a function of the Gravity Number (Ng). A trend (TOP/TSI increasing with the gravity number) is observed but the points are scattered. It was also noticed that the (TOP/TSI) increased as the Peclet Number (*Pe*) decreases **(Figure 5.4)**. Both N_g and *Pe* have significant impact on (TOP/TSI) and their effects are opposite to each other. From **Figures 5.3** to **5.5** it is clear that N_g, *Pe* or combination of both alone are not sufficient enough to represent the efficiency of the process through a strong correlation.

Assuming the dispersion through the fracture is Taylor type dispersion, the first dimensionless group shown in column two of **Table 5.2**, dispersion-diffusion ratio, can also be presented in the form of the Peclet number (*Pe*). When plotted against the ratio (TOP/TSI) for all the experiments performed, the newly proposed dimensionless number, $N_{M\text{-}FD}$, in Eq. 5.15 showed a trend with a power law behavior as shown in **Figure 5.6**.

Viscous flow is dominant in the fracture while the diffusion process accounts for the mass-transport from fracture to the matrix. When applied at high solvent injection rate, after a quick recovery of the fracture oil through viscous flow, the solvent breaks through. The recovery from matrix is slower compared to the lower rates due to less contact time with the

A version of this chapter has been published
Trivedi J.J. and Babadagli T., 2008. J. Pet. Sci. Eng. doi:10.1016/j.petrol.2008.03.001.

matrix in order for the diffusion into matrix to take place. This yields a higher ($N_{M\text{-}FD}$). In the case of lower injection rates, the diffusion dominates the recovery resulting in lower ($N_{M\text{-}FD}$). Hence, higher $N_{M\text{-}FD}$ indicates a faster recovery with more solvent injection. On the other hand, a low value of the ($N_{M\text{-}FD}$) is an indication of slow but more efficient recovery, i.e., less solvent injection is required. This might even yield higher ultimate recoveries from the matrix compared to the extremely high injection rate cases. Hence, one needs to define a critical rate or critical $N_{M\text{-}FD}$ as a more universal indicator of the efficiency of the process.

One can observe a characteristic trend of ($N_{M\text{-}FD}$) change with (TOP/TSI) in **Figure 5.6**. When the injection rate reaches a certain value, flow is only through the fracture and not enough residing time is allowed for an effective diffusional matrix-fracture interaction. This rate yields a progressing flat line parallel to x-axis, almost constant (TOP/TSI) with increasing ($N_{M\text{-}FD}$). This $N_{M\text{-}FD}$ value is called critical point and beyond this point, the diffusional recovery in a fractured porous media can be considered as an inefficient process. The critical $N_{M\text{-}FD}$ was found to be between 2E+07 to 3.5 E+07.

Previously we have proposed a similar group (Trivedi and Babadagli, 2006), Fracture Diffusion Index (FDI), without any DA or IA study and found to be very much alike the group defined here:

$$FDI = \frac{\sqrt{k_f} * v * f(\theta) * \rho_s}{k_m * D * \rho_o} \quad \text{.....(5.19)}$$

where v is the volumetric injection rate of the diffusing phase and D is the diffusion co-efficient between oil and solvent. $f(\theta)$ is the wettability indicator.

The FDI was presented as the ratio of viscous force acting into fracture and diffusion force into matrix which has matrix permeability term (k_m). The main difference between $N_{F\text{-}MD}$ and the FDI is the velocity terms [$(u_T)^2$ term in $N_{F\text{-}MD}$ instead of v in the FDI and the absence of k_m in the $N_{F\text{-}MD}$. It is interesting to note that the Darcy equation has been applied only to fracture, when assuming no flow into the matrix. Due to this, the final groups derived from the IA do not have matrix permeability term. Matrix porosity is present in the group given in G2 and has significant impact on analysis of the process. For comparison purpose we have

A version of this chapter has been published
Trivedi J.J. and Babadagli T., 2008. J. Pet. Sci. Eng. doi:10.1016/j.petrol.2008.03.001.

plotted the FDI against (TOP/TSI) in **Figure 5.7**. The critical FDI for the same set of experiments is between 6.5 E+14 to 9 E+14. Both groups have power law behavior against (TOP/TSI) with a good match and can be used in determining the efficiency of the process. Importance of matrix permeability in the effectiveness of the diffusional matrix-fracture interaction needs more physical tests.

5.7 Concluding Remarks

If the amount of oil produced per amount of solvent injected is the critical efficiency parameter, one can define a critical rate. We proposed a more universal approach and derived a new dimensionless group, $N_{M\text{-}FD}$, to analyze the efficiency of the process. The critical $N_{M\text{-}FD}$ was found to be between 2 E+07 and 3.5 E+07. Within this range, the process is called efficient from the recovery/solvent injection and recovery time points of view. If it is less than 2 E+07, the process is effective for the amount of oil produced but not very efficient in terms of time. This approach for efficiency evaluation is also useful in greenhouse gas sequestration and groundwater contamination practices. Those processes target to maximize the storage of injected material in the matrix and this requires an effective matrix-fracture transfer due to diffusion. This could be controlled by the rate that would be determined by matrix properties.

Figure 5.1 Geometrical representation of matrix-fracture system used in this study.

A version of this chapter has been published
Trivedi J.J. and Babadagli T., 2008. J. Pet. Sci. Eng. doi:10.1016/j.petrol.2008.03.001.

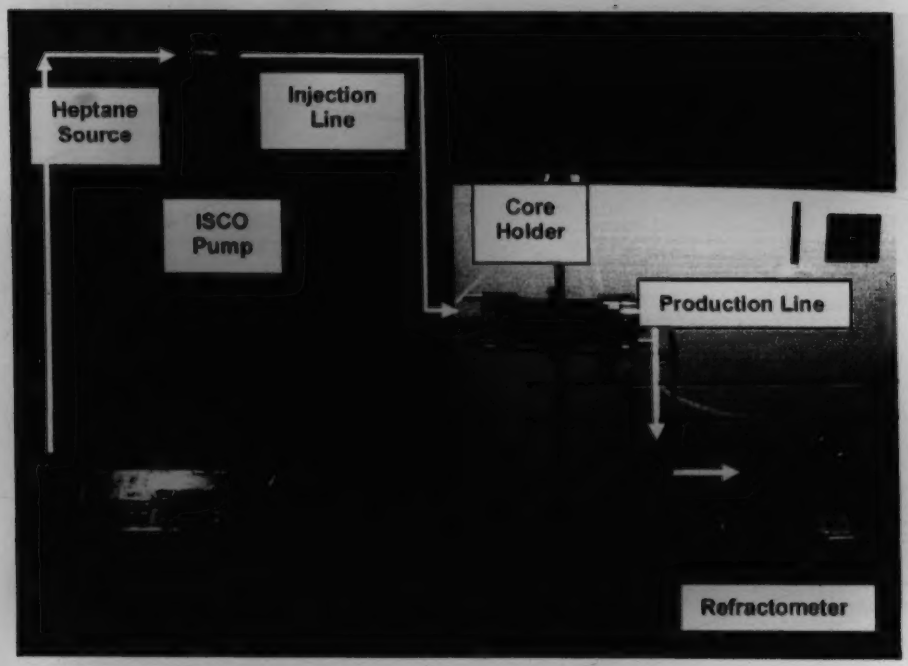

Figure 5.2: Experimental set-up

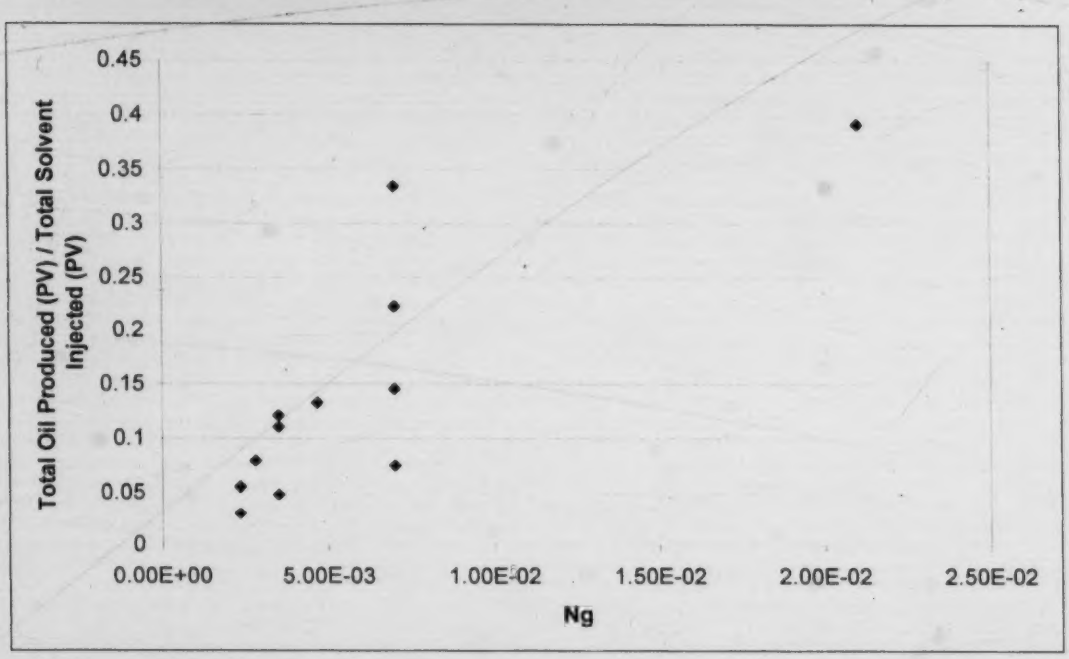

Figure 5.3: Normalized oil production with respect to amount of solvent injected as a function of the gravity number (Ng).

A version of this chapter has been published
Trivedi J.J. and Babadagli T., 2008. J. Pet. Sci. Eng. doi:10.1016/j.petrol.2008.03.001.

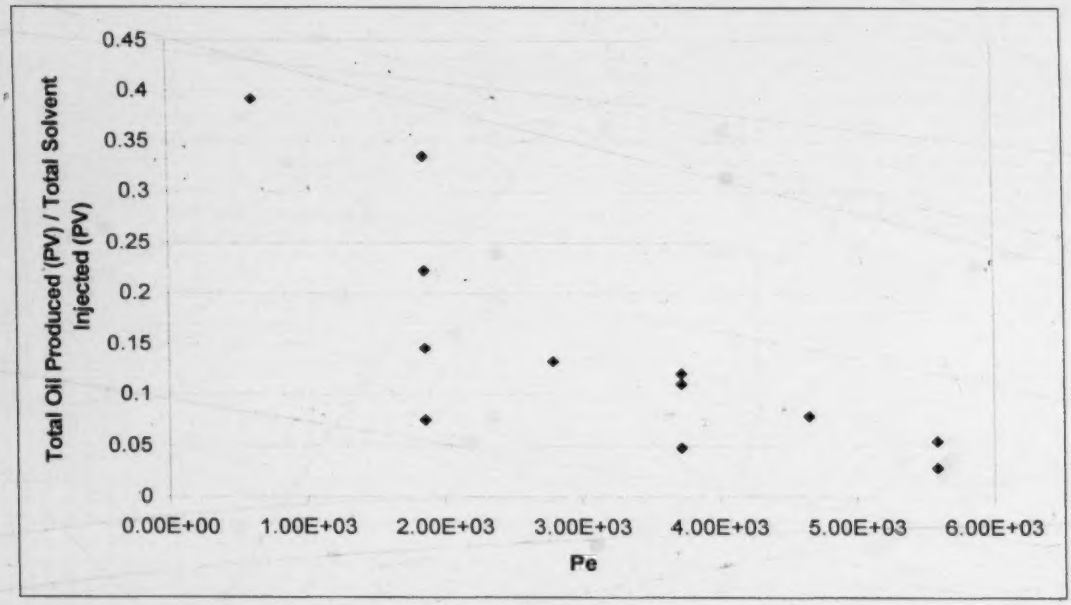

Figure 5.4: Normalized oil production with respect to amount of solvent injected as a function of the Peclet number (*Pe*).

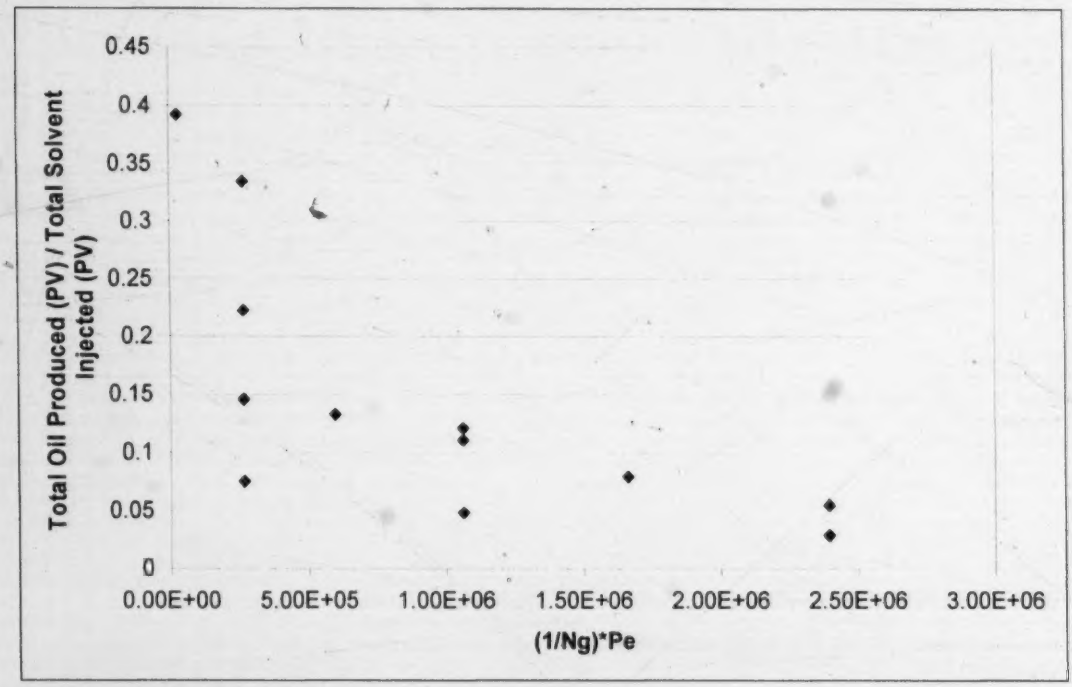

Figure 5.5: Normalized oil production with respect to amount of solvent injected as a function of (Peclet Number/Gravity Number).

A version of this chapter has been published
Trivedi J.J. and Babadagli T., 2008. J. Pet. Sci. Eng. doi:10.1016/j.petrol.2008.03.001.

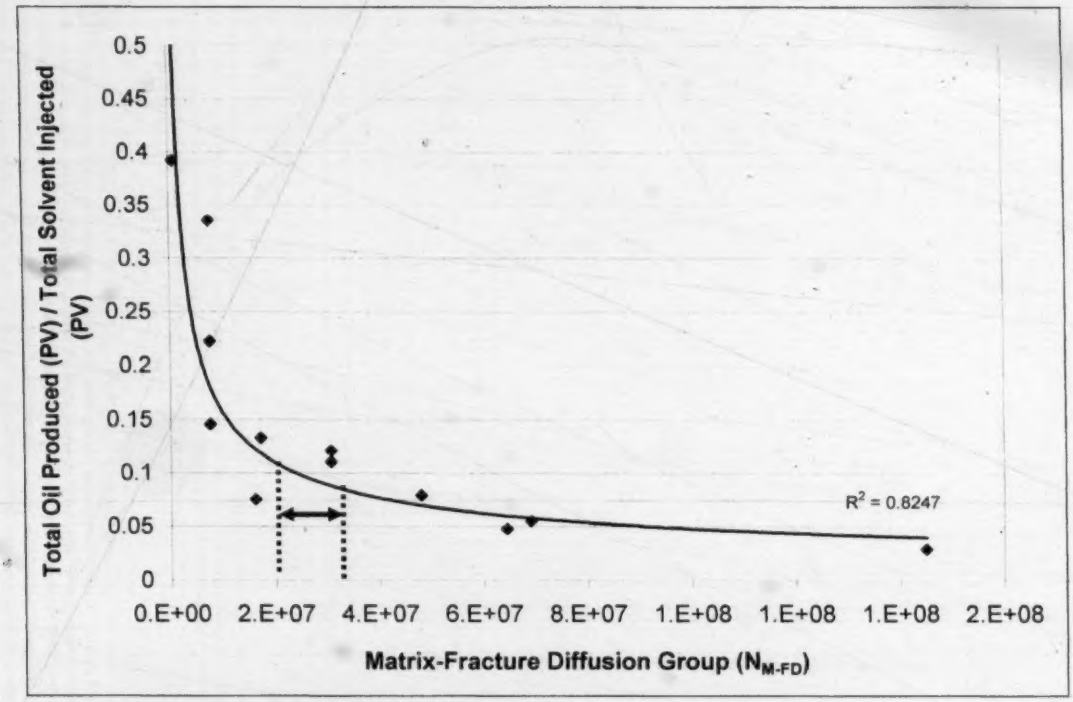

Figure 5.6: Normalized oil production with respect to amount of solvent injected as a function of Matrix-Fracture Diffusion Group (N_{M-FD}).

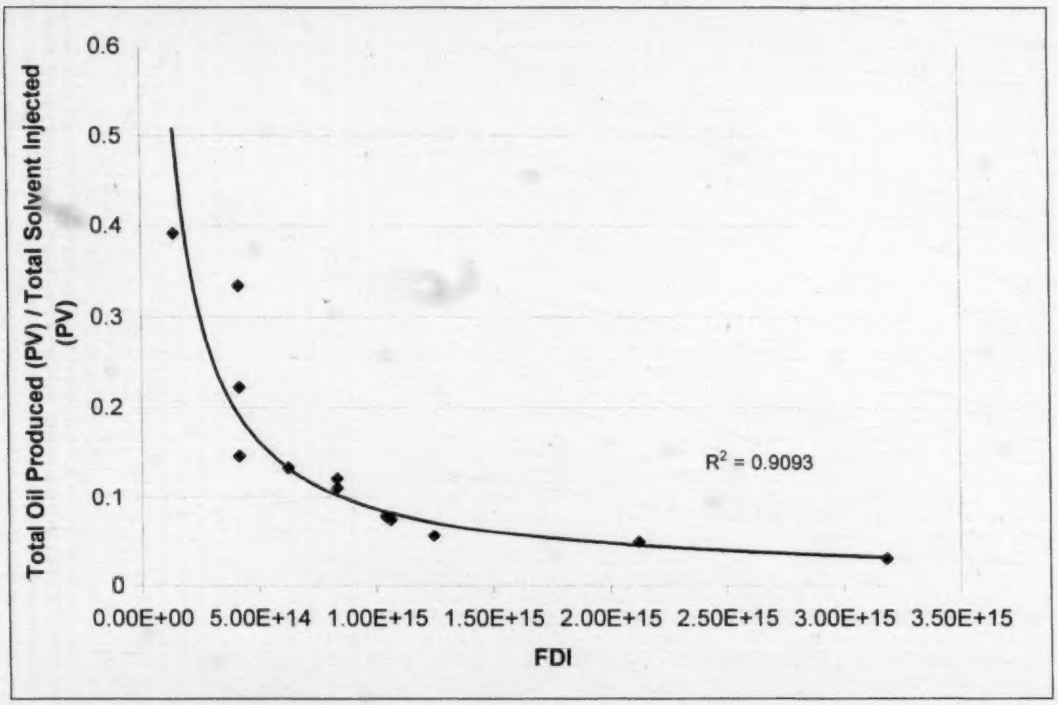

Figure 5.7: Normalized oil production with respect to amount of solvent injected as a function of Fracture Diffusion Index (FDI).

A version of this chapter has been published
Trivedi J.J. and Babadagli T., 2008. J. Pet. Sci. Eng. doi:10.1016/j.petrol.2008.03.001.

6 EXPERIMENTAL INVESTIGATIONS ON THE FLOW DYNAMICS AND ABANDONMENT PRESSURE FOR CO_2 SEQUESTRATION AND INCREMENTAL OIL RECOVERY IN FRACTURED RESERVOIRS: THE MIDALE FIELD CASE

6.1 Introduction

Very limited number of experimental work has been reported in context to oil recovery from naturally fractured reservoir using carbon dioxide as a solvent, and of these, sequestration related ones are even less. With the success of miscible flooding in different ongoing projects, researchers and industry have come together to focus on sequestration as well recently. Studies performed in these contexts are summarized below:

- Karimaie et al. (2007) performed experiments for secondary and tertiary injection of CO_2 and N_2 in a fractured carbonate rock. In their work, 2 mm gap between core cylinder and core was used as a fracture while the core acted as a matrix. They used binary mixture of C1-C7 at 170 bar and 85 ^{0}C as solute. Gas was injected at 5 cc/min into the fracture to drain the oil (in secondary injection) or water (in tertiary injection) and then reduced to 1 cc/min. Within 10 hrs of secondary CO_2 injection, 75% of oil was recovered while it took 400 hrs (~17days) to recover 15% of oil using secondary N_2.

- Darvish et al. (2006a; 2006b) used 96.6 mm long and 46 mm in diameter (4 mD, 44%) chalk cores. After saturating the core with live oil at 300 bar and 130 ^{0}C, CO_2 was injected at 5.6 cc/min to displace the oil from the fracture and then the rate was reduced to 1 cc/min.

- Chakravarthy et al. (2006) used WAG and polymer gels to delay the breakthrough during CO_2 injection into fractured cores. They studied immiscible condition and used Berea cores (D = 2.5 cm (1 inch); L = 10 cm (3.9 inches)). They injected CO_2 continuously at 0.03 cc/min and 0.1 cc/min and compared core flooding experiments with continuous CO_2

A version of this chapter has been published
Trivedi J.J. and Babadagli T., 2008. # 2008-092, 59th Ann. Tech. Meeting, CIPC/SPE GTS, Calgary.17-19 June.

injection, viscosified water injection followed by CO_2, and gel injection into fractured Berea sandstone.

- Muralidharan et al. (2004) conducted experimental and simulation studies to investigate the effect of different stress conditions (overburden pressure) on fracture/matrix permeability and fracture width. They concluded that during constant injection average fracture permeability decreased about 91% and the average mean fracture aperture decreased about 71% while increasing overburden pressure from 500 psi to 1500 psi.

- Torabi and Asghari (2007) studied CO_2 huff-and-puff performance on two Berea sandstone cores (k = 100 md and 1000 md; L = 30.48 cm; D = 5.08 cm). CO_2 was injected into 0.5 cm annular space between core and core holder acting as a fracture. In their experiments, they injected CO_2 at six different pressure steps of constant pressure into saturated core. It followed by production at atmospheric pressure for 24 hours and removing CO_2/flash fluid from the top. Each step was continued until production ceases. No consideration was taken for sequestration. They observed drastic increase in the recovery factor from immiscible to near miscible/miscible conditions.

- Asghari and Torabi (2007) performed gravity drainage experiments in sandstone core samples with fracture at the annular space and concluded that miscibility can increase the production substantially. One of their findings was that the recovery may decrease far above the miscibility. Injection and production was not at controlled rate, hence sudden increase or decrease in pressure may affect the results when comparing and also sequestration cannot be accomplished.

All these works used standard sandstone samples, usually Berea sandstone. Studies using -fractured- carbonate rocks or low permeable matrix are very rare (Karimaie et al., 2007; Darvish et al., 2006a & 2006b; Chakravarthy et al., 2006). Moreover, most of the works presented above focused on the enhanced oil recovery aspect rather than the CO_2 sequestration. Keeping in mind that sequestration during enhanced oil recovery experiments at high pressure reservoir conditions on fractured cores are involved in numerous difficulties, solution to this kind of problems was sought using simulation studies. Due to the limitations of simulators to describe matrix-fracture transfer functions and multiphase

A version of this chapter has been published
Trivedi J.J. and Babadagli T., 2008. # 2008-092, 59th Ann. Tech. Meeting, CIPC/SPE GTS, Calgary.17-19 June.

diffusion/mass transfer mechanism experimental results prove more critical in terms of understanding the complex physics of the process.

6.2 Experimental Components

6.2.1 Diffusion Cell (Core Holder)

The diffusion cell is a 21 in. long and 3 inch in diameter steel made core holder. It is capable of holding cores up to 21 inches in length and 2 inches in diameter. Both ends have ferrule assembly by installing ferrule to the end caps with screws. Rubber sleeve is installed around both ferrules. The sleeve-ferrule assembly is inserted into the holder body from one side. The other ferrule assembly is then installed and tightened. The core is inserted through ferrule into the rubber sleeve using spacers if needed. Core lengths can be reduced by using spacers and by using the length adjustment available in the retainers.

The annulus between the outer diameter of the sleeve and the inner diameter of the body is filled with the hydraulic oil which is used to supply overburden using hydraulic hand pump. The maximum pressure rating of the cell is 4000 psi and maximum temperature is 100 ^{O}C.

The holder has an inlet for applying overburden pressure around the rubber sleeve. The radial stress is applied to the core using high pressure nitrogen cylinder from the overburden line. The both end of has three 1/8" holes. One of the holes at the inlet touching the center where fracture is located is used as an injection port, the other two for pressure transducer and pressure relief valve. Similarly at the production end the hole touching the fracture is used as a production port. The experimental set-up is shown in **Figure 6.1**.

6.2.2 Injection Set-up

Two ISCO 500D pumps were used for injection of oil and CO_2. The ISCO syringe pumps can operate at flow rates as low as 0.01 ml/min. The maximum pressure rating for the pump is 3750 psi at 200 ml/min. The pumps can be set to operate either at constant flow or at constant pressure using a controller attached. 500 mL capacity piston type (Model 500D) that can maintain constant flow to within +/- 0.5%.

A version of this chapter has been published
Trivedi J.J. and Babadagli T., 2008. # 2008-092, 59th Ann. Tech. Meeting, CIPC/SPE GTS, Calgary.17-19 June.

The liquid CO_2 cylinder has pressure only 850 psi. The accumulator of the pump has a capacity of only 508 ml. Therefore, every time after the refill, the syringe pumps were used to increase the pressure up to the desired level. N_2 cylinder supplying constant pressure using high pressure regulator at the overburden line is used to apply the loads and stresses. In some experiments water using ISCO pump was used to supply overburden pressure.

ISCO pumps are connected to RS-232 serial interface for controlling and operating parameters using the LabVIEW program.

6.2.3 Production System

6.2.3.1 Back Pressure Regulator

A KPB series medium to high pressure piston-sensing back pressure regulator provided by Swagelok was used. The regulator was connected to the production line to maintain the system pressure. It provided back-pressure control in gas/liquid application.

6.2.3.2 Separator

A separator is used for oil and gas separation coming through the backpressure regulator.

6.2.3.3 Flow Meter

A volume/mass flow meter was attached to the top of the separator.

6.2.4 Data Acquisition System (DAQ)

Data acquisition from the thermocouples and pressure transducers is performed using the National Instruments cDAQ-9172 module equipped with NI Bus 9211 and 9215, which is connected to a host PC. The LabVIEW software is used to monitor the entire process and perform the appropriate programs for I/O applications.

All the necessary data, as listed below, are collected using this system:

- The flow rate, volume remaining and pump pressure signals output from the ISCO pump controller,

- Digital scale value and weight of oil production data with time. The time steps can be varied for frequent data collection at the early stage of experiments,
- CO_2 mass flow, volume flow, temperature and pressure data,
- Pressure data through transducers attached to the two ends of the core holder.

6.2.5 Core Properties and Core Preparation

Cores were cut through the center in direction of longitudinal axis using the special saw **(Figure 6.2)**. The cut cores were weighted and placed in a desiccator filled with oil. The desiccator was connected to a vacuum pump. The core was saturated under constant vacuum for 48 hours. The weight of the core after saturation was measured. Porosity of the matrix was calculated from the difference in the weight of saturated and unsaturated core. The porosity of Berea sandstone cores ranges from 19 to 21 %. The porosity of Midale cores ranges from 27 to 31 %. The average permeabilities are 500 mD and 10 mD for Berea sandstones and the Midale sample, respectively.

The Midale reservoir is described by two distinct layers: (1) the Marly (upper layers) and (2) the Vuggy (lower layers) zones. The upper layers consist of micro-crystalline dolomite while the lower layers consist of micro to coarsely crystalline fragmental limestone. The zones are separated by a thinner, tighter carbonate zone permeable to vertical fluid flow.

The core used in this experiment was selected from the Marly zone (between the depth of 1422.81m and 1424.57m) which contains highly porous crystalline dolomitic mudstones and wackestones. The fracture intensity in the Vuggy intershoal is higher than that of the overlying Marly. The Vuggy shoal is the least fractured. In a separate set of experiment, a core from the caprock was taken and tested for its breakthrough capacity.

6.3 Experimental Procedure

The following steps were followed for preparation to CO_2 flooding:

- Core was cut and dried in the oven to remove the water content. Before this, the Midale cores were subjected to a cleaning process using the Soxhlet device.

A version of this chapter has been published
Trivedi J.J. and Babadagli T., 2008. # 2008-092, 59th Ann. Tech. Meeting, CIPC/SPE GTS, Calgary.17-19 June.

- Dried core was cut into two pieces in the longitudinal direction using a diamond saw and the sides of the cores were smoothened as possible. The cut cores were weighted. Core was coated with aluminum foil except the two ends.
- Two pieces of cut cores were put in the desiccator filled with n-decane/Midale crude oil and connected to the vacuum pump assembly. Cores were saturated under vacuum for 48 hours.
- The weight of the core after saturation was measured. Porosity of the matrix was calculated from the difference in the weight of saturated and unsaturated core.
- Saturated two core pieces were held together and the fractured core was placed into the core holder assembly.
- Once the core is placed into the core holder and injection/production lines are connected properly, overburden pressure using high pressure nitrogen cylinder was applied. The overburden was always kept 300 psi higher than the injection pressure.
- Oil was injected into the fractured core at the desired pressure until the flow rate stabilizes while keeping the back pressure fully closed. Core was saturated for 24 hrs to achieve complete saturation.
- Pump was switched to constant flow and oil was injected at desired flow rate and system pressure was maintained by adjusting the opening of the back pressure regulator.
- Once the back pressure regulator is set, the oil injection was stopped and pressure inside the CO_2 pump was increased 50 to 100 psi higher than the desired experimental pressure. Then, the CO_2 pump was switched to run at constant rate flow.
- Once the oil saturated sample was ready, CO_2 injection was started and two different steps were followed during injection as explained below.

6.3.1 Continuous CO_2 Diffusion for Oil Recovery

CO_2 was injected at different very low rates: 5ml/hr, 10ml/hr and 20 ml/hr with injection pressure of 1200 psi and backpressure regulator operating at 1200 psi, a near miscible/miscible pressure condition for CO_2/n-decane system for the Berea sandstone cases. To study the CO_2 behavior at immiscible condition, two experiments at the injection

rate of 5ml/hr and 10 ml/hr were carried out at 950 psi core pressure by keeping initial injection pressure and backpressure regulator at 950 psi. Another pressure, 1400 psi, was selected to obtain fully miscible displacement and compare the results with other two cases. At 1400 psi, one CO_2 injection rate (10 ml/hr) was tested. For the Midale core experiment, injection was carried out at 10 ml/hr rate while keeping the core pressure 950 psi. This represents a pressure slightly below the miscibility pressure. The system was continuously supplied with constant overburden pressure of 1500 psi using water injection using ISCO pump in all the experiments. Pressure variations and amount of oil/gas production were closely monitored and logged during the experiment run.

6.3.2 Blow Down

After the continuous injection was stopped, the production valve at the bottom of the core-holder and the backpressure valve were closed. The system was totally shut-down for 36 hrs. During this period CO_2 and oil diffusion and back diffusion took place. Change in pressure at the injection/production ends was monitored. After 36 hrs, production valve and back pressure was opened to produce CO_2 and oil. Production continues until the pressure inside the core lowers to 250 psi. The shut-down and pressure blow down cycle was then repeated for every 250 psi pressure steps. The amount of oil and CO_2 production were measured at every pressure steps to determine the CO_2 sequestration capacity at particular pressure and ultimate oil recovered after the blow down.

6.4 Effect of Rate – Existence of Critical Rate

Many researchers showed the importance of critical rate on the oil recovery process during gas and liquid injection. Slobod and Howlett (1964) and Thompson and Mungan (1969) showed that the critical velocity defines the fingering behavior in displacement of more viscous and denser fluid in a miscible process. If the density difference is lower, increase in rate will allow more viscous force domination which leads to viscous fingering. Higher the density difference, higher the gravity force. Hence, higher density difference will cause the CO_2 flow to the path of least resistance through the fracture to the production end.

A version of this chapter has been published
Trivedi J.J. and Babadagli T., 2008. # 2008-092, 59th Ann. Tech. Meeting, CIPC/SPE GTS, Calgary.17-19 June.

Mahmoud (2006) and Wood et al. (2006) showed that the presence of vertical fracture improved the oil recovery through immiscible gas assisted gravity drainage (GAGD) compared to the unfractured counterpart. Gas will try to stay on the top and expand laterally. They also mentioned that if the gravity force loses its dominance to viscous forces then adverse effect of fractures can be observed.

The effect of rate or definition of critical rate on fracture reservoirs is different. Higher rates causes early breakthrough through fractures without enough contact with matrix in order for the diffusion between matrix and fracture to occur (Trivedi and Babadagli, 2008a & 2008c; Babadagli, 2000).

There is always an existence of critical injection rate for optimal recovery in the fractured reservoirs. Maintaining the same pressure condition in the reservoir by adjusting the backpressure regulator and injecting CO_2 at different rates of 5 ml/hr, 10 ml/hr and 20 ml/hr **(Figure 6.3)** shows the importance of knowing the critical rate before the start of CO_2-EOR project. 5ml/hr injection in Exp-2 is proven to be very slow and the recovery is extremely low. 20 ml/hr injection rate (Exp-6) causes an early breakthrough **(Figure 6.4)** of CO_2. Dispersion driven flow in the fracture and mass transfer between matrix and fracture driven by diffusion are the two major governing mechanism of oil recovery during the CO_2 injection into fracture-matrix system. Flux transfer may also governed by flow into the fracture. 5ml/hr is too slow causing an ineffective dispersion in fracture. The diffusive transfer to matrix is effective due to delayed breakthrough in the fracture but the process is too slow and therefore assumed to be inefficient in terms of oil recovery. On the other hand, 20ml/hr is proved to be more efficient for recovery compared to 5ml/hr despite early breakthrough and high CO_2 production. The intermediate rate of 10ml/hr injection resulted in even higher recovery compared to 20ml/hr, and hence suggesting the occurrence of critical injection rate. Looking at the results of storage in **Figure 6.5**, again 10 ml/hr showed maximum storage scenario followed by the 5ml/hr and 20 ml/hr cases. These experimental results have triggered the need of a new rate dependent transfer function which can define the critical rate for enhanced oil recovery as well as sequestration (Trivedi and Babadagli, 2008a & 2008c; Babadagli, 2000).

A version of this chapter has been published
Trivedi J.J. and Babadagli T., 2008. # 2008-092, 59th Ann. Tech. Meeting, CIPC/SPE GTS, Calgary.17-19 June.

6.5 Sequestration – Time and Economical Aspects

It is well understood that greenhouse gas sequestration with EOR is one of the viable choices for cost effective solution. In early stages of the production, the EOR aspect of the process is more critical than sequestration. When CO_2 flooding is continued for long time and eventually the oil cut has gone extremely low values, most of the injected CO_2 is recycled or reservoir pressure is reduced for additional recovery by pressure depletion (blow-down period). The time when continuous CO_2 flooding should be stopped and determining the minimum reservoir abandonment pressure are the two important aspects of the process in terms of optimal economical balance between oil recovery and amount of CO_2 sequestered.

Figure 6.6 represents the amount sequestered with time during continuous injection of CO_2. The shapes of the curves follow similar kind of trends in all the experiments with 10ml/hr injection. Two distinct slopes can be seen. Initially the storage is almost following a 45° line, suggesting almost all the injected CO_2 is being stored. The start of second line slope suggests the major breakthrough of CO_2. With the increase in reservoir pressure the amount of sequestered CO_2 also increases due to CO_2 compressibility. At the same time, the volume of CO_2 produced also goes high with higher reservoir pressure, which causes the higher CO_2 handling and recycling cost. The rate also impacts the sequestration and production volume. Comparing the Exp-2, Exp-4 and Exp-6, one may observe that the CO_2 sequestered increases for 5 ml/hr to 10 ml/hr rate cases with increase in injection rate while maintaining the same reservoir pressure. But further increase in injection rate, 20 ml/hr, has caused lowest amount sequestered and highest production of CO_2 compared to other two cases.

6.6 Effect of Miscibility – Sequestration and EOR

The miscibility pressure between the CO_2 and n-decane is ~1200 psi at the room temperature. CO_2 was injected at constant rate with maintaining different miscibility conditions: immiscible (~950 psi), near miscible (~1175-1225 psi) and above miscible (~1400 psi). Injecting at a same rate and at these three different pressure condition yields different results for EOR and sequestration. As seen in **Figure 6.3**, during the continuous CO_2 injection period with rate at 10 ml/hr the recoveries of immiscible, near miscible and

A version of this chapter has been published
Trivedi J.J. and Babadagli T., 2008. # 2008-092, 59th Ann. Tech. Meeting, CIPC/SPE GTS, Calgary.17-19 June.

above miscible conditions are 47%, 67% and 60%, respectively. Increasing the pressure above a point is not beneficial to incremental oil recovery and near miscible injection proved to be more useful. Increase in pressure causes variation in density as well as in viscosity of the CO_2 which plays a critical role when flow is through the fracture. **Figures 6.4** and **Figure 6.5** present the amount of CO_2 produced and amount of CO_2 stored, respectively, against total CO_2 injected. The higher the pressure above the miscible pressure, the higher the amount of CO_2 produced and CO_2 sequestered.

6.7 Rock Type – Sandstone and Limestone

Though the porosity of Midale and Berea sandstones are very high, the permeability variation can cause major impact on recovery and sequestration. Oil recovery from the selected Marly zone core is ~ 23%, lower than from sandstone with similar injection and pressure condition **(Figure 6.3)** at the end of continuous injection period. Note that oil types are different in Berea sandstone and Midale core cases as well even though they were both light oils **(Table 6.1)**. Amount of sequestered and produced gas is, however, very much equal to that of sandstone counterpart results in **Figures 6.4** and **Figure 6.5** despite the differences in oil and rock type. After nearly 5 hrs of injection into the Midale core, the produced amount of CO_2 was at very high rate and oil cut went very low. Hence the continuous injection of CO_2 was carried out for shorter time for the Midale case compared to the Berea sandstone cases (~18 hrs).

6.8 Blow Down – Sequestration and EOR

After the continuous injection period, the production and injection valves were closed for about 36 hrs for each experiment. The peak incremental oil production was noticed right after the blow down to 750 psi followed by shutdown period and the amount of produced oil varied for each experiment **(Figure 6.3)**. With the CO_2 injection rate of 10 ml/hr at different miscibility conditions, the maximum oil production during the first blow down was noticed for ~950 psi reservoir pressure which is just below the minimum miscibility pressure of CO_2 – n-decane system. Recoveries during the first blow down became lower with increasing pressure (increasing miscibility). For the Midale case, recovery after the first shut

A version of this chapter has been published
Trivedi J.J. and Babadagli T., 2008. # 2008-092, 59th Ann. Tech. Meeting, CIPC/SPE GTS, Calgary.17-19 June.

down period increased from 23 % to 41% **(Figure 6.3)**. In the Berea sandstone counterpart case (Exp-5), the oil recovery increased significantly from 47 % to 80 % during the first blow down cycle. This could be attributed to oil characteristics mainly. The permeability effect was considered to be secondary importance.

It is quite noticeable that for each experimental run, the oil production increased to significant amounts during the blow down to 750 psi after the first shut down period of 36 hrs. This could be a very vital issue in terms of oil recovery obtained mainly by gravity drainage. During the subsequent blow down cycles oil production was not quite significant.

6.9 Critical Observations

Due to the early breakthrough of CO_2 through fracture, oil was not swept well in the matrix around the production end, compared to the matrix near the injection end. After finishing the Exp-4, cores were visually inspected. Yellowish dark color identified the unrecovered oil zones. It clearly showed that the most of the oil was swept near the production part and at the injection end unswept zones were visible in the cross-section. This difference is due to the fact that a great portion of oil was recovered during the shut-in and blow down period. During shut-in, because of gravity, the lateral migration of CO_2 inside the matrix near to the production zone is more compared to the migration at the top of the matrix. The mechanism clearly suggesting the huff-and-puff application would be useful to recover unswept oil after continuous CO_2 flooding even though this may not be ideal for sequestration. More experimental support is required to justify the choice of huff-and-puff after continuous flooding with CO_2.

Density was (measured during the experiments and at the end) not changed during the experiments with CO_2-decane system, being a single component. Realistically a change in density with CO_2 is expected with the crude oil because of different CO_2 dissolution rate with different components; this was observed with CO_2-Midale oil system.

When the injection of CO_2 was stopped, the pressure decrease inside the core was observed. Interestingly the pressure decreased up to a certain value in all the experiments. The change in pressure with time was plotted for the three experiments (Exps. 4, 5, and 6) in **Figure 6.7**.

To understand the reasons of this strange behavior and avoid any thoughts of leakage or adsorption, the shutdown period was kept ~92 hrs during the case-6. It is evident from **Figure 6.7** that the decrease in pressure reached to a certain value and then it was stabilized. This pressure is around 860 psi at the experimental temperature. This is believed to be due to phase change mechanism. Looking at the CO_2 phase diagram, this point follows the sublimation line, a line between liquid and gas phase. At this point liquid requires a large volume change to do the phase change. Hence, the pressure tends to stabilize to reach the equilibrium. Given the change in pressure by external means, the CO_2 inside the core will be changing the phase hence the properties of CO_2 will change very abruptly and may affect the recovery as well as storage process in the subsequent blow down periods.

If the reservoir temperature is higher, this phase change pressure also increases. The CO_2 expands/diffuse inside the pores after the oil production. Also it can be seen as lost of miscible region, where CO_2 diffuses as a separate phase than oil inside the reservoir. This enhances the oil production during the first blow down as discussed earlier. In this process of migration mainly due to diffusion inside the matrix and convective mass transfer between fracture-matrix, a state of dynamic equilibrium is reached and pressure tends to stabilize. During the blow down period this aspect also needs to be taken care of.

In the case of Midale core (Exp-7), the pressure reduction (stabilized at ~915 psi) and the CO_2 diffusion during the first shut down period was less due to carbonate nature of the rock and much denser oil type. Comparing the Exp-5 and Exp-7, where the only difference is oil and rock type while injection pressure and rate are same, CO_2 has to diffuse into much tighter rock and more denser as well as viscous oil. This resulted into lower recovery during the first blow down cycle to 750 psi compared to that of the Berea counterpart (Exp-5) as discussed earlier and shown in Figure 6.3.

6.10 Cap Rock Sealing

In a separate set of experiment, oven dried cap rock core was placed inside the core holder. The overburden was applied using water line. CO_2 was continuously injected with constant pressure injection at different pressure steps. Once a test pressure is reached, injection valve

A version of this chapter has been published
Trivedi J.J. and Babadagli T., 2008. # 2008-092, 59th Ann. Tech. Meeting, CIPC/SPE GTS, Calgary.17-19 June.

was closed and CO_2 production at the other end was monitored. The injection was done from the bottom of the core against the gravity to mimic the real field situation. For the next step pressure was increased 50 psi higher. Change in pressure at both the ends was monitored closely. The change in pressure at the production end suggests the overcoming of capillary pressure forces and causing the breakthrough. This pressure was noted in between 1650 psi to 1700 psi **(Figure 6.8)**. Interestingly, Li et al. (2005) reported similar values of sealing pressure capacity for Weyburn field (~ 1400 psi to 1700 psi). In their study, the cap rock was first saturated with water and then the capillary pressure using CO_2 was measured. The effect of variable water saturation on cap rock sealing pressure was beyond the scope of the present paper. It should be emphasized that this pressure range is around the miscibility pressure and therefore, the pressure applied in the field.

6.11 Conclusions and Remarks

Critical rate is one of the important factors to be considered while designing an EOR and sequestration project. 10 ml/hr has proven to be the most effective continuous injection rate into fractured sandstones. For sequestration, 10 ml/hr was also observed as the critical rate yielding the maximum storage. Maintaining near miscible pressure conditions is the most effective for incremental oil recovery. Going beyond the near miscible pressure condition is proven to be beneficial for sequestration purpose but can cause reduction in production. Blow down for additional recovery at the end of the CO_2 injection project life, can increase the recovery by 10% up to a certain pressure (~750 psi here). Going below this pressure will affect sequestration adversely without much benefit of recovering oil. CO_2 phase behavior/change during the project is very crucial and should be studied carefully with density and viscosity change into consideration. The reservoirs with lower temperature can also be targeted for sequestration and EOR. Recovery from the Midale carbonate was only 23 % but after a first cycle of blow down it reached 41 % due to CO_2 diffusion and gravity drainage. The storage capacity of the Midale carbonate was, however, almost half then that of the sandstone rock while maintaining other operational parameter similar.

A version of this chapter has been published
Trivedi J.J. and Babadagli T., 2008. # 2008-092, 59th Ann. Tech. Meeting, CIPC/SPE GTS, Calgary.17-19 June.

Table 6.1: Core and fluid properties and experimental details

Exp. No	Core type	Flow rate (cc/hr)	Length (inches)	Oil type	Pressure (psi)	Porosity (%)	Swi (%)
1	Berea Sandstone	5	6	decane	900	20-22	No
2	Berea Sandstone	5	6	decane	1200	20-22	No
3	Berea Sandstone	10	6	decane	1400	20-22	No
4	Berea Sandstone	10	6	decane	1200	20-22	No
5	Berea Sandstone	10	6	decane	975	20-22	No
6	Berea Sandstone	20	6	decane	1250	20-22	No
7	Midale core (Marly zone)	10	6	Midale crude oil (dead)	950	27-31	No

Oil Type	Density (g/cc)	Viscosity (cp)
n-decane	0.73	0.92 at 20 ^{0}C
Midale cure oil (dead)	0.91	33 at 25 ^{0}C

A version of this chapter has been published
Trivedi J.J. and Babadagli T., 2008. # 2008-092, 59th Ann. Tech. Meeting, CIPC/SPE GTS, Calgary.17-19 June.

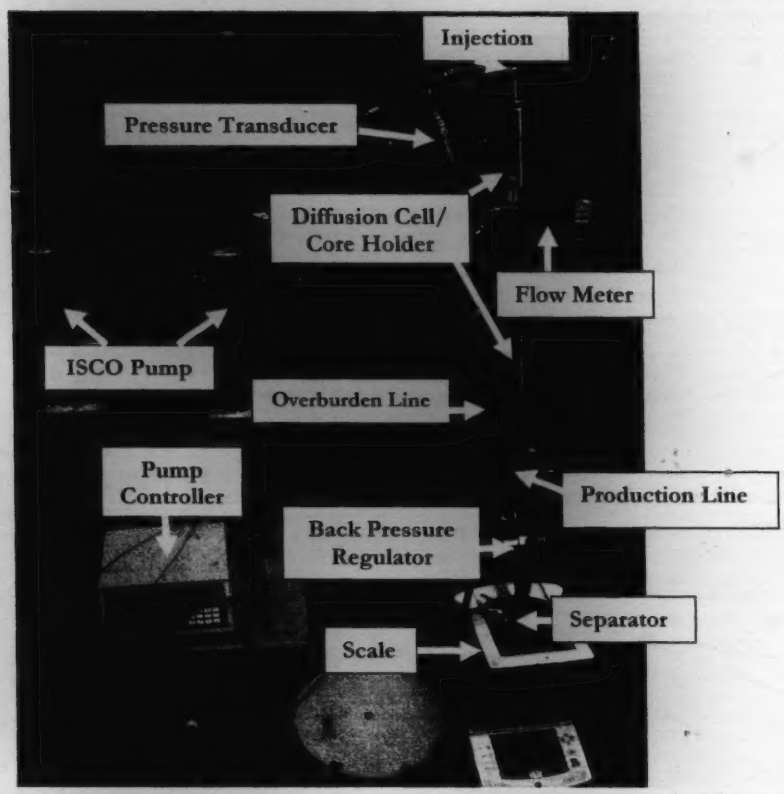

Figure 6.1: Experimental set-up (A schematic is presented in chapter 7, Figure 7.2).

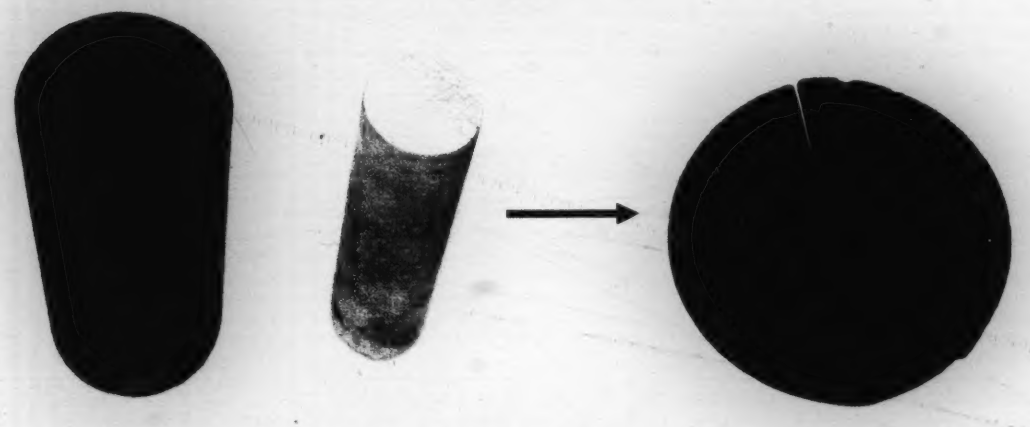

Figure 6.2: Core cutting, cleaning and fracture preparation.

A version of this chapter has been published
Trivedi J.J. and Babadagli T., 2008. # 2008-092, 59th Ann. Tech. Meeting, CIPC/SPE GTS, Calgary.17-19 June.

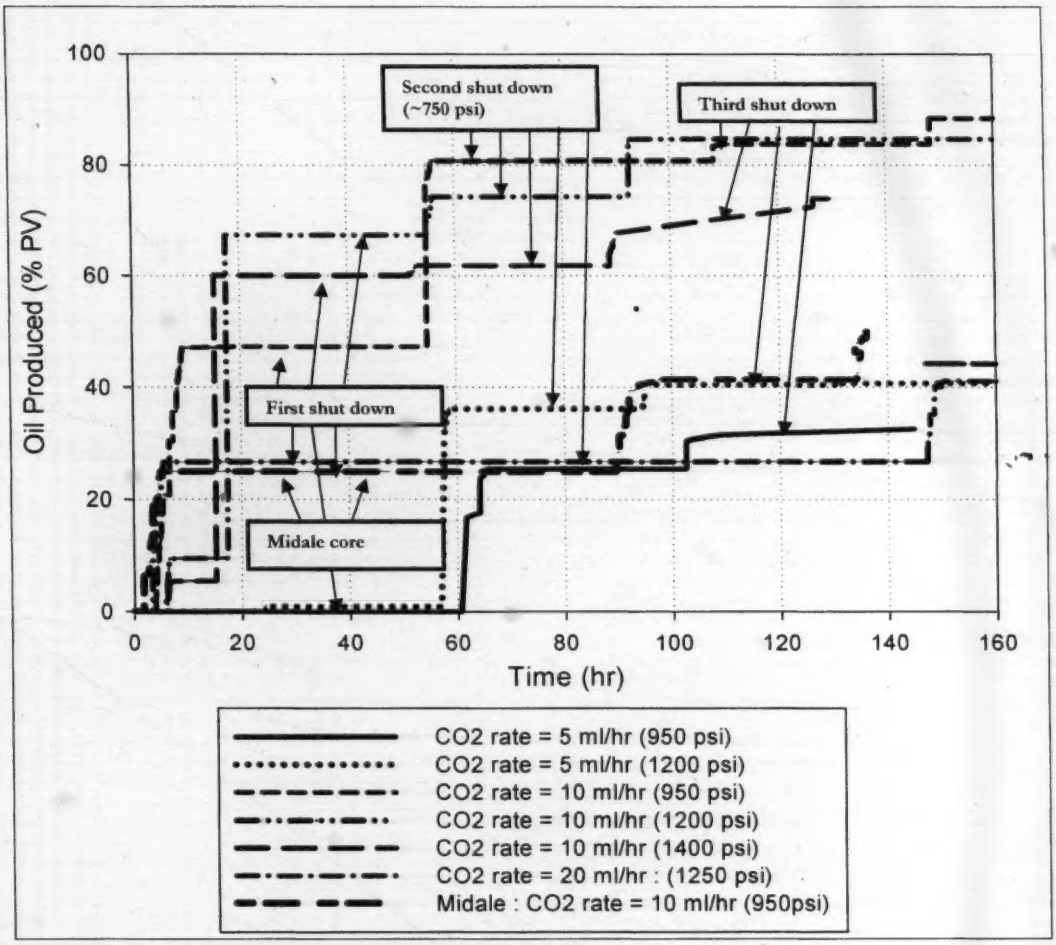

Figure 6.3: Oil production for different rates and pressures.

A version of this chapter has been published
Trivedi J.J. and Babadagli T., 2008. # 2008-092, 59th Ann. Tech. Meeting, CIPC/SPE GTS, Calgary.17-19 June.

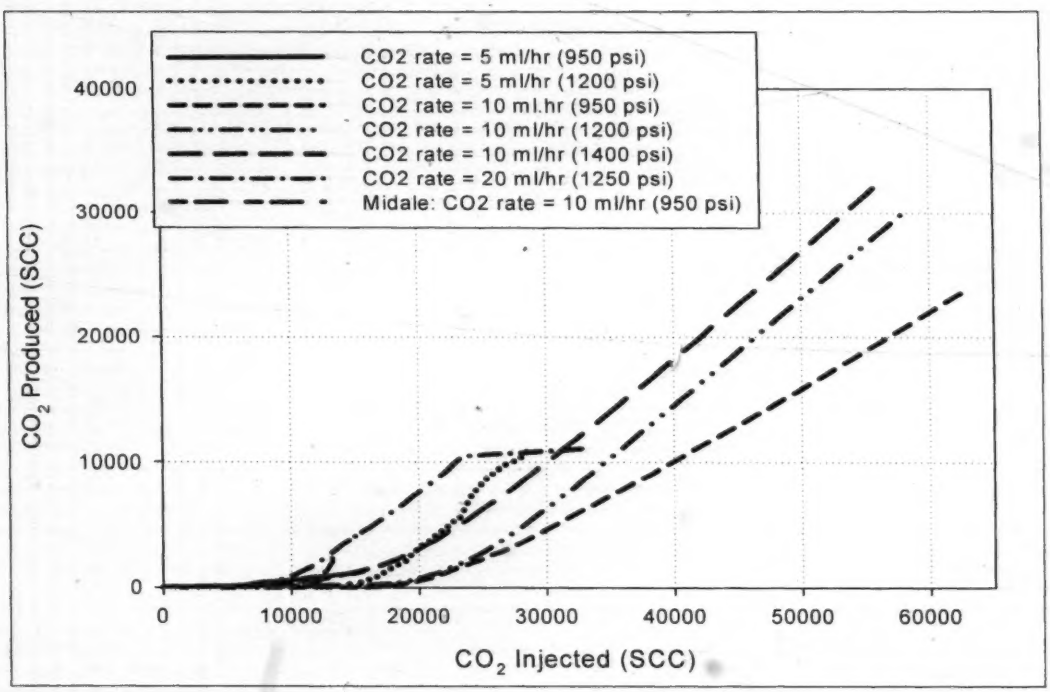

Figure 6.4: CO2 produced per amount of CO2 injected for different rates and pressures.

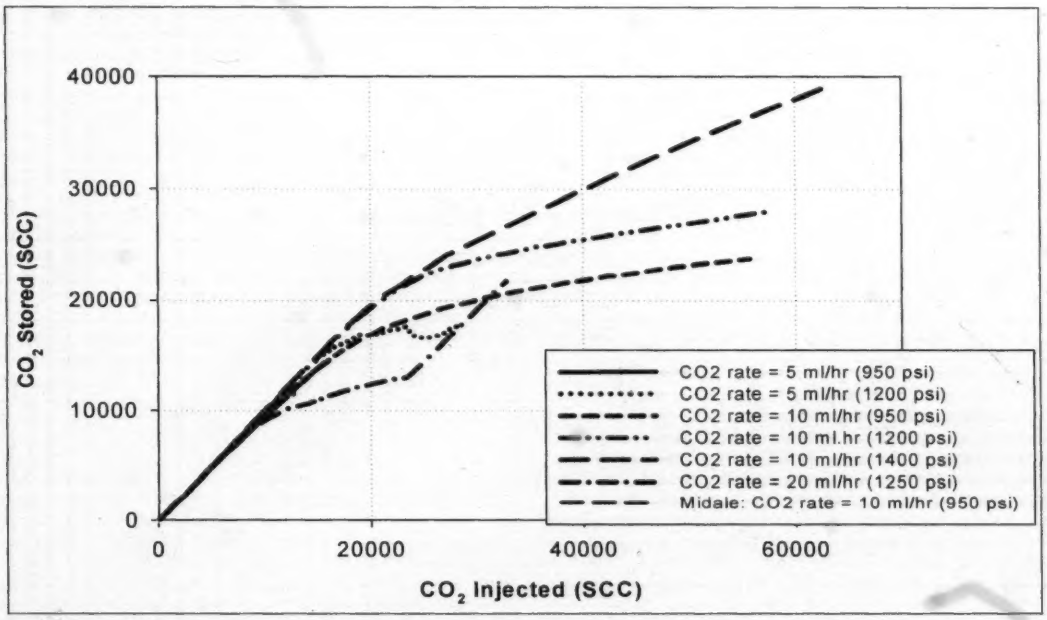
CO2 rate = 5 ml/hr (950 psi)
CO2 rate = 5 ml/hr (1200 psi)
CO2 rate = 10 ml/hr (950 psi)
CO2 rate = 10 ml.hr (1200 psi)
CO2 rate = 10 ml/hr (1400 psi)
CO2 rate = 20 ml/hr (1250 psi)
Midale: CO2 rate = 10 ml/hr (950 psi)
CO2 Stored (SCC)
CO2 Injected (SCC)
0
10000
20000
30000
40000
60000

Figure 6.5: CO2 stored per amount of CO2 injected for different rates and pressures.

A version of this chapter has been published
Trivedi J.J. and Babadagli T., 2008. # 2008-092, 59th Ann. Tech. Meeting, CIPC/SPE GTS, Calgary.17-19 June.

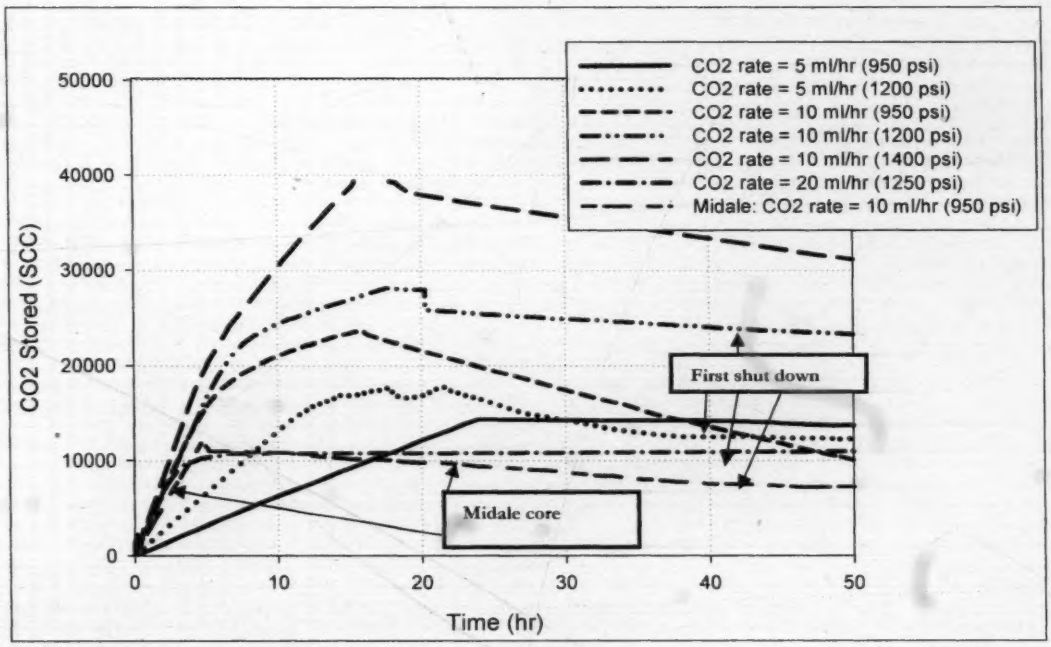

Figure 6.6: CO2 stored with time for different rates and pressures.

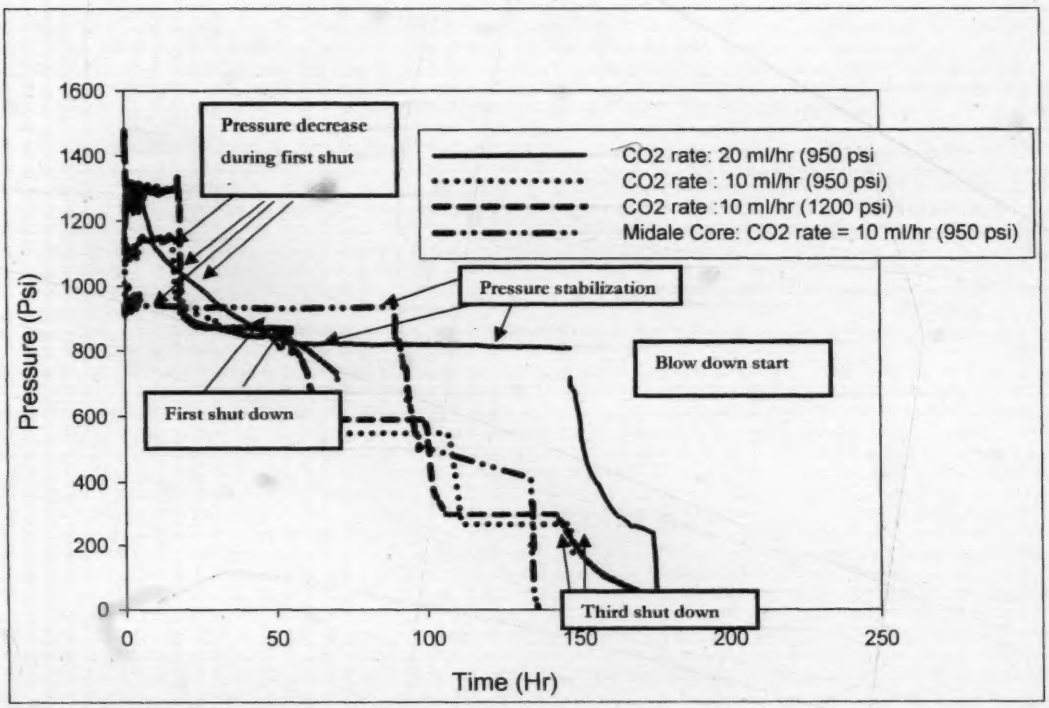

Figure 6.7: Core pressure change against time for four different cases.

A version of this chapter has been published
Trivedi J.J. and Babadagli T., 2008. # 2008-092, 59th Ann. Tech. Meeting, CIPC/SPE GTS, Calgary.17-19 June.

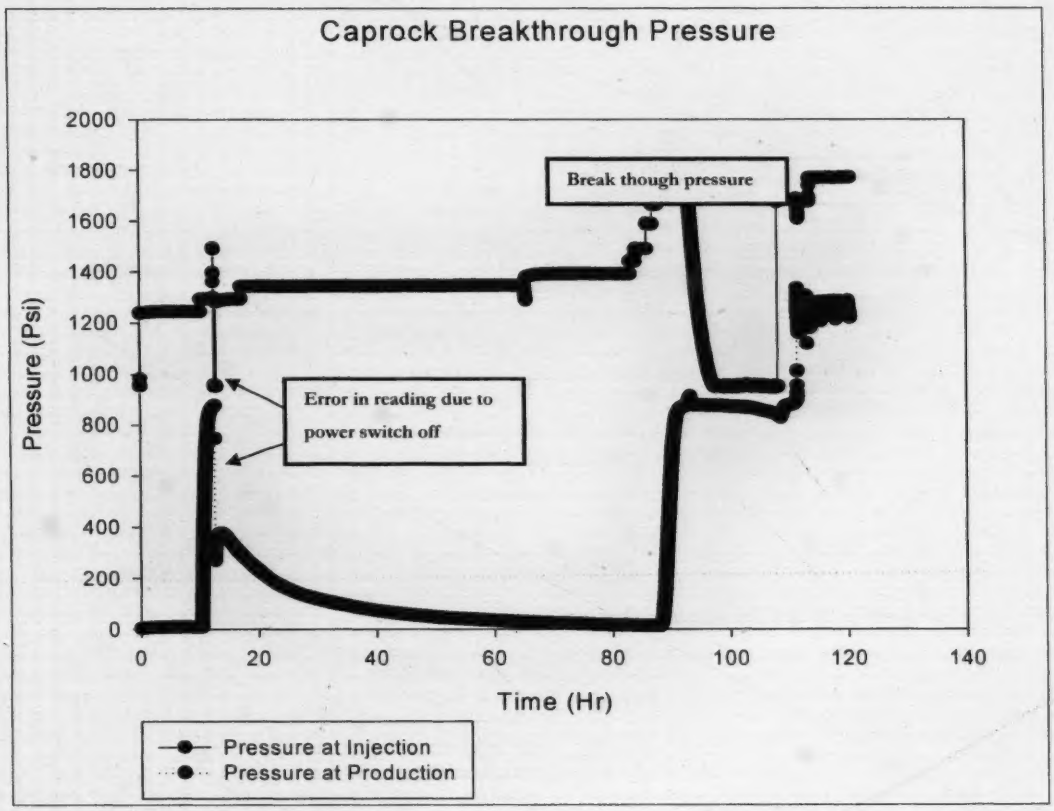

Figure 6.8: Cap rock sealing capacity test.

A version of this chapter has been published
Trivedi J.J. and Babadagli T., 2008. # 2008-092, 59th Ann. Tech. Meeting, CIPC/SPE GTS, Calgary.17-19 June.

7 EXPERIMENTAL ANALYSIS OF CO_2 SEQUESTRATION EFFICIENCY DURING OIL RECOVERY IN NATURALLY FRACTURED RESERVOIRS

7.1 Overview

In the previous chapter, we dealt with different recovery and sequestration aspects during continuous injection and consecutive blow down periods. In this chapter, we analyzed the recovery mechanisms during continuous injection and soaking (towards huff-n-puff) of the previous experimental results given in Chapter 6 with an additional experiment on the Midale field core and crude oil.

7.2 Introduction

Although there exists considerable amount of experimental work on modeling matrix-fracture interaction using first contact miscible solvents to mimic fully miscible CO_2 injection (Burger and Mohanty, 1997; Burger et al., 1996; Gabitto, 1998; Firoozabadi and Markeset, 1994; Trivedi and Babadagli, 2008a), experimental studies using CO_2 as solvent are limited. Mostly Berea sandstones are used in these researches because of their readily availability, ease of cleaning and homogeneous structures. Studies using fractured carbonate rocks or low permeable matrix are rare (Karimaie et al., 2007; Darvish et al., 2006a and 2006b). In one of its kind experimental work, Chakravarthy et al. (2006) used polymer gels to show the effect of delayed breakthrough during immiscible CO_2 injection into fractured Berea cores. Improved recovery was observed during huff-and-puff performance in miscible range over immiscible injection of CO_2 (Asghari and Torabi, 2007; Torabi and Asghari, 2007). Because of the complexity and duration involved into the diffusion experiments as well as limitations of simulators to precisely predict the multiphase diffusion/mass transfer functions, the previous attempts to understand the physical mechanism are highly valuable. None of these works, however, considered the sequestration aspect during EOR. In the first part of this chapter, we performed dynamic diffusion experiments to show that oil recovery from the matrix can be enhanced as well as greenhouse gas storage can be accomplished by

A version of this paper has been published
Trivedi J.J and Babadagli T. 2008. SPE 117606. SPE Eastern Regional/AAPG Eastern Section Joint Meeting Pittsburgh.11–15 October 2008.

optimizing flow dynamics. In the second part, we provided a quantitative analysis showing the efficiency limits of the process.

7.2.1 Importance/Role of Diffusivity in Miscible and Immiscible Matrix-Fracture Transfer Process

Different miscible injection processes using carbon dioxide, nitrogen, flue gas, natural gas, or other hydrocarbon gases such as methane, ethane, propane and butane as solvent were tested for the purpose of enhanced oil/gas recovery. One of the most important issues in common is that they all dissolve into the oil phase by diffusion mechanism. The efficiency of the mixing or dissolving is typically measured or characterized by a mutual diffusion coefficient of solvent into the oil phase. Solute transport in rough fractures is controlled by diffusion as well as advective processes. The fracture dispersion coefficient and effective matrix diffusion coefficient are the most important parameters for matrix oil recovery. In fractured porous media, the matrix diffusion is of primary importance in the processes such as geological disposal of nuclear waste, contaminant transport during ground water contamination, enhanced oil recovery in naturally fractured reservoirs and greenhouse gas sequestration in fractured geological formations.

Experimental methods to measure diffusivity could be direct or indirect. Direct method is the one which requires the compositional analysis of the diffusing species while the indirect method involves in measuring the parameters affected by diffusion such as volume change, pressure variation or solute volatization. As reported in literature, direct methods are time consuming and expensive (Sigmund, 1976; Upreti and Mehrotra, 2002). Recently, several studies reported new approaches for indirect method (Upreti and Mehrotra, 2002; Riazi, 1996; Tharanivasan et al., 2004; Zhang et al., 2000; Sheikha et al., 2005). These methods typically measure the change in pressure due to gas diffusion into liquid. Most of the research works until now did not consider the flow (or hydrodynamics) in the porous media while calculating the diffusion coefficient. In this study we obtained diffusion coefficients by simulating and matching the CO_2 gas injection into oil saturated fractured porous media

A version of this paper has been published
Trivedi J.J and Babadagli T. 2008. SPE 117606. SPE Eastern Regional/AAPG Eastern Section Joint Meeting
Pittsburgh.11–15 October 2008.

experimental results. Diffusion/dispersion into fractured porous media was then quantified by newly defined dimensionless groups.

7.3 Experimental Components

7.3.1 Core Properties and Core Preparation

Cores were cut through the center in the direction of longitudinal axis using the special saw (**Figure 7.1**). The cores were then weighted and placed in a desiccator filled with oil. The desiccator was connected to a vacuum pump. The core was saturated under constant vacuum for 48 hours. The weight of the core after saturation was measured. Porosity of the matrix was calculated from the difference in the weight of saturated and unsaturated core. The porosity of Berea sandstone cores ranges from 19 to 21 %. The porosity of Midale cores ranges from 27 to 31 %. The average permeabilities are 500 mD and 10 mD for Berea sandstones and the Midale sample, respectively.

7.3.2 Diffusion Cell (Core Holder)

The diffusion cell is a 21 in. long and 3 inch in diameter steel made core holder. It is capable of holding cores up to 21 inches in length and 2 inches in diameter. Both ends have ferrule assembly by installing ferrule to the end caps with screws. The rubber sleeve is installed around both ferrules. The sleeve-ferrule assembly is inserted into the holder body from one side. The other ferrule assembly is then installed and tightened. The core is inserted through ferrule into the rubber sleeve using spacers if needed. Core lengths can be reduced by using spacers and by using the length adjustment available in the retainers.

The annulus between the outer diameter of the sleeve and the inner diameter of the body is filled with the hydraulic oil which is used to supply overburden using hydraulic hand pump. The maximum pressure rating of the cell is 4000 psi and maximum temperature is 100 ^{0}C. The holder has an inlet for applying overburden pressure around the rubber sleeve. The radial stress is applied to the core using high pressure nitrogen cylinder from the overburden line. The both end of has three 1/8" holes. One of the holes at the inlet touching the center where fracture is located is used as an injection port, the other two for pressure

A version of this paper has been published
Trivedi J.J and Babadagli T. 2008. SPE 117606. SPE Eastern Regional/AAPG Eastern Section Joint Meeting Pittsburgh.11–15 October 2008.

transducer and pressure relief valve. Similarly at the production end the hole touching the fracture is used as a production port. The experimental set-up is shown in **Figure 7.2**.

7.3.3 Injection Set-up

Two ISCO 500D pumps were used for injection of oil and CO_2. The ISCO syringe pumps can operate at flow rates as low as 0.01 ml/min. The maximum pressure rating for the pump is 3750 psi at 200 ml/min. The pumps can be set to operate either at constant flow or at constant pressure using a controller attached. 500 mL capacity piston type (Model 500D) that can maintain constant flow to within +/- 0.5%. The liquid CO_2 cylinder has pressure only 850 psi. The accumulator of the pump has a capacity of only 508 ml. Therefore, every time after the refill, the syringe pumps were used to increase the pressure up to the desired level. N_2 cylinder supplying constant pressure using high pressure regulator at the overburden line is used to apply the loads and stresses. In some experiments water using ISCO pump was used to supply overburden pressure. ISCO pumps are connected to RS-232 serial interface for controlling and operating parameters using the LabVIEW program.

7.3.4 Production System

Production unit is comprised of a back pressure regulator, a custom made separator and a flow meter unit. A KPB series medium to high pressure piston-sensing back pressure regulator provided by Swagelok was used. The regulator is connected to the production line coming out at bottom of the core holder. By closing and opening of the regulator knob desired pressure inside the core holder was maintained. A separator is connected to back pressure regulator for oil and gas separation coming through the backpressure regulator. Separated oil is collected into a graduated cylinder on an electric balance while the amount of gas coming out was passed through a volume/mass flow meter.

7.3.5 Data Acquisition System (DAQ)

Data acquisition from the thermocouples and pressure transducers is performed using the National Instruments DAQ-9172 module equipped with NI Bus 9211 and 9215, which is connected to a host PC. The LabVIEW software is used to monitor the entire process and

A version of this paper has been published
Trivedi J.J and Babadagli T. 2008. SPE 117606. SPE Eastern Regional/AAPG Eastern Section Joint Meeting
Pittsburgh.11–15 October 2008.

perform the appropriate programs for I/O applications. All the necessary data, as listed below, are collected using this system. ISCO pumps and weight balance are connected through RS-232 serial interface for controlling and operating parameters using the LabVIEW program, while the flow meter is connected through s-video to RS-232 convertor interface. The flow rate, amount of volume injected and pump pressure data from the ISCO pump, gas mass/volume flow from the flow meter, pressure data through transducers connected at the injection and production line and weight data from the electric balance are collected at different time steps using LabVIEW program.

7.4 Experimental Procedure

The cores were cut and dried in the oven to remove the water content. Before this, the Midale cores were subjected to a cleaning process using the Soxhlet device. Dried core was cut into two pieces in the longitudinal direction using a diamond saw and the sides of the cores were smoothened. The cut cores were weighted and coated with aluminum foil except the two ends. Two pieces of cut cores were put in the desiccator filled with n-decane/Midale crude oil and connected to the vacuum pump assembly. Cores were saturated under vacuum for 48 hours. The weight of the core after saturation was measured. Porosity of the matrix was calculated from the difference in the weight of saturated and unsaturated core. Saturated two core pieces were held together and the fractured core was placed into the core holder assembly. Once the prepared core is placed into the core holder and injection/production lines are connected properly, overburden pressure using high pressure nitrogen cylinder was applied. The overburden was always kept 300 psi higher than the injection pressure. Oil was injected into the fractured core at the desired pressure until the flow rate stabilizes while keeping the back pressure fully closed. Core was saturated for 24 hrs to achieve complete saturation. The pump was switched to constant flow and oil was injected at desired flow rate and system pressure was maintained by adjusting the opening of the back pressure regulator. Once the back pressure regulator is set, the oil injection was stopped and pressure inside the CO_2 pump was increased 50 to 100 psi higher than the desired experimental pressure. Then, the CO_2 pump was switched to run at constant rate flow.

A version of this paper has been published
Trivedi J.J and Babadagli T. 2008. SPE 117606. SPE Eastern Regional/AAPG Eastern Section Joint Meeting Pittsburgh.11–15 October 2008.

In one of the Midale core experiments, sudden change in pressure was observed while injecting oil into the core situated in the core assembly as discussed earlier. Hence core was removed from the holder before even starting the CO_2 injection and we found the core completely crushed into pieces. Upon repetition of the same problem, we modified the design using a lead metal cover jacket surrounding the core and only exposing the fracture portion. The overburden and core pressure was increased simultaneously so that the core was not exposed to sudden pressure change.

7.4.1 Continuous CO_2 Diffusion for Oil Recovery

CO_2 was injected at different very low rates: 5ml/hr, 10ml/hr and 20 ml/hr with an injection pressure of 1200 psi and backpressure regulator operating at 1200 psi, a near miscible/miscible pressure condition for CO_2/n-decane system for the Berea sandstone cases. To study the CO_2 behavior at immiscible condition, one experiment at the injection rate of 5ml/hr and was carried out at 950 psi core pressure by keeping initial injection pressure and backpressure regulator at 950 psi. Another pressure, 1400 psi, was selected to obtain fully miscible (above miscible) displacement and compare the results with other two cases. At 1400 psi, one CO_2 injection rate (10 ml/hr) was tested. For the Midale core experiments, injection was carried out at 10 ml/hr rate while keeping the core pressure 950 psi and 1700 psi in two different cases. At 950 psi, Midale crude oil is immiscible with CO_2 while at 1700 psi it is at near miscible condition. The system was continuously supplied with constant overburden pressure of 1500 psi using water injection using ISCO pump in all the experiments except in case-8 where overburden was maintained at 1850 psi. Pressure variations and amount of oil/gas production were closely monitored and logged during the experiment run.

7.4.2 Blow Down

After the continuous injection was stopped, the production valve at the bottom of the core-holder and the backpressure valve were closed. The system was fully shut-down for 36 hrs. During this period CO_2 and oil diffusion and back diffusion took place. Change in pressure at the injection/production ends was monitored. After 36 hrs, production valve and back pressure was opened to produce CO_2 and oil. Production continues until the pressure inside

A version of this paper has been published
Trivedi J.J and Babadagli T. 2008. SPE 117606. SPE Eastern Regional/AAPG Eastern Section Joint Meeting Pittsburgh.11–15 October 2008.

the core lowers to 250 psi. The shut-down and pressure blow down cycle was then repeated for every 250 psi pressure steps. The amount of oil and CO_2 production were measured at every pressure steps to determine the CO_2 sequestration capacity at particular pressure and ultimate oil recovered after the blow down.

7.5 Experimental Results and Discussion

Figures 7.3 and **7.4** show the amount of oil produced with respect to the reservoir (core) pressure during the project life. It can be seen that the production trend for all cases of injection follows modified hyperbolic relationship (y0 + a*P/ (b + P)) with the core pressure. As seen from the graphical representation of oil recovery with blow-down pressure, most of the oil is produced during the first cycle of blowdown period up to 750 psi. For Cases 7 and 8, where CO_2 was injected at 10 ml/hr into Midale core saturated with Midale oil at pressure 950 psi and 1700 psi respectively, the recovery increased until the pressure reduction reaches 400 psi, which is lower than the Berea sandstones. The pressure stabilization for Case 8 was around 1100 psi during shut down higher than Berea. After the first blowdown, the recovery at 800-700 psi for the Cases 7 and 8 are almost the same even though, at the end of during continuous injection, 1700 psi initial pressure (case 8) showed ~8% higher recovery with less amount of CO_2 PV injection.

The normalized recovery factor (R.F. = % Recovery / PV Inj) based on per volume of CO_2 injected was presented in **Figures 7.9** and **7.10**. It is a log-log representation of R.F. with PV of CO_2 injected during the continuous injection period. The Cases 5 and 6 follow a similar trend and are parallel in nature. But 20 ml/hr injection rate has a higher R.F. value. Here the difference in initial injection pressure does not have much difference in values hence difficult to reach any sound conclusion. But in **Figure 7.8**, where initial injection pressure are 950 psi and 1700 psi, the difference in the R.F. clearly suggests the miscible process having advantage over immiscible case. After ~0.3 PV of CO_2 injection, the R.F. for both cases approaches to the same value. Hence, further continuations of miscible process can impair the economics of the project due to high compression cost of CO_2 to achieve miscible condition. At this point switching to maintaining lower pressure would be more economical.

A version of this paper has been published
Trivedi J.J and Babadagli T. 2008. SPE 117606. SPE Eastern Regional/AAPG Eastern Section Joint Meeting Pittsburgh.11–15 October 2008.

To check the viability of storage during pressure reduction for oil production, we showed the results of CO_2 production at different pressures in **Figures 7.5** and 7.**6**. CO_2 storage at different pressures for the same cases is given in **Figures 7.7** and **7.8** after the continuous injection was stopped. Up to 600 psi, it follows a linear trend of CO_2 storage reduction but below 600 psi the storage drops drastically. The trend of CO_2 storage with blowdown pressure for the Midale cores initially saturated with dead Midale crude oil is also shown in **Figure 7.8**. The detailed results and discussion of the experiments are presented in another study (Trivedi and Babadagli, 2008e).

When a non-equilibrium gas comes in contact with a liquid phase in a constant volume and constant temperature system, the system will approach to a new equilibrium state with changed pressure and temperature condition governed by diffusion process. The time required to reach this new equilibrium condition depends on the diffusion coefficient of the gas into the liquid phase, matrix properties (mainly width). The amount of gas transferred into the oil phase depends on gas solubility while the transfer rate is governed by diffusion coefficient. During the continuous injection of CO_2 into oil saturated porous media, injection was stopped when the oil production was very low compared to gas production. At this stage, the phase at the injection and production ports located at the centre of the core where the fracture is lying was occupied mainly by CO_2. During the shutdown period after the continuous injection was stopped caused a drop in pressure. As shown in **Figure 7.11**, during shutdown the pressure declined and reached a stable value, a point of quasi-equilibrium. This clearly suggests the diffusion of CO_2 into the hydrocarbon phase. During this period, mobilization of heavier hydrocarbon component of the oil occurs. This phenomenon is due to increased extraction/condensation, a result of diffusion and solubilization.

The pressure decay behavior was observed and used by many authors (Upreti and Mehrotra, 2002; Riazi, 1996; Tharanivasan et al., 2004; Zhang et al., 2000; Sheikha et al., 2005; Fjelde et al., 2008) to calculate solvent gas/CO_2 diffusivity into heavy oil/bitumen as well as into light hydrocarbons. In this method, more commonly known as pressure decay method, two pairs of fluids are place in a closed chamber (Sapphire cell) at test conditions and pressure response of the constant volume system are modeled by applying appropriate boundary

A version of this paper has been published
Trivedi J.J and Babadagli T. 2008. SPE 117606. SPE Eastern Regional/AAPG Eastern Section Joint Meeting Pittsburgh.11–15 October 2008.

conditions to calculate diffusion coefficients. So far, we have not come across any work where interaction between any phase (gas, liquid or supercritical) of a gas and oil saturated porous media was used to study pressure decay method hence the interpretation of the results during our experiments are more critical and valuable. The value of diffusion coefficient is dependent on the final equilibrium pressure and times required to reach this pressure. The steeper the pressure decline with time, the higher the value of diffusion coefficient. As seen in **Figure 7.11**, in the Case 7, where injection of CO_2 was at immiscible condition into Midale carbonate core, the pressure decay behavior was not observed. In contrast, for the Case 8, the decay was observed as near miscible condition was maintained during CO_2 injection but still it was not as steep decline as observed for the Cases 4, 5 and 6. This discrepancy is due to diffusion characteristics in different rock types: Berea sandstones (Cases 4 to 6) and Midale carbonates (Cases 7 and 8). Also in the Case 6 the decay is gradual, while in the Cases 4 and 5 the decay is very steep. Injection in the Case 6 was stopped earlier and the total amount of CO_2 injected was much lower due to injection/production at higher rates compared to the Cases 4 and 5. Hence, indicating that shutdown after slower rate injection for a longer period of time will yield higher diffusion and higher amount of oil recovered during the first blowdown compared to a faster rate injection for a shorter period of time. This conclusion is complemented by oil production with pressure depletion shown in **Figure 7.3** for the Case 4 and 6.

During the first blow down period after the first shutdown, significant amount of oil production was noticed while further consecutive shutdowns were ineffective for production. The reason being, during the first shutdown, the quasi-equilibrium is reached as the pressure stabilizes after the decay. This means that further solubility of gas into oil phase is very much reduced. To increase the oil production requires addition of fresh gas phase to create non-equilibrium into the system which subsequently will increase the solubility as well as the rate of molecular transfer controlled by diffusion coefficient. CO_2 solubility also is a function of pressure and increases with pressure. The shutdown at higher pressure will increase the chances of CO_2 contacting larger portion of oil.

The hydrocarbon distribution of the oil recovered for the Case 8 is shown in **Figure 7.12**. The samples collected at initial stage (stock tank oil used for saturation of the core), during

continuous injection, during the first blowdown followed by quasi-equilibrium during first shutdown and during the last cycle of blowdown were analyzed using GC-MS for carbon distribution and are presented here. Maintaining near miscible condition and injecting at continuous rate, oil swelling and extraction capacity of CO_2 increased. Recovery is also governed by the extraction process during the development of miscibility. While in the shutdown period, as the pressure decreases, condensation due to lose of miscibility occurs. The heavier carbon components dissolve in the CO_2 rich phase inside the matrix. Thus, it creates a middle phase and recovery of heavier component increases. As shown in **Figure 7.12**, during this period, C14-C17 as well as C18-C22 recovery was increased almost 13% and $C22^+$ recovery increased by ~9%. Interestingly, there were almost zero $C10^-$ components in the production. This emphasizes the role of density and gravity during quasi-equilibrium. Until the pressure reduces to the stabilization point (quasi-equilibrium), condensation and diffusion are the major driving mechanisms. After that, oil recovery is due to mobilization of oil inside the fracture due to pressure reduction which is very low in percentage amount and also lighter in hydrocarbon enrichment compared to the one obtained during the quasi-equilibrium state. The carbon distribution found was similar to the initial stock tank oil but still somewhat higher in heavier hydrocarbons. Below 600 psi, CO_2 is in a gas phase and further decrease in pressure only results in gas production.

7.6 Matrix-Fracture Diffusion Simulation

Fracture-matrix transfer process was modeled numerically and presented in the form of dimensionless groups to analyze the effects of different parameters quantitatively. The process experimentally analyzed in the previous section was simulated using finite element modeling with the governing advection-convection equations and the Darcy equation. Only parameters other than those unavailable from the laboratory scale experiments are the diffusion/dispersion coefficients and mass transfer coefficients in the matrix and fracture. These parameters were obtained through matching the numerical modeling results to their experimental equivalents and then they were correlated to fluid-rock properties and flow velocity.

A version of this paper has been published
Trivedi J.J and Babadagli T. 2008. SPE 117606. SPE Eastern Regional/AAPG Eastern Section Joint Meeting Pittsburgh.11–15 October 2008.

Figure 7.1 presents the matrix-fracture system (length = L and radius = 2r) with inlet, outlet as well as the boundary conditions. The x-axis is the principle flow direction, while the y-axis is the direction perpendicular to the flow. The pore space of the matrix is initially filled with oil (C = 0) and is flooded with a CO_2 (C = 1) from one side x = 0 at the center, where fracture (half aperture = b) is located. The oil is assumed to be dispersed uniformly into the porous matrix. It is assumed that both fluids, displacing and displaced, are incompressible and complete mixing across the fracture width takes place at all times. Both media has uniform properties. In this analysis, we do not impose any restriction on the geometric shape of the fracture, except that the cross section of the fracture is invariant with the axial position. The displacing fluid (CO_2) flows/injected at constant rate through fracture at the inlet x = 0; there is no flow in the matrix surrounding fracture. Under these conditions, Equations governing the system are shown below with the appropriate initial and boundary conditions. Assuming the diffusive flux from fracture to matrix is acting perpendicular to the fracture, the coupling parameter between matrix and fracture are the continuity of fluxes and concentrations along the interface (Tang et al., 1981).

The dead volume of the oil in the injection and production line have been subtracted from the final experimental results and then used for simulation of flow and diffusion behavior only inside the porous media. During the closing and opening of BPR valve the pressure fluctuation in a range of +/- 20 psi occurs. This fluctuation has been neglected while the performing simulation and flow at the bottom exit at the fracture has assumed to be regulated by constant outlet pressure.

Domain 1 – Fracture

$$\frac{\partial CF_1}{\partial t} - D_L \frac{\partial^2 CF_1}{\partial x^2} - D_L \frac{\partial^2 CF_1}{\partial y^2} = -u_F \frac{\partial CF_1}{\partial x} \quad \text{.....(7.1)}$$

$$\frac{\partial CF_2}{\partial t} - D_L \frac{\partial^2 CF_2}{\partial x^2} - D_L \frac{\partial^2 CF_2}{\partial y^2} = -u_F \frac{\partial CF2}{\partial x} \quad \text{.....(7.2)}$$

A version of this paper has been published
Trivedi J.J and Babadagli T. 2008. SPE 117606. SPE Eastern Regional/AAPG Eastern Section Joint Meeting
Pittsburgh.11–15 October 2008.

Domain 2 – Matrix

$$\frac{\partial CM_1}{\partial t} - D_e \frac{\partial^2 CM_1}{\partial x^2} - D_e \frac{\partial^2 CM_1}{\partial y^2} = 0 \quad \text{..... (7.3)}$$

$$\frac{\partial CM_2}{\partial t} - D_e \frac{\partial^2 CM_2}{\partial x^2} - D_e \frac{\partial^2 CM_2}{\partial y^2} = 0 \quad \text{..... (7.4)}$$

Initial conditions:

$$CF1(x, y, 0) = 0; CM1(x, y, 0) = 0; CF2(x, y, 0) = 1; CM2(x, y, 0) = 1; CF1(0, t) = CF0 \quad \text{..... (7.5)}$$

Boundary conditions:

$$\left.\frac{\partial CM_1}{\partial y}\right|_{(x,r,t)} = 0 \qquad \left.\frac{\partial CM_2}{\partial y}\right|_{(x,r,t)} = 0 \quad \text{..... (7.6)}$$

$$\left.\frac{\partial CF_1}{\partial x}\right|_{(\infty,t)} = 0 \qquad \left.\frac{\partial CF_2}{\partial x}\right|_{(\infty,t)} = 0 \quad \text{..... (7.7)}$$

$$D_L \frac{\partial CF_1}{\partial y} = -D_e \frac{\partial CM_1}{\partial y}; \; D_L \frac{\partial CF_2}{\partial y} = -D_e \frac{\partial CM_2}{\partial y} \quad \text{at t = t} \;\; \forall x, b \quad \text{..... (7.8)}$$

The simulation results were compared with the results of experimental performed earlier. Through matching the experimental results with the numerical ones, the values of D_L and D_e were obtained.

7.7 Correlation for CO_2 Sequestration and Oil Production

In previous attempts, different studies derived dimensionless groups to represent the efficiency of the immiscible or miscible EOR processes. Mostly all of them were for homogeneous systems and only a few focused on heterogeneous reservoirs. Gharbi et al. (1998) and Gharbi (2002) used inspection analysis to investigate the miscible displacement in

A version of this paper has been published
Trivedi J.J and Babadagli T. 2008. SPE 117606. SPE Eastern Regional/AAPG Eastern Section Joint Meeting Pittsburgh.11–15 October 2008.

homogeneous porous media. Grattoni et al. (2001) defined a new dimensionless group combining the effects of gravity; viscous and capillary forces which showed a linear relationship with the total recovery. For the application of the dimensionless groups, Kulkarni and Rao (2006) presented the effect of major dimensionless groups on the final recovery based on various miscible and immiscible gas assisted gravity drainage field data and laboratory experimental data. In another study (Wood et al. 2006) dimensionless groups were derived for tertiary enhanced oil recovery (EOR) using CO_2 flooding in waterflooded reservoirs and presented a screening model for EOR and storage in Gulf Coast reservoirs. For transfer in fractured porous media a dimensionless group, FDI (Fracture Diffusion Index), was proposed (Trivedi and Babadagli, 2006) as a ratio of viscous forces in the fracture and diffusion forces in the matrix using the analogy to capillary imbibition controlled immiscible displacement in fractured porous medium. In a recent attempt, Trivedi and Babadagli (2008d) derived a new dimensionless group with its physical significance towards the efficiency of miscible recovery process into fractured porous media. In the present analysis, we used the same group – Matrix-Fracture Diffusion group ($N_{M\text{-}FD}$) – for our experimental results to analyze the efficiency. ($N_{M\text{-}FD}$) is defined as follws:

$$(N_{M\text{-}FD}) = \left(\frac{\mu_0 u_T^2 b}{k_F \Delta\rho g D_m}\right)\left(\frac{L}{\phi_m r}\right) = \frac{Pe^* Ar_M}{N_g}$$

where,

$$Pe = \frac{u_T^* b}{D_m} \quad ; \qquad N_g = \left(\frac{k_F \Delta\rho g}{\mu_0 u_T}\right); \qquad Ar_M = \left(\frac{L}{\phi_m r}\right)$$

The TOP/TSI (total oil produced / total solvent injected) ratio is of particular interest when it comes to optimization and the critical rate determination. In previous attempts, dimensionless numbers (empirical and derived) were correlated to TOP/TSI and also with TSS/TSI using the experimental results for solvent injection (Babadagli and Trivedi, 2006 and 2008a). They used the first contact miscible solvent to mimic the CO_2 injection process whereas we used the results of CO_2/oil experiments performed in this study for the same type of analyses. Well known dimensionless numbers, Peclet number (Pe), gravity number (N_g) and matrix-fracture diffusion group ($N_{M\text{-}FD}$) for different experiments condcuted in this

A version of this paper has been published
Trivedi J.J and Babadagli T. 2008. SPE 117606. SPE Eastern Regional/AAPG Eastern Section Joint Meeting
Pittsburgh.11–15 October 2008.

study, are shown in **Table 7.3**. We also included the results from Trivedi and Babadagli (2008a) (Cases 8, 9, and 10) and Firoozabadi and Markeset (1994) (Cases 11, 12, and 13) which were performed under similar experimental conditions but different solvent/solute pairs. As presented in **Figure 7.13**, $N_{M\text{-}FD}$ shows a power law relation with high accuracy with the TOP/TSI values for all experiments. In many enhanced oil recovery processes the time to reach the ultimate recovery could be more critical compared to the amount of solvent injected while sometimes the compression cost associated with the amount of CO_2 injected could be important considering overall economics of the project. Higher $N_{M\text{-}FD}$ indicates a faster recovery with more solvent injection. On the other hand, a low value of the $N_{M\text{-}FD}$ is an indication of slow but higher normalized recovery due to less amount of total solvent injected. The process having too low $N_{M\text{-}FD}$ also cannot be considered as the best scenario because of extremely slow nature of the process. The optimal/critical value of $N_{M\text{-}FD}$ group would be the one which is time effective as well as effective in terms of amount of solvent injected or produced minimization and define the critical rate. The critical $N_{M\text{-}FD}$ value found here is between 3.5 E+3 to 1 E+4.

7.8 Conclusions

The heavier hydrocarbon components recovery is increased by a large fraction during shutdown after continuous injection of CO_2. The shutdown after slower rate injection for a longer period of time yielded higher diffusion and higher amount of oil recovered during first blowdown compared to faster injection rate case for a shorter period of time. The pressure decay during this shutdown period gives a measure of diffusion as well as recovery enhancement phenomenon in fractured porous media. During the project life blowing down reservoir for an economic benefit of oil recovery is not viable after a particular pressure stage and that pressure was found to be around 600-700 psi for Berea sandstone and 400 psi for Midale carbonate cores. Similarly, while considering greenhouse gas sequestration same pressure was proved to be the bottom limit to exceed for viable range.

Understanding of diffusion/dispersion phenomenon into the matrix-fracture system and its quantification were achieved using successful simulation match of very slow rate CO_2 injection into oil saturated fractured porous media experimental results. Efficiency of the

A version of this paper has been published
Trivedi J.J and Babadagli T. 2008. SPE 117606. SPE Eastern Regional/AAPG Eastern Section Joint Meeting
Pittsburgh.11–15 October 2008.

miscible gravity drainage process in the fractured porous media can be generalized using a dimensionless group $N_{M\text{-}FD}$. The critical value of dimensionless matrix-fracture diffusion group was found to be in a range of 3.5 E+3 to 1 E+4.

Table 7.1: Experiments details

Case No	Core type	Flow rate (cc/hr)	Length (inches)	Oil type	Pressure (psi)	Porosity (%)
1	Berea Sandstone	5	6	decane	950	20-22
2	Berea Sandstone	5	6	decane	1200	20-22
3	Berea Sandstone	10	6	decane	1400	20-22
4	Berea Sandstone	5-10	6	decane	1250	20-22
5	Berea Sandstone	10	6	decane	1000	20-22
6	Berea Sandstone	20	6	decane	1250	20-22
7	Midale core (Marly zone)	10	6	Midale crude oil (dead)	950	27-31
8	Midale core (Marly zone)	10	6	Midale crude oil (dead)	1700	27-31

Table 7.2: Hyperbolic behavior for oil recovery during production life

Case No	y_0	a	b	R^2
1	61.99	4.99	-1059	0.9985
2	41.68	3.488	-1357	1
3	74	12.66	-1989	0.9832
4	85.98	13.89	-1488	0.9949
5	90.74	10.45	-1997	0.9729
6	44.32	7.748	-1849	0.9989
7	48.13	10.53	-1379	0.9316
8	52.28	17.23	-2420	0.8361

A version of this paper has been published
Trivedi J.J and Babadagli T. 2008. SPE 117606. SPE Eastern Regional/AAPG Eastern Section Joint Meeting Pittsburgh.11–15 October 2008.

Table 7.3: Dimensionless numbers and TOP/TSI predicted values using $N_{M\text{-}FD}$.

No	q_i (ml/hr)	Pressure (psi)	Pe	N_g	$N_{M\text{-}FD}$	TOP/TSI (predicted)	TOP/TSI (Experimental)
1	5	1250	300	3.9636	2149.6187	0.55	0.5825
2	10	1250	600	1.7341	9826.8282	0.3707	0.3656
3	20	1250	1200	0.9909	34393.899	0.2676	0.2842
4	10	950	1714.286	0.6606	73701.212	0.219	0.22
5	10	1350	150	0.4955	8598.4747	0.384	0.3645
6	10	1200	800	0.6606	34393.899	0.268	0.314
7	10	1700	240	1.6515	3852.1167	0.47	0.39
8	1	15	62.1055	1.6765	1068.912	0.659	0.62
9	3	15	186.3165	0.5588	9620.206	0.372	0.334
10	6	15	372.6329	0.2794	38480.82	0.259	0.23
11	0.0026087 (velocity)	15	80.8697	2.3891	418.542	0.842	0.98
12	0.01435 (velocity)	15	81.7739	0.4343	2328.069	0.539	0.51
13	0.04348 (velocity)	15	82.184	0.1433	7089.021	0.403	0.383

A version of this paper has been published
Trivedi J.J and Babadagli T. 2008. SPE 117606. SPE Eastern Regional/AAPG Eastern Section Joint Meeting Pittsburgh.11–15 October 2008.

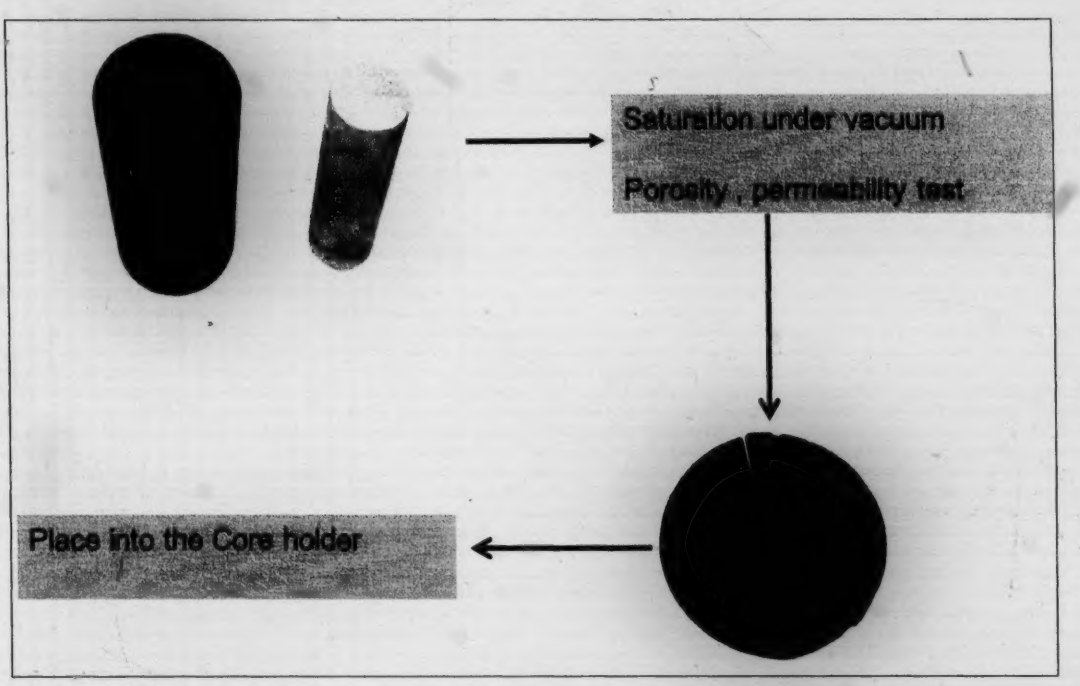

Figure 7.1: Core Preparation.

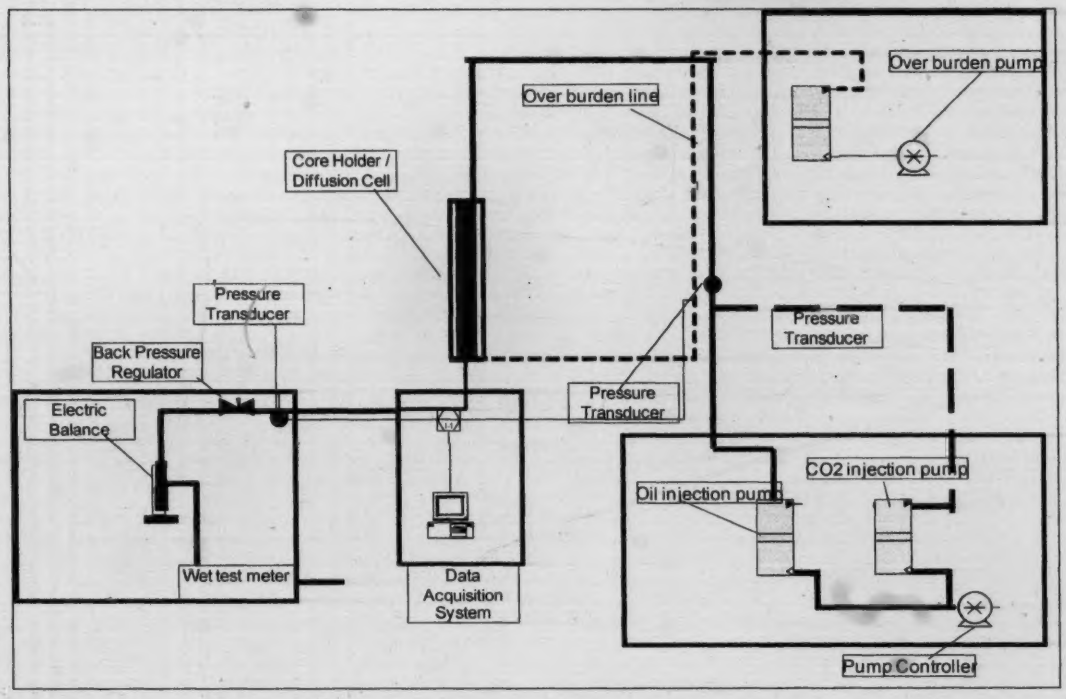

Figure 7.2: Experimental Setup (Photo of the set-up is shown in Figure 6.1).

A version of this paper has been published
Trivedi J.J and Babadagli T. 2008. SPE 117606. SPE Eastern Regional/AAPG Eastern Section Joint Meeting
Pittsburgh.11–15 October 2008.

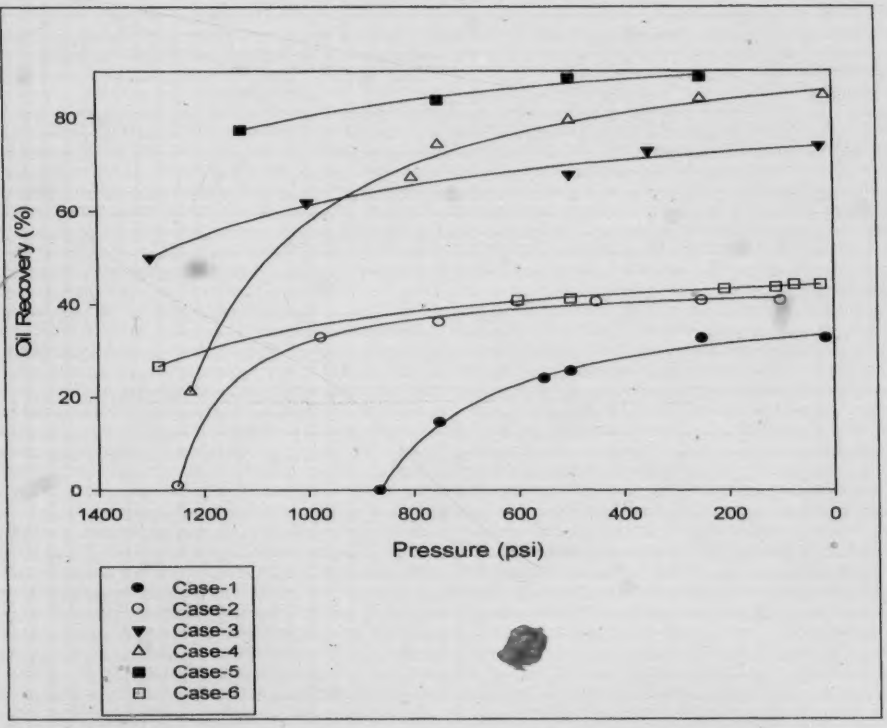

Figure 7.3: Oil recovery with the pressure blowdown for Berea sandstone.

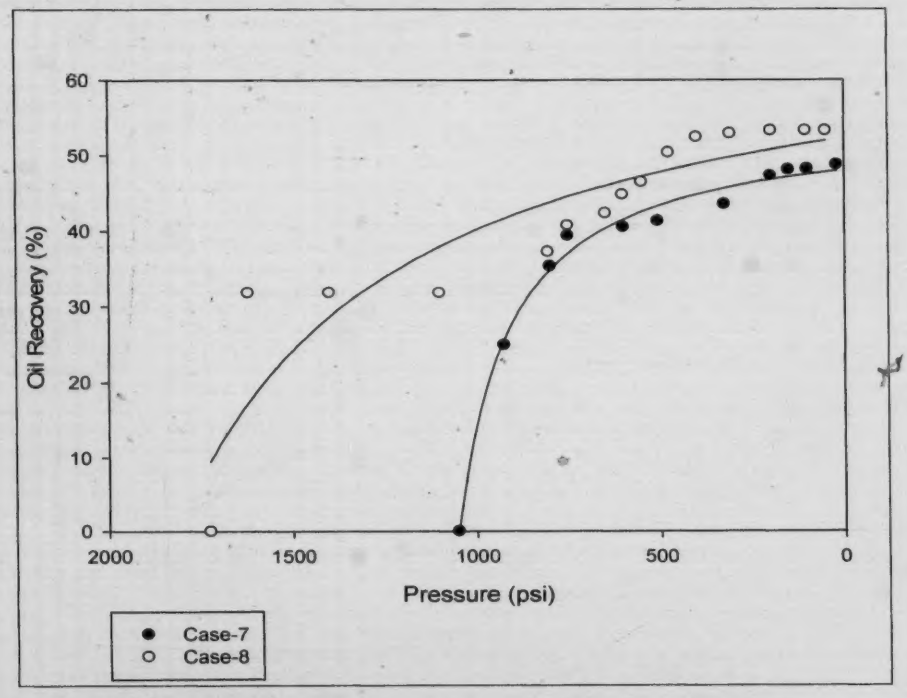

Figure 7.4: Oil recovery with the pressure blowdown for Midale carbonate.

A version of this paper has been published
Trivedi J.J and Babadagli T. 2008. SPE 117606. SPE Eastern Regional/AAPG Eastern Section Joint Meeting Pittsburgh.11–15 October 2008.

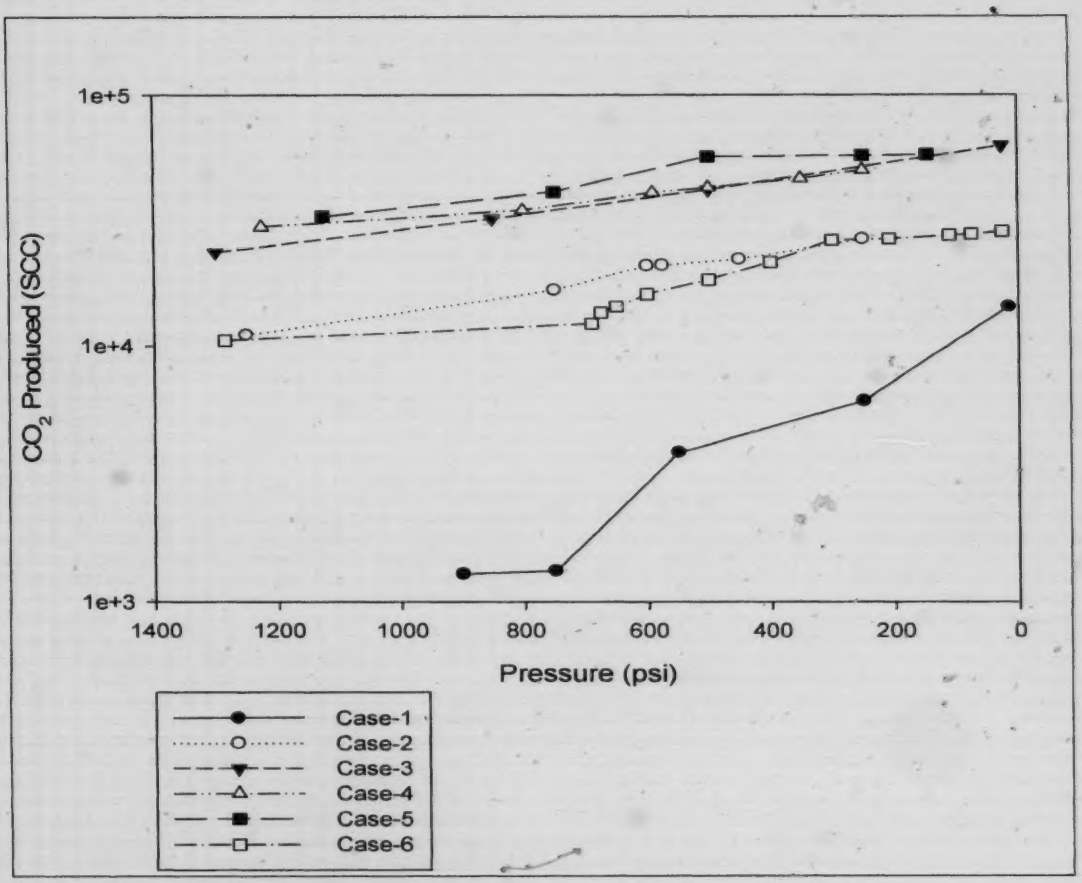

Figure 7.5: CO_2 production with the pressure blowdown for Berea sandstone.

A version of this paper has been published
Trivedi J.J and Babadagli T. 2008. SPE 117606. SPE Eastern Regional/AAPG Eastern Section Joint Meeting
Pittsburgh.11–15 October 2008.

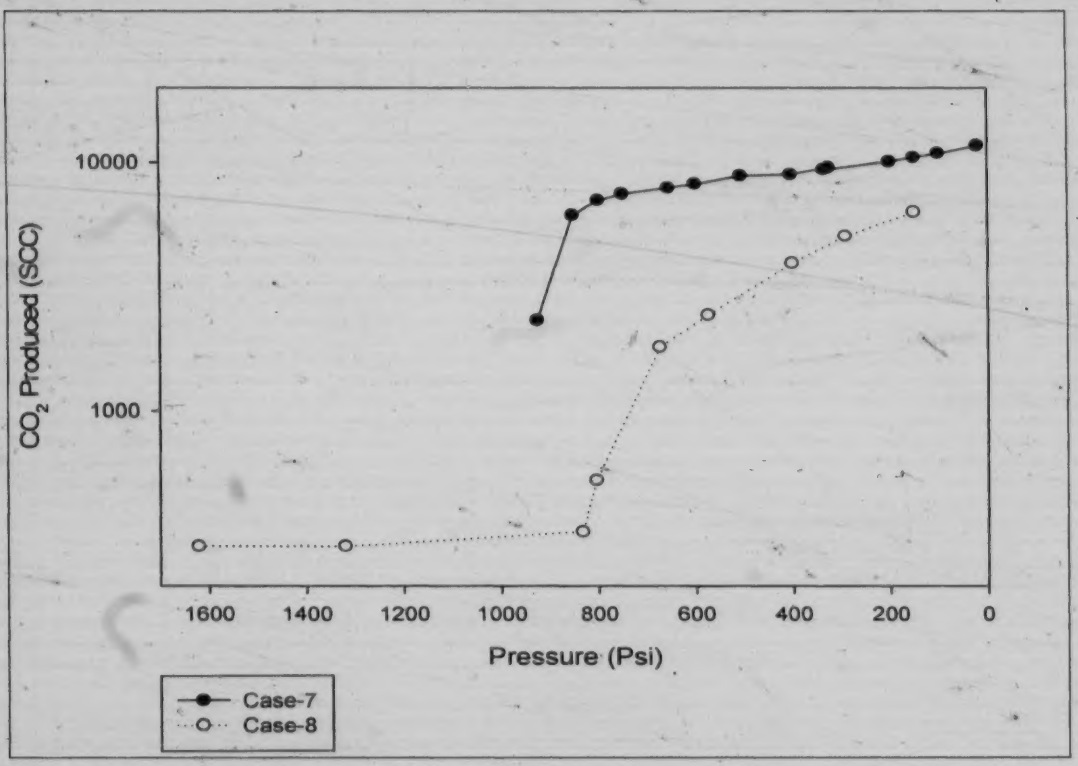

Figure 7.6: CO_2 production with the pressure blowdown for Midale carbonate.

A version of this paper has been published
Trivedi J.J and Babadagli T. 2008. SPE 117606. SPE Eastern Regional/AAPG Eastern Section Joint Meeting Pittsburgh.11–15 October 2008.

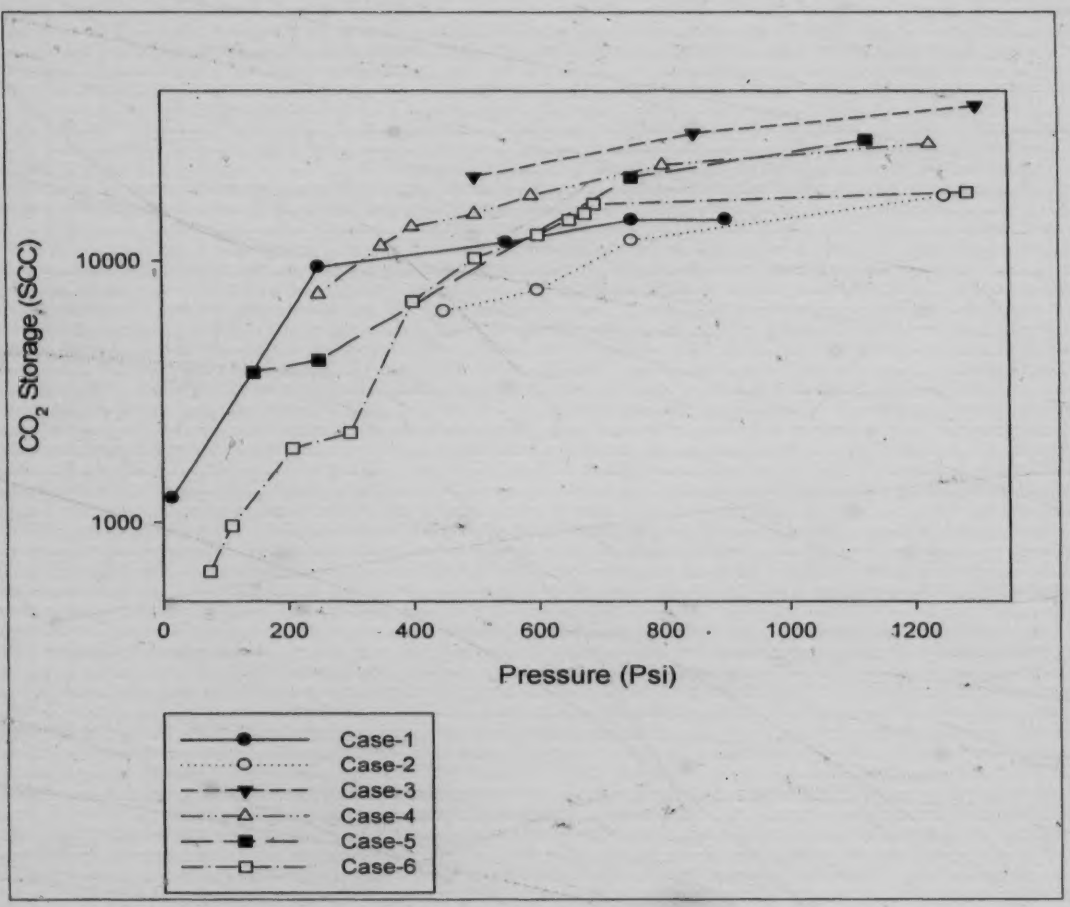

Figure 7.7: CO_2 storage with the pressure blowdown for Berea sandstone.

A version of this paper has been published
Trivedi J.J and Babadagli T. 2008. SPE 117606. SPE Eastern Regional/AAPG Eastern Section Joint Meeting Pittsburgh.11–15 October 2008.

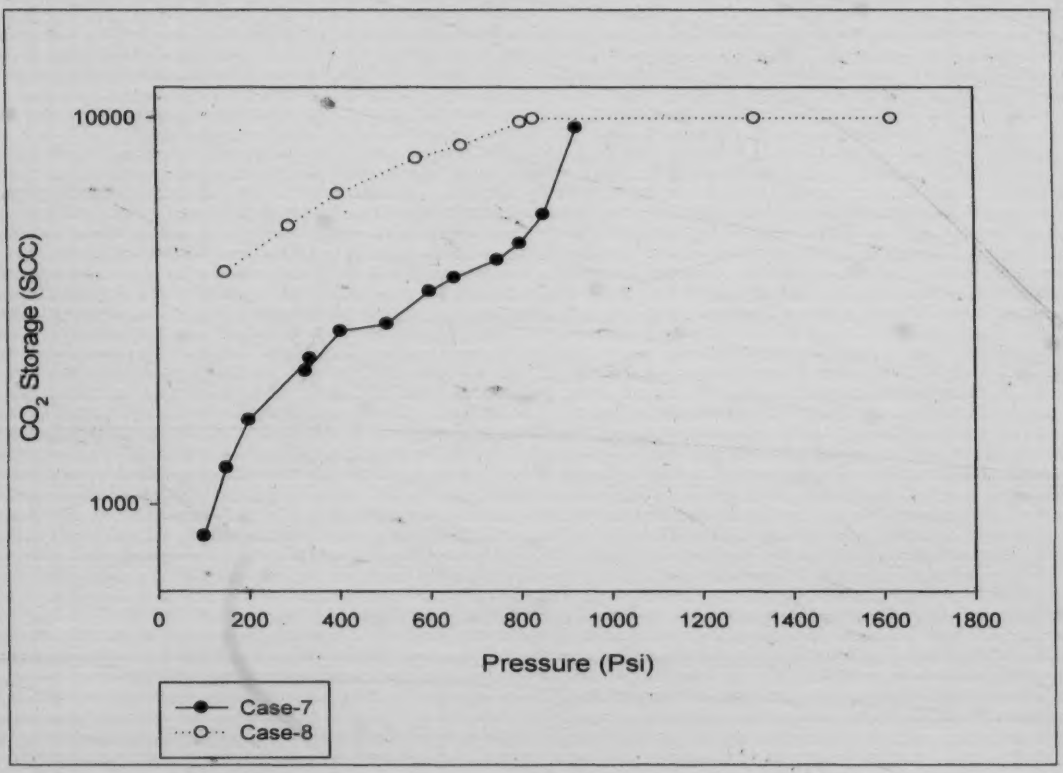

Figure 7.8: CO_2 storage with the pressure blowdown for Midale carbonate.

A version of this paper has been published
Trivedi J.J and Babadagli T. 2008. SPE 117606. SPE Eastern Regional/AAPG Eastern Section Joint Meeting
Pittsburgh.11–15 October 2008.

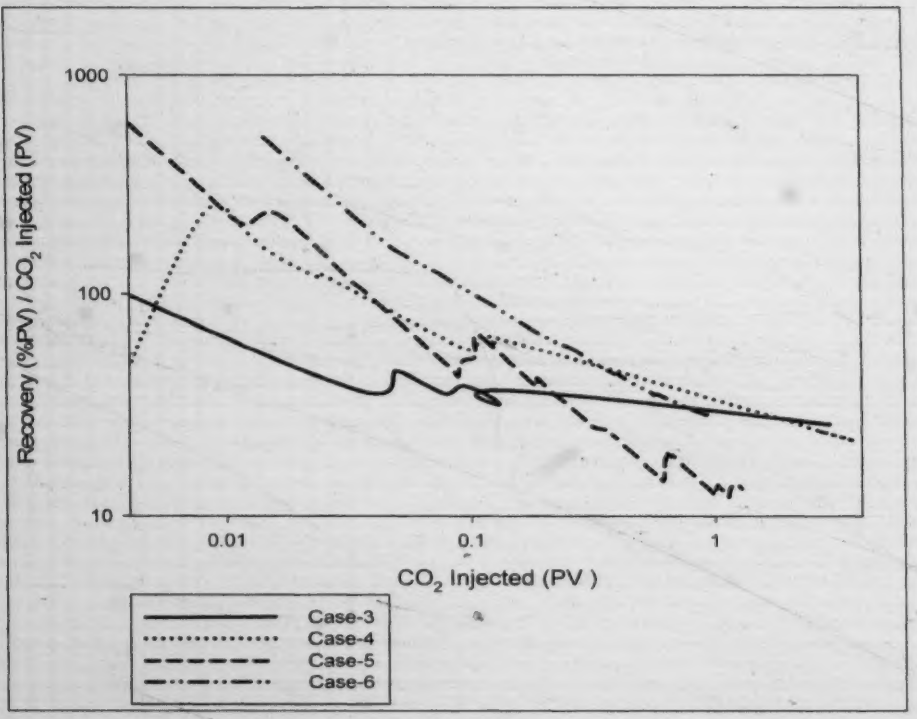

Figure 7.9: Normalized recovery factor with the CO_2 PV injected for Berea sandstone.

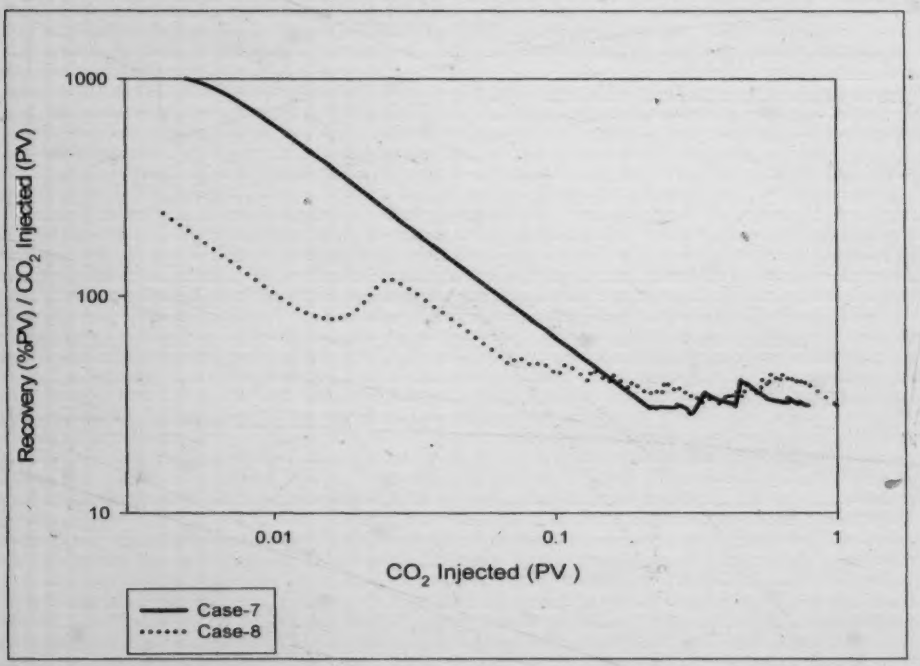

Figure 7.10: Normalized recovery factor with the CO_2 PV injected for Midale carbonate.

A version of this paper has been published
Trivedi J.J and Babadagli T. 2008. SPE 117606. SPE Eastern Regional/AAPG Eastern Section Joint Meeting Pittsburgh.11–15 October 2008.

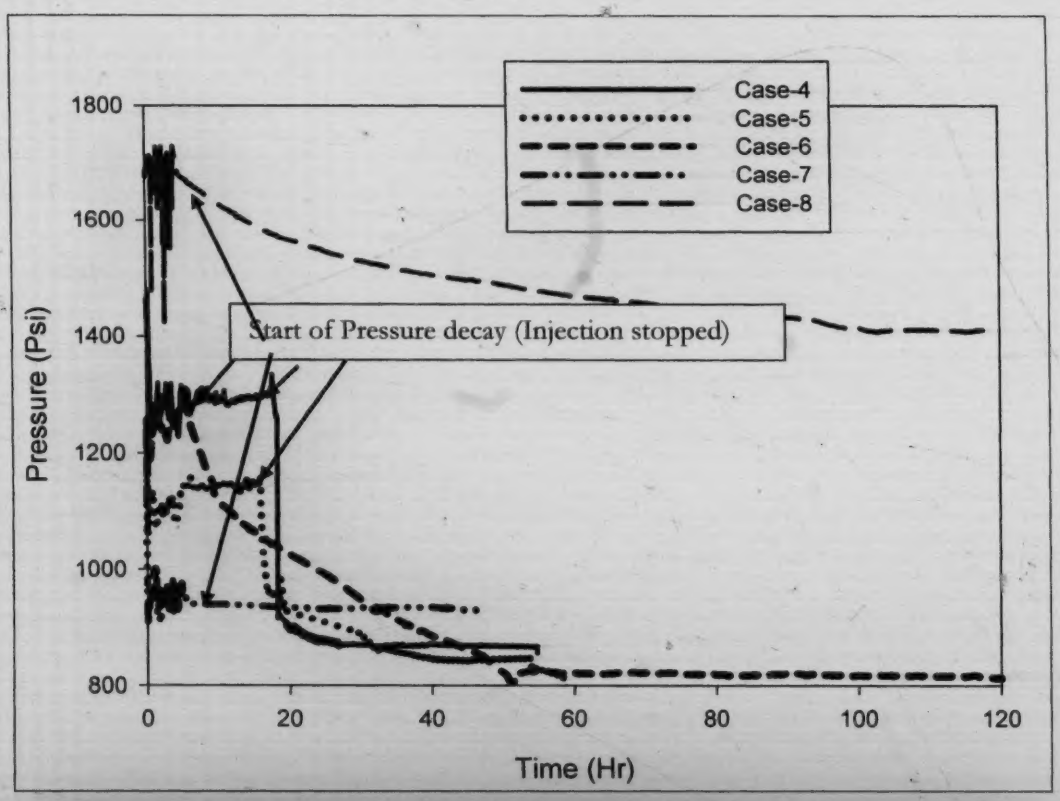

Figure 7.11: Pressure decay and attainment of quasi-equilibrium behavior.

Figure 7.12: Hydrocarbon recovery distribution for the Case-8 at different stages of the production life.

A version of this paper has been published
Trivedi J.J and Babadagli T. 2008. SPE 117606. SPE Eastern Regional/AAPG Eastern Section Joint Meeting
Pittsburgh.11–15 October 2008.

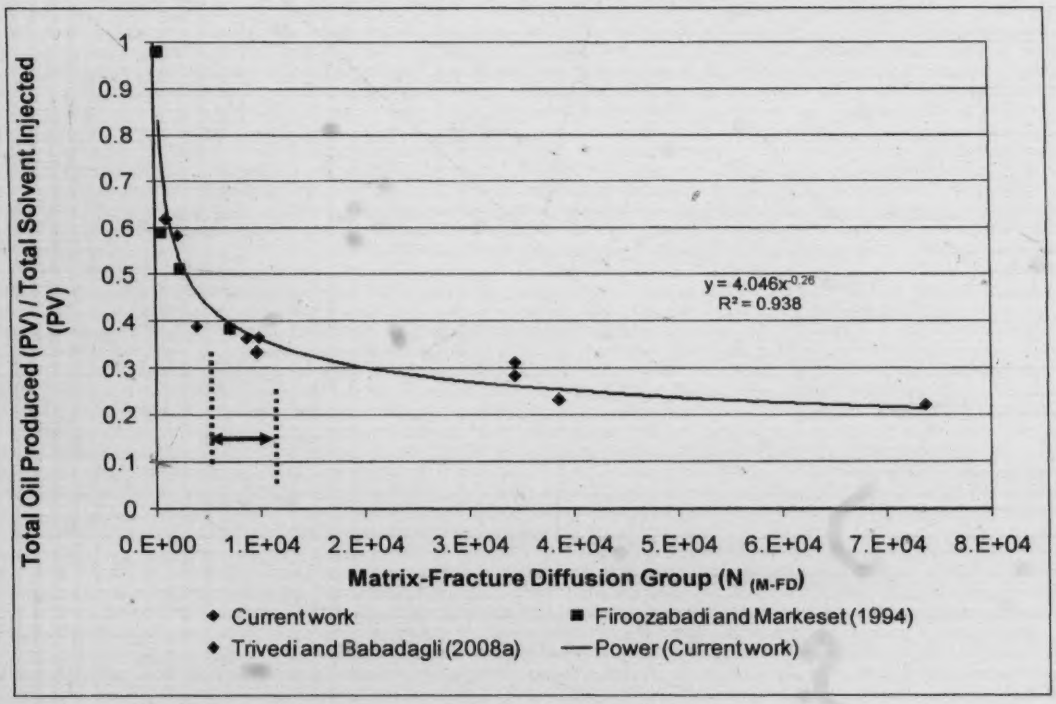

Figure 7.13: (TOP/TSI) with matrix-fracture diffusion group (N_{M-FD}).

A version of this paper has been published
Trivedi J.J and Babadagli T. 2008. SPE 117606. SPE Eastern Regional/AAPG Eastern Section Joint Meeting
Pittsburgh.11–15 October 2008.

8 ANALYSIS OF OBSERVATIONS ON THE MECHANICS OF MISCIBLE GRAVITY DRAINAGE IN FRACTURED SYSTEMS

8.1 Problem Statement

- The understanding of gravity drainage mechanism in fractured systems is still below par. Hence, the modeling of the process is a challenge yet and more attempts are needed towards the clarifications on the physics of the process for accuracy.

- Injected gas flowing in fracture could be in equilibrium or non-equilibrium with the oil phase in porous matrix. Depending on that the recovery mechanism varies quite significantly.

- Moreover, the heterogeneity or presence of fracture adds more dimensions to the difficulty level of the problem.

- The mechanistic difference between gravity stable gas injection and gravity drainage for non-equilibrium gas (special consideration of CO_2) is not studied thoroughly.

- The detailed literature review on the failure of most of the existing models to differentiate the drainage and displacement mechanisms is studied by Kulkarni et al. (2006). Three different mechanisms hypothesized by them for gravity drainage have very limited experimental support in the literature to the best of our knowledge.

- Only attempts to describe the miscible gravity drainage mechanism in NFRs clearly were done by Alavian and Whitson (2005), Darvish et al. (2004) and by Verlaan and Boerrigter (2006) in a simulation study as well as experimental study from Schechter and Guo (1996).

- When the non-equilibrium gas like CO_2 is injected into matrix-fracture system, mechanisms like molecular diffusion, dispersion mixing, swelling, IFT reduction,

viscous displacement, CO_2 solubility effect and properties of fracture as well as matrix may play important role other than the three described by Kulkarni et al.

- The mechanisms may vary depending on the well configuration (location), i.e., injection and production wells located in the fracture or in the matrix.

8.2 Mechanisms: Miscible Gravity Drainage in NFRs

In the experimental study, it was observed that oil produced at different time have different composition than the original oil suggesting the existence of extraction process simultaneously acting with other mechanism. If no extraction has taken place or the oil is only displaced (miscibly or immiscibly), then wt% or the components should remain constant (in terms of normalized concentration it should remain about 1). When a component is preferentially extracted, a change in wt % should be observed; its increase means higher extraction of that particular component (increase in normalized concentration above 1).

1) Drainage in fracture:

At the initial period the composition change was not observed, indicating the recovery from the fracture before much of the CO_2 diffuses into the core. This period is dominant by pure drainage from the fracture. The recovery during this period is affected by flow rate, injection pressure (initial pressure) and density difference.

2) Induced drainage and extraction in matrix with forced drainage in fracture:

In this phase, the oil produced has higher percentage of medium components. The governing mechanism is extraction of oil (swelling due to CO_2-oil contact) and reduction in IFT caused by lateral diffusion of CO_2 and then driven by free fall gravity drainage within matrix and forced drainage in fracture. The oil components that vaporized to the gas phase are transported to the fracture by molecular diffusion due to compositional difference between gas in the fracture and in the matrix. The diffusion is the limiting mechanism here.

3) Extraction of heavier hydrocarbon with forced drainage in fracture:

As the diffusion coefficients of heavier components are comparatively higher, a preferential extraction occurs. At this level the heavier components are extracted.

8.3 Soaking: Improving Extraction Mechanism

If continued long enough, a point will be reached during the second phase at which the recovery becomes uneconomical and there still exists high amount of oil saturation in the matrix to be recovered. To recover this oil, more and more CO_2 needs to be injected but a great portion of it will be quickly produced without producing economical matrix oil making the project inefficient. To enhance the recovery, we propose a new approach. During the late 2nd stage and at the start of 3rd stage when the CO_2 recycling cost begins to increase and oil cut goes down, a soaking of injected CO_2 until this point can increase the recovery. This will allow the third level of recovery mechanism to become effective and heavier components can be preferentially extracted. During soaking, the governing mechanism is extraction and "free fall gravity drainage" (process believed to occur in NFRs after depleting all oil in the fractures or there exists only injected gas in the fractures -Schechter and Guo, 1996).

As shown by Darvish et al. (2004), when the gas saturation in the matrix increases, the oil viscosity drastically increases. During the soaking period when the gas saturation of the matrix increases, oil mobility reduces to very low due to increase in viscosity. This is extraction mechanism where heavier components of residual oil vaporize into the gas phase. This fact has been verified by chromatographic analysis.

Time to reach gas saturation its maximum value and benefit from the recovery by extraction in NFRs could require great amount of time and CO_2 injection as well as recycling depending on the matrix size. This may not be economical in most of the cases. To overcome this problem, we suggest that soaking period would help to gain the recovery through extraction. The length of the soaking period should be limited until the pressure of the closed system (non-equilibrium gas and porous media containing residual oil) reaches a quasi-equilibrium stage.

8.4 Effect of Diffusion/Dispersion and Injection Rate

Diffusion of solvent from the fracture to matrix creates a zone of mixing inside the matrix. The mixing increases with time. In this mixed zone, the oil viscosity and density are reduced. To understand the effect of lateral transfer and diffusion in gravity drainage, first contact miscible experiments were performed as given in Chapter 2. This neglects the effects of compositional change (hence extraction) due to solvent of solute with two distinct components (heptane and mineral oil) as well as capillary and IFT change (both are zero due to first contact miscible nature). The results presented in our previous work shows the oil production rate does not drop drastically supporting the hypothesis, simulation results and experimental trends of previous researches differentiating the drainage and displacement mechanisms. Some of the conclusions gave insights into the importance of lateral flow and diffusion flow:

- When compared with horizontal displacement with vertical drainage, the presence of gravity effect was evident. The effect of gravity was more profound when the rate was higher.

- At early stage, when less amount of solvent is present, the governing mechanism in the process is viscous displacement resulting most recovery from fracture and is higher for higher injection rate.

- The recovery curve at lower solvent injection rate overpasses the one at higher solvent injection rate after a certain amount of solvent injected indicating slower the rate is being more towards free fall drainage into the matrix.

- At high rates, mixing of oil and solvent is higher, resulting in lower viscosity and density in the mixing zone. The mixing zone increases with time and so does the gravity drainage rate. These observations were made by Verlaan and Boerrigter (2006) in their simulation study giving justification to the higher production recovery obtained at higher rate injection with same amount of solvent injected compared to lower rates.

- The mixing zone moves faster with higher injection rate as "fresh solvent" is present in the fracture zone to diffuse into matrix. Subsequently, the drainage rate in the matrix and the rate of oil (solute) drained out to fracture increases (due to the difference of drainage rate between mixing zone and oil zone). This is purely driven by diffusion due to concentration gradient.

- With the increase of injection rate, bypassing of oil zone, i.e. matrix, is more pronounced and this results in lower ultimate recovery. Oil trapping increases as the injection rate and thereby the gravitational force increase. The forced gravity drainage becomes unstable as the injection rate increases. This conclusion was also supported by forced gravity drainage experiments in fractured system by Dastyari et al. (2005). They performed forced drainage experiments using glass micromodels with immiscible pair of fluids. This gives justification to the conclusion that the slower injection rate though resulting slower ultimate recovery but efficient for ultimate recovery.

9 CONTRIBUTIONS AND RECOMMENDATIONS

9.1 Contributions and Conclusions

9.1.1 First Contact Miscible Experiments

- Dominance of the phase diffusion into matrix through fracture over viscous flow in the fracture was shown in this study. Though the higher solvent injection rate yields high production rate of oil in the initial period of the project life, considering the long run, the low rate solvent injection strategy is the best with most of the production contribution from matrix through the diffusion process. Solvent injected at lower rate has more time to diffuse into matrix in transverse direction before it breaks through, hence results in higher ultimate recovery than that of higher rate solvent injection strategy.

- With some water existing in the rock from previous waterflooding, one can still obtain oil recovery from matrix by the diffusion process. Note that the ultimate recovery obtained from the waterflooding followed by the solvent diffusion process would be much lower than the cases with solvent diffusion only.

- The efficiency of the process was investigated using two different parameters. When the amount of oil produced per time is the critical efficiency parameter, a rate of 6 ml/hr was found to be the optimal rate for almost all the cases except less water-wet samples. This approach for efficiency analysis is useful for enhanced oil recovery applications.

- In this study, we have not varied two critical parameters; the size of the matrix (length or width) and oil type (mainly for viscosity variation). Further attempts were made in subsequent studies where the process has been theoretically modeled using

the experimental observations and considering those parameters (Trivedi and Babadagli, 2007a-b).

9.1.2 Scaling of Matrix-Fracture Miscible Process and Critical Rate Definition

- If the amount of oil produced per amount of solvent injected is the critical efficiency parameter, one can define a critical rate.

- Inspectorial Analysis (IA) was applied on governing equations representing miscible matrix-fracture interaction when solvent is injected into oil saturated porous matrix. Seven different independent dimensionless groups were derived by applying linear (affine) transformation to the groups obtained by IA.

- The critical parameter defining the efficiency of the process could be the amount of solvent introduced per oil produced as in the case of enhanced oil recovery applications (the opposite is the case in greenhouse gas sequestration or groundwater contamination processes). None of the scaling groups individually can define the efficiency of the process of interest (Total Oil Produced (TOP) / Total Solvent Injected (TSI)) ratio obtained from miscible experiments. Hence a new dimensionless group combining varying strength of all forces acting as different dimensionless groups during the process was proposed.

- Higher $N_{M\text{-}FD}$ indicates a faster recovery with more solvent injection. On the other hand, a low value of the ($N_{M\text{-}FD}$) is an indication of slow but more efficient recovery, i.e., less solvent injection is required. This might even yield higher ultimate recoveries from the matrix compared to the extremely high injection rate cases.

- This approach for efficiency evaluation is also useful in greenhouse gas sequestration and groundwater contamination practices. Those processes target to maximize the storage of injected material in the matrix and this requires an effective matrix-

fracture transfer due to diffusion. This could be controlled by the rate that would be determined by matrix properties.

9.1.3 Simulation of Matrix-Fracture Process

- The experimental results indicated that the recovery through the fracture (less contribution from matrix) is dominated by the Peclet number (dispersion effect) and mass transfer rate constant (K_r). Hence, at the earlier stage of the production life (when the fracture oil recovery is effective) higher rate solvent injection should be preferred.

- Considering overall effect and assuming the solute inside the matrix pores is larger in amount compared to that in the fracture, the effective diffusion coefficient (D_e^M) is the major controlling parameter and slower rate solvent injection with more retention time for effective diffusive flux to transfer from matrix yields efficient recovery.

- The porous media aged over a period of time behaved different than that of non-aged one depending on the solute properties. The wettability factor presented here and further used in the study proved handy tool for inclusion of aging effect.

- Length of the matrix being one of the important parameter because of the solvent breakthrough was noticed during experiments. The shorter cores, having less time for solvent to diffuse in transverse direction into porous matrix, showed lower solute recovery in a given time and rate compared to the longer ones. We, however, did not observe significant effect of matrix size on the mass transfer rate constant (K_r) and effective diffusion coefficient in matrix (D_e^M).

- The mass transfer rate and effective matrix diffusion coefficient were found to be linearly dependent on the average fluid velocity through fracture and also affected by wettability as well as rock properties.

- K_v and D_e^M, not available from any means of laboratory experiments, can be easily computed for miscible solvent processes in fractured porous media using the correlations provided here with fairly good amount of accuracy.

9.1.4 Multi-Contact CO_2 Experiments

- Critical rate is one of the important factors to be considered while designing an EOR and sequestration project.

- Maintaining near miscible pressure conditions is the most effective for incremental oil recovery. Going beyond the near miscible pressure condition is proven to be beneficial for sequestration purpose but can cause reduction in production.

- The reservoirs with lower temperature can also be targeted for sequestration and EOR.

- The oil recovery from the Midale carbonate cores was only 23 % but after a first cycle of blow down it reached 41 % due to CO_2 diffusion and gravity drainage. The storage capacity of the Midale carbonate was, however, almost half than that of the sandstone rock while maintaining other operational parameter similar.

- The pressure decay during this shutdown (soaking) period gives a measure of diffusion as well as recovery enhancement phenomenon in fractured porous media.

- The recovery of heavier hydrocarbon components is increased by a large fraction during shutdown (soaking) after continuous injection of CO_2. The shutdown after a relatively slow injection rate for a longer period of time yielded higher diffusion and higher amount of oil recovered during the first blowdown compared to faster injection rate case for a shorter period of time.

- Blow down for additional recovery at the end of the CO_2 injection project life, can increase the recovery by 10% up to a certain pressure (~750 psi here). Going below this pressure will affect sequestration adversely without much benefit of recovering oil. CO_2 phase behavior/change during the project is very crucial and should be studied carefully with density and viscosity change into consideration.

- During the project life blowing down reservoir for an economic benefit of oil recovery is not viable after a particular pressure stage and that pressure was found to be around 600-700 psi for Berea sandstone and 400 psi for the Midale carbonate cores. Similarly, while considering greenhouse gas sequestration, the same pressure was proved to be the bottom limit not to exceed the viable range.

- "Huff and Puff" after continuous injection could prove very effective for EOR in fractured reservoirs. The Huff cycle should be at miscible/near miscible condition followed by a shutdown (soaking) until the quasi-equilibrium is reached and then a Puff cycle. The Puff cycle should only be limited to pressure reduction until ~600 psi and then followed by and Huff cycle to again reach miscible pressure.

- Understanding of diffusion/dispersion phenomenon into the matrix-fracture system and its quantification were achieved using successful simulation match of very slow rate CO_2 injection into oil saturated fractured porous media experimental results. Efficiency of the miscible gravity drainage process in fractured porous media can be generalized using a dimensionless group $N_{M\text{-}I/D}$.

- The multicontact miscible diffusion at reservoir temperature and pressure is more complex. This case requires more effort and could be critical especially in the CO_2 injection for EOR and sequestration.

9.2 Recommendations for Future Research

- To predict the efficiency of EOR and sequestration we proposed a critical value of matrix-fracture diffusion group which contains the Peclet and gravity number. More experimental data with a wider range of porosity and permeability, wider scales of viscosity and more oil wet systems for the validation will be ideal for necessary modification in matrix-fracture diffusion group and its use as a transfer functions or as a critical injection rate determination purpose.

- Current reservoir simulation tools consider matrix-fracture interaction to some extent. The phenomenon observed in experiments such as pressure decay to reach quasi-equilibrium and extraction of heavier components during shutdown cannot be dealt easily with current forms of commercial reservoir simulation tools. Modifications such as diffusion coefficient as a function of concentration and pressure conditions also non-equilibrium boundary concepts should be incorporated.

- A micro-model and glass bead model with sandstone and carbonate replicas for miscible CO_2 diffusion and oil swelling behavior at reservoir condition should be tested. The visual and quantitative results will lead to better understating of lighter and heavier component phase diffusion and are necessary to solidify the implicative conclusive statement.

- "Huff and Puff" after continuous injection could prove very effective for EOR in fractured reservoirs. The "Huff" cycle should be at miscible/near miscible condition followed by a shutdown until the quasi-equilibrium is reached and then a "Puff" cycle should be implemented. The "Puff" cycle should only be limited to pressure

reduction till 600-500 psi and then followed by "Huff" cycle to again reach miscible pressure. Further analysis for optimal application schemes for the "Huff" and "Puff" process is needed.

- Since CO_2 was able to recover heavier hydrocarbon components of the crude oil, CO_2 in conjunction with steam injection should be tested in heavy oil NFRs for EOR and CO_2 sequestration.

10 NOMENCLATURE

Chapter - 3

A = Total area for the core, m^2

$2b$ = Fracture aperture, m

CF = Concentration in fracture, fraction

CM = Concentration in matrix, fraction

D_m = Mutual diffusion coefficient, m^2/s

D_L = Effective dispersion coefficient in fracture, m^2/s

D_e^M = Effective diffusion coefficient in matrix for matrix-fracture system, m^2/s

D_{eff} = Effective diffusion coefficient, m^2/s

D_{mech} = Mechanical dispersion coefficient, m^2/s

g = gravitational force, m/s^2

K_V = Mass transfer rate constant, s^{-1}

N = Flux

P = Pressure, N/m^2

Pe = Peclet number, Dimensionless

Q_S = Source term,

Q = Amount imbibed, m^3

r = Half fracture spacing, m

S = Saturation, fraction

t = time, s

V = Average fluid velocity in the fracture, m/s

W_{factor} = Wettability factor, Dimensionless

x = coordinate direction along the fracture, m

y = coordinate direction normal to the fracture, m

Greek Letters

κ = Permeability, m^2

ρ_f = Density, kg/m^3

μ = Viscosity, kg/m.s

Subscripts

1 = Solvent

2 = Solute

h = Hydraulic

m = Mass transfer

M = Matrix

F = Fracture

R = Reaction

C = Convection

S = Surface

C = Capillary

K = Kerosene

W = Water

Chapter - 4

b = Fracture width, m

Bi_m = Biot number, Dimensionless

$< C_A >$ = Cup-mixing concentration (transverse averaged concentration weighted with respect to the normalized longitudinal velocity, fraction

C_{AW} = Circumferentially averaged concentration at the fluid-solid interface, fraction

Da = Damkohler number, Dimensionless

D_L = Effective dispersion coefficient in fracture, m^2/s

D_e^M = Effective diffusion coefficient in matrix for matrix-fracture system, m^2/s

K_V = Mass transfer rate constant, s^{-1}

K_m = mass-transfer coefficient between bulk fluid phase and matrix fluid phase, m/s.

L = Characteristic length, m

P = Pressure, N/m^2

Pe = Peclet number, Dimensionless

R = Core radius, m

Re = Reynolds number, Dimensionless

Sh = Sherwood number, Dimensionless

t = time, s (Defined in Table 4.1)

v = Average fluid velocity in the fracture, m/s

W_{factor} = Wettability factor, Dimensionless

Greek Letters

ρ = Density, kg/m^3

μ = Viscosity, kg/m.s

ϕ = Thiele modulus, Dimensionless

η = Effectiveness factor, Dimensionless

Subscript

1 = Solvent

2 = Solute

∞ = Asymptotic Value

C = Capillary

G = Global

K = Kerosene

L = Local

r = radial direction

z = transverse direction

Chapter - 5

b = Fracture width m,

C_e = Concentration at equilibrium

D_L = Effective dispersion coefficient in fracture m^2/s,

D_e^M = Effective diffusion coefficient in matrix for matrix-fracture system m^2/s,

FDI = Fracture diffusion index, dimensionless,

g = Gravity force m/s,

k_f = Fracture permeability m^2,

k_m = Matrix permeability m^2,

L = Length of Fracture m,

L_x = Matrix size in x direction m,

L_y = Matrix size in y direction m,

$N_{f,Ca}$ = Facture capillary number, dimensionless

$P_{c,eff}$ = Effective capillary pressure, dimensionless,

$P_{c,max}$ = Maximum capillary pressure value (P_c at S_{wi}=0), dimensionless,

Q_I = Amount of solvent injected (Pore volume)

Q_P = Amount of solute produced (Pore volume)

r = Matrix width m,

u_f = Flow velocity m/s,

Symbols

μ_w = Viscosity of water, cp,

σ = Interfacial tension, N/m,

ρ_s = Density of injected (solvent) phase, kg/m^3,

ρ_o = Density of displaced (oil) phase, kg/m^3,

$\emptyset_f$ = Porosity (Fracture)

$\emptyset_M$ = Porosity (matrix)

μ_s = Solvent viscosity, kg/m.s,

μ_o = Solute viscosity, kg/m.s,

$\Delta\mu$ = Viscosity difference, kg/m.s,

$\Delta\varrho$ = Density difference, kg/m^3

Chapter - 7

b = Fracture width m,

D_l = Effective dispersion coefficient in fracture m^2/s,

D_e = Effective diffusion coefficient in matrix for matrix-fracture system m2/s,

g = Gravity force m/s,

k_f = Fracture permeability m^2,

k_m = Matrix permeability m^2,

L = Length of Fracture m,

Lx = Matrix size in x direction m,

Ly = Matrix size in y direction m,

r = Matrix width m,

u_f = Flow velocity m/s,

Symbols

ρ_s = Density of injected (solvent) phase, kg/m^3,

ρ_o = Density of displaced (oil) phase, kg/m^3,

$\emptyset_f$ = Porosity (Fracture)

$\emptyset_M$ = Porosity (matrix)

μ_s = Solvent viscosity, kg/m.s,

μ_o = Solute viscosity, kg/m.s,

$\Delta\mu$ = Viscosity difference, kg/m.s,

$\Delta\rho$ = Density difference, kg/m^3

11 APPENDIX

Fracture:

$$\frac{\partial C_F}{\partial t} + u_{Fx}\frac{\partial C_F}{\partial x} - D_L\frac{\partial^2 C_F}{\partial x^2} + \frac{\phi_m D_m}{b}\frac{\partial C_M}{\partial y} = 0 \quad \text{.....(10.1)}$$

For matrix:

$$\frac{\partial C_M}{\partial t} - D_m\frac{\partial^2 C_M}{\partial y^2} = 0 \quad \text{.....(10.2)}$$

$$u_{FX} = -\frac{k_F}{\mu_F}\left(\frac{\partial P_F}{\partial x} + \rho_F g\right) \quad \text{.....(10.3)}$$

$C = 0$ at $t = 0$ $\quad \forall x, y$ .....(10.4)

$u_y = 0$ at $y = 0$ $\quad \forall x, t$ .....(10.5)

$u_y = 0$ at $y = b$ $\quad \forall x, t$ .....(10.6)

$$\frac{1}{b}\int_0^b u_{FX}\,dy = u_T \quad \text{At x=0} \quad \text{.....(10.7)}$$

$$P_F = P_{wf} + \rho_m g(b - y) \quad \text{at x=L} \quad \text{.....(10.8)}$$

Dimensionless variables for non-dimensionalizing the above equations related to our system are as follows:

$$x = \left(X_1^* X_D + X_2^*\right) \quad \text{.....(10.9)}$$

$$y = \left(y_1^* y_D + y_2^*\right) \text{ (Within fracture)} \quad \text{(10.10)}$$

$$y = \left(Y_1^* Y_D + Y_2^*\right) \text{ (Within matrix)} \quad \text{(10.11)}$$

$$t = \left(t_1^* t_D + t_2^*\right) \quad \text{(10.12)}$$

$$C_F = (C_{F1}^* C_{FD} + C_{F2}^*) \quad \text{(10.13)}$$

$$C_M = (C_{M1}^* C_{MD} + C_{M2}^*) \quad \text{(10.14)}$$

$$u_{Fx} = (u_{FX1}^* u_{FXD} + u_{FX2}^*) \quad \text{(10.15)}$$

$$P_F = (P_{F1}^* P_{FD} + P_{F2}^*) \quad \text{(10.16)}$$

Using these dimensionless variables (Equations 10.9 to 10.16) the advection-convection equation (Eq. 10.1) for fracture can be written as:

$$\left(\frac{C_{F1}^*}{t_1^*}\right)\frac{\partial C_{FD}}{\partial t_D} + (u_{FX1}^* u_{FXD} + u_{FX2}^*)\left(\frac{C_{F1}^*}{X_1^*}\right)\frac{\partial C_{FD}}{\partial X_D} - D_L\left(\frac{C_{F1}^*}{(X_1^*)^2}\right)\frac{\partial^2 C_{FD}}{\partial X_D^2} + \phi_m D_m\left(\frac{C_{M1}^*}{Y_1^*}\right)\frac{\partial C_{MD}}{\partial Y_D} = 0 \quad \text{(10.1A)}$$

$$\frac{\partial C_{FD}}{\partial t_D} + \left(\frac{t_1^* u_{FX1}^*}{X_1^*}\right) u_{FXD}\frac{\partial C_{FD}}{\partial X_D} + \left(\frac{t_1^* u_{FX2}^*}{X_1^*}\right)\frac{\partial C_{FD}}{\partial X_D} - \left(\frac{D_L t_1^*}{(X_1^*)^2}\right)\frac{\partial^2 C_{FD}}{\partial X_D^2} + \left(\frac{\varphi_m D_m t_1^*}{Y_1^*}\right)\frac{\partial C_{MD}}{\partial Y_D} = 0 \quad \text{(10.1B)}$$

Using these dimensionless variables (Equations 9 to 16) the advection-convection equation (Eq. 2) for matrix can be written as:

$$\frac{\partial C_{MD}}{\partial t_D} - \left(\frac{D_m t_1^*}{(Y_1^*)^2}\right)\frac{\partial^2 C_{MD}}{\partial Y_D^2} = 0 \quad \text{(10.2A)}$$

Similarly, using the dimensionless variables in Equations 10.9 to 10.16, one can present Equations 10.3 to 10.8 in the dimensionless form:

$$\left(u^*_{FX1}u_{FXD}+u^*_{FX2}\right)=k_F\left[\mu_0+(C^*_{F1}C_{FD}+C^*_{F2})(\mu_S-\mu_0)\right]^{-1}\left(\left(\frac{P^*_{F1}}{X^*_1}\right)\frac{\partial P_{FD}}{\partial X_D}+\left(\rho_0+(C^*_{F1}C_{FD}+C^*_{F2})\Delta\rho\right)g\right) \quad \text{.....(10.3A)}$$

$$u_{FXD}=-\left[\left\{\left(\frac{C^*_{F1}X^*_1u^*_{FX1}\mu_0}{k_FP^*_{F1}}\right)-\left(\frac{C^*_{F1}X^*_1u^*_{FX1}\mu_S}{k_FP^*_{F1}}\right)\right\}C_D+\left(\frac{C^*_{F2}X^*_1u^*_{FX1}\Delta\mu}{k_FP^*_{F1}}\right)+\left(\frac{X^*_1u^*_{FX1}\mu_0}{k_FP^*_{F1}}\right)\right]^{-1}$$

$$\left[\frac{\partial P_{XD}}{\partial X_D}+\left(\frac{\Delta\rho gX^*_1C^*_{F1}}{P^*_{F1}}\right)C_D+\left(\frac{\rho_0gX^*_1}{P^*_{F1}}\right)+\left(\frac{\Delta\rho gX^*_1C^*_{F2}}{P^*_{F1}}\right)\right]-\left(\frac{u^*_{FX2}}{u^*_{FX1}}\right) \quad \text{.....(10.3B)}$$

$$(C^*_{F1}C_{FD}+C^*_{F2})=0 \quad \text{at } t^*_1t_D+t^*_2=0 \quad \forall X_D,y_D \quad \text{.....(10.4A)}$$

$$C_{FD}=\left(-\frac{C^*_{F2}}{C^*_{F1}}\right) \quad \text{at } t_D=\left(-\frac{t^*_2}{t^*_1}\right) \quad \forall X_D,y_D \quad \text{.....(10.4B)}$$

$$(u^*_{Fy1}u_{FyD}+u^*_{Fy2})=0 \quad \text{at } y^*_1y_D+y^*_2=0 \quad \forall X_D,t_D \quad \text{.....(10.5A)}$$

$$u_{FyD}=\left(-\frac{u^*_{Fy2}}{u^*_{Fy1}}\right) \quad \text{at } y_D=\left(-\frac{y^*_2}{y^*_1}\right) \quad \forall X_D,t_D \quad \text{.....(10.5B)}$$

$$(u^*_{Fy1}u_{FyD}+u^*_{Fy2})=0 \quad \text{at } y^*_1y_D+y^*_2=b \quad \forall X_D,t_D \quad \text{.....(10.6A)}$$

$$u_{FyD}=\left(-\frac{u^*_{Fy2}}{u^*_{Fy1}}\right) \quad \text{at } y_D=\left(\frac{b-y^*_2}{y^*_1}\right) \quad \forall X_D,t_D \quad \text{.....(10.6B)}$$

$$\left(\frac{y^*_1}{b}\right)\int_0^{(b-y^*_2)/y^*_1}\left(u^*_{FX1}u_{FXD}+u^*_{FX2}\right)dY_D=u_T \quad \text{at } \left(X^*_1X_D+X^*_2\right)=0 \quad \forall t_D \quad \text{.....(10.7A)}$$

$$\int_0^{(b-y^*_2)/y^*_1}\left(u_{FXD}+\left(\frac{u^*_{FX2}}{u^*_{FX1}}\right)\right)dy_D=\left(\frac{u_Tb}{y^*_1u^*_{FX1}}\right) \quad \text{at } X_D=\left(-\frac{X^*_2}{X^*_1}\right) \quad \forall t_D \quad \text{.....(10.7B)}$$

$$(P^*_{F1}P_{FD} + P^*_{F2}) = P_{wf} + \left[\rho_0 + \Delta\rho\left(\left(\frac{y^*_1}{b}\right)\int_0^{(b-y^*_2)/y^*_1}\left(u^*_{FX1}u_{FXD} + u^*_{FX2}\right)dY_D\right)\left(g\left(b - y^*_1 y_D - y^*_2\right)\right)\right]$$

$$\text{at } \left(X^*_1 X_D + X^*_2\right) = L \;; \qquad 0 \le \left(y^*_1 y_D + y^*_2\right) \le b \quad \text{.....(10.8A)}$$

$$\text{at } X_D = \left(\frac{\mathbf{L - X^*_2}}{\mathbf{X^*_1}}\right); \qquad \left(-\frac{\mathbf{y^*_2}}{\mathbf{y^*_1}}\right) \le y_D \le \left(\frac{\mathbf{b - y^*_2}}{\mathbf{y^*_1}}\right) \quad \text{.....(10.8B)}$$

Table 10.1: The unique dimensionless group from the above equations (marked as bold letters)

$\left(\frac{t^*_1 u^*_{FX1}}{X^*_1}\right)$	$\left(\frac{X^*_1 u^*_{FX1}\mu_0}{k_F P^*_{F1}}\right)$	$\left(-\frac{\mathbf{u^*_{FX2}}}{\mathbf{u^*_{FX1}}}\right)$
$\left(\frac{t^*_1 u^*_{FX2}}{X^*_1}\right)$	$\left(\frac{\Delta\rho g X^*_1 C^*_{F1}}{P^*_{F1}}\right)$	$\left(-\frac{\mathbf{y^*_2}}{\mathbf{y^*_1}}\right)$
$\left(\frac{D_L t^*_1}{(X^*_1)^2}\right)$	$\left(\frac{\rho_0 g X^*_1}{P^*_{F1}}\right)$	$\left(\frac{\mathbf{b - y^*_2}}{\mathbf{y^*_1}}\right)$
$\left(\frac{\phi_m D_m t^*_1}{Y^*_1}\right)$	$\left(\frac{\Delta\rho g X^*_1 C^*_{F2}}{P^*_{F1}}\right)$	$\left(\frac{u_T b}{y^*_1 u^*_{FX1}}\right)$
$\left(\frac{D_m t^*_1}{(Y^*_1)^2}\right)$	$\left(\frac{u^*_{FX2}}{u^*_{FX1}}\right)$	$\left(-\frac{\mathbf{X^*_2}}{\mathbf{X^*_1}}\right)$
$\left(\frac{C^*_{F1} X^*_1 u^*_{FX1}\mu_0}{k_F P^*_{F1}}\right)$	$\left(-\frac{\mathbf{C^*_{F2}}}{\mathbf{C^*_{F1}}}\right)$	$\left(\frac{P_{wf} - P^*_{F2}}{P^*_{F1}}\right)$
$\left(\frac{C^*_{F1} X^*_1 u^*_{FX1}\mu_S}{k_F P^*_{F1}}\right)$	$\left(-\frac{\mathbf{t^*_2}}{\mathbf{t^*_1}}\right)$	$\left(\frac{\mathbf{L - X^*_2}}{\mathbf{X^*_1}}\right)$
$\left(\frac{C^*_{F2} X^*_1 u^*_{FX1}\Delta\mu}{k_F P^*_{F1}}\right)$	$\left(-\frac{\mathbf{u^*_{Fy2}}}{\mathbf{u^*_{Fy1}}}\right)$	

For eliminating extra dimensionless group from these 23 groups obtained from above equations, the arbitrary scale factors being 0 and 1 can be assigned:

Hence, setting;

$$\left(\frac{C^*_{F2}X^*_1u^*_{FX1}\Delta\mu}{k_F P^*_{F1}}\right)=0 \quad ; \quad \left(\frac{u^*_{FX2}}{u^*_{FX1}}\right)=0 \quad ; \quad \left(\frac{C^*_{F2}}{C^*_{F1}}\right)=0$$

$$\left(\frac{t^*_2}{t^*_1}\right)=0 \quad ; \quad \left(\frac{X^*_2}{X^*_1}\right)=0 \quad ; \quad \left(\frac{P_{wf}-P^*_{F2}}{P^*_{F1}}\right)=0$$

and,

$$C^*_{F1}=1 \quad ; \quad C^*_{M1}=1 \quad ; \quad \left(\frac{L-X^*_2}{X^*_1}\right)=1 \quad ; \quad \left(\frac{t^*_1u^*_{FX1}}{X^*_1}\right)=1 \; ;$$

$$\left(\frac{C^*_{F1}X^*_1u^*_{FX1}\mu_0}{k_F P^*_{F1}}\right)=1 \; ; \quad \left(\frac{X^*_1u^*_{FX1}\mu_0}{k_F P^*_{F1}}\right)=1 \; ; \quad \left(\frac{u_T b}{Y^*_1u^*_{FX1}}\right)=1 \; ; \quad \left(\frac{b-y^*_2}{y^*_1}\right)=1$$

We obtain the scale factors:

$$X^*_1=L \quad ; \quad t^*_1=\left(\frac{L}{u_T}\right) \quad ; \quad P^*_{F1}=\left(\frac{\mu_0 L u_T}{k_F}\right) \quad ;$$

$$u^*_{FX1}=u_T \quad ; \quad y^*_1=b$$

Thus, the Equations (10.1B), (10.2B), (10.3B), (10.4B) and (10.5B) can be reduced to following dimensionless equations:

$$\frac{\partial C_{FD}}{\partial t_D} + u_{FxD}\frac{\partial C_{FD}}{\partial x_D} - \left(\frac{D_L}{Lu_T}\right)\frac{\partial^2 C_F}{\partial x^2} + \left(\frac{\phi_m D_m L}{bru_T}\right)\frac{\partial C_{MD}}{\partial Y_D} = 0 \quad \text{..... (10.1C)}$$

$$\frac{\partial C_{MD}}{\partial t_D} - \left(\frac{D_m L}{r^2 u_T}\right)\frac{\partial^2 C_{MD}}{\partial Y_D{}^2} = 0 \quad \text{..... (10.2C)}$$

$$u_{FXD} = -\left[\left(1-\left(\frac{\mu_S}{\mu_0}\right)\right)C_D + 1\right]^{-1}\left[\frac{\partial P_{FD}}{\partial X_D} + \left(\frac{k_F \Delta\rho g}{\mu_0 u_T}\right)C_D + \left(\frac{k_F \rho_0 g}{\mu_0 u_T}\right)\right] \quad \text{..... (10.3C)}$$

$C_{FD} = 0$ at $t_D = 0$ $\forall X_D, y_D$ ..... (10.4C)

$u_{FyD} = 0$ at $y_D = 0$ $\forall X_D, t_D$ ..... (10.5C)

$u_{FyD} = 0$ at $y_D = 1$ $\forall X_D, t_D$ ..... (10.6C)

$\int_0^1 (u_{FXD})dy_D = 1$ at $X_D = 0$ $\forall t_D$ ..... (10.7C)

$$P_{FD} = \left[\left(\frac{k_F \rho_0 gb}{\mu_0 u_T L}\right) + \left(\frac{k_F \Delta\rho gb}{\mu_0 u_T L}\right)\int_0^1 u_{FXD}\,dy_D\right](1-y_D) \quad \text{at } X_D = 1, \quad 0 \le y_D \le 1 \text{ ..... (10.8C)}$$

The dimensionless groups from the above equations (10.1C to 10.5C) are:

$\left(\frac{D_L}{Lu_T}\right)$ ..... (G'-1)

$\left(\frac{\phi_m D_m L}{bru_T}\right)$ ..... (G'-2)

$\left(\frac{D_m L}{r^2 u_T}\right)$ ..... (G'-3)

$\left(\frac{\mu_S}{\mu_0}\right)$ ..... (G'-4)

$$\left(\frac{k_F \Delta\rho g}{\mu_0 u_T}\right) \quad \text{(G'-5)}$$

$$\left(\frac{k_F \rho_0 g}{\mu_0 u_T}\right) \quad \text{(G'-6)}$$

$$\left(\frac{k_F \rho_0 g b}{\mu_0 u_T L}\right) \quad \text{(G'-7)}$$

$$\left(\frac{k_F \Delta\rho g b}{\mu_0 u_T L}\right) \quad \text{(G'-8)}$$

The coefficient matrix of these groups:

D_L	L	u_T	ϕ_m	D_m	b	r	μ_0	μ_S	k_F	$\Delta\rho$	g	ρ_o
1	−1	−1	0	0	0	0	0	0	0	0	0	0
0	1	−1	1	1	−1	−1	0	0	0	0	0	0
0	1	−1	0	1	0	2	0	0	0	0	0	0
0	0	0	0	0	0	0	−1	1	0	0	0	0
0	0	−1	0	0	0	0	−1	0	1	1	1	0
0	0	−1	0	0	0	0	−1	0	1	0	1	1
0	−1	−1	0	0	1	0	−1	0	1	0	1	1
0	−1	−1	0	0	1	0	−1	0	1	1	1	0

Dimensionless scaling groups can be reduced to using the raw elimination method on coefficient matrix:

$$
\begin{array}{cccccccccccc}
D_L & L & u_T & \phi_m & D_m & b & r & \mu_0 & \mu_S & k_F & \Delta\rho & g & \rho_o \\
\left|\begin{array}{cccccccccccc}
1 & 0 & 0 & 0 & -1 & 0 & 0 & 0 & 0 & 0 & 0 & 0 & 0 \\
0 & -1 & 0 & 1 & 0 & 0 & 1 & 0 & 0 & 0 & 0 & 0 & 0 \\
0 & 0 & -1 & 0 & 1 & -1 & 0 & 0 & 0 & 0 & 0 & 0 & 0 \\
0 & 0 & 0 & 0 & 0 & 0 & 0 & -1 & 1 & 0 & 0 & 0 & 0 \\
0 & 0 & 0 & 0 & 0 & 0 & 0 & 0 & 0 & 0 & 1 & 0 & -1 \\
0 & 0 & -1 & 0 & 0 & 0 & 0 & -1 & 0 & 1 & 1 & 1 & 0 \\
0 & -1 & 0 & 0 & 0 & 1 & 0 & 0 & 0 & 0 & 0 & 0 & 0
\end{array}\right|
\end{array}
$$

Hence we obtain the final dimensionless groups as;

$\left(\frac{D_L}{D_m}\right)$ = (Dispersion diffusion ratio) ..... (G1)

$\left(\frac{\phi_m r}{L}\right)$ = (1/aspect ratio for matrix) ..... (G2)

$\left(\frac{D_m}{bu_T}\right)$ = (1/*Pe*) ..... (G3)

$\left(\frac{\mu_S}{\mu_0}\right)$ = (1/M) = (1/Mobility factor) ..... (G4)

$\left(\frac{\Delta\rho}{\rho_0}\right)$ = Density Number ..... (G5)

$\left(\frac{k_F \Delta\rho g}{\mu_0 u_T}\right)$ = Gravity Number ..... (G6)

$\left(\frac{b}{L}\right)$ = (1/Aspect ratio for fracture) ..... (G7)

12 BIBLIOGRAPHY

Aris R., 1956. On dispersion of a solute in a fluid flowing through a tube. Proc. R. Soc. London A. 235 (1200): 66.

Alavian S. A. and Whitson C. H., 2005. CO_2 IOR Potential in Naturally Fractured Haft Kel Field, Iran. IPTC 10641, International Petroleum Technology Conference. Doha, Qatar. November.

Asghari K. and Torabi F., 2007. Experimental Study of Extent and Rate of Gravity Drainage of Oil From Matrix into Fractures in Presence of Miscible and Immiscible CO_2. Paper 2007-120, 58th Annual Technical Meeting, Canadian International Petroleum Conference, Calgary, AB, Canada, 12-14 June.

Babadagli T. and Ershaghi I., 1993. Improved Modeling of Oil/Water Flow in Naturally Fractured Reservoirs Using Effective Fracture Relative Permeabilities. SPE 26076, SPE Western Regional Meet., Anchorage, Alaska, May 26-28.

Babadagli T. and Zeidani K., 2004. Evaluation of Matrix-Fracture Imbibition Transfer Functions for Different Types of Oil, Rock and Aqueous Phases. SPE 89450, paper presented at the 14th SPE/DOE Symposium on Improved Oil Recovery, Tulsa, OK, April.

Babadagli T., 2000. Efficiency of Capillary Imbibition Dominated Displacement of Non-Wetting Phase by Wetting Phase in Fractured Porous Media. Transport in Porous Media. 40: 323.

Babadagli T., 2002. Scaling capillary imbibition during static thermal and dynamic fracture flow conditions. J. Pet. Sci. Eng. 33: 223.

Babadagli T., Hatiboglu C. U. and Hamida T., 2005. Evaluation of Matrix-Transfer Functions for Counter-Current Capillary Imbibition. SPE 92111, SPE Asia Pacific Oil & Gas Conference and Exhibition, Jakarta, Indonesia, April.

Bachu S., 2002. Sequestration of CO2 in Geological Media: Criteria and Approach for Site Selection in Response to Climate Change. Energy Convers. Manag. 41: 953.

Bear J., 1988. Dynamics of fluids in porous media. New York: Dover Publications Inc.

Bear J., 1979. Hydraulics of groundwater. McGraw Hill.

Bhattacharya M., Harold M. P. and Balakotaiah V., 2000. Mass-transfer coefficients in washcoated monoliths. AICHE J. 50: 2939.

Burger J. E., Springate G. and Mohanty K. K., 1996. Experiments on Bypassing during Gas Floods in Heterogeneous Porous Media. SPERE. 11 (2): 109.

Burger J.E. and Mohanty K. K., 1997. Mass transfer from bypassed zones during gas injection. SPERE. 12 (2): 124.

Chakravarthy D., Muralidaharan V., Putra E., Hidayati D. T. and Schechter D. S., 2006. Mitigating Oil Bypassed in Fractured Cores During CO2 Flooding Using WAG and Polymer Gel Injections. SPE 97228, SPE/DOE Symposium on Improved Oil Recovery, Tulsa, OK, USA, 22-26 April.

Civan F. and Rasmussen M. L., 2002. Improved measurement of gas diffusivity for miscible gas flooding under nonequilibrium and equilibrium conditions. SPE 75135, SPE/DOE Improved Oil Recovery Symposium. Tulsa, OK. April.

Civan F. and Rasmussen M. L., 2005. Determination of Parameters for Matrix-Fracture Transfer Functions From Laboratory Data. SPE 94267, SPE Production & Operation Symposium, Oklahoma City, OK, April.

Comings F. W. and Sherwood T. K., 1934. The drying of solids, moisture movement by capillarity in drying granular materials. Ind. & Eng. Chemistry. 26: 1096.

Correa A. C. F. and Firoozabadi A., 1996. Concept of Gravity Drainage in Layered Porous Media. SPEJ. March. 101-111.

COMSOL. 2006. COMSQL Multiphysics; 3.2 ed. Stockholm, Sweden.

Cybulski A. and Moulin J. A., 1994. Monoliths in Heterogeneous Catalysis. Catal. Rev. Sci. Eng. 36: 179.

Cybulski A. and Moulin J. A., 1998. Structured catalysis and reactors. New York: Marcel Dekker.

Darvish G. R., Lindeberg E., Holt T., Utne S. A. and Kleppe J., 2006a. Reservoir-Condition Laboratory Experiments of CO_2 Injection into Fractured Cores. SPE 99650, SPE Europe/EAGE Annual Conference and Exhibition, Vienna, Austria, 12-15 June.

Darvish G. R., Lindeberg E., Holt T. and Utne S. A., 2006b. Reservoir-Condition Laboratory Experiments of CO_2 Injection into Fractured Cores. SPE 99649, SPE Europe/EAGE Annual Conference and Exhibition, Vienna, Austria, 12-15 June.

Da Silva F. L. and Belery P., 1989. Molecular Diffusion in Naturally Fractured Reservoirs: A Decisive Recovery Mechanism. SPE 19672, 64th SPE Fall Meeting, San Antonio, TX, October.

Dastyari A., Bashukooh B., Shariatpanahi S. F., Haghighi M. and Sahimi M., 2005. Visualization of Gravity Drainage in a Fractured System During Gas Injection Using Glass Micromodel. SPE 93673, 14th SPE Middle East Oil & Gas Confefence, Behrain. March.

Dindoruk B. and Firoozabadi A., 1997. Crossflow in Fractured/Layered Media Incorporating Gravity, Viscous, and Phase Behavior Effects. SPEJ. June. 120-135.

Dronfield D. G. and Silliman S. E., 1993. Velocity dependence of dispersion for transport through a single fracture of variable roughness. Water Resour. Res. 29(10): 3477.

Detwiler R. L., Rajaram H. and Glass R. J., 2000. Solute transport in variable-aperture fractures: an investigation of the relative importance of Taylor dispersion and macrodispersion. Water Resour. Res. 36(7): 1611.

Firoozabadi A. and Markeset T. I., 1994. Miscible Displacement in Fractured Porous Media: Part I – Experiments. SPE 27743, SPE/DOE 9th Symposium on Improved Oil Recovery, Tulsa, OK. April.

Fischer H. B., List E. J., Koh R. C. Y., Imberger J. and Brooks N. H., 1979. Mixing in Inland and Coastal Waters. Academic, San Diego, Calif.

Fjelde I., Zuta J. and Duyilemi O. V., 2008. Oil Recovery from Matrix during CO_2-Foam Flooding of Fractured Carbonate Oil Reservoirs. SPE 113880, SPE Europec/EAGE Annual Conference and Exhibition, Rome, Italy, 9-12 June.

Forzatti P., 2001. Present Status and Perspectives in de-NOx SCR Analysis. Appl. Catal. A. Gen. 222: 221.

Fox R. W. and McDonlad T. A., 1998. Introduction to Fluid Mechanics. John Willey & Sons Canada, Ltd.

Freeze R. A. and Cherry J. A., 1979. Groundwater. Prentice- Hall, Englewood Cliffs, NJ.

Froment G. F. and Bischoff K. B., 1990. Chemical reactor analysis and design (2nd Edition) Wiley, New York.

Gabitto J. F., 1998. Matrix-fracture mass transfer. SPE 39702, paper presented at SPE/DOE Improved Oil Recovery Symposium. Tulsa, OK. April.

Gharbi R., Peters E. and Elkamel A., 1998. Scaling Miscible Fluid Displacement in Porous Media. Energy & Fuels. 12: 801.

Gharbi R., 2002. Dimensionally Scaled Miscible Displacement in Heterogeneous Permeable Media. Transport in Porous Media. 48: 271.

Ghorayeb K. and Firoozabadi A., 2000. Numerical Study of Natural Convection and Diffusion in Fractured Porous Media. SPEJ. 5 (1):12.

Grattoni C. A., Jing X. D. and Dawe R. A., 2001. Dimensionless Groups for Three-Phase Gravity Drainage Flow in Porous Media. Journal of Petroleum Science and Engineering. 29: 53.

Gillham R. and Cerry J.A., 1982. Contaminant migration in saturated unconsolidated geologic deposits. In Recent trends in hydrogeology. Edited by T. N. Narasimhan. Geological Society of America, Special Paper 189, 3:1-62.

Handy L., 1960. Determination of effective capillary pressure for porous media from imbibition data. AIME Trans. 219: 75.

Hatiboglu C. U. and Babadagli T., 2004. Experimental analysis of primary and secondary oil recovery from matrix by counter-current diffusion and spontaneous imbibition. SPE 90312, SPE Annual Technical Conference and Exhibition. Houston, TX. September.

Hatiboglu C. U. and Babadagli T., 2006. Primary and Secondary Oil Recovery from Different Rocks by Countercurrent Diffusion and Spontaneous Imbibition. SPE 94120, SPE/DOE Symposium on Improved Oil Recovery, Tulsa, OK, April.

Horne R. N. and Rodriguez F., 1983. Dispersion in tracer flow in fractured geothermal systems. Geophys. Res. Let. 10 (4): 289.

Hu H., Whitson C. H. and Ai Y., 1991. A study of recovery mechanisms in a nitrogen diffusion Experiment. SPE 21893, unsolicited paper available in Society of Petroleum Engineers e-library.

Hujun Li., Putra E., Schechter D. S. and Grigg R. B., 2000. Experimental investigation of CO2 gravity drainage in a fractured system. SPE 64510, SPE Asia Pacific Oil & Gas Conference and Exhibition. Brisbane, Australia. October.

Ippolito I., Daccord G., Hinch E. J. and Hulin. J. P., 1984. Echo tracer dispersion in model fractures with a rectangular geometry. J. Contam. Hydrol. 16 (1): 87.

Jamshidnezhad M., Montazer-Rahmati M. and Sajjadian V. A., 2004. Theoretical and experimental investigations of miscible displacement in fractured porous media. Transport in Porous Media. 57 (1): 59.

Jessen K., Kovscek A. R. and Orr F. M., 2005. Increasing CO2 Storage in Oil Recovery. Energy Convers. Mgmt. 46: 293.

Jensen T. B., Sharma M. P., Harris H. G. and Whitman D. L., 1992. Numerical investigations of steam and hot-water flooding in fractured porous media. SPE 24172, paper presented at the SPE/DOE 8th Symposium on Enhanced Oil Recovery. Tulsa, OK. April.

Johnson R. W., 1998. The Handbook of Fluid Dynamics. CRC Press.

Karimaie H., Darvish G. R., Lindeberg E. and Torsaeter O., 2007. Experimental Investigation of Secondary and Tertiary Gas Injection in Fractured Carbonate Rock. SPE 107187, SPE Europe/EAGE Annual Conference and Exhibition, London, UK, 11-14 June.

Keller A. A., Roberts P. V., Martin M. J., 1999. Effect of fracture aperture variations on the dispersion of solutes. Water Resour. Res. 35(1): 55.

Kovscek A. R., 2002. Screening Criteria for CO2 Storage in Oil Reservoir. Petroleum Science and Technology. 20 (7-8): 841.

Kulkarni M. M. and Rao D. N., 2006a. Characterization of Operative Mechanisms in Gravity Drainage Field Projects through Dimensionless Analysis. SPE 103230, SPE Annual Technical Conference and Exhibition, San Antonio, TX. September.

Kulkarni M. M. and Rao D. N., 2006a. Analytical Modeling of the Forced Gravity Drainage GAGD Process. AIChE paper # 72361, AIChE Annual Meeting. San Francisco, CA. November.

LaBolle E. M., Quastel J., Fogg G. E. and Gravner J., 2000. Diffusion Processes in Composite Porous Media and their Numerical Integration by Random Walks: Generalized Stochastic Differential Equations with Discontinuous Coefficients. Water Resources Research. 36: 651.

Lenormand R., Le Romancer J. F., Le Gallo Y. and Bourbiaux B., 1998. Modeling the Diffusion Flux Between Matrix and Fissure in a Fissured Reservoir. SPE 49007, SPE Annual Technical Conference and Exhibition, New Orleans, LA, September.

Le Romancer J. F., Defives D. F., and Fernandes G., 1994. Mechanism of oil recovery by gas diffusion in fractured reservoir in presence of water. SPE 27746, SPE/DOE 9th Symposium on Improved Oil Recovery, Tulsa, OK. April.

Li S., Dong M., Li Z., Huang S., Qing H. and Nickel E., 2005. Gas Breakthrough Pressure for Hydrocarbon Reservoir Seal Rocks: Implication for Security of Long-term CO2 Storage in the Weyburn Field. Geofluids. 5: 326-334.

Mohanty K. K and Salter S. J., 1982. Multiphase flow in porous media: II- pore-level modeling. SPE 11018, SPE Annual Technical Conference and Exhibition. New Orleans. September.

Mahmoud N.N., 2006. Demonstration and Performance Characterization of the Gas Assisted Gravity Drainage (GAGD) Process using A Visual Model. Thesis, Louisiana State University.

Morel D. D., Bourbiaux B., Latil M. and Thiebot B., 1993. Diffusion effects in gas flooded light oil fractured reservoirs. SPE-Adv. Tech. Series. 1 (2): 100-109.

Muralidharan V., Putra E. and Schechter D. S., 2004. Experimental and Simulation Analysis of Fractured Reservoir Experiencing Different Stress Conditions. Paper 2004-229, 55th Annual Technical Meeting, Canadian International Petroleum Conference, Calgary, Canada, June 8-10.

Pande K. K. and Orr F. M. Jr., 1990. Analytical computation of breakthrough recovery for CO2 floods in layered reservoirs. SPE 20177, unsolicited paper available in Society of Petroleum Engineers e-library.

Part M., 1993. Percolation model of drying under isothermal conditions in porous media. Int. J. Multiphase Flow. 19: 693.

Perkins T. K and Johnston O. C., 1963. A review of diffusion and dispersion in porous media. SPEJ. 3(4):70, Trans. AIME. 228 (1): 70.

Rangel-German E. R. and Kovscek A. R., 2000. Matrix-Fracture Interaction in Single Matrix Blocks. Proceedings of 25th Workshop on Geothermal Reservoir Engineering. January.

Riazi M. R., 1996. A New Method for Experimental Measurement of Diffusion Coefficients in Reservoir Fluids. J. Pet. Sci. Eng. 14 (3-4): 235.

Roux S., Plouraboue F. and Hulin J. P., 1998. Tracer dispersion in rough open cracks. Trans. Porous Media. 32 (1): 97.

Saidi A. M., 1987. Reservoir Engineering of Fractured Reservoir. Total Edition Press.

Sahimi M., Heiba A. A., Hughes B. D., Davis H. T. and Scriven L. E., 1982. Dispersion in flow through porous media. SPE 10969, SPE Annual Technical Conference and Exhibition. New Orleans. September.

Schechter D. S. and Guo B., 1996. Mathematical Modeling of Gravity Drainage after Gas Injection into Fractured Reservoirs. SPE 35170, SPE Improved Oil Recovery Symposium. Tulsa, OK. April.

Sheikha H., Pooladi-Darvish M. and Mehrotra A. K., 2005. Development of Graphical Methods for Estimating the Diffusivity Coefficient of Gases in Bitumen from Pressure-Decay Data. Energy & Fuels. 19 (5): 2041.

Shook M., Li D. and Lake L. W., 1992. Scaling immiscible flow through permeable media by inspectional analysis. In-Situ 4: 311.

Sigmund P.M., 1976. Prediction of Molecular Diffusion at Reservoir Conditions: Part I. Measurement and Prediction of Binary Dense Gas Diffusion Coefficients. J. Can. Pet. Tech. 15: 48– 57.

Slobod R. L. and Howlett W. E., 1964. The Effect o Gravity Segregation in Studies of Miscible Displacement in Vertical Unconsolidated Porous Media. SPEJ. :1-8.

Stubos A. K. and Poulou S., 1999. Oil recovery potential from fractured reservoirs by mass transfer processes. SPE 56415, SPE Annual Technical Conference and Exhibition. Houston, TX. October.

Taber J. J., Martin F. D. and Seright R. S., 1997a. EOR Screening Criteria Revisited-Part 1: Introduction to Screening Criteria and Enhanced Recovery Field Projects. SPE Res. Eng. 189.

Taber J. J., Martin F. D. and Seright R. S., 1997b. EOR Screening Criteria Revisited-Part 2: Applications and Impact of Oil Process. SPE Res. Eng. 199.

Tang D. H., Frind E. O. and Sudicky E. A., 1981. Contaminant Transport in Fractured Porous Media: Analytical Solution for a Single Fracture. Water Resour. Res. 17: 555.

Taylor G., 1953. Dispersion of soluble matter in solvent flowing slowly through a tube. Proc. R. Soc. A. 219 (1137):186.

Tharanivasan A. K., Yang C. and Gu Y., 2004. Comparison of Three Different Interface Mass Transfer Models Used in the Experimental Measurement of Solvent Diffusivity in Heavy Oil. J. Pet. Sci. Eng. 44 (3-4): 269.

Thompson J. L. and Mungan N., 1969. A laboratory study of gravity drainage in fractured systems under miscible conditions. SPEJ. June. 247.

Torabi F. and Asghari K., 2007. Performance of CO2 Huff-and-Puff Process in Fractured Media (Experimental Results). Paper 2007-119, 58th Annual Technical Meeting, Canadian International Petroleum Conference, Calgary, AB, Canada, 12-14 June.

Trivedi J. J. and Babadagli T., 2006. Efficiency of Miscible Displacement in Fractured Porous Media. SPE 100411, SPE Western Regional/AAPG Pacific Section/GSA Cordilleran Section Joint Meeting. Anchorage, Alaska, 8-10 May.

Trivedi J. and Babadagli T., 2008a. Efficiency of Diffusion Controlled Miscible Displacement in Fractured Porous Media. Transport in Porous Media. 71(3): 379.

Trivedi J. and Babadagli T., 2008b. Experiment and Numerical Modeling of the Mass Transfer between Rock Matrix and Fracture. Chemical Eng. J. doi:10.1016/j.cej.2008.05.032.

Trivedi J. and Babadagli T., 2008c. Efficiency Analysis of Greenhouse Gas Sequestration during Miscible CO_2 Injection into Fractured Oil Reservoirs. Accepted for publication in Env. Sci and Tech.

Trivedi J. and Babadagli T., 2008d. Scaling Miscible Displacement in Fractured Porous Media Using Dimensionless Groups. J. Pet. Sci. Eng. doi:10.1016/j.petrol.2008.03.001.

Trivedi J. J. and Babadagli T., 2008e. Experimental Investigations on the Flow Dynamics and Abandonment Pressure for CO_2 Sequestration and Incremental Oil Recovery in